KU LEUVEN

ARENBERG DOCTORAL SCHOOL
FACULTY OF ENGINEERING SCIENCE

A NOVEL ANISOTROPIC COMPOSITE FOAM CONCEPT FOR IMPROVED HEAD PROTECTION IN OBLIQUE IMPACTS

Yasmine Mosleh

Supervisor:
prof.dr.ir. Jan Ivens

Dissertation presented in partial fulfilment of the requirements for the degree of Doctor of Engineering Science (PhD): Materials Engineering

August 2018

A NOVEL ANISOTROPIC COMPOSITE FOAM CONCEPT FOR IMPROVED HEAD PROTECTION IN OBLIQUE IMPACTS

Yasmine Mosleh

Supervisor:
prof.dr.ir. Jan Ivens

Members of the Examination Committee:
prof.dr.ir. Bart Depreitere
prof.dr.ir. Jos Vander Sloten
prof.dr.ir. Bert Verlinden
prof.dr.ir. Ignaas Verpoest
prof.dr.ir. Peter Halldin
prof.dr.ir. Larry Lessard
prof.dr.ir. Omer Van der Biest, Chairman

Dissertation presented in partial fulfilment of the requirements for the degree of Doctor of Engineering Science (PhD): Materials Engineering

August 2018

Acknowledgements

This thesis could not have been completed without collaboration and help of so many people to whom I express my enormous gratitude.

First of all, I would like to express my gratitude to my promoter prof. Jan Ivens, offering me this opportunity in the first place and his trust in me no matter how difficult the project seemed. I thank him for his support and guidance.

I wish to thank the Flemish Scientific Research Council FWO who provided financial support to this research through the Levenslijn project (G.0C67.13).

I would like to thank prof. Jos Vander Sloten and prof. Bart Depreitere as members of my supervisory team who both had a huge influence on leading this multidisciplinary project and the Leuven Bicycle Helmet Group. Thank you for your guidance and the encouragements you gave to us all during these years.

I would like to sincerely thank the other jury members of my thesis in KU Leuven, em. prof. Ignaas Verpoest, prof. Bert Verlinden and prof. Omer Van der Biest for reading my thesis and being part of my assessory committee and for their insightful comments.

I also thank em. prof. Ignaas Verpoest for his guidance during my participation in the steel fibre composite project (SFRP).

I would like to thank prof. Peter Halldin from Royal Institute of Technology KTH, for his kind and generous assistance to me and Dr. Kelly Vanden Bosche, during our project visit to Stockholm and for sharing with us his vast expertise and insight in the subject matter. I also thank him for being assessor of my thesis and for his constructive suggestions.

I specially thank prof. Larry Lessard from McGill University for coming such a long way to be a part of my committee, for his very good suggestions, and also for the engaging lecture he presented to us during his visit to Leuven.

I sincerely thank Dr. Sheron Shamuilia and Dr. Wim De Clercq from LRD for their diligent support and advise during writing and filing of my patent.

I would like to thank Dr. Leonard Pastrav from the Mechanical Engineering Department at Campus GroupT of KU Leuven for his essential help and guidance. His insight in electromechanics helped us in development of the set-ups.

Special thanks to Dr. Kelly Vanden Bosche from whom I inherited the project, without whom I could not have had a good start. I am grateful to you for so many different aspects, for your continuous support of me and your words of encouragements and your insight. During the transfer of the project, I found out that you are one of the best teachers I know. Thank you for being such a pleasant colleague and more importantly a good friend!

Thanks of course to all my master students from the Faculty of Engineering Technology: Bart, Jeroen, Sven, Olivier, Jamie, Joachim, Maarten, Frederic, and Serdar; it was a pleasure for me to work with you during these years. Thank you for your cooperation and for your full trust in me to guide you. Your success in your thesis was as fulfilling for me as if it were my own.

The performance of this heavily experimental work in the lab was not possible without cooperation of technicians Ing. Bart Pelgrims, Ing. Marc Peeters, and Kris Van de Staey in the the composites lab, and Joop Van Deursen in the workshop. I am thankful to them all.

I like to thank all my friends and colleagues in the Bicycle Helmet Group, Zhaoyin, Gracia, Dries, Nele, Markos and Dimitris for creating a pleasant environment, for their cooperation and the useful discussions during our meetings.

I was blessed to share office with kind hearted and generous people during my time in Leuven, Lina, Eduardo, Carlos, Ngoc, Morissa, Stijn, and Kirill thank you for being my friends!

Other friends and colleagues in the CMG group and MTM, were an indispensable part of the good memories which I take; I do not mention names in fear that I may miss out somebody.

My deepest gratitude goes to my Mother; from her I know what perseverance means, being dedicated and hardworking, and to have no fear to explore different paths, and how to find a way to light no matter how dark the path is. I am blessed to have my beloved brother with whom I share pleasant experiences and memories, for being a soulmate no matter near or far... I cherish the loving memory of my father who would have been the happiest about this achievement.
I thank my parents-in-law for being so encouraging and kind to me. And last, I thank my husband to be my best pal, and my stimulus to finish this degree.

Abstract

Oblique impact is the most common accident situation that occupants in traffic accidents or athletes in professional sports experience. During oblique impact, the human head is subjected to a combination of linear and rotational (angular) accelerations. Rotational (angular) acceleration and also velocity of the head are known to be responsible for traumatic brain injuries and must be minimised.

Cyclists are amongst the most vulnerable road users in traffic and helmets are the only means offering them head protection. Conventional helmets are proven to be effective at mitigation of head linear accelerations. However, they lack dedicated mechanisms to specifically aim at rotational acceleration mitigation, which is also still not a requirement in helmet test standards. Within the KU Leuven Bicycle Helmet Group (newly called IMPACT), it was proposed around the year 2008 that by using (transversely) anisotropic foam with the direction of anisotropy perpendicular to the head surface, the rotational acceleration (deceleration) transferred to the head can be reduced. Early studies demonstrated that a highly anisotropic polyethersulfone foam (PES) with large shape anisotropy ratio could outperform conventional isotropic expanded polystyrene foam (EPS) as helmet liner to reduce both linear and rotational accelerations of the head. However, the better performance of PES foam in comparison to EPS foam could not be solely attributed to anisotropy. This was due to simultaneously different density and solid material properties of PES

foam in comparison to EPS. Moreover, processing the highly anisotropic PES foam into complex geometries e.g. of bicycle helmets proved to be challenging and hindered its practical realization as alternative material for helmet liners on large industrial scale.

In this thesis, composite foam with column/matrix configuration is presented as a novel concept for head protection in applications such as protective helmets or headliners in interiors of crashworthy vehicles. This concept creates anisotropy in foam at the ''macro level'' and also enabled to finally perform a clear ''proof of principle study'' to show that the anisotropy of the foam can lead to mitigation of rotational acceleration and velocity transferred to the head in an oblique impact. Moreover, through experimental and numerical parametric studies, it is shown that in the composite foam concept, the level of anisotropy and hence mitigation of rotational acceleration and velocity can be tailored by changing parameters such as the diameter of the foam columns in the structure and the compliance of the matrix foam. The experimental parametric study was carried out by performing biaxial shear-compression and oblique impact experiments on different configurations of composite foams. The numerical parametric study was carried out by simulating oblique impact of a simplified head model, with finite elements. Results have shown reductions in rotational acceleration up to 44% as compared to standard EPS 80 foam by using composite foam. Simulations matched the experimental results and also showed that the shape of the columns of high density foam is less critical.

Another focus of this thesis has been the further development and presentation of test set-ups which can be utilised for preliminary and final assessment of foam materials for helmets in oblique loading, namely a biaxial shear-compression tester and an oblique impact set-up. The biaxial shear-compression test set-up was utilized to study the effect of foam anisotropy on the energy absorption capacity of foams under different loading angles. Moreover, the correlation between combined shear-compression properties of the foams and their behaviour in oblique impact tests was investigated and confirmed. Additionally, in this thesis, further development of the KU Leuven oblique impact set-up was undertaken. For this, a critical comparison between KU Leuven and KTH (Stockholm) oblique impact set-ups was made. Furthermore, a thorough analysis on the instrumentation of the KU Leuven set-up was carried out by designing an apparatus which allowed calibration of its Angular Rate Sensor (ARS) in its wide

working range. Moreover, the KU Leuven set-up was simplified by designing and incorporating a solid angled anvil instead of a rotating impact surface. The oblique impact set-up can be utilised for testing foams as flat foam samples as well as for helmet testing.

Samenvatting

Impact onder een hoek, is de meest voorkomende situatie tijdens ongelukken in het verkeer of bij professionele sporters. Tijdens impact onder een hoek wordt het menselijk hoofd blootgesteld aan een combinatie van lineaire en rotationele (hoek) versnellingen. Rotationele versnelling en snelheid zijn verantwoordelijk voor traumatische hersenschade en moeten geminimaliseerd worden.
Fietsers behoren tot de meest kwetsbare weggebruikers en helmen zijn het enige middel om hen bescherming van het hoofd te bieden. Conventionele helmen zijn bewezen goed in het opvangen van lineaire versnellingen van het hoofd. Ze hebben echter geen speciale mechanismen om rotationele versnellingen op te vangen, wat ook nog steeds geen vereiste is in testnormen voor helmen.
Binnen de fietshelmen groep van de KU Leuven (recentelijk genoemd IMPACT) was in 2008 voorgesteld dat door het gebruik van anisotroop schuim met de richting van anisotropie loodrecht op het oppervlak van het hoofd, de rotationele versnelling die op het hoofd wordt uitgeoefend kan worden verkleind. Eerste studies lieten zien dat een zeer anisotroop polyethersulfon (PES) schuim een betere reductie van lineaire en rotationele versnellingen kon laten zien dan conventioneel isotroop ge-expandeerd polystyreen (EPS). Maar de verbetering in eigenschappen kon niet uitsluitend worden toegewezen aan anistropie, omdat de PES tegelijkertijd ook een verschillende densiteit en polymeereigenschappen liet zien t.o.v. EPS. Tenslotte, bleek ook verwerking van het zeer anisotrope PES schuim in complexe vormen zoals van een helm, zeer moeilijk, zodat de praktische uitvoerbaarheid op industriële schaal vooralsnog verhinderd is.

In deze thesis, wordt composietschuim met een kolom/matrix configuratie voorgesteld als een nieuw concept voor bescherming van het hoofd in applicaties zoals beschermende helmen of zogenaamde headliners in het interieur van crash-bestendige voertuigen. Dit concept creëert anisotropie in een schuim op macro-niveau en liet ook toe om uiteindelijk een duidelijke "proof of principle" studie te doen om aan te tonen dat anisotropie in het schuim kan leiden tot onderdrukking van rotationele versnelling en snelheid van het hoofd in een impactbelasting onder een hoek. Hierop verdergaand, met hulp van experimentele en numerieke parameter studies, wordt aangetoond dat met het concept van composietschuim, het niveau van anisotropie en hierdoor van onderdrukking van rotationele versnelling en snelheid kan worden ingesteld door het veranderen van parameters als de diameter van de schuimkolommen in de struktuur en de compliantie van het matrixschuim. De experimentele parameterstudie werd uitgevoerd door het doen van bi-axiale afschuif-en-compressie testen alsmede van impactexperimenten onder een hoek, op verschillende configuraties van composietschuim. De numerieke parameterstudie werd uitgevoerd door het simuleren van impact onder een hoek met een gesimplificeerd eindige elementen model van het hoofd. Resultaten laten een reductie zien in rotationele versnellingen tot 44% in vergelijking met standaard EPS 80 polystyreenschuim door het gebruik van composietschuim. Het model liet een goede overeenkomst zien met de experimentele resultaten en liet ook zien dat de vorm van de kolommen van hoge dichtheid schuim minder kritisch is.
Een andere focus van deze thesis was de verdere ontwikkeling en presentatie van testopstellingen die kunnen gebruikt worden voor de pre-liminaire en uiteindelijke beoordeling van schuimmaterialen voor helmen bij belasting onder een hoek, met name een bi-axiale testopstelling voor gecombineerde afschuiving en compressie en een opstelling voor impact onder een hoek. De bi-axiale afschuiving en compressie opstelling werd gebruikt voor de studie van het effect van schuimanisotropie op de energieabsorptie van schuimen belast onder verschillende hoeken. Ook werd de correlatie onderzocht en bevestigd tussen gecombineerde afschuif-compressie eigenschappen van de schuimen en hun gedrag tijdens impact onder een hoek. Verder werd in deze thesis verdere ontwikkeling gedaan van de KU Leuven opstelling voor impact onder een hoek. Hiertoe werd een kritische vergelijking gemaakt tussen de opstellingen van KU Leuven en de KTH in Stockholm. Een grondige analyse werd gedaan van de

instrumentatie van de KU Leuven opstelling door het ontwerp van een opstelling voor de calibratie van de hoeksnelheidssensor in een breed werkingsgebied. Daarenboven werd de KU Leuven opstelling gesimplificeerd door het ontwerp en de implementatie van een vaste opstelling met een helling onder een hoek in plaats van een opstelling met een roterende band. De impactopstelling onder een hoek kan gebruikt worden voor het testen van vlakke schuimmonsters alsmede voor het testen van helmen.

Symbols and Abbreviations

Symbols

a_x	linear acceleration of the centre of mass of a rigid body (in the x direction)
a_y	linear acceleration of the centre of mass of a rigid body (in the y direction)
a_z	linear acceleration of the centre of mass of a rigid body (in the z direction)
a_r	resultant linear acceleration
a_{cr}	critical linear acceleration
$a_{r,\,max}$	peak (maximum) resultant linear acceleration
C	compression displacement rate
d	cylinder diameter
E	elastic modulus
E^*	elastic modulus of foam

E_s	elastic modulus of solid polymer
F_N	normal force
F_T	tangential force
g	gravitational acceleration constant = 9.81 ms^{-2}
G^*	shear modulus of the foam
h	height of a foam cell edge
I_{xx} , I_{yy} *and* I_{zz}	rotational moments of inertia of a rigid body (around the x, y and z axes)
k	densification constant
l	length (width) of foam cell edge
l/d	cylinder aspect ratio
P_{wall}	contribution of the load carried in the cell wall
p_0	initial gas pressure in an uncompressed foam cell
R	aspect ratio of a foam cell = h/l
R_ρ	relative density of foam = ρ^*/ρ_s
S	shear displacement rate; intercylinder distance
t	time; thickness of foam cell edge
T	Temperature
T_g	glass transition temperature
V_t	tangential linear velocity
W	work (energy stored/dissipated) per unit volume

α_r	resultant rotational acceleration
α_{cr}	critical rotational acceleration
$\alpha_{r,\ max}$	peak (maximum) resultant rotational acceleration
α_x , α_y , α_z	rotational acceleration (around the x, y and z axes)
γ	shear strain
Δt	impact pulse duration (time of impact)
$\omega_{r,max}$	maximum resultant rotational velocity
ε	Strain
ε_D	densification strain
θ	deformation angle, anvil angle with respect to horizontal line
ν	Volume fraction
ρ^*	density of foam
ρ_s	density of solid polymer
ρ_{actual}	actual foam density
$\rho_{overall}$	overall foam density
μ	viscosity of air
σ^*	stress in a foam
σ_{cr}	brittle crushing strength of foam
σ_{el}	elastic buckling stress of foam
σ_{max}	maximum allowable compressive stress

σ_p	peak stress in a foam
σ_{pl}	plastic collapse stress of foam
$\sigma_{s,y}$	yield strength of polymer
$\sigma_{p,A}$	yield strength of foam when compressed on plane A
$\sigma_{p,C}$	yield strength of foam when compressed on plane C
τ	shear stress
ω_{max}	peak (maximum) resultant rotational velocity
ω_r	resultant rotational velocity
$\omega_x\, \omega_y\, \omega_z$	rotational velocity (in the x, y and z directions)

Abbreviations

AIM	Angular Impact Mitigation System
ARS	Angular Rate Sensor
ASDH	Acute SubDural Daematoma
ASTM	American Society of the International Association for Testing and Materials
BRIC	BRain Injury Criterion
CPSC	Consumer Product Safety Committee standard
CSA/CAN	Canadian Standards Association standard
DAI	Diffuse Axonal Injury
EN (CEN)	Common European Norm (standard)
E-PLA	Expanded-PolyLactic Acid

EPP	Expanded PolyPropylene foam
EPS	Expanded PolyStyrene foam
FEM	Finite Element Modelling
GAMBIT	Generalized Acceleration Model for Brain Injury Threshold
HDPE	High Density PolyEthylene
HIC_{15} HIC_{36}	Head Injury Criterion maximized over 15 or 36 seconds
HIC_{rot}	Rotational Head Injury Criterion
HIP_{max}	maximum Head Impact Power
KTH	Royal Institute of Technology, Stockholm, Sweden
KU	KU Leuven
MAF	Modified Arcan test Fixture
MIPS	Multidirectional Impact Protection System
PC	PolyCarbonate
PES	PolyEtherSulfone
PET	PolyEthylene Terepthalate
PU	PolyUrethane
PVC	PolyVinyl Chloride
S/C	Shear deformation/Compression deformation ratio
UBTD	Universal Biaxial Testing Device
HDPE-MA	High Density PolyEthylene Modified with Maleic Anhydride
XPS	Extruded PolyStyrene foam

Table of Contents

Chapter 1
General introduction

Cycling is a healthy activity and can be an efficient form of transport. As sport or leisure, cycling can help with respiratory, cardiovascular, and mental health [1-3]. As a means of transportation, cycling contributes to less air pollution, a cleaner environment, and reduced traffic. Moreover, cycling for transportation can be economically beneficial by saving the fuel expense and for commuting inside busy cities cycling is often faster than some of the other modes of transport.

Like other types of sports, cycling is not without risk. Head injuries are an important fraction of cycling-related injuries. Numerous reports have identified head injuries as the major cause of severe dysfunction or mortality for both cyclists and pedestrians [4-6]. Some studies identified head injuries as the main cause of death in 69–93% of fatal bicycle accidents [6]. A case control study of cycling fatalities in Ontario, Canada, between 2006 and 2010 also indicated an association between occurrence of fatalities and sustaining a head injury [7].

Cyclists, motorcyclists, and pedestrians are the most vulnerable road users in comparison to vehicle occupants [8]. Car occupants, for example, are protected by safety belts, airbags, and the body structure of the car whilst helmets are the only tool offering protection to the cyclists.

Current bicycle helmets are typically comprised of an energy absorbing helmet liner covered by a hard plastic shell which helps to distribute the impact over a larger area. The helmet can be adjusted and fixed on the head using a chin strap. Helmet liners which are often polymer foams, typically expanded polystyrene (EPS), are designed to absorb impact energy whilst keeping translational forces/accelerations transmitted to the head below a certain threshold defined by standards [9-10].

Up to now many studies have evaluated the effectiveness of bicycle helmets. In the first case-control study, it was found that using helmets reduces the head and brain injury occurrence by 85% and 88%, respectively for all age groups [11]. In a study by Bambach, et al. [12], it was found that cyclists who do not wear helmets face a higher chance of sustaining a head injury by 1.98–3.89 times. In particular, the risk of skull fracture, intracranial injuries and open head wounds was increased by 2.29–4.61, 1.60–3.52, and 5 times, respectively. In a Cochrane review of case-control studies, it was concluded that bicycle helmets reduced the risk of head and brain injuries for all ages of bicyclists by 63 to 88%. Also bicycle helmets seemed to offer similar level of protection for all crashes (including crashes involving motor vehicles) [13]. Attewell et al. [14] evaluated the bicycle helmet efficacy using a meta-analytic approach based on peer-reviewed research papers published between 1987-1998. In this study, it was concluded that the bicycle helmets prevent serious head injury, brain injury, facial injury, and even death. Moreover, in this study, it was proposed that the use of the helmet for all riders should be further encouraged. In another meta-analysis study carried out by Olivier and Creighton [15], it was concluded that bicycle helmet use is associated with reduced odds of head injury, serious head injury, facial injury, and fatal head injury. In a more recent meta-analysis study on effectiveness of bicycle helmets on crash involved cyclists between 1989–2017, Hoye [16] concluded that the use of bicycle helmets reduces head injury by 48%, serious head injury by 60%, traumatic brain injury by 53%, face injury by 23%, and the total number of killed or seriously injured cyclists by 34%. Apart from case-control and population based studies, the efficacy of helmets in reducing head injuries was also confirmed by laboratory experiments and accident simulation studies [17 -18].

In order to certify a helmet for entering the market, it needs to pass a standardization test. In current bicycle helmet standards such as the European cyclist helmet standard (EN1078) [19], the American standard (CPSC, 1998) [20], and the Australian/New Zealand standard (AS/NZS 2063) [21], the helmet is dropped vertically onto a horizontal or kerbstone surface and the used head-form is guided and constrained in order to prevent rotational (angular) acceleration. In these standards only linear acceleration is considered as a criterion for evaluation of the protective effect of the helmet.

Different studies indicate that oblique impacts are the most common impact situations that a cyclist experiences in traffic accidents [22-24]. In an oblique impact, the human head undergoes normal and tangential force components which give rise to linear (translational) and rotational (angular) accelerations. The normal force components that are not directed to the centre of rotation of the head also result in a rotational moment. Rotation of the head is linked to traumatic brain injuries e.g. contusions, subdural haematoma (SDH), and diffuse axonal injury (DAI), [25-29]. Large rotational accelerations can cause relative motion between the brain and the skull leading to significant tensile and possibly shear strains on bridging veins. Rupture of over-strained bridging veins can lead to acute SDH, ASDH, [30]. The brain tissue is nearly incompressible and its bulk modulus is around six orders of magnitude larger than its shear modulus [31], hence for a given impact, the brain is more prone to shear deformation. Kleiven concluded that the strain in the brain is more sensitive to rotational rather than linear movement [32]. It can be concluded that rotational movement has a bigger role in inducing traumatic brain injuries and can certainly not be disregarded when developing protective gear.

The awareness of the role of rotational movement of the head in inducing traumatic brain injury encouraged further research aiming at introducing an oblique impact testing set-up [33-36] and rotational acceleration/velocity based acceptance criteria and thresholds in the next generation bicycle helmet standards [37] and also to design functionally more advanced helmets aiming specifically at reducing the rotational movement of the head during impact. The efforts on developing helmets which can reduce head rotational movement were focused on either improving the helmet liner itself [38-40] or on proposing new helmet designs [41-43].

In an effort to improve the helmet liner, it was proposed within the bicycle helmet group (recently renamed to IMPACT group) at KU Leuven that by using an anisotropic foam liner with direction of anisotropy perpendicular to the head surface instead of a conventional isotropic foam, the rotational acceleration of the head could be further mitigated [38]. A first study was set up to investigate if a highly anisotropic polyethersulfone foam (PES) with large shape anisotropy ratio (R~10) and low density (57 kg/m^3), could outperform conventional isotropic EPS foam in terms of reducing rotational movement of the head when used as helmet liner [24]. To demonstrate the validity of the innovative proposal, bicycle prototype helmets were produced using this PES foam; the performance of prototype helmets in oblique impact was benchmarked against commercial helmets with isotropic EPS foam as liner. Results showed that the prototype helmets could significantly reduce peak resultant linear acceleration, rotational acceleration, and rotational velocity of the head simultaneously. However, it should be noted that PES foam used as liner in the prototype helmets has a lower density (57 kg/m^3) than EPS (80 kg/m^3) in reference helmets and obviously the solid polymer material in both foams was different; this hindered to assess the effect of foam anisotropy as the only and independent varying parameter in this proof of principle study. Moreover, the practical realization of PES foam as an alternative material for helmet liners in terms of processing showed significant challenges. This is because the highly anisotropic PES foam could only be processed in the form of flat panels and transforming the flat PES foam into the intricate shape of a helmet without damaging the cell structure appeared very time consuming and labour intensive and obviously not suited for commercial application [39, 44].

In this thesis, a novel anisotropic material concept, namely composite foam, is proposed as a smart structural solution to introduce the mechanical anisotropy in a foam at ''macro level'' without changing the overall density, thickness, or solid material in a foam. The composite foam concept comprises of two different densities of a foam (e.g. EPS foam) in a column/matrix configuration in which high density column foam must be aligned in radial direction (perpendicular to the head surface) when used in a helmet. This concept enables to finally prove that anisotropy as a single variable in foam can lead to mitigation of rotational acceleration and velocity in oblique head impacts. Moreover,

in this concept, the level of anisotropy can be easily tailored for a given weight and thickness of the foam liner. Additionally, the composite foam structure is optimized for the further reduction in rotational movement using experimental and numerical parametric studies. This concept has the potential to be produced in industrial manner.

Another focus of this thesis is the further development of the characterization methods and test set-ups for preliminary and final assessment of foam materials in oblique loading at coupon and helmet level. A biaxial shear-compression test set-up was utilized to study the possible correlation between combined shear-compression properties of the foam with the level of linear and rotational accelerations transferred to the head during oblique impact tests. Moreover, further development of the KU Leuven oblique impact set-up was undertaken. For this, a thorough analysis of the instrumentation of the set-up was carried out by designing an apparatus which allowed calibration of its Angular Rate Sensor (ARS) which measures rotational velocity (about x, y, and z axis) in a wide working range. Moreover, the KU Leuven set-up was simplified by designing and incorporation of a solid inclined anvil instead of a rotating impact surface which had previously shown to be complex.

References

1. Lusk, A.C., et al. Bicycle riding, walking, and weight gain in premenopausal women. Archives of Internal Medicine, 2010. 170(12): p. 1050-1056.
2. Børrestad, L.A.B., et al. Experiences from a randomised, controlled trial on cycling to school: Does cycling increase cardiorespiratory fitness? Scandinavian Journal of Public Health, 2012. 40(3): p. 245-252.
3. Ohta, M., et al. Effect of the Physical Activities in Leisure Time and Commuting to Work on Mental Health. Journal of Occupational Health, 2007. 49(1): p. 46-52.
4. Eilert-Petersson, E. and Schelp, L. An epidemiological study of bicycle-related injuries. Accident Analysis & Prevention, 1997. 29(3): p. 363-372.

5. Fredriksson, R., Rosénb, E., Kullgrena, A. Priorities of pedestrian protection—A real-life study of severe injuries and car sources. Accident Analysis & Prevention 2010. 42(6):p.1672–1681.
6. Oström, M., Björnstig, U., Näslund, K., Eriksson, A. Pedal cycling fatalities in Northern Sweden. International Journal of Epidemiology, 1993; 22: p.483-488.
7. Persaud, N., Coleman, E., Zwolakowski, D., Lauwers, B., Cass, D. Nonuse of bicycle helmets and risk of fatal head injury: A proportional mortality, case-control study. CMAJ, 2012. 184(17):p.921–923.
8. WHO, 2013. Global Status Report on Road Saefty 2013 - Supporting a decade of action.
9. Di Landro, L., Sala, G., and Olivieri, D. Deformation mechanisms and energy absorption of polystyrene foams for protective helmets. Polymer Testing, 2002. 21(2):p. 217–228.
10. Miltz, J., Ramon, O. Energy absorption characteristics of polymeric foams used as cushioning materials, Polymer Engineering and Science, 1990. 30: p.129–133.
11. Thompson, R.S., Rivara F.P., and Thompson, D.C. A Case-Control Study of the Effectiveness of Bicycle Safety Helmets. New England Journal of Medicine, 1989. 320(21): p. 1361-1367.
12. Bambach, M.R., et al. The effectiveness of helmets in bicycle collisions with motor vehicles: A case–control study. Accident Analysis & Prevention, 2013. 53: p. 78-88.
13. Thompson, D.C., Rivara, F., Thompson, R. Helmets for preventing head and facial injuries in bicyclists. Cochrane Database of Systematic Reviews, *1999.* DOI: 10.1002/14651858.CD001855.
14. Attewell, R.G., Glase, K., McFadden, M. Bicycle helmet efficacy: a meta-analysis. Accident Analysis and Prevention, 2001. 33(3):p.345-52.
15. Olivier, J., Creighton, P. Bicycle injuries and helmet use: a systematic review and meta-analysis. International Journal of Epidemiology, 2017. 46(1):p.278-292.

16. Hoye, A. Bicycle helmets-To wear or not to wear? A meta-analyses of the effects of bicycle helmets on injuries. Accident Analysis and Prevention, 2018. 117:p.85–97.
17. McIntosh, A.S., Lai, A., Schilter, E. Bicycle helmets: head impact dynamics in helmeted and unhelmeted oblique impact tests. Traffic Injury Prevention, 2013. 14:p.501–508.
18. Fahlstedt, M., Halldin, P., Kleiven, S. The protective effect of a helmet in three bicycle accidents - a finite element study. Accident Analysis and Prevention, 2016. 91:p.135–143.
19. EN1078, 2012. European Standard EN1078:2012. Helmets for Pedal and for Users of Skateboards and Roller Skates.
20. CPSC, 1998. Safety Standard for Bicycle Helmets; Final Rule. Federal Register 63, 11711–11747.
21. AS/NZS 2063:2008, 2008. Australian/New Zealand Standard - Bicycle Helmets.
22. Otte, D., et al. Contribution to Final Report COST 327, University of Hannover. 1999
23. Bourdet, N., Deck, C., Serre, T., Perrin C., Llari, M., Willinger R. In-depth real-world bicycle accident reconstructions. International Journal of Crashworthiness, 2014. 19(3): p. 222-232.
24. Verschueren, P. Biomechanical Analysis of Head Injuries Related to Bicycle Accidents and a New Bicycle Helmet Concept (Ph.D. thesis). KU Leuven, 2009
25. Holborn, A.H.S. Mechanics of head injury. Lancet, 1943. 2: p.438- 441.
26. Gennarelli, T.A., Ommaya A.K., Thibault L.E. Comparison of translational and rotational head motions in experimental cerebral concussion. Proceedings of 15ThStapp Car Crash Conference, SAE P-39, 1971: p.797-803.
27. Gennarelli TA, Thibault LE. Biomechanics of acute subdural hematoma. Journal of Trauma, 1982. 22 (8): p.680–686.
28. Ommaya, A.K. Biomechanics of head injury: experimental aspects. Biomechanics of Trauma. Appleton-Century-Crofts, East Norwalk, CT; 1985:p.245–271

29. Gennarelli, T.A., et al. Diffuse axonal injury and traumatic coma in the primate. Annals of Neurology, 1982. 12(6): p. 564-574.
30. Depreitere, B., Van Lierde, C., Vander Sloten, J., Van der Perre, G., Van Audekercke, R., Plets, C., Goffin, J. Mechanics of acute subdural hematoma resulting from brigding vein rupture. Journal of Neurosurgery, 2006. 104(6): p.950– 956.
31. McElhaney, J.H., Roberts, V. L., Hilyard J. F. Properties of human tissues and components: nervous tissues. in Handbook of Human Tolerance Automobile Research Institute Inc. Tokyo, Japan, 1976. 143.
32. Kleiven, S. Evaluation of head injury criteria using an FE model validated against experiments on localized brain motion, intra-cerebral acceleration, and intra-cranial pressure. International Journal Crashworthiness, 2006. 11(1): p.65–79.
33. Deck, C., Bourdet, N., Calleguo, A., Carreira, P.R., Willinger, R. Proposal of an improved bicycle helmet standard. In International Crashworthiness Conference Proceedings, Milan, Italy, July 2012.
34. Halldin, P., Gilchrist, A., Mills, N.J. A New Oblique Impact Test for Motorcycle Helmets. International Journal of Crashworthiness, 2001. 6(1): p.53–64.
35. Mills, N.J., Gilchrist, A. Oblique Impact Testing of Bicycle Helmets. International Journal of Impact Engineering, 2008. 35(9): p.1075–1086.
36. Pang, T.Y., Thai, K.T., McIntosh, A.S., Grzebieta, R., Schilter, E., Dal Nevo, R., Rechnitzer, G. Head and Neck Responses in Oblique Motorcycle Helmet Impacts: A Novel Laboratory Test Method. International Journal of Crashworthiness, 2011. 16 (3): p.297–307.
37. CEN/TC158-WG11. CEN/TC 158 - WG11 Rotational test methods. 2014.
38. Depreitere, B., et al., Protective helmet, EP 1 776 022 B1, 2008 (Patent).
39. Vanden Bosche, K., Mosleh, Y., Depreitere, B., Vander Sloten, J., Verpoest, I., Ivens J. Anisotropic polyethersulfone foam for

bicycle helmet liners to reduce rotational acceleration during oblique impact. Proceedings of the Institution of Mechanical Engineers H, Journal of Engineering in Medicine, 2017. 231(9): p.851-861.

40. Hansen, K., et al., Angular Impact Mitigation system for bicycle helmets to reduce head acceleration and risk of traumatic brain injury. Accident Analysis & Prevention, 2013. 59: p. 109-117.
41. http://mipshelmet.com
42. http://www.lazerhelmets.com/innovations/superskin.
43. http://www.6dhelmets.com
44. Vanden Bosche, K.,Development and characterization of novelanisotropic foam for bicycle helmets, 2016, PhD Thesis, Katholieke Universiteit Leuven: Leuven.

Chapter 2
Statement of purpose

The current PhD thesis focuses on two main goals:

1. **Proposition of a new anisotropic foam concept for protective helmets:** (e.g. bicycle helmets, motorcycle helmets, ski helmets, and equestrian helmets) to aim at reducing rotational acceleration and velocity. To achieve this goal, following questions should be addressed:

- Given the complications of chemical processing of anisotropic foam and more importantly its processing into intricate geometries for some applications, e.g. helmets, what can be a smart structural solution to create the anisotropy in foam without going through the difficulties of a chemical processing foaming route?

- Can the shear and compressive properties of a foam in oblique loading be decoupled from each other without changing the overall density of the foam?

- Does anisotropy in a foam liner as a single variable (without changing other parameters such as foam density, solid foam

material or foam thickness) lead to reduction of rotational acceleration and velocity?

- When a suitable material concept is found, what parameters within the concept can be varied to optimise the performance of the foam liner?

- Can the proposed anisotropic material concept be applied to complex geometries such as bicycle helmets?

- What is the effect of helmet shell material on its impact performance when impacted by sharp and blunt projectiles?

2. Further development and utilization of relevant testing machines: To develop and evaluate new anisotropic foam concepts, specific testing set-ups namely a combined shear-compression tester and an oblique impact set-up should be further developed, verified and utilised.

2.1 Biaxial combined shear-compression tester: Further validation of the test set-up by performing experiments on isotropic EPS foams with different densities and also on PES foam with anisotropy ratio around 2.4 is performed. In addition, the following questions should be addressed:

- Does the biaxial shear-compression test set-up generate reproducible and consistent results?

- What is the effect of foam anisotropy and shear-compression load ratio on the energy absorption capability of foams in biaxial shear-compression loading?

2.2 Oblique impact set-up: In the initial evaluation of the KU Leuven oblique impact set-up it was found that there is a significant discrepancy in the helmet testing results obtained

from the KU Leuven set-up and KTH-MIPS moving sled set-up. Therefore, a systematic evaluation of different parts of the KU Leuven oblique impact set-up is performed which includes the design of a set-up for calibration of the Angular Rate Sensor (ARS sensor, incorporated in a dummy head) in its full working range. Moreover, the initial design of the KU Leuven oblique impact set-up includes a rotary band impact surface which makes it more expensive and complicated to be adopted for regular helmet evaluation in industry and hence its simplification was another pursuit in this thesis. By achieving these goals following questions should be addressed:

- What are the sources of difference in the initial design of the KU Leuven oblique impact set-up with the KTH moving sled set-up? Impact surface? Sensoring system? Data acquisition box?

- How can the ARS be calibrated in the relevant angular velocity range?

- Is there a relationship between the quasi-static combined shear-compression performance of the foam materials and their behaviour in oblique impact?

Outline of the thesis

In chapter 1 a brief introduction to the subject of the thesis accompanied with the problem statement is presented. The research goals and outline of the thesis are described in chapter 2. Chapter 3 is a literature review which summarises the most common head injuries in cycling accidents and discusses the design of conventional bicycle helmets, with polymer foams and their mechanical properties as the most common helmet liner materials. Additionally in chapter 3 a survey of proposed innovative designs or liners for bicycle helmets for rotational acceleration mitigation is presented. Chapter 4 describes the combined shear-compression test method and also investigates the effect of foam anisotropy on the foam energy absorption under

different deformation angles. Chapter 5 proposes the layered composite foam concept to introduce mechanical anisotropy in foams at ''macro level''. Further development of the KU Leuven oblique impact test set-up and its critical comparison to the KTH moving sled oblique impact set-up is described in chapter 6. In chapter 7, the composite foam concept with a column-matrix configuration is proposed for head protection applications (particularly in helmets) to reduce rotational acceleration. In this chapter, oblique impact tests together with biaxial shear-compression tests on flat composite foams are performed and compared to single layer foam of equivalent density and thickness. Moreover, in chapter 7, through a parametric study, the structure of the composite foam (with column/matrix configuration) is optimized for the best performance in reduction of head rotation during oblique impacts. Chapter 8 investigates the performance of composite foam with column/matrix configuration in reducing rotational movement of the head via a numerical approach. In this chapter, oblique impact tests on flat and helmet shape composite foams are simulated and the effect of various parameters in the structure of composite foams on their performance is investigated. Chapter 9 pursues two objectives. The first objective is to study the effect of the helmet shell material on the helmet performance when impacted by sharp and blunt projectiles. The second objective in chapter 9 is to investigate the performance of multi-layer helmet liners in linear and oblique impacts via experimental and numerical approaches. Chapter 10 presents the conclusions of this work and outlines further research.

Chapter 3
Introduction and background

The objective of this chapter is to provide the reader with a brief overview of necessary background knowledge related to different subjects discussed throughout this thesis. This chapter begins with an introduction on human head anatomy, common head injuries in cycling accidents, and a survey of the most common global head injury criteria in the field. In the next sections, conventional bicycle helmets, their structure and design considerations will be discussed. This will be followed by a brief introduction to polymer foams and their mechanical properties as the most common helmet liner materials. Then, a survey of existing helmet testing standards and subsequently various oblique impact test set-ups in different research labs will be presented. The rest of this chapter will discuss different design considerations for bicycle helmets and a survey of proposed innovative designs or liners for bicycle helmets aiming at improved head protection against rotational movement will be presented.

3.1 Anatomy of the human head

The human head consists of three main parts, the skull, the brain, and the scalp. The brain and the spinal cord are two main parts of central nervous system which controls the activities of all body parts by receiving, analysing and coordinating the information and sending commands to the muscles and the rest of the body. This makes brain the most vital organ in the body. Figure 3-1 demonstrates different layers which comprise the brain protective barriers. The outermost

layer is the scalp, covering the skull. The scalp has viscoelastic material properties and behaves as physical barrier and provides immunologic protection and thermal insulation. The thickness of the scalp is around 5-7 mm and varies depending on age and location [1-3]. Below the scalp is the periosteum, which is a loose tissue covering the skull [5]. The skull bone is a very important structure which protects the brain against head impact.

The three meninges layers just beneath the skull envelop the brain as illustrated in Figure 3-1. They consist of three layers: the dura, the arachnoid and the pia mater. The outermost layer is the dura mater which is a thick membrane adhered to the skull. The dura mater surrounds the large venous channels (superior sagittal sinus) carrying blood from the brain towards the heart. The middle of the three meninges layers is the arachnoid membrane with its spider web-like structure which gives it a cushioning effect. The pia mater is a delicate membrane which firmly adheres to the surface of the brain and follows its contours. Another important element in the head/brain anatomy is the bridging veins. The bridging veins, which bridge the space between the brain and the skull, traverse the subdural space and puncture through the dura mater to join into the superior sagittal sinus to transport the blood [6].

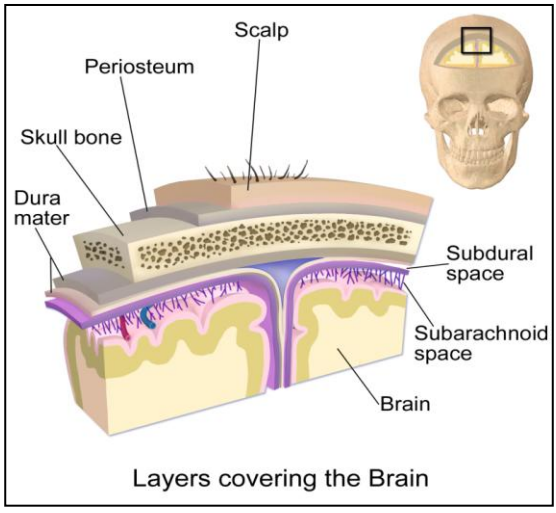

Figure 3-1: Illustration of coronal section through skull and meninges. From [4].

3.2 Head injury

Deformation of the tissues beyond a recoverable limit is the most common origin of injury. Deformation of a tissue or structure is measured based on the change in shape or strain beyond their limit [7]. In mechanics these limits are defined as yield and failure strain levels or energy-based level such as an elastic energy criterion [8-9]. The two main types of strains that can damage tissues are tensile strain and shear strain; a third type is compressive strain, which is responsible for crushing injuries. Shear strain occurs when forces oppose each other across a tissue. For example, the differential movement of the brain with respect to the accelerated skull during head impact causes a combination of shear and tensile strain at the interface between brain and skull [10-11].

Head injuries involve damage to the scalp, skull and brain. Brain injuries are categorized to focal and diffuse brain injuries. Head injuries can be induced by a contact load or an inertial load. The contact load may lead to skull fracture or focal brain injury like epidural haematoma, subdural haematoma, and contusions. Rapid contact loading can produce shock waves throughout the head. Contact force can also induce relative motion between the brain and skull leading to contusions and rupture of the bridging veins, causing subdural haematoma.

This relative motion can also cause focal injuries of the brain tissue by generating compression and shear strain in the brain due to coup and counter coup effect. Finally, a contact force can cause acceleration or deceleration of the head and the injury mechanisms, described below for the inertial loading, also apply in the same way.

Inertial forces cause the head to accelerate or decelerate. This acceleration/deceleration can be translational, rotational or a combination of both. Translational acceleration typically leads to focal brain injuries while rotational acceleration can cause both focal and diffuse brain injuries. Similar to contact loading, the acceleration of the head in a non-contact loading may result in a relative movement between the brain and the skull. This is because the brain has different inertia than the skull and will lag behind when a sudden head movement occurs. This relative movement as mentioned earlier causes strain on bridging veins leading to subdural haematoma. The brain tissue will also be strained when it comes in contact with the bony protrusions leading to brain contusions. Moreover, rotational accelerations can generate shear deformations in the brain, which

leads to diffuse brain injuries such as diffuse axonal injury by stretching the axons [6].

3.2.1 Epidemiological study of cyclists accidents and most common head injury types

In a retrospective epidemiological study conducted by Depreitere et al. [12], the main head injury types of 86 pedal cyclist patients were identified. These pedal cyclists underwent a neurosurgical intervention for head injury at the University Hospitals Leuven between January 1990 and June 2000. Depreitere et al. identified skull fracture (86%), brain contusions (73%), and acute subdural haematoma (43%) are three most frequent bicycle related head injuries. Other types of head injury as diffuse axonal injury (DAI), intraventricular bleeding, and gliding contusions were more frequent in the bicycle accidents in which a motor vehicle was involved; their mechanism of occurrence to their opinion is most likely related to the long impact pulse duration. It is noteworthy to mention that the use of a helmet was established for only 3 of all cases included in this study, an aspect definitively playing an important role on the distribution of the head injuries. In the next sections the most common injuries mentioned above will be briefly explained.

3.2.1.1 Skull fracture

A break in the cranial vault, which protects the brain from direct contact with external objects, is called a skull fracture. They occur when the head is impacted by another object with an energy or force beyond the tolerance limit of the skull. The skull fracture is a focal injury which is associated with translational acceleration of the head as a result of radial force. The direct criterion for skull fracture is considered to be the failure stress or strain of the bone material. Wood [13] measured the failure strain value around 0.5–0.7%. Moreover, it was found that the failure stress was highly dependent on the strain rate. In a study by Yoganandan et al [14], they found that the fracture force limit varied from 6kN in quasi-static tests to 12kN in impact tests. Mertz et al. [15] suggested (from their dummy experiments) a 5% risk of skull fracture if the peak linear acceleration exceeded 180g and 40% risk if the peak linear acceleration exceeded 250g. Verschuren [16] and Monea et al. [17] proposed a criterion for skull fracture based on absorbed energy. This criterion proposes energy absorption limit of

22-24 J for frontal skull fracture and 5-15 J for the thinner temporal area.

3.2.1.2 Brain contusions

A contusion is amongst most common focal brain injuries. Contusion is the bruise of the brain tissue which can be associated with many small micro-haemorrhages of ruptured blood vessels [18, 19]. Based on the impact location and the location of the contusion, they can be categorised as *coup* and *contrecoup* contusions which are illustrated in Figure 3-2. A coup contusion develops at the site of impact when the brain impacts the skull, whereas the contrecoup contusion is caused by a secondary impact when the rebounding brain impacts the opposite wall of the skull.

Shear stresses in the brain, caused by relative rotational movement of the brain-skull system, were also proposed as a cause of brain contusions by Ommaya et al. [20]. Willinger et al. [21] proposed that the relative motion between brain and skull is a function of the frequency of the applied load to the head. By investigating volunteer MRI scans and skull vibration experiments, Depreitere [18] and Van Lierde [22] proposed that contusions are caused by compressive strains in the cortex of the brain and uplifting or down-smiting of the inferior surface of the frontal and temporal lobes caused by rotation. Contusions occur more often in the frontal and temporal (side) lobes of the brain, [18].

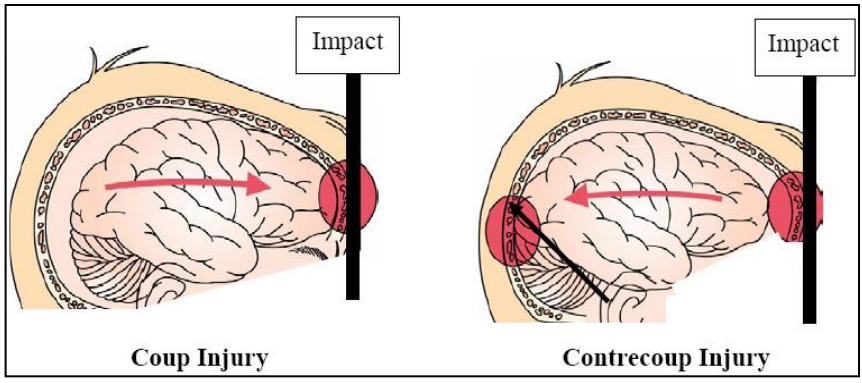

Figure 3-2: Illustration of coup (left) and contrecoup (right) contusions at the site of the impact, adopted from, [16].

3.2.1.3 Acute Subdural Haematoma

Acute subdural haematoma (ASDH) is a particular haemorrhage type characterised by large volumes of blood in the subdural region. The large volume of blood pressurises the underlying brain tissue. It is believed that ASDH has two main causes: 1) Large contusions which lead to bleeding in the subdural space, and 2) rupture of parasagittal bridging veins.

According to Gennarelli et al. [8], ASDH is related to high rate rotational acceleration of the head in the sagittal plane. Moreover, they concluded that purely translational motions cannot induce ASDH and the importance of rotational acceleration for the rupture of bridging veins has been stated by other researchers [8, 18, 24, 25]. Huang et al, [25] indicated that a sudden pure rotation of the brain causes the highest strains in the bridging veins. Monea et al. [18] proposed a limiting strain of 5mm or 25% for rupture of bridging vein. Löwenhielm et al. [26] proposed a threshold of 4500 rad/s^2 for ASDH. Figure 3-3 illustrates acute subdural haematoma (ASDH).

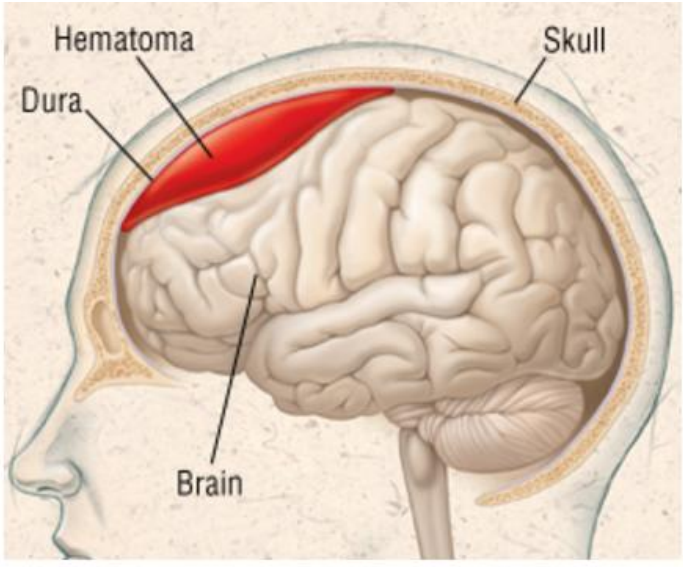

Figure 3-3: Illustration of subdural haematoma. From [27].

3.2.1.4 Diffuse axonal injury

Diffuse axonal injury (DAI) is related to disruption of axons when they are stretched due to shear strains in the brain. Axons are part of neuron cells and their duty is to transmit signals from one neuron to another or to other tissue cells. Tearing of axons as a result of stretch can initially lead to mechanical damage of the axon. It is found that there is also biochemical damage to the axons in response to the initial mechanical damage, which happens hours to days after initial injury. Diffuse axonal injury or DAI is one of the major causes of unconsciousness and persistent vegetative state [28]. In pioneering work of Strich [29], DAI was referred to as "diffuse degeneration of white matter". DAI is correlated with rotational accelerations of the brain via experiments on primates [30]. A threshold of rotational acceleration limit of 10 krad s^{-2} and a peak change in rotational velocity of 100 rad s^{-1} was proposed for DAI by Margulies and Thibault [31]. It can be concluded that rotational acceleration by creating shear forces is more responsible for traumatic brain injuries than linear acceleration, and aside from the focal traumatic injuries such as contusions and ASDH, it can also result in diffuse traumatic brain injuries such as diffuse axonal injury.

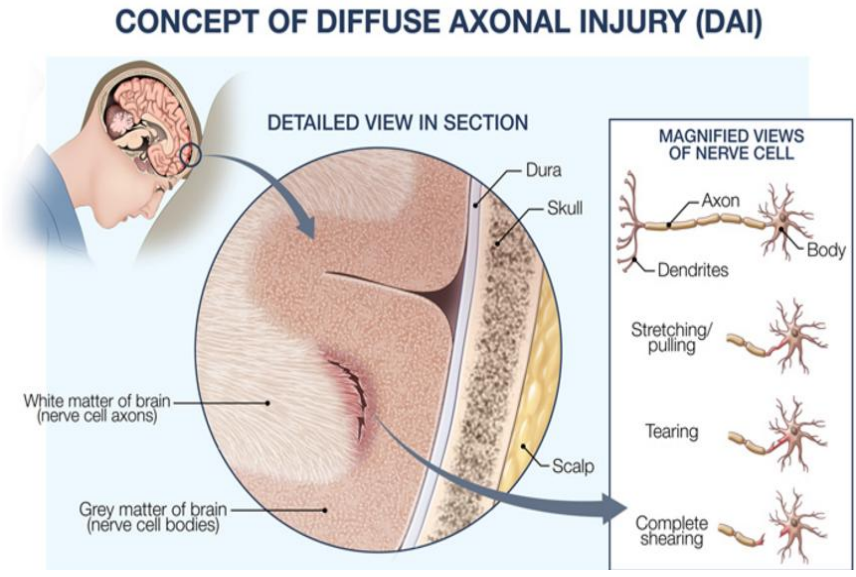

Figure 3-4: Mechanism of DAI. From [32].

3.3 Most common global injury criteria

Injury criteria are categorized into local and global injury criteria. They are used for evaluating the response of the head to impact (performed by experiments or FE modelling). In global injury criteria the global head kinematics (linear and rotational motions) are used as input into some empirical equations to provide a direct relation between the global head kinematics and the possibility of head injury occurrence. Global injury criteria are easy to use (especially for benchmark studies in industry) and they can give a good comparative evaluation in parametric studies where the protective effect of different materials is the subject of the study or the effect of different impact conditions on the head injury occurrence is under investigation. However, it should be noted that global injury criteria cannot quantitatively predict the occurrence of some serious brain injuries (e.g. ASDH and DAI). Local injury criteria are the next generation of injury assessment tools and they are still the topic of further investigation. In local injury criteria, the global head kinematics are used as input to a finite element head model to define the internal mechanical response of the head [6]. The various local head injury criteria, proposed by different studies, are pressure, von Mises stress, principal strain, strain energy, strain rate, and the product of strain and strain rate [6]. The peak values of these parameters are utilised to assess the occurrence of a particular head injury. The finite element head models provide the scientists the tool to investigate the injury mechanisms and to define the tolerance limits of the head for different head injuries. Some examples of these FE head models are KTH head model [33], Université de Strasbourg finite element head model [34], and University College Dublin brain trauma model [35].

Baeck in her PhD showed that the response of different head models to the same loading condition is different [6]. This results in different thresholds for local injury criteria.

The evaluation of impact results, throughout this dissertation, is based on global injury criteria and in the following section the most common global injury criteria are described.

3.3.1 Head Injury Criterion (HIC)

The Head Impact Criterion (HIC) introduced by American National Highway Transportation Safety Administration (NHTSA) is the most common tolerance criterion in the field. HIC takes only the resultant linear acceleration, $a(t)$ into account and integrates the resultant linear

acceleration over the pulse duration, *t*, to the power 2.5. The dimensional unit of *a(t)* is in g's meaning *a(t)* in m/s^2 divided by 9.81 m/s^2 and *t* is in seconds [36].

$$HIC_{15} = \left\{ \left({}^{1}/_{(t_2 - t_1)} \int_{t_1}^{t_2} a(t) \right)^{2.5} (t_2 - t_1) \right\}_{max} \qquad (3.1)$$

In the HIC formula, which is given by equation 3.1, the time interval t_2-t_1 should be chosen in a way that the solution of the equation is maximized. The initial proposition of time interval was 36 ms (HIC_{36}). Later on the time interval of 15 ms (HIC_{15}) was proposed by Eppinger et al. [37]. A tolerance limit of 1000 for HIC_{36} and 700 for HIC_{15} were suggested for a 50th percentile male dummy head [37].

3.3.2 Rotational Injury Criterion (RIC)

In order to evaluate the effect of head rotation, Rotational Injury Criterion (RIC) was proposed in the same form as HIC and is described by equation 3.2, in which *α(t)* stands for resultant rotational acceleration in rad/s^2 and *t* is in seconds, [38].

$$\mathrm{RIC} = \left\{ \left({}^{1}/_{(t_2 - t_1)} \int_{t_1}^{t_2} \alpha(t)/20 \right)^{2.5} (t_2 - t_1) \right\}_{max} \qquad (3.2)$$

There are currently no limiting values suggested for RIC, however, the RIC values can be calculated and used for benchmarking studies on different helmet liner materials.

3.3.3 Generalised Acceleration Model for Brain Injury Threshold (GAMBIT)

HIC and RIC criteria consider the translational and rotational behaviours separately. However, in real life impact, the head/brain undergoes multi-axial loading and hence both linear (translational) and rotational accelerations are simultaneously present. Therefore, both rotation and translation are needed for accurate prediction or modelling of brain injury. For this, Generalized Acceleration Model for Brain Injury Threshold (GAMBIT), is proposed which incorporates

both linear and rotational accelerations [39]. This criterion described by equation 3.3 incorporates both peak linear and rotational acceleration in the evaluation of head injury probability. In equation 3.3, a_{max} and α_{max} stand for the maximum linear and rotational acceleration. These values are derived from impact simulations and are defined as a_{cr}=250 g, and α_{cr}=25000 rad/s^2, [39].

$$GAMBIT = \left\{ \left({}^{a_{max}}/_{a_{cr}} \right)^2 + \left({}^{\alpha_{max}}/_{\alpha_{cr}} \right)^2 \right\}^{\frac{1}{2}} \quad (3.3)$$

3.3.4 Head Impact Power (HIP)

The lack of pulse duration in the equation 3.3 is a drawback to GAMBIT model. Another suggestion to combine both linear and rotational accelerations into a criterion and also take impact pulse duration into account, Newman et al. [40] proposed the head impact power (HIP) which is described in equation 3.4. HIP is an empirical expression and suggests that the rate of change of linear and rotational kinetic energy (power) can be a suitable biomechanical assessment tool for brain injury.

$$\begin{aligned} HIP = {} & ma_x \int a_x(t)dt + ma_y \int a_y(t)dt + ma_z \int a_z(t)dt \\ & + I_{xx}\alpha_x \int \alpha_x(t)dt + I_{yy}\alpha_y \int \alpha_y(t)dt + I_{zz}\alpha_z \int \alpha_z(t)dt \end{aligned} \quad (3.4)$$

Where m is the mass of the dummy head and helmet (in kg), a is linear acceleration (in m/s^2), I stands for moment of inertia of the head (in kg.m^2) and α is rotational acceleration (in rad/s^2). Though the HIP value can be determined at any time during an impact, for simplicity in impact evaluation, HIP is not reported as a curve, but as a maximum value, or HIP_{max}. To calculate the HIP_{max} values in this thesis, the physical properties of the dummy head were used. The Hybrid III 50th percentile male dummy head which is used in oblique impact tests in this thesis has a mass of 4.54 kg. The moment of inertia around the y-axis (ear to ear axis), I_{yy}, is 0.0234 kg·m^2. I_{xx} and I_{zz} moments of inertia are not explicitly defined by the Hybrid III dummy head data sheet, so values typical for the human head (on which the Hybrid III dummy

head was designed), I_{xx} = 0.016 kg·m^2 and I_{zz} = 0.022 kg·m^2, are used to calculate HIP_{max} values in chapter 7 of this thesis, [40,41].

3.3.5 Brain Injury Criterion (BRIC)

It is proposed by Kleiven [42] that the rotational velocity can better correlate to mild traumatic brain injuries than angular acceleration. In an attempt to consider rotational velocity also in an injury criterion, Takhounts et al. [43] proposed BRain Injury Criterion (BRIC). BRIC is defined by equation 3.5 where ω_{max} and α_{max} are the maximum rotational (angular) velocity and acceleration for each test, respectively. The critical values derived for the Hybrid III dummy were ω_{cr} = 46.41 rad/s, and α_{cr} = 39,774.87 rad/s^2.

$$BRIC = \omega_{max} / \omega_{cr} + \alpha_{max}/\alpha_{cr} \quad (3.5)$$

3.4 Bicycle helmets

Cyclists are one of the most vulnerable road users and helmets are the only means available in the market to protect them from head injuries. Bicycle helmets are designed to absorb the majority of the impact energy whilst reducing the forces/accelerations transmitted to the head during an impact. Bicycle helmet should fulfil following requirements:

- To absorb the impact energy.
- To reduce the linear acceleration transferred to the head below a critical acceleration (determined by helmet standards).
- To reduce rotational acceleration (however, not yet included as evaluation parameter in helmet standards).
- To offer good coverage of the head without hindering the vision.
- To avoid sharp object penetration during impact.
- To remain fixed to the head during impact.
- To be mechanically and thermally easy to wear by being light, small and well ventilated.
- To have a good aerodynamic shape and to be fashionable

Earlier helmets were made of pith which is a crushable natural material and breaks after a single impact. Around the turn of the 20th century racing cyclists started using helmets made of strips of leather-covered paddings. These rudimentary helmets were called hairnets and during 1970's, the interior padding of the hairnets were made of foams [44]. An example of a hairnet is shown in Figure 3-5a. Although hairnets did not provide much impact protection, they did prevent some abrasion to the scalp, face, and ears. Through the years the helmet design evolved based on the materials available in the market and the knowledge acquired through extensive research. Nowadays, a typical bicycle helmet consists of several main features as shown in Figure 3-5b-c:

- Outer shell
- Liner
- Comfort padding
- Retention and fixation system
- Ventilation holes

In the following sections the function of each part of the helmet will be briefly explained

Figure 3-5: (a) Example of a hairnet, from [44]; (b) a conventional helmet and its different features such as plastic shell, ventilation holes, and chin strap, from [45]; (c) interior of a commercial helmet from SportAtlas containing comfort puddings, from [46].

3.4.1 Function of helmet shell

One of the functions of the smooth outer shell in a helmet is to distribute the impact energy over a larger area and avoiding concentrated loads from puncturing the helmet [47]. Another function of the smooth shell is to reduce the sliding frictional forces between the helmet and impacted surface. A lower friction between the helmet and the impact surface allows for easier sliding and thus reduces the tangential forces acting on the head during impact and thereby reduce the rotation of the head. Moreover, high friction between the helmet and the road surface can transfer high forces to the neck.

In commercial bicycle helmets, a very thin shell of thermoplastic material such as polyvinyl chloride (PVC), polycarbonate (PC), acrylonitrile-butadiene-styrene copolymer (ABS) or polymer composites are used [16, 48]. Recently, commercial bicycle helmets are produced using an in-mould production process in which the shell is moulded into the liner material. In older helmet versions, the shell was glued to the helmets. In those helmets, aging of the glue could cause the risk of contact loss between the shell and liner during the impact which could lead to high friction contact between the liner and the road surface.

In order to investigate the effect of a helmet shell in the reduction of friction forces and therefore rotational acceleration transmitted to the head, Hodgson et al. [49] proposed the Wayne State Skid Test (see Figure 3-6).

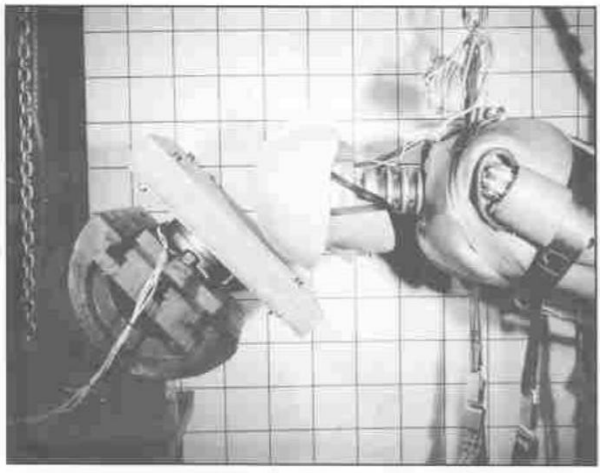

Figure 3-6: Wayne State Skid Test setup [49].

In their study, helmeted hybrid III dummy head was dropped on an angled anvil. The surface of angled anvil was a rough concrete slab with small pebbles embedded into it. To measure both normal and transverse forces transferred to the angled anvil, loadcells were used. A triaxial accelerometer was placed in the centre of mass of the head in combination with a linear accelerometer, placed at some distance from the triaxial accelerometer, to measure the ear-to-ear rotational acceleration.
They tested helmets with hard shell, micro-shell, no-shell with attached external rubber straps and no shell. They concluded that the helmets with shell were found to be safer than helmets without the shell by further reducing rotational acceleration [49].

3.4.2 Function of ventilation holes

The ventilation holes ensure a good helmet-head climate by letting fresh air ducted into the helmet and humidity vented out. It was proposed by De Bruyne [50] that strategic placing of the ventilation holes (one inlet at the front, three on the top, and a wide vent at the rear) leads to better temperature control.

3.4.3 Function of retention system and fixation System

A good retention and fixation system (chin straps) ensure that the helmet is placed firmly on the head and stays on the head of the rider during impact while avoiding strangulation.

3.4.4 Function of comfort Padding

In order to ensure a good fit of the helmet on the head, the comfort padding which consists of a soft and flexible foam (e.g. low density polyurethane foam) covered with a skin-friendly fabric is used. The comfort pads do not significantly contribute to the energy absorption capacity of the helmet, but it is hypothesized that they could be beneficial in reducing the rotational acceleration transferred to the head by lowering the sliding friction between the helmet and the head resembling the effect of human skin and fat tissue surrounding the skull (provided they are not completely crushed by the compressive stress) [16, 51]. It is claimed that the placement of the padding does influence the air flow underneath the helmet and helps with thermal comfort of the cyclist [16, 52, 53].

3.4.5 Function of helmet Liner

The liner protects the cyclist's head by absorbing the impact energy whilst reducing the impact forces transferred to the head below injurious level [48]. The liner located on the inside of the shell is made of lightweight and highly impact-absorbing materials often foams particularly EPS expanded polystyrene (EPS) or expanded polyethylene (EPP). There are also other liners proposed in the market or in literature such as environmentally friendly expanded poly-lactic acid (E-PLA) [54], polyurethane (PU) honeycomb [55], corrugated waterproof cardboard honeycomb [56], bundled hollow Koroyd™ tubular polymer straws which are welded together like a honeycomb [57], air bag helmets [58], and semi-spherical cone liner design [59]. The helmets made of those suggested liners are claimed to perform better than standard helmet in linear impact. However, this conclusion is based on limited impact results and some of them e.g. helmets made with paper honeycomb are not tested in all directions, nor under all required test conditions (e.g. wet). Moreover, the claimed superiority of these innovative liners is not tested in oblique impact which is the most common accident situation. Still it is believed that polymer foam helmet liners can compete with other designs in the market due to its high impact absorption capacity, low cost, and easy processing. In this thesis the focus is on the proposition of new anisotropic foam concepts for protective helmets (especially bicycle helmets) to provide additional functionality of reducing rotational accelerations resulting in better head protection in oblique impact. In the next sections the properties of foams in terms of their structure, mechanical properties and their unique energy absorption capability will be discussed.

3.5 Polymer foams

One of the most common materials to be used as head liner in a helmet is foam and more specifically polymer foams e.g. expanded polystyrene (EPS) [60]. The high energy absorption capability of polymer foams together with their light weight makes them an excellent choice for head and body protection applications. Foams are categorised as cellular materials which are interconnected networks of solid struts and planes forming edges and faces of cells [61]. In polymer foams, the process of expansion of a nonporous polymer into a porous one is realised by chemical or physical means. In order to produce polymer foams, cells must nucleate and grow within the polymeric material. Foams are either open cell, meaning that they have solid only at the

edges of the polyhedral cell, and/or closed cell, containing solid membranes over the faces of polyhedral cells [61].

3.5.1 Structure of polymer foams

Polymer foam is a three dimensional network of interconnected cells as shown in Figure 3-7 left. Polymer foam can be differentiated from a solid material with isolated pores (Figure 3-7 right) below a theoretical relative density of $R_\rho \approx 0.3$.

The relative density of a foam, R_ρ, is defined as the density of polymer foam, ρ_*, divided by the density of the solid polymer, ρ_s, and is presented in equation 3.6.

$$R_\rho = \frac{\rho_*}{\rho_s} \qquad (3.6)$$

The value of 0.3 is derived from the volume fraction of polymer in a foam in which the foam growth has reached to the extent that the cells (in the shape of spheres) impinge each other in a centred cubic arrangement [61]. A sphere is not a space filling structure. Impinging spherical cells will result in deforming the spherical cellular shape and will develop into space filling shapes which equilibrate as shapes with minimized surface area and energy.

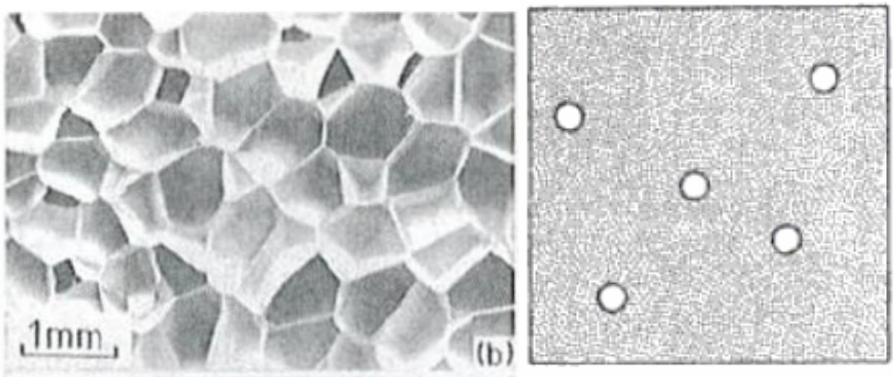

Figure 3-7: Closed cell polyethylene foam (left); A solid material with isolated pores, R_ρ > 0.3 (right), adopted from [61].

For a long time, it was thought that the idealised space-filling cell which minimizes surface area per unit volume was Kelvin's tetrakaidecahedron with slightly curved faces shown in Figure 3-8 [62]. Later on, with the aid of computer software for minimization of surface area, Weaire and Phelan [63] have identified a unit cell of even lower surface area per unit volume (Figure 3-8b). The Kelvin structure consists of tetra(kai)decahedra which is a truncated octahedral with 8 hexagonal faces and 6 square faces in which the faces are slightly curved [61]. The Weaire-Phelan structure contains eight cells in its repeat unit: two irregular dodecahedra with 12 pentagonal faces, and six tetradecahedra [61]. It should be noted that the efficient space-filling is not the only factor influencing cell shape. Other factors such as polymer viscosity, external forces due to gravity and mould geometry, and the polymer solidification kinetics are other factors influencing the cell shape. All these parameters hinder the foam cells from adopting idealised shapes. In addition, in reality, a range of cell sizes are present. This is due to nucleation and growth phenomena and the fact that the cells are not nucleated at the same time [60].

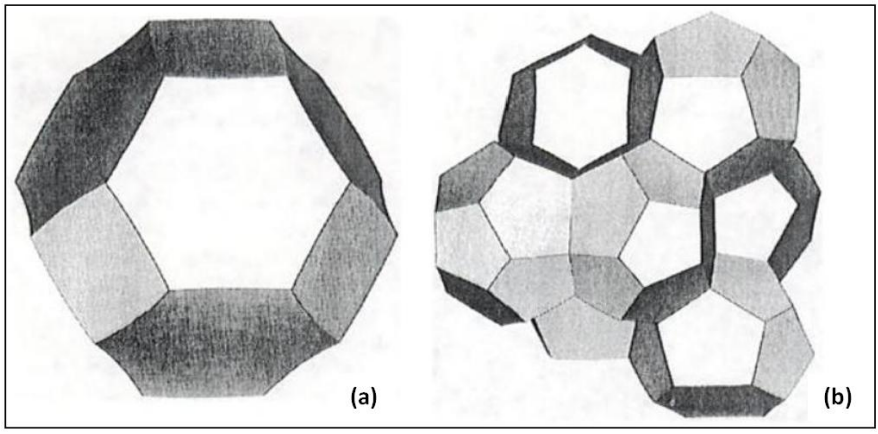

Figure 3-8: (a) Illustration of Kelvin's tetrakaidecahedral unit cell; (b) Weaire and Phelan's unit cell, consisting of six 14-sided polyhedra and two 12-sided polyhedral, [61].

3.5.2 Mechanical properties of polymeric foams

The macroscopic mechanical behaviour of foams is determined by interplay between the intrinsic mechanical properties of the solid polymer which the cells are made of and the microstructure of the cells

(shape anisotropy degree and percentage of closed/open cells), and the foam relative density (R_ρ).
In the following sections a brief overview of mechanical response of polymer foams in compression, and impact loadings will be briefly explained. For more information readers are referred to the book of Ashby and Gibson [61].

3.5.2.1 Compression behaviour

Figure 3-9 shows schematic compressive stress-strain curves for elastomeric (Figure 3-9 top left), elastic-plastic (Figure 3-9 top right), and brittle foams (Figure 3-9 middle). It can be observed that the compressive stress-strain curves of foams irrespective of their material type consist of three main successive regions: 1) linear elastic region, 2) plateau region and 3) densification region.
At small strains, usually less than 5%, the behaviour of foam is linear elastic, with a slope equal to the Young's modulus of the foam (E). Dominant deformation mechanism in this region is strut bending as shown in Figure 3-9 (bottom right). As the load increases, the foam cells begin to collapse by elastic buckling, plastic yielding, or brittle crushing, depending on the mechanical properties of the solid material that the cell walls are comprised of. Collapse progresses at approximately constant load in plateau region, until the opposing walls in the cells touch and densification starts.
In the densification region the stress increases sharply. In Figure 3-9, $\sigma_{el,}$ σ_{pl} , and σ_{cr} *represent* elastic buckling stress, plastic collapse stress, and brittle crushing strength, respectively for three different classes of polymeric foams. The plateau stress, can be different from the stress at the initial deviation from elasticity (σ_{el} , σ_{pl}, and σ_{cr}). For plastic and brittle foams, σ^* can often be less than σ_{pl} or σ_{cr}, due to the damage in one layer of deformed cells after yielding or crushing. The plateau stress of closed foams can be higher than the elastic stress limit (yield stress), due to the effect of enclosed gas compression and contribution of the cell walls. For open cell foams, plateau region is generally a horizontal line as the cells throughout the material collapse by the mechanism determined by the matrix polymer.

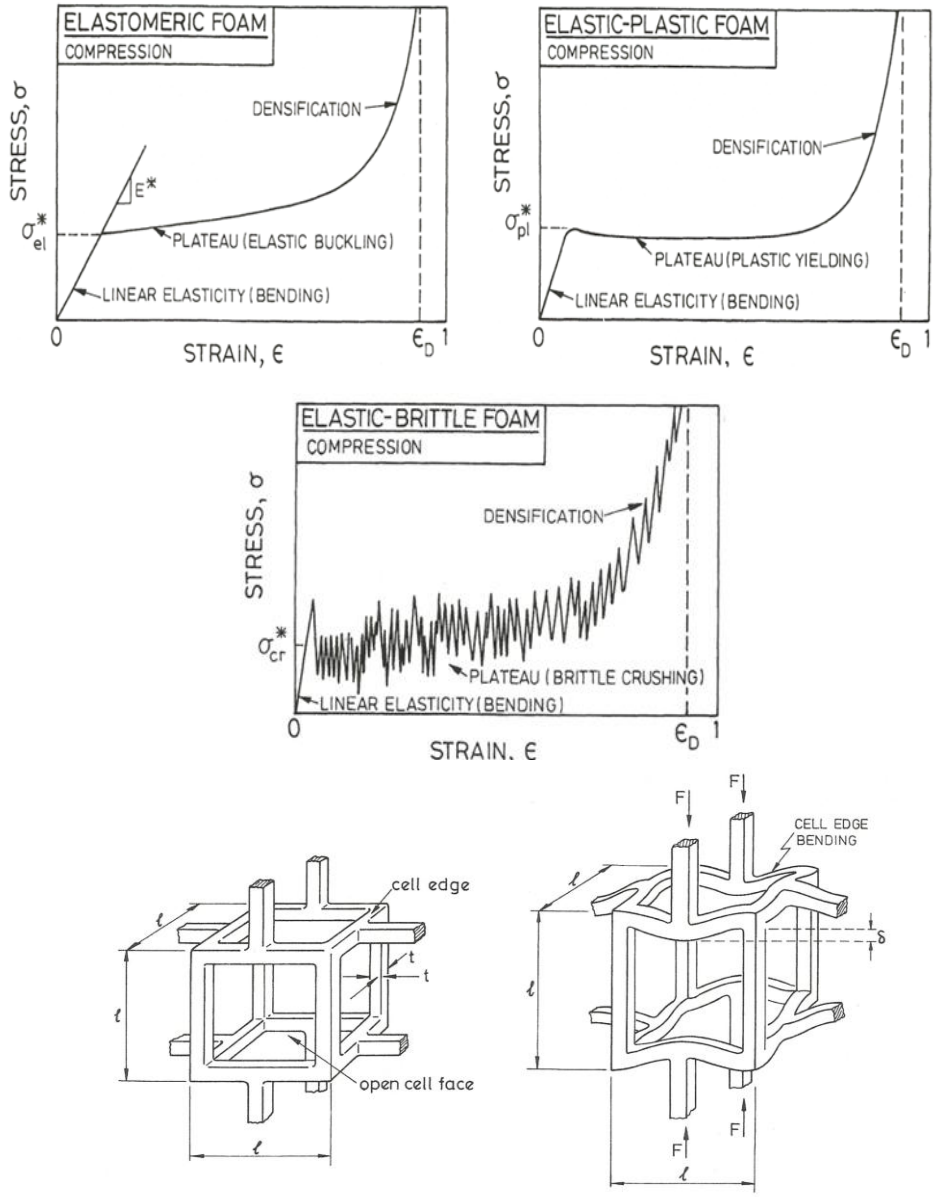

Figure 3-9: Compressive stress-strain curves of elastomeric foam (top left); elastic-plastic foam (top right) and elastic-brittle foam (middle); simplified model showing an open foam cell and elastic bending of its cell struts (bottom). From [61].

3.5.2.1.1 Effect of density on compression behaviour of foams

The effect of foam density on compressive stress–strain responses of foams is shown in Figure 3-10. As observed, there is a direct dependency of compressive behaviour of foams on foam density. The elastic modulus, collapse (yield) stress, and plateau stress levels increase with increasing foam density whereas the length of plateau region and the strain at the start of densification decreases with an increase in foam density. The relationship between relative density, ρ^*/ρ_s, and foam elastic modulus, E^*, for open cell foams is expressed by equation 3.7 and is derived based on the simplified cubic cell model shown in Figure 3-9. For more detail about the derivation of such expression, readers are referred to [61]. In equation 3.7, E_s and C stand for the elastic modulus of solid polymer and the proportionality constant, respectively. The value of C (the proportionality constant) is determined by experimental data to be 1 for isotropic open-cell foams [61].

$$E^* = CE_s\left(\frac{\rho^*}{\rho_s}\right)^2 \qquad (3.7)$$

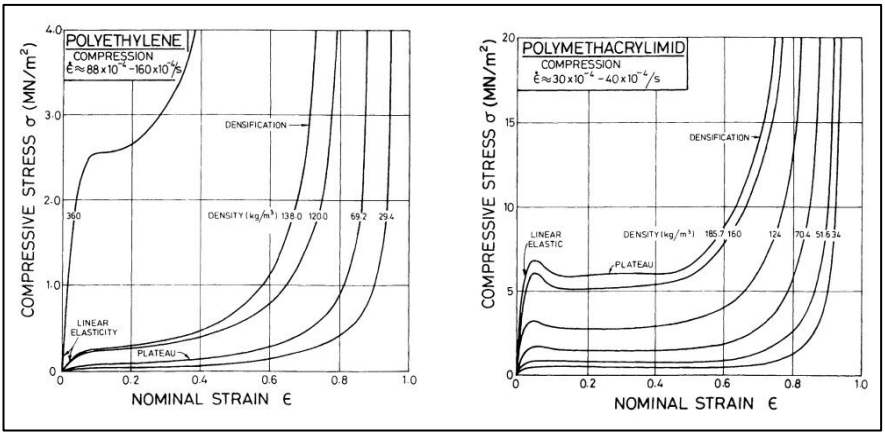

Figure 3-10: Compressive stress-strain curves of foams with increasing the density for a fixed strain rate: (Left) polyethylene foam; (Right) polymethacrylimid. From [61].

An expression for shear modulus of the foam, G^*, can be derived in a similar way and is described by equation 3.8. For an open-cell, isotropic foam experimental data suggests a value of 3/8 for C, [61].

$$G^*=CE_s(\frac{\rho^*}{\rho_s})^2 \quad (3.8)$$

In a similar derivation to that for the elastic modulus, Gibson and Ashby [61] give the derivation for elastic collapse, σ_{el}, also driven by beam bending:

$$\sigma_{el}=CE_sR_\rho^2 \quad (3.9)$$

In this case, the empirical value of C for open-cell isotropic foams is 0.05.
In the case of plastic collapse strength (σ_{pl}), equation 3.10 is found. $\sigma_{s,y}$ stands for solid polymer yielding stress.

$$\sigma_{pl} = C\sigma_{s,y}R_\rho^{3/2} \quad (3.10)$$

In this case, the empirical data suggests a value of 0.3 for C. For brittle foams, same equation as 3.10 holds but the proportionality constant is determined to be 0.65.
In closed-cell foams, in the plateau region, two other parameters contribute to the mechanical response of the closed cell foam (mainly elastic and elasto-plastic foams). One of these contributions comes from the cell walls (they can laterally stretch), which help to carry the compressive load during larger deformations. The second contribution is related to the gas in the cells which increases in pressure during the compression based on Boyle's law. The gas pressure contribution can be seen in the plateau region with a positive gradient contrary to a horizontal plateau for the open cell polymer foams. The contribution of the gas pressure (σ^g) to the overall stress within the foam is described by equation 3.11.

$$\sigma^g = p_0\left(\frac{\varepsilon}{1-\varepsilon-R_\rho}\right) \quad (3.11)$$

Thus in closed cell polymer foams the plateau stress (σ*) can be regarded as a variable and can expressed by equation 3.12 in which σ_{el} is the elastic buckling (described by equation 3.9), the second term is the contribution of the gas pressure due to Boyle's law for isothermal compression and the third term is related to the load-carrying capacity of the cell wall (P_{wall}). p_0 is the initial gas pressure within the cells.

$$\sigma^* = \sigma_{el} + p_0\left(\frac{\varepsilon}{1-\varepsilon-R_\rho}\right) + P_{wall} \quad (3.12)$$

In shear, the contribution due to gas pressure is not present because pure shear is not expected to cause any change in volume of the material.
The densification strain, ε_D, is determined experimentally by equation 3.13 where *k* is an empirical constant. It can be inferred that the foams with lower relative density have a longer plateau region [61].

$$\varepsilon_D = 1 - kR_\rho \quad (3.13)$$

3.5.2.1.2 Effect of temperature and strain rate

Most foams are used in ambient temperatures (temperature range between -20° C and 40°C) but there are other applications such as thermal insulators or heat exchangers in which the temperature range is much wider. The range of strain-rates depends on the application and can vary from $1s^{-1}$ to strain rates as high as 10^5 s^{-1} (e.g. in high performance packaging or crash protection) [61]. This thesis focuses on foams used for protective helmets (e.g. bicycle helmet) in which the foams can undergo strain rates in the range of 200-350 s^{-1} during impacts and thus the strain rate dependence of foams can affect impact forces transferred to the cyclist's head. There are two separate

phenomena that contribute to the temperature and strain rate dependency of the foams. The first contribution derives from the solid of which the foam is made. Here the focus is mainly on polymer foams. Polymeric materials generally demonstrate viscoelastic behaviour and near or above their glass transition temperature, they show temperature and strain rate dependency.
The second contribution is related to the fluid which fills the foam cells. When the foam is deformed, the pore fluid (often gas in polymeric foam) is either deformed or forced to flow out (in closed cell foam, through perforated cell walls). In closed cell foams, the compressibility of a gas depends on the temperature and hence a new temperature-dependence is introduced by its presence. In open-cell foams, the pore fluid is expelled out the foam as it deforms and the work done against the viscosity of the fluid introduces a new strain-rate dependence. For polymers well below their glass temperatures, T_g, the compressive modulus varies almost linearly with temperature, and its rate-dependence is negligible. The relationship between the elastic modulus, the temperature, and the strain rate is described by equation 3.14 in which α_m is a constant and E_s^0 stands for the modulus of solid polymer at 0°K.

$$E_s = E_s^0(1 - \alpha_m \frac{T}{T_g}) \tag{3.14}$$

The plastic collapse as a function of the temperature and the strain rate is described in equation 3.15 in which $(\sigma_{pl}^*)^0$ is the plastic collapse stress of the foam at 0°K, and A and $\dot{\varepsilon}_0$ are material properties. A linear decrease in the yield strength by increasing the temperature and a logarithmic increase in the yield strength with increase in $\dot{\varepsilon}$ can be inferred from equation 3.15.

$$\sigma_{pl}^* = (\sigma_{pl}^*)^0 \ (1 - \frac{AT}{T_g} \ln \frac{\dot{\varepsilon}_0}{\dot{\varepsilon}}) \tag{3.15}$$

As mentioned earlier, the strain rate dependency in the foams can originate from the compression of the fluid in the foam cells. In open cell polymer foams, compression forces the viscous air to flow out the

interconnected cells as shown in Figure 3-11. The cell size strongly influences air-flow properties. The faster the foam is deformed, the more work is done. This dependence can be described by equation 3.16 in which C_5 is a proportionality constant of order unity, L is the base length of the foam and l is the edge cell length. The contribution of air flow to the strength σ* of a foam is therefore proportional to the strain rate and the viscosity of air (μ) and to the inverse of the cell size to the power two.

$$\sigma_g^* = \frac{C_5 \mu \dot{\varepsilon}}{1-\varepsilon} \left(\frac{L}{l}\right)^2 \qquad (3.16)$$

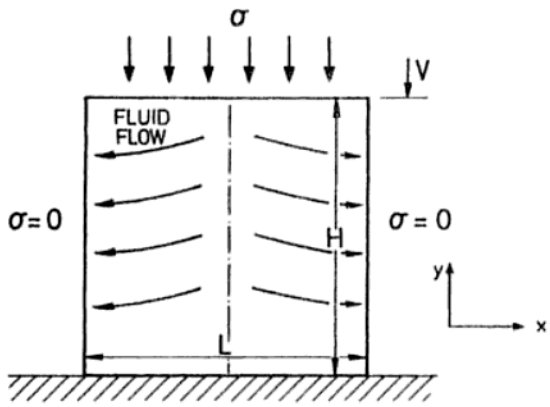

Figure 3-11: The compression of fluid- filled, open-cell foam with a pressure gradient of order σ/L. From [61].

3.5.2.2 Impact behaviour of polymer foams

One of the key characteristics of polymer foams is their excellent energy absorption, which together with their light weight makes them an excellent choice in areas such as industrial packaging or head and body protection. Due to the cushioning effect of the foams, the kinetic energy of the impact converts to other types of energy e.g. heat via plasticity, viscosity, viscoelasticity or friction, and this must be done whilst keeping the peak force (and thus the deceleration or

acceleration) on the packaged object, the head or the body part below a certain threshold [61]. The direction of the impact is often unpredictable; hence the package or body wear must offer multi-directional impact energy absorption.
In elastomeric foams (used in cushions and in soft paddings) much of the external work stored during loading is released upon unloading; however, due to damping or hysteresis, not all stored work is recovered. In plastic and brittle foams, the work done in the plateau region is completely dissipated as plastic work. These foams are effective in high performance applications such as helmets (the focus of this thesis). This is because they give large and controlled energy absorption with no rebound. The rebound during impact can be as damaging as initial impact.

The deformation of the fluid within the cells is another factor which affects the impact behaviour of the foams. In open-cell foams, the pore fluid is expelled whilst deforming. This causes viscous dissipation and it is strongly dependent on strain-rate. In closed-cell foams, the cell fluid is compressed as the foam deforms, storing energy which is largely recovered when the foam is unloaded (particularly if the deformation is still within linear elastic region). Unlike viscose dissipation, this storage mechanism is almost independent of the strain-rate [61].

Figure 3-12 (left) compares the energy-absorbing capacity of the foam to the solid material of which it is made of during compression loading. The area under the stress-strain curve indicates the work done per unit volume of the foam material at a given strain or in other words the energy stored or dissipated in the material at a specific strain. As observed, for the same stress level, *the energy absorption per unit volume* (w) of the foam is significantly higher. The stress is proportional to the force and hence acceleration/deceleration transferred to the packaged object or body part (head in helmet application). In the linear elastic region of the foams, very little energy is absorbed whilst most energy is absorbed during the long plateau region of the stress-strain curve at near-constant load. Therefore, the plateau region is the most important region in applications such as packaging or helmets. For a given amount of energy to be absorbed, there is also an optimum foam density in which the stress is minimised as illustrated in Figure 3-12 (right).

As shown, for too low density foams (ρ_3), the energy may not be completely absorbed in the plateau region and foam ''bottoms out'' generating high peak stresses due to densification. Too high density foam (ρ_1) generates high peak stress for the given energy absorption due to the higher plateau stress. Between these two extremes, there is an optimum density (ρ_2) which absorbs the same energy whilst keeping the stress levels lower [61].

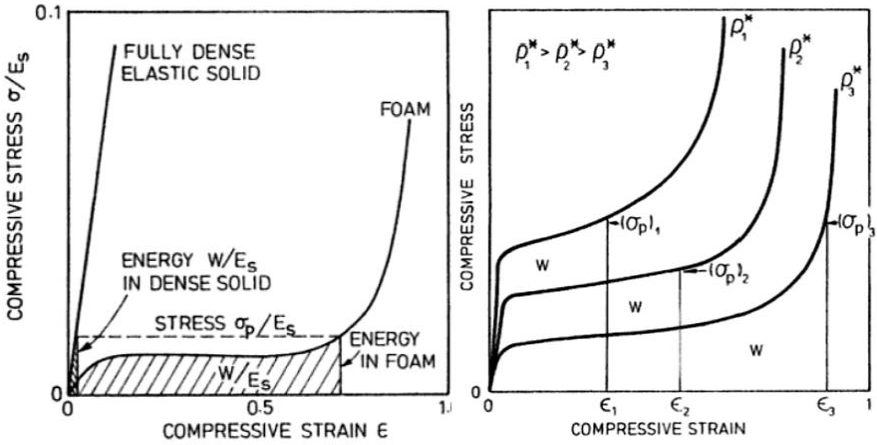

Figure 3-12: (left) Comparison between dense solid and foam for a given absorbed energy per volume, w during compression loading; (right) optimization of the foam density for the lowest maximum stress for a given energy absorbed per unit volume, w. From [61].

3.5.2.2.1 Foam energy absorption diagrams

Energy-absorption diagrams, proposed by Maiti et al. [64], offer a method of optimizing the foam selection. To plot energy diagrams, as shown in Figure 3-13a-c, a range of densities for a given foam is tested in compression at a fixed strain-rate and temperature. The stress-strain curves are integrated up to a stress σ_p which is the maximum permitted stress. This area is the energy absorbed per unit volume, *w.* Both *w* and σ_p values are normalised by the modulus of the solid, E_s, allowing foams with different solid materials to be plotted together. The normalised *w* value is plotted as a function of normalised σ_p, for each curve as shown in Figure 3-13b. Plotting these curves show that different foam densities will produce "shoulders" that lie along a line, called an envelope which is shown in Figure 3-13b. Beyond this

shoulder, the peak stress sharply increases whilst increase in energy absorption capabilities is not significant thanks to the foam entering the densification region. In Figure 3-13c, the envelope is replotted on the same axes and marked with density points and the same procedure is repeated for other strain rates. Finally, the density points are connected to give a collection of intersecting contours. From these curves it can be learned that for a given relative density, a higher strain rate results in more energy absorption at the expense of a higher normalized peak stress.

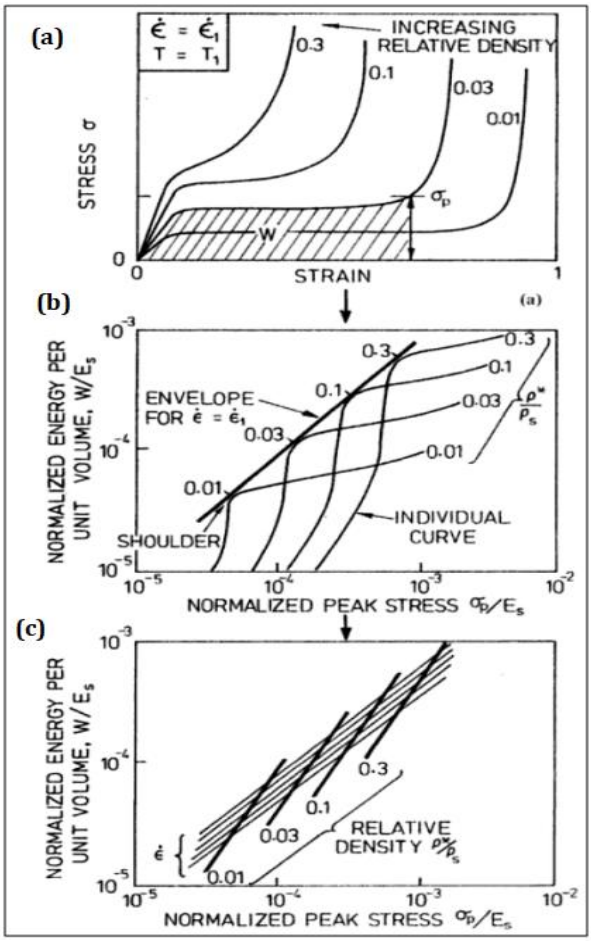

Figure 3-13: Procedure of plotting energy-absorption diagrams. From [61].

3.5.3 Anisotropy in foams

Most foams are anisotropic. Anisotropy in foams can arise from material anisotropy or structural anisotropy. The material anisotropy in foams is related to the properties of the solid material that the foam is made of e.g. in wood (solid material of wood has a fibrous composite nature). The other type of anisotropy in foams is structural anisotropy meaning direction-dependent foam properties directly attributable to the shape of the cells. This means that the foam cells are elongated in a certain direction and the properties in the direction of elongation of the cells are different than other directions. In polymer foams the geometrical cell anisotropy is induced during the foaming process, the reason being that foams undergo external forces (e.g. gravity, constraint forces of mould, and pressure gradients) during their production process which cause the foam cells to be elongated in a certain direction [61]. Figure 3-14 illustrates a simplified axisymmetric open cell exemplifying a typical elongated cell in anisotropic foam. The elongation direction (X_3) is also called the rise direction. The geometrical anisotropy of the foam cells is defined as the ratio of the largest cell dimension (h) to the smallest (l). This ratio, ***R=h/l,*** is called shape anisotropy ratio [65].

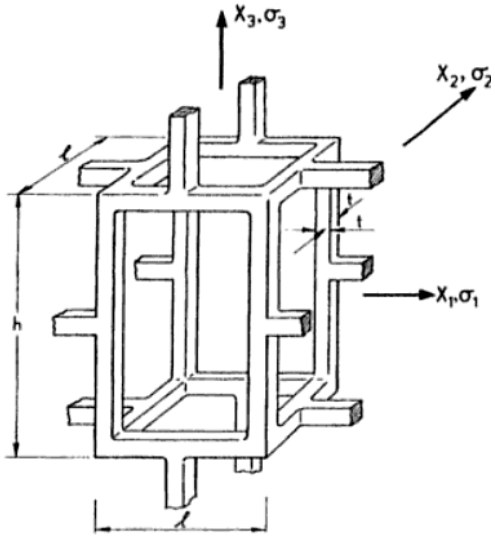

Figure 3-14: An axisymmetric unit cell with anisotropy ratio of R=h/l. From [61].

Figure 3-15 shows the load-deflection curves of anisotropic elastic foam (left) and anisotropic plastic foam (right) when compressed in three orthogonal directions of X_1, X_2, and X_3. As observed, elongation of the cell in X_3 direction leads to different mechanical properties in this direction than in the X_1 and X_2 directions whilst mechanical properties in X_1 and X_2 directions (orthogonal to the rise direction, X_3) are nearly identical. The overall behaviour can be described as transversely isotropic. As observed in Figure 3-15 (right) the mechanical anisotropy of the plastic foam is much more pronounced than for the elastic foam.
Gibson and Ashby [61] modelled the effect of shape anisotropy on based on simplified cell geometry shown in Figure 3-14 and found expressions which relate the shape anisotropy to mechanical properties such as Young's modulus and plastic yield strength which will be briefly mentioned here. Young's modulus and plastic yield strength, and elastic strength ratios as a function of cell shape anisotropy ratio, R, in transversely isotropic foams are described by equations 3.17-3.19.

$$\frac{E_3^*}{E_1^*} = \frac{2R^2}{1+(1/R)^3} \tag{3.17}$$

$$\frac{\sigma_{pl,3}^*}{\sigma_{pl,1}^*} = \frac{2R}{1+\frac{1}{R}} \tag{3.18}$$

According to equation 3.18, in plastic foams, the cells are stronger in the rise direction, although the effect of anisotropy on plastic strength is not as large as in stiffness. The foam cells with the shape anisotropy of 2 have 8 times larger stiffness and 2.6 times larger plastic collapse strength in their anisotropy direction.

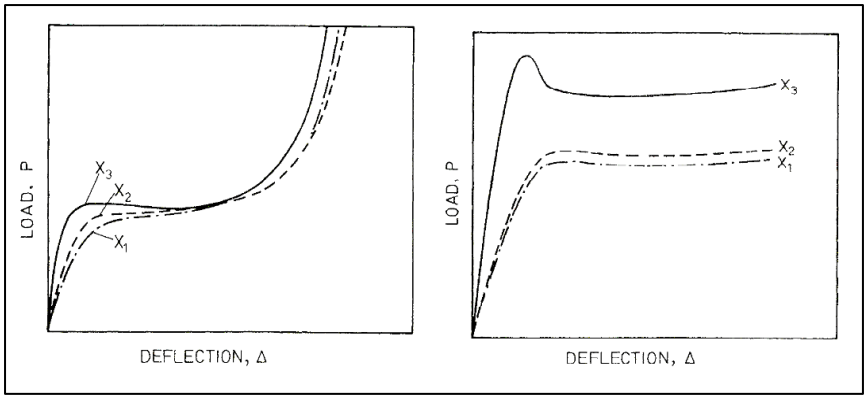

Figure 3-15: Load-deflection curves of foams measured whilst loading in three orthogonal directions of X_1, X_2, and X_3: (Left) fully elastic foam, (right) plastic foam. From [61].

The elastic strength ratio is described by equation 3.19, where n_3 stands for the rotational stiffness of the beam ends (cell edges) in X_3 direction. Here, two effects compete in determining the ratio; the longer beams would buckle more easily, but are more constrained. Experiments show that the competing effects almost cancel each other, giving a weak dependence of elastic stress ratio on *R.*

$$\frac{\sigma^*_{el,3}}{\sigma^*_{el,1}} = \frac{n_3^2}{n_1^2}\frac{1}{R} \tag{3.19}$$

An expression for shear modulus ratio is given by equation 3.20.

$$\frac{G^*_{31}}{G^*_{12}} = \frac{2}{1+R} \tag{3.20}$$

From equation 3.20 it can be inferred that shear stiffness perpendicular to the direction of cell elongation (rise direction) is lower than the shear stiffness in planes in the rise direction (see figure 3-14). This is because elongated struts and walls would bend easier when loaded in shear. Therefore, it is hypothesized that for a given

compression stiffness and density, anisotropic foams with elongated cells and high anisotropy ratio would demonstrate lower transverse shear stiffness.
Moreover, the energy absorption capacity of isotropic foams is independent of the direction of loading. This is due to their identical mechanical properties in all directions. In anisotropic foams, however, mechanical properties differ in anisotropy direction (direction of cell elongation) from the direction perpendicular to it which can give direction dependent energy absorption capacity to the foam. This hypothesis will be investigated in chapter 4 of this thesis.

3.6 Current Bicycle helmet test standards

A helmet needs to pass a standardization test in order to be certified for entering the market. The first standardization test for pedal cyclist was British Standard 4544 introduced in 1970. Standardization tests evaluate the performance of commercial helmets in attenuation of impact energy and reducing the linear acceleration levels transferred to the head. Moreover, they serve as a guideline for the design of new helmets by imposing requirements such as chin-strap retention system strength, required field of vision, and the head coverage. Nowadays, there are different standards worldwide for bicycle helmet certifications such as American standard CPSC [66], Canadian standard CAN/CSA-D113.2-M [67], European standards (EN 1078 [68] for adults and EN 1080 [69] for young children), Australian/New Zealand standard AS/NZS 2063 [70], and Snell standard Snell B-95, [71]. Each standardization group has a different procedure to evaluate the helmets. In these different standards, helmets can be impacted on one to three different surfaces depending on the standard. Moreover, the maximum allowable linear acceleration varies in different standards meaning a helmet that passes one standard may not pass another. Table 3-1 summarizes impact conditions such as impact energy, drop height, impact velocity, impact surface, and acceleration limit for American and European standards.

The impact set-up and instrumentation of American standard CPSC and European standard (EN1078 and EN1080) for evaluation bicycle

helmets will be briefly explained here. A comprehensive summary of all different standards and their requirements can be found in Hynd et al. [72] and the thesis of Vanden Bosche [46].

Table 3-1: Input parameters and requirements of American and European cycling helmet standardization tests.

Standard	Impact surface	Input criteria	Drop height	weight	Output criteria
CPSC (USA)	**Flat** D = 125 mm	Impact velocity 6.2 ms^{-1}	2 m	5 kg	300 g resultant
	Kerbstone Θ=105°, R =15mm	4.8 ms^{-1}	1.2 m		
	Hemisphere R = 48 mm	4.8 ms^{-1}	1.2 m		
EN 1078/1080	**Flat** D = 130 mm	5.42 ms^{-1}	1.497m	3.1-6.2 kg	250 g resultant
	Kerbstone Θ=105°, R =15mm	4.57 ms^{-1}	1.064m		

As summarized in table 3-1, the American standard CPSC [66] suggests a linear acceleration pass criterion of 300g at an impact velocity of 4.8 m/s and 6.2 m/s for kerbstone and flat impact surfaces, respectively. The CPSC impact test apparatus is shown in Figure 3-16. As observed in Figure 3-16, a guided fall impact using support arm on the rail is required for testing. The weight of the headform drop assembly is specified as 5 kg. Moreover, in this test set-up, a single uniaxial accelerometer is placed at the centre of mass of the headform and the line of impact is restrained to within the measurement axis. The headform material is suggested to be a low resonance K-1A magnesium alloy. The base of the test apparatus should be sufficiently heavy.

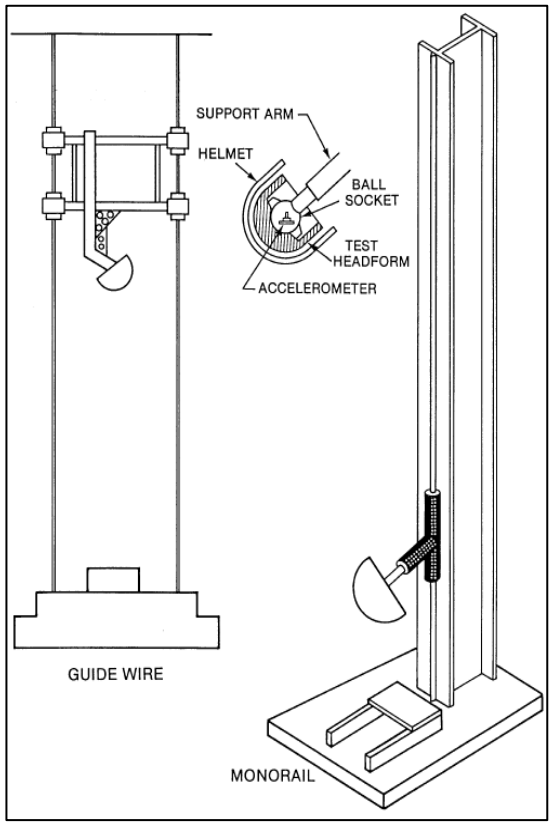

Figure 3-16: Illustration of CPSC impact set-up. From [66]

The European standards (EN1078 and EN1080) require a linear acceleration limit of 250g for a helmet to be certified. The EN1078 and 1080 impact set-up which is illustrated in Figure 3-17, in which a helmeted headform rests on a guided frame, drops on the flat and kerbstone surfaces at a velocity of 5.42 m/s and 4.57 m/s, respectively. In this set-up, the frame drops away at the point of impact, and the helmet is free to move. The European (EN) standards require a triaxial accelerometer at the centre of gravity such that the vector resultant linear acceleration pulse can be calculated.

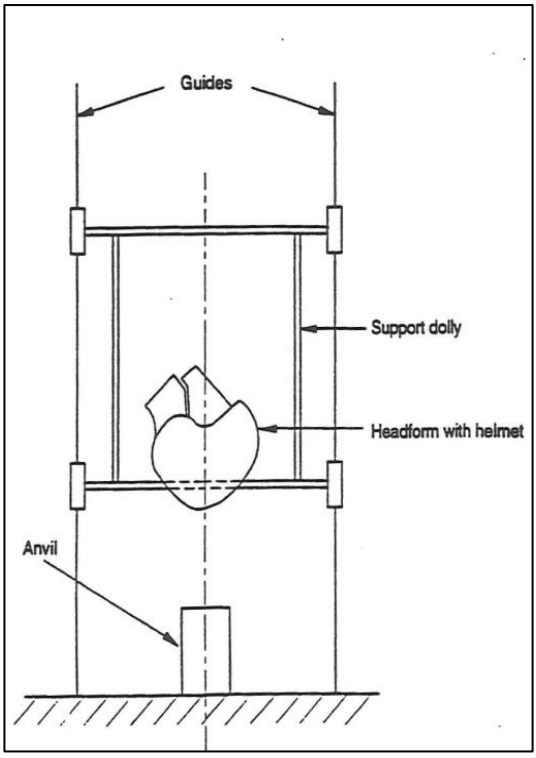

Figure 3-17: Illustration of EN 1078 and 1080 impact set-up. From [68-69].

Among the standards mentioned before, the Australian standard is the only one that takes into consideration not only the peak acceleration but also the time pulse for helmet impact efficiency evaluation. This standard allows for a peak acceleration of 250 g, with accelerations of greater than 150 g to be limited to 6 ms, and 200 g limited to 3 ms.

3.7 Oblique impact test methods

In oblique impact experiments, the head experiences a combination of two force components namely normal and tangential to the head surface and the resultant force is applied to the head in an oblique angle. In this experiment, both the linear and rotational accelerations experienced by the head are measured as a function of impact duration. One major criticism to the current bicycle helmet standard tests is that they do not evaluate the helmets in oblique impact which is

the prevalent impact condition. The only official helmet testing standard that includes an oblique impact is the ECE (United Nations Economic Commission for Europe) regulation 22.05 [73] for motorcycle helmets in which a helmeted headform is dropped onto an inclined 15° anvil (with respect to the vertical line) with abrasive and protruded surface. The anvil is equipped with load cells which can measure the tangential force. This set-up is intended to assess the effect of the protrusions and the surface friction on the motorcycle helmets, and is not aimed for the direct measurement of rotational acceleration. Moreover, the angle of 15° is not large enough to induce a sufficient level of rotation [74]. The real bicycle accident reconstruction by Bourdet et al. [75] showed that the typical impact angles are larger than 30° (33°±20°).

Another criticism to the current testing methods is that the linear acceleration is the only measured parameter for evaluation of the helmet performance and the helmets are certified solely based on the peak linear acceleration limit. The above mentioned criticisms and the knowledge of the important role of rotational kinematics in inducing traumatic brain injuries encouraged further research on alternative oblique impact testing designs [76-82]. These testing designs allow for performing oblique impacts and also the measurement of rotational acceleration and velocity of the headform. Currently, there is an ongoing effort for proposition of a new European bicycle helmet standard in which oblique impact testing and rotational acceleration limits will be incorporated [83]. In the next sections, a brief summary of different oblique test rigs will be presented. In some of these oblique impact designs, the helmeted head is dropped on a moving plate [76-79] whilst in some other the helmeted head is dropped on an angled anvil [70-82]. In these tests the head is either free [77, 78, 80] or attached to a neck [79, 81].

3.7.1 KTH moving sled oblique impact set-up

In this oblique impact set-up developed by Halldin et al. [76], in the lab of KTH and their spin-off company MIPS, a guided helmeted head is dropped onto a horizontally moving sled as illustrated in Figure 3-18a. The horizontal motion is provided by a moving sled. The sled is shot under the drop tower using pneumatic pressure. The moving (shooting) sled is synchronized in a way that it is directly under the drop tower at the moment of the impact of the helmeted head. In this set-up a Hybrid III dummy head is used. The reason is that of all

available dummy heads, the hybrid III head has the moment of inertia which is closest to the average human head, though it is only biofidelic for rotation around the Y (ear-to-ear) axis. The set-up instrumentation initially included an array of 4 accelerometers which later on was changed to an array of 9 linear accelerometers which is shown in Figure 3-18b. This array of 9 accelerometers enables the measurement of linear and rotational accelerations in three directions of x, y and z [77]. More recently the set-up has been equipped with a pneumatic clamp to hold the head whilst falling in a guided drop tower until just before impact. From 2014, the moving sled in the KTH set-up has been replaced by an angled anvil to reduce the complexity of the set-up and make it more compact.

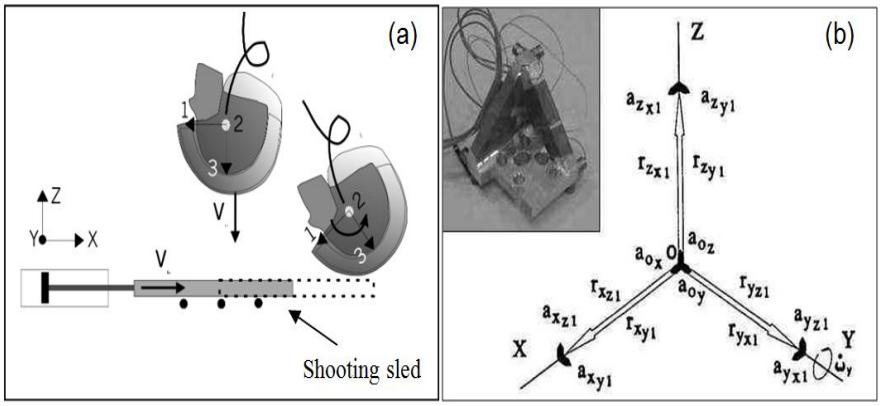

Figure 3-18: (a) Illustration of KTH moving sled set-up; an array of 9 accelerometers which will be placed in the centre of mass of the dummy head. From [77].

3.7.2 Birmingham test design

The Birmingham set-up has been developed by Mills and Gilchrist [78] in a similar way as the KTH moving sled set-up. It consists of a free-falling headform impacting a horizontally moving aluminium sandwich plate of total mass of 7.458 kg. The sled is moved by a pneumatic cylinder of 1m stroke. One difference between KTH and Birmingham set-ups is the sensor arrangements. In Birmingham set-up, the horizontally moving plate is equipped with two triaxial force transducers measuring normal and tangential forces on the top plate.

Furthermore, the headform in this set-up is a hollow aluminium dummy head with an external PVC plastisol skin. The headform is equipped with a triaxial linear accelerometer and two rotational accelerometers, one aligned with the neck-to-crown (z) axis, and one that was adaptable to either the ear-to-ear (y) axis or on the nose-to-rear (x) axis. To keep the helmet in place during the vertical fall, a supporting U-shaped aluminium honeycomb frame is attached to a vertical monorail via a 4-wheeled carriage [78]. Figure 3-19 demonstrates Birmingham oblique impact set-up.

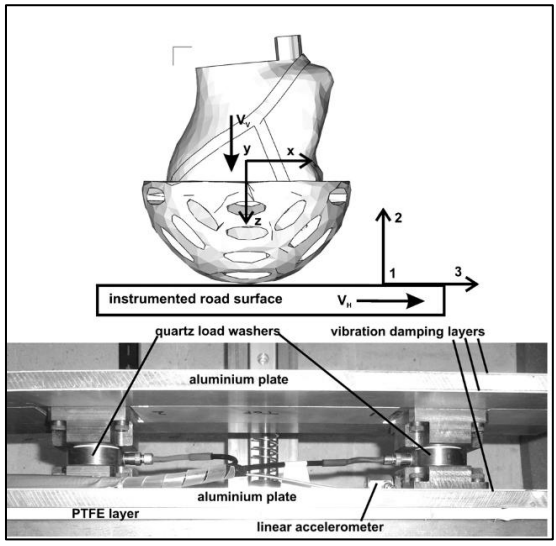

Figure 3-19: Birmingham test set-up with the force transducers and linear accelerometer under the aluminium impact plate. From [78].

3.7.3 KU Leuven set-up

The initial design of the KU Leuven oblique impact set-up was inspired by the KTH moving sled oblique impact set-up. The KU Leuven set-up utilises a drop impact tower in which a hybrid III dummy head is incorporated via a four point gripping system. In the KU Leuven set-up, a rotating belt is used as impact surface instead of a moving (shooting) sled. For instrumentation, an array of a triaxial gyroscope (Angular Rate Sensor) and three linear accelerometers is located in the centre of the mass of the dummy head. A 4-point support system for guided drop of the helmeted head till just before the impact is incorporated in this

set-up [46, 84]. Further investigation of this set-up will be described in chapter 6 of this thesis.

3.7.4 University of New South Wales set-up

Figure 3-20 shows the oblique impact test set-up developed by Pang et al. [79] which is another adaptation to the moving sled design. The test rig utilises a Hybrid III head and neck, but it can be adapted to any dummy head–neck combination. The presence of the neck changes the centre of rotation away from the centre of gravity of the head and closer to the pivot joint with the neck. The set-up was constructed using two vertical steel columns as shown in Figure 3-20. A ball joint connection to hold and orientate the head–neck assembly allows for the maximum freedom of configuration.

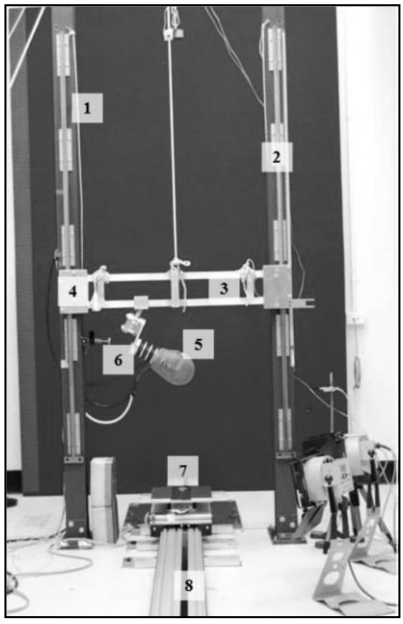

Figure 3-20: Oblique impact test set-up in University of New South Wales, including a stiff Hybrid III head-neck assembly. From [79].

The 50th percentile male Hybrid III dummy head was equipped with three linear accelerometers mounted orthogonally at the centre of mass to acquire data in the local x, y, and z coordinate system of the head. The dummy head was also fitted with two angular

accelerometers which measured the accelerations in the coronal and sagittal planes. The entire drop assembly moves in guided free fall. The total mass of the assembly is 20.7 kg.
The necessity of including a neck in the design of an oblique impact set-up is one of the ongoing debates in the standardization committee. Some researchers pointed out the influence of the neck and the rest of the body on the rotational kinematics of the head [85-87] while some other researchers believed that the effect of the neck in short impact pulses is negligible [16, 87, 88, 89]. The effect of the body and neck on kinematic of rotation and prediction of brain injuries during oblique impact and the necessity of including the neck in oblique impact test rigs are still under further investigation.

3.7.5 Wayne State University set-up

Figures 3-21 demonstrates the oblique impact set-up of Wayne State University. This set-up comprises of a mini sled with the Hybrid III head-neck structure which moves along the horizontal rails. The sled was pneumatically accelerated up to the desired velocity and decelerated whilst crushing the foam target attached to an aluminium plate. The aluminium plate is mounted in the end of the rail making a 30° angle with the vertical plane. The vinyl skin covering the rigid dummy skull was of the type without a nose to avoid interference during testing. The head-neck structure was rigidly supported during sled acceleration but was released during sled transit to allow an unhindered reaction during the impact event. For instrumentation, the aluminium plate is equipped with two load cells which were attached to a stationary frame. Two independent systems of multiple translational accelerometers were used to measure sagittal plane angular acceleration. The purpose of using two independent accelerometer systems is to increase the reliability of the estimate. An upper neck load cell is used to measure upper neck load and upper neck torque in x, y, z axes. To measure sled deceleration a uniaxial accelerometer is rigidly attached to the sled. Two uniaxial load cells behind the inclined aluminium plate record the headform contact force in the direction of sled motion. The sled velocity prior to head-foam contact is measured by a digital velocity meter [81].

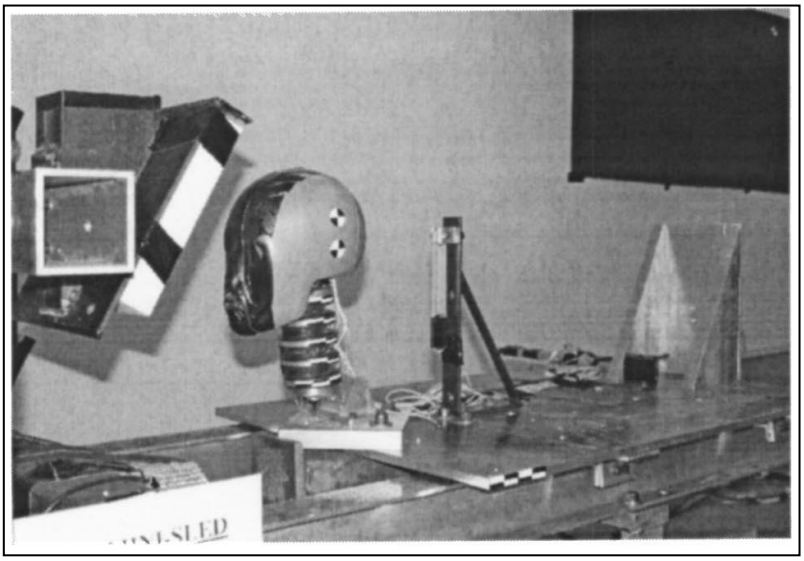

Figure 3-21: The Wayne State University mini-sled set-up just prior to the dummy head contacts the foam [81].

3.7.6 Legacy Research Institute test set-up

This oblique impact set-up which is shown in Figure 3-22, uses a falling impact on an angled anvil. This set-up includes a ISO (DIS) 6220/ EN 920 magnesium headform which is connected to drop assembly via a Hybrid III neck (which is stiffer than the human neck). The neck provides quasi-physiologic head restraints and enables head rotation only about the neck. In this set-up, sensors are added to the headform and neck to measure the angular head accelerations and the neck loading. The headform is instrumented with two biaxial accelerometers, one located at the centre of mass of the head and the second one located 78.5 mm anterior and 28.1 mm inferior of the centre of mass. Both accelerometers measure the angular acceleration of the headform about the ear-to-ear axis. Additionally, the base of the surrogate neck was instrumented is a 3-axis load cell that measures neck shear, neck compression and the neck flexion/extension moment [82].

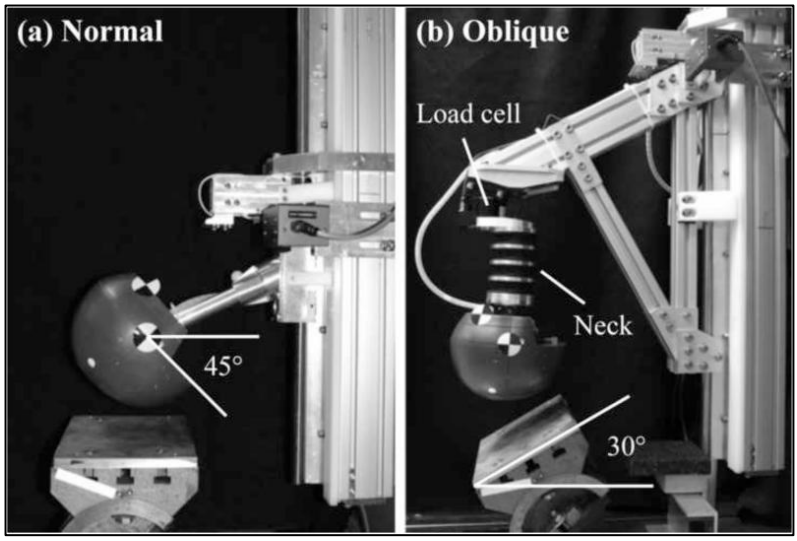

Figure 3-22: Legacy research institute test set-up: (left) linear impact, (right) oblique impact. From [82].

3.8 Important aspects in designing bicycle helmets

3.8.1 Foam selection

As mentioned earlier, a helmet for head protection has two main functions, firstly absorbing the impact energy and secondly minimizing the acceleration/deceleration experienced by the head below an allowable limit. The allowable limit of linear acceleration is defined by the specific helmet standard used. A brief description of relevant European and American bicycle helmet standards was given in section 3.6.

Apart from these two main functions of bicycle helmets, there are also other design considerations which will be explained in the following paragraphs. First, the conventional selection parameters for the helmet liners such as thickness and the density will be discussed. As explained earlier, integrating the stress-strain curve of the foam liner gives the absorbed energy per unit volume. By increasing the foam thickness, the total volume can be increased thus increasing the energy

absorption. However, there is a limit to the thickness of the foam liner in a helmet which is determined by standards, aerodynamics and fashion constraints. Moreover, a too thick helmet liner increases the rotational moment of inertia which can lead to higher rotational acceleration, as will be further explained in the next section.
The other parameter is the foam density. For a given foam thickness, by increasing the foam density, the plateau stress level increases leading to an increase in energy absorption. However, at the same time, the level of force transferred to the head also increases and hence there will be an optimum density as shown in Figure 3-12. The choice of the solid material of the foam liner is also important; the foam should be able to dissipate the energy during the first impact to avoid multiple impacts (due to bouncing) which can lead to neck injury and several successive head impacts. Therefore, elastic foams are less suitable for this application. Also for the helmet application, the foam material should maintain its mechanical properties and energy absorption capacity for different environmental conditions (e.g. a temperature range between -20°C and +50°C). Expanded polystyrene foams (EPS) is the most suitable foam available for helmet application so far, for its high energy absorption capacity, easy processing, relatively low cost and maintaining its impact performance in a wide temperature range.
The weight and the aerodynamic shape of the helmet are other important parameters for the helmet design. Helmets should be light and comfortable to wear. Moreover, by adopting a more aerodynamically favourable shape for the helmet, cyclists face lesser wind resistance during a ride.
Temperature and humidity in the helmet is controlled by introducing vent holes in the helmet design. In a study by De Bruyne [50], it was proposed that reducing the number of ventilation holes but placing them in strategic locations could result in better control of temperature. Moreover, it should be noted that the excessive vent holes in a helmet reduce the total volume of the foam liner. Limiting the effective volume of the foam liner reduces the energy absorption capacity. To compensate for this, higher density foam or thicker foam must be used.
Sufficient head coverage and field of vision are also other important parameters in helmet design. Depreitere et al. [90] proposed to lower the temporal region in adult helmets design (like in children‘s helmets) to better protect the thin temporal bone region.

3.8.2 Designing a helmet aiming at rotational acceleration mitigation

Oblique impacts are the most common impact situation that cyclists go through during traffic accidents [91, 75]. In an oblique impact, the human head undergoes normal and tangential force components which give rise to linear (translational) and rotational (angular) accelerations. The normal force components that do not act through the centre of rotation of the head also result in a rotational moment.

Figure 3-23 illustrates a simplified model of a helmeted head which undergoes an oblique load (F_o). In this model, the head is assumed to be a sphere covered with a hemispherical helmet. The oblique resultant force comprises of two force components F_N (normal force, which passes through the centre of gravity, CG) and F_T (tangential force).

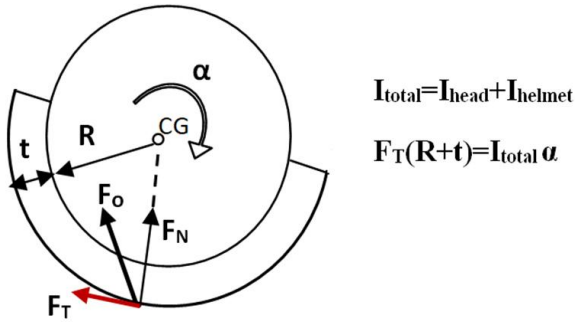

Figure 3-23: Simplified model of helmeted head undergoing simultaneous normal (F_N) and tangential (F_T) force components.

As mentioned, the tangential force component causes rotation of the head. In this model R is the radius of the spherical head, t stands for the overall thickness of the helmet (foam liner+shell), and I is the moment of inertia. As shown in equation 3.21, the rotational acceleration (α) depends on the tangential force (F_T), the lever arm ($R+t$) and overall moment of inertia of the head and helmet, I_{total}.

$$F_T(R+t)=I_{total}\alpha \qquad (3.21)$$

There can be several ways to limit rotational acceleration based on this simplified model shown in Figure 3-23:

- Reducing the overall thickness of the helmet can reduce the lever arm but it can also decrease the moment of inertia of the helmet which leads to a competing effect on rotational acceleration (see equation 3.21). It is shown in PhD thesis of Kelly Vanden Bosche [46] (for the same simplified model) that the effect of lever arm on rotational acceleration is greater than the effect of the helmet thickness, meaning decreasing the helmet thickness can lead to reduction of rotational acceleration in general.
- Reducing the tangential forces (F_T) transferred to the head via helmet can reduce rotational acceleration of the head. This can be achieved by choosing a liner with lower shear resistance or by adopting innovative designs which cause slip between the head and the helmet and thus reducing transferred tangential forces.

3.8.2.1 Helmet designs specifically aiming at rotational acceleration mitigation

Conventional helmets are effective at mitigation of head linear acceleration. However, they lack dedicated mechanisms to specifically aim at rotational acceleration mitigation. The role of rotational (angular) acceleration in serious head injuries was initially demonstrated by Holborn [92]. There is substantial evidence indicating that the rotational acceleration contributes more than linear acceleration to traumatic brain injuries such as concussions, diffuse axonal injuries (DAI), and acute subdural haematoma (ASDH) [8, 30, 93, 94, 95]. The awareness of the correlation between rotational acceleration (and velocity) of the head with traumatic brain injuries encouraged further research on new protective helmet designs aiming at rotational acceleration and velocity mitigation. These efforts were focused on either improving the foam liner [46, 82, 96] or introducing innovative designs such as adding a slip layer in the helmet structure e.g. in the MIPS system [97] and Lazer SuperSkin [98] or using dampers between a sandwich of EPS foam liners in 6D helmet technology [99]. In the following sections, the abovementioned helmet concepts will be briefly discussed.

3.8.2.1.1 Lazer SuperSkin

SuperSkin helmets utilise Phillips Head Protection System [98] which is licensed by LazerSport and aimed mainly for motorcycle helmets. SuperSkin helmet design is inspired by natural protection of the head by the scalp and is comprised of a stretchy flexible polymer membrane with a low friction fluid that has been added over the hard shell of the helmet as shown in Figure 3-24. During oblique impact, the polymer membrane slips over the inner shell of the helmet and mitigates the tangential forces and thus rotational acceleration. It is stated by the manufacturer that SuperSkin helmets can reduce the rotational accelerations and tangential forces causing injuries by 50% and 67.5%, respectively. It is cumbersome to use this concept in bicycle helmets because of their venting holes and complex aerodynamic shape. Moreover, questions can be raised concerning ageing effects of both the membrane and the low friction fluid.

Figure 3-24: Illustration of natural protection of the head by the skin (left) and the stretchable low friction layer in SuperSkin helmet (right). From [98].

3.8.2.1.2 MIPS helmets

MIPS stands for ''Multi-directional Impact Protection System''. MIPS technology for helmets was introduced in the market by Swedish company of the same name. MIPS technology incorporates a slip layer (similar to SuperSkin) in the helmet structure. The slip layer in MIPS helmets is a thin plastic shell, with a thickness of 0.5-0.7 mm. MIPS developed two models, MIPS-1 and MIPS-2. In MIPS-1 an external shell

slip layer is added around the outside of the helmet and is originally developed for helmets with a smoother external surface (e.g. motorcycle helmet, ski helmet, equestrian helmet). In MIPS-2, the slip layer is incorporated between the inner surface of the liner and the retention system. MIPS-2 is aimed for bicycle helmets which have more complex geometries due to various venting holes and aerodynamic shape. When a helmet with MIPS system is subjected to an oblique impact, the low friction layer enables the helmet to slide relative to the head as shown in Figure 3-25. This relative movement according to MIPS adds protection to the helmets against the rotational motion. Results from ski helmet testing showed that MIPS-1 reduces the rotational acceleration and rotational velocity up to 38% and 23%, respectively [97]. An American consumer report indicated that helmets equipped with the MIPS-2 system reduced the transmitted lower tangential force up to 43% [100].

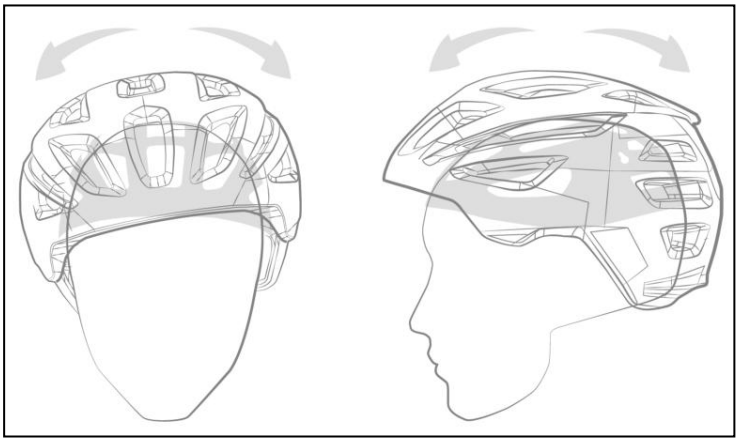

Figure 3-25: Illustration of MIPS-2 bicycle helmet with low friction layer, between helmet liner and the head, allowing the helmet slide relative to the head in oblique impacts. From [97].

In a study by Klug et al. [101], the performance of different commercial helmets (including MIPS-2 helmet) in oblique impact was investigated and compared. It was found that MIPS-2 helmet with low friction layer could significantly reduce all injury criteria values (e.g. HIC, HIP, GAMBIT, and BrIC) far more than other helmet types in this study.

According to Dr. Peter Halldin from MIPS, internal oblique impact testing results of MIPS helmets demonstrate reduction in angular acceleration in the range of 20-60%, and angular velocity mitigation between 10-40%. These tests were validated by the Biokinetics test laboratory in Canada. The large variation is due to differing positions of impact and there is no clear distinction between the MIPS-1 and MIPS-2 systems [46].

3.8.2.1.3 AIM system

AIM system stands for "Angular Impact Mitigation" and is proposed in a research paper by Hansen et al. [82] for bicycle helmets. The AIM system consists of a 17 mm thick aluminium honeycomb liner elastically suspended between an inner liner which is a 0.8 mm thick polyethylene terephthalate (PET) liner and an outer ABS shell as shown in Figure 3-26. The honeycomb in the AIM system is attached to the crown of the outer shell and to the periphery of the inner liner by a permanent adhesive. According to the authors, the aluminium honeycomb provides a non-elastic crumple zone which can absorb the normal component of the impact force (directed perpendicular to the outer helmet shell) while the suspension method mitigates angular acceleration by allowing relative movement between the helmet shell and the head as shown in Figure 3-26.

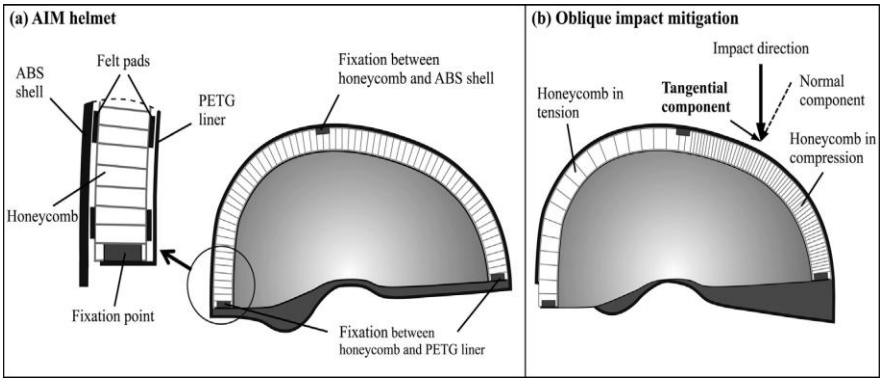

Figure 3-26: Illustration of the AIM helmet (left) and rotation of the shell around the liner by a transverse compression of the honeycomb (right). From [82].

The helmets with AIM system were prepared by replacing the EPS foam liner of 85 kg/m^3 density with aluminium honeycomb of the same thickness and density of 50 kg/m^3. Linear and oblique impact tests were performed on AIM helmets and standard helmets. To perform the oblique impacts, a helmeted dummy head was dropped on a 30° anvil. According to the authors, the AIM system resulted in a reduction of the peak linear acceleration by 14% in linear impacts and the reduction of peak angular acceleration by 34% in oblique impacts. Moreover, computational modelling predicted that AIM helmets reduced the risk of concussion and DAI by 27% and 44%.

3.8.2.1.4 6D helmet technology

6D helmet technology is a patented design concept comprising of a suspended dual liner system. In this helmet concept, shearable dampers shown in Figure 3-27 are sandwiched between two EPS foam liners. These dampers enable the liners to move relative to each other. This design allows for 6 degrees of free freedom (6D) of displacement of dual liners during an impact regardless of the head shape, the impact angle, and the tightness of the helmet on the head. The manufacturer's website alleges the reduction of the peak rotational acceleration for low velocity (3 m/s) and high velocity (6 m/s) impacts up to around 20% and 50%, respectively. This reduction is accompanied by prolongation of impact duration (about two times longer than for standard helmets) which according to the manufacturer is the key component of reducing the severity and magnitude of any impact [99].

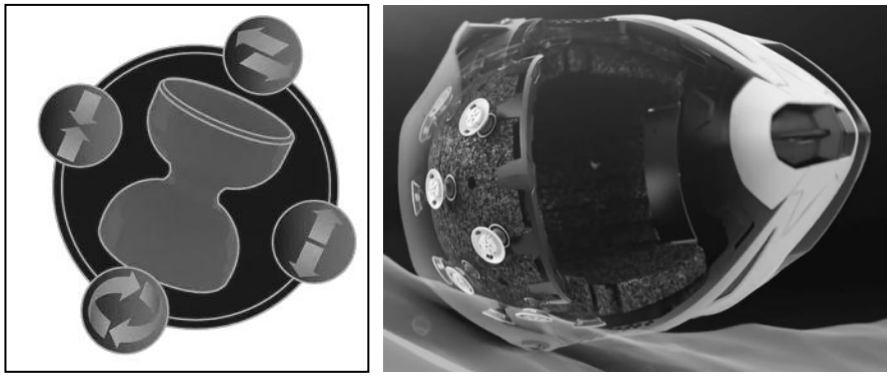

Figure 3-27: Illustration of the shearable dampers which can move with 6 degrees of freedom (left) and an example of a 6D helmet design hitting a surface (right). From [99]

Of course, if the impact force/acceleration peak is reduced, the prolongation of impact duration is expected to maintain the same change in momentum. However, the prolongation of impact duration is not always a positive phenomenon in terms of head protection during impact. This is because the probability of head injury is derived from a combination of acceleration and impact duration, as described in several head injury criteria. Therefore, for helmet evaluation a combination of peak acceleration and impact duration must be considered; it can be that lowering peak acceleration at the price of much longer impact duration causes the same injury severity to the head as a higher peak acceleration in a shorter impact duration. Moreover, it should be noted that this system increases the thickness of the helmet.

3.8.2.1.5 Proposed concept of KU Leuven

A novel concept for protective helmets (including bicycle helmets) aiming at reducing rotational acceleration transferred to the head was proposed by multidisciplinary bicycle helmet group in KU Leuven. In this concept which is patented [102], it is proposed to add so called ''internal slip'' functionality in the liner itself by using a highly anisotropic foam liner with its direction of anisotropy perpendicular to the surface of the head as shown in Figure 3-28.

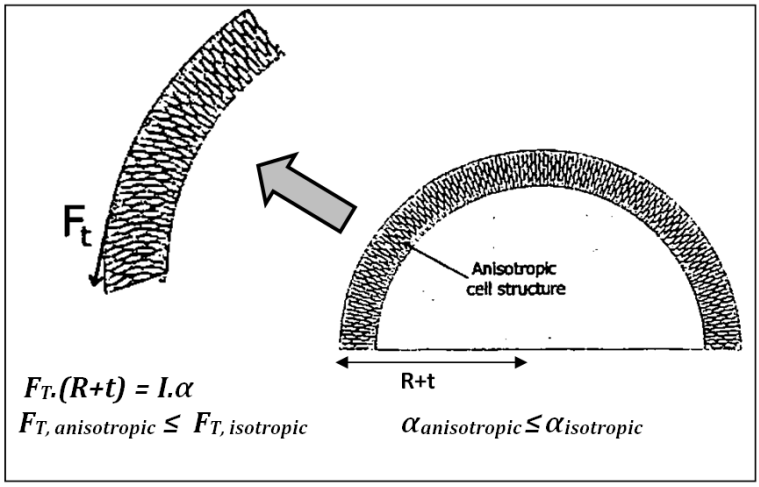

Figure 3-28: Anisotropic foam with highly elongated cells aligned perpendicular to the head surface; lower tangential force transferred to the head via anisotropic foam leads to lower rotational acceleration.

The idea is that for the same initial kinematic impact conditions, the anisotropic foam demonstrates lower shear resistance than the reference isotropic foam used in a standard helmet (e.g. EPS). It is hypothesized that by using the anisotropic foam liner the rotational acceleration could be mitigated via reducing the tangential forces/shear stress transferred to the head. This is because anisotropic foam demonstrates lower shear resistance in comparison to an equivalent isotropic foam counterpart. This is described by the simple mechanical equation shown in Figure 3-28 in which F_T is the tangential force, (R+t) is the lever arm, α and I stand for rotational acceleration and moment of inertia of the helmeted head, respectively. The compressive behaviour in the anisotropic foam, however, should be comparable to its isotropic foam counterpart to be able to perform well in the standard drop tower tests and provide sufficient protection against linear accelerations as demanded in the current standards. In theory the idea of using an anisotropic foam liner instead of a separate slip layer (e.g. in MIPS) has the advantage that the total thickness of the helmet could stay unchanged and this internal slip can act in any direction regardless of the helmet shape whilst in helmets with slip layer depending of the tightness of the helmet fit and the shape of the skull the relative movement between helmet and head can have constraints.
A preliminary study to compare the performance of isotropic and anisotropic foam for bicycle helmet application was performed in PhD thesis of Peter Verschueren [16]. In this thesis three different anisotropic polymer foams namely polyvinyl chloride (PVC), polyurethane (PU) and expanded polyethersulfone (PES) foams were compared with isotropic expanded polystyrene (EPS) foam as reference material. Table 3-2 summarizes these foams and their densities. The anisotropy ratio of these foams is not specified though.

The test set-up used in this study is illustrated in figure 3-29 which enables testing foams in combined shear-compression impact trying to mimic an oblique impact of a head/helmet system. In this set-up, a polyester ball is attached rigidly to a rigid steel pendulum arm. The foam specimens were thermoformed into a curved shape and attached to the polyester ball, and were impacted against an angled plate. The tilt angle of the force platform is β. The rotational acceleration can be calculated by placing a linear accelerometer on the pendulum while

one triaxial accelerometer is positioned on the far left side of the polyester ball.

Table 3-2: Specifications of the foam investigated. From [16].

Foam type	**isotropic EPS**	**anisotropic PU**	**anisotropic PVC**	**anisotropic PES**
Commercial name		Kapex® C51	Airex® C70.40	Ultratect®
Density (kg/m^3)	25-57	40	60	57
Compression strength (MPa)	0.3-1	0.45	0.45	0.74
Shear strength (MPa)	-	0.45	0.45	0.47

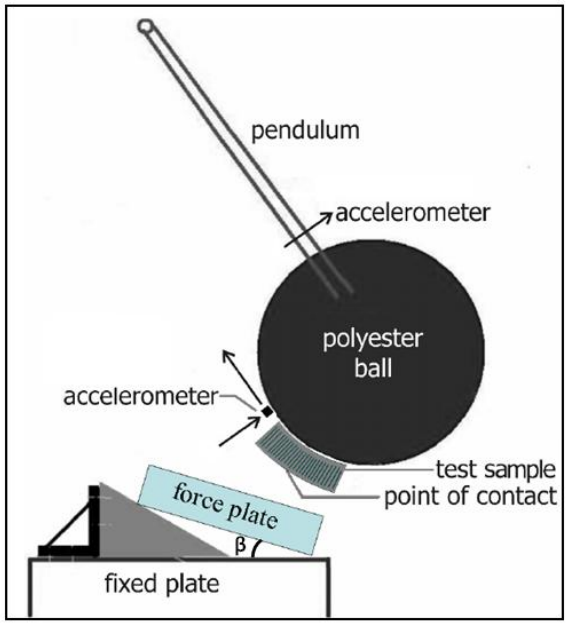

Figure 3-29: An illustration of shear-compression impact set-up. From [16].

As observed in Figure 3-30, preliminary results show that using an anisotropic foam showed lower peak rotational accelerations when stricken by the ball in comparison to isotropic EPS foams. Although the test method was different than testing the foams in real oblique impact but it could give a good comparative indication. From the preliminary findings in the thesis of Peter Verschuren [16], anisotropic PES foam was indicated as the best performing foam in reducing rotational acceleration and was chosen for proof of principal prototype testing during the PhD thesis of Kelly Vanden Bosche, [46].

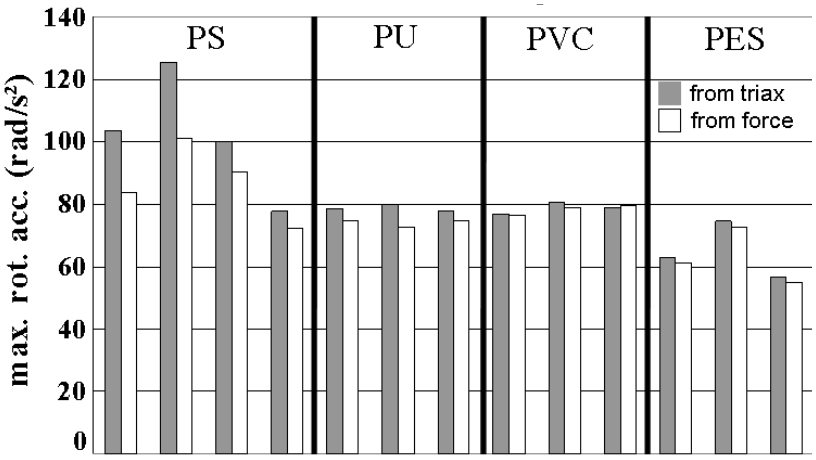

Figure 3-30: Peak rotational acceleration obtained from shear-compression impact test at β=20°. From [16].

For the prototype testing study, a commercial children's helmet named ''Hardtop Mini'' in size medium was sourced from the Swedish company SportAtlas. Prototypes of PES foams were prepared by using the shell of the commercial helmet, removing the EPS foam and refilling it with PES foam. The EPS foam in the reference helmets has a density of 80 kg/m^3. The anisotropic PES foam used for the prototype study has a large shape anisotropy ratio (R~10) and a low density (57 kg/m^3); it was supplied by Thermoplast Composite GmbH.
The rotational impact tests in this study were carried out on the oblique impact test rig of the Royal Institute of Technology (KTH) in Stockholm [74]. The impact tests were performed at two different resultant impact velocities (V_r) of 7.8 and 8.5 m/s .The oblique impact

angles were set at 28.5° and 37.5°, respectively. The results indicated that the prototype PES helmets cause lower peak linear and rotational accelerations of the head compared to the reference helmets up to 39% and 42%, respectively. Moreover, the evaluation of the results based on the global head injury criterion such as HIC and RIC also showed the superior performance of PES prototype helmets over standard helmets [46].

However, there is a fundamental question in this proof of principle study and that is whether the favourable performance of PES foam over EPS foam can be solely attributed to the cell anisotropy in PES foam. The PES foam has a lower density (57 kg/m^3) than EPS foam (80 kg/m^3) and it is made of a different polymer solid material. To answer this question, in this thesis, the effect of the helmet foam liner anisotropy on the reduction of rotational movement of the head in oblique impact is studied as the only varying parameter. For this, a novel concept will be introduced in chapter 5 which allows producing anisotropic foam and comparing its behaviour in oblique impact with its isotropic foam counterpart of the same solid material, density, and thickness.

Another practical problem in using PES foam for helmets is that the PES foam with such cell anisotropy is only available in the slab form. This is due to its special processing method described in a patent from BASF [103]. In this processing method, PES pellets are introduced with a blowing agent into large press and heated while applying significant pressure to the pellets causing them to melt. In the next step the pressure is released at such fast rate that the cells nucleate, grow, and immediately freeze in place. The cells become significantly anisotropic in the direction of the growth. Because of this particular processing method, the macroscopic geometry of this anisotropic PES foam is significantly limited and can only be made in blocks and subsequently cut into flat sheets. Moreover, thermoforming of PES foam can damage the cell structure [46]. Therefore, despite favourable oblique impact performance, PES foam is not suitable for the helmet production in an industrial scale.

Producing highly anisotropic polymer foams is not straightforward. This is because in highly anisotropic foam, the cell growth must be guided along a specific direction (e.g. via applying external negative pressure or stretching the foam) and at the same time elongated foam cells must be frozen and preserved in this elongated geometry (e.g. rapid cooling). Hence there is limited number of polymer foams with

significant degree of anisotropy (R>3) available in the market. In an attempt to produce highly anisotropic foam, a two step expansion batch process to produce cross-linked high density poly ethylene (x-HDPE) was proposed during the PhD thesis of Kelly Vanden Bosche in collaboration with University of Valladolid, [46]. This method consists of a 2-step expansion process, separated by a cross-linking matrix stabilization step, in a mould that constrained the foam growth to one direction to produce highly anisotropic cells. Using this method, x-HDPE foam could be produced with cell shape anisotropy ratio around R ~3.5 about one third of the shape anisotropy in PES foam (R~10) in a small cylindrical mould with internal diameter of 30 mm and internal height of 30 mm. The produced x-HDPE foam could achieve 30% of the plastic collapse strength ratio and 20% of the elastic modulus ratio of anisotropic PES foam. Because the x-HDPE foam was not as anisotropic as the PES material, a parametric study was attempted to improve and optimize the foam; however, it did not lead to any improvement due to many coupled processing parameters. Moreover, it was initially hypothesized that this process could be used for complex shapes, such as a bicycle helmet. However, in practice, it turned out to be extremely difficult to up-scale the foam to a bigger mould than initial 30 mm mould let alone more complicated geometries [46] due to significant temperature gradients inside the moulding material.
Therefore, one of the main focuses of this thesis is to develop a material concept to produce anisotropic foam with an eye on the possibility of processing into intricate geometries such as in helmets (e.g. for bicycle, ski, motorcycle or equestrian helmets).

3.9 References

1. Galford, J.E., McElhaney, J.H. A viscoelastic study of scalp, brain and dura. Journal of Biomechanics, 1970. 3(2): p.211-221.
2. Hori, H., Moretti, G., Rebora, A., Crovato, F.The Thickness of Human Scalp: Normal and Bald. The Journal of Investigative Dermatology, 1972. 58(6): p. 396-399.
3. Seery, G.E. Surgical Anatomy of the Scalp. Dermatologic Surgery, 2002. 28(7): p.581–587.
4. Blaus, B. Blausen gallery 2014. Wikiversity Journal of Medicine (2014).

5. Gray, H. Gray's Anatomy: The Anatomical Basis of Medicine and Surgery. Churchill-Livingstone, Elsevier, 40th Edition, 2008.
6. Baeck, K. Biomechanical modeling of head impacts: A critical analysis of finite element modeling approaches. PhD thesis, KU Leuven, 2013.
7. Fung, Y. C. Biomechanics-Mechanical Properties of Living Tissues. Springer Verlag, 1981.
8. Gennarelli, T., and Thibault, L. Biomechanics of acute subdural hematoma. Journal of trauma, 1982. 22 (8): p.680–686.
9. Monea, A. G., Baeck, K., Verbeken, E., Verpoest, I., Vander Sloten, J., Goffin, J., and Depreitere, B. The biomechanical behaviour of the bridging vein-superior sagittal sinus complex with implications for the mechanopathology of acute subdural haematoma. Journal of the mechanical behaviour of biomedical materials, 2013. 32: p.155–165.
10. Injury in America: A Continuing Public Health Problem Committee on Trauma Research, Institute of Medicine, National Research Council, 1985.
11. Courville, C. B. The mechanism of coup-contre-coup injuries of the brain: A critical review of recent experimental studies in the light of clinical observations. Bulletin of Los Angeles Neurological Societies, 1950. 15: p.72-86.
12. Depreitere, B., et al., Bicycle-related head injury: a study of 86 cases. Accident Analysis & Prevention, 2004. 36(4): p. 561-567.
13. Wood, J.L., Dynamic response of human cranial bone. Journal of Biomechanics, 1971. 4(1): p. 1-12.
14. Yoganandan, N., et al. Biomechanics of Skull Fracture. Journal of Neurotrauma, 1995. 12(4): p. 659-668.
15. Mertz, H.J., Prasad, P., Irwin, A.L. Injury Risk Curves for Children and Adults in Frontal and Rear Collisions. In Proceedings of the 41th Stapp Car Crash Conference. Lake Buena Vista, Florida, US, 1997. pp. 13–30.
16. Verschueren, P., Biomechanical analysis of head injuries related to bicycle accidents and a new bicycle helmet concept, 2009, PhD Thesis, Katholieke Universiteit Leuven: Leuven.

17. Monea, A.G., et al., The relation between mechanical impact parameters and most frequent bicycle related head injuries. Journal of the Mechanical Behaviour of Biomedical Materials, 2014. 33: p. 3-15.
18. Depreitere, B., A rational approach to pedal cyclist head protection, 2004, PhD Thesis, Katholieke Universiteit Leuven: Leuven.
19. Hardman, J.M., Manoukian, A. Pathology of head trauma Neuroimaging Clinics of North America, 2002. 12(2): p.175-187.
20. Ommaya, A. K., Grubb, R. L. Jr., and Naumann, R. A. Coup and contre-coup injury: Observations on the mechanics of visible brain injuries in the rhesus monkey. Journal of Neurosurgery, 1971. 35: p.503-516.
21. Willinger, R., Taleb, R.L., Kopp, C.M. Modal and temporal analysis of head mathematical models. Journal of Neurotrauma, 1995. 12(4): p.743-754.
22. Van Lierde, C. Biomechanics of head injury - Damage criteria for skull and brain lesions. 2005, PhD dissertation, K.U.Leuven.
23. Maxeiner, H. Detection of ruptured cerebral bridging veins at autopsy. Forensic Science International, 1997. 89(1): p.103-110.
24. Gennarelli, T., Thibault, L., Ommaya A.K. Pathophysiologic responses to rotational and translational accelerations of the head. Stapp car crash journal, 1972. 16: p.296–308.
25. Huang, H.-M. M. Three-Dimensional Finite Element Analysis of Subdural Hematoma. Journal of Trauma-Injury Infection & Critical Care, 1999. 47(3): p.538–544.
26. Löwenhielm, P. Dynamic properties of the parasagittal bridging veins., Zeitschrift fur Rechtsmedizin, 1974. 74(1): p.55–62.
27. http://www.health.harvard.edu/diseases-and-conditions/subdural-hematoma
28. Wasserman, J., Koenigsberg, R.A. (2007). Diffuse axonal injury. Emedicine.com retrieved on 2008-01-26.

29. Strich, S.J. Diffuse Degeneration of the Cerebral White Matter in Severe Dementia Following Head Injury. Journal of Neurology, Neurosurgery, and Psychiatry, 1956. 19: p.163–185.
30. Gennarelli, T.A., et al. Diffuse axonal injury and traumatic coma in the primate. Annals of Neurology, 1982. 12(6): p. 564-74.
31. Margulies, S.S., Thibault, L.E. A Proposed Tolerance Criterion for Diffuse Axonal Injury in Man. Journal of Biomechanics, 1992. 25: p.917–923.
32. http://kryski.com/medicolegal-visuals
33. Kleiven, S. Predictors for traumatic brain injuries evaluated through accident reconstructions. Stapp car crash journal, 2007. 51: p.81–114.
34. Willinger, R. and Baumgartner, D. Human head tolerance limits to specific injury mechanisms. International Journal of Crashworthines, 2003. 8(6): p.605–617.
35. Horgan, T. and Gilchrist, M. D. The creation of three-dimensional finite element models for simulating head impact biomechanics. International Journal of Crashworthines, 2003. 8(4): p.353–366.
36. Versace, J., A review of the severity index. In 15th Stapp Car Crash Conference1971. p. 771-796.
37. Eppinger, R., et al. Supplement: Development of Improved Injury Criteria for the Assessment of Advanced Automotive Restraint Systems (II). National Highway Traffic Safety Administration, 2000.
38. Kimpara, H., Iwamoto, M. Mild traumatic brain injury predictors based on angular accelerations during impacts. Annals of Biomedical Engineering, 2012. 40(1): p.114–126.
39. Newman J. A generalized acceleration model for brain injury threshold (GAMBIT), In: Proceedings of the International Research Council on Biomechanics of Injury (IRCOBI) Conference, 1986. p.121–131.
40. Newman, J.A.S., N.; and Welbourne, E., A proposed new biomechanical head injury assessment function—the maximum power index,. Strapp Car Crash Journal, 2000. 44: p.215-47.

41. Yoganandan, N., Pintar F. A., Zhang, J., Baisden, J.L. Physical properties of the human head: mass,centerofgravity and moment of inertia. Journal of Biomechanics, 2009. 42(9): p. 1177-1192.
42. Kleiven, S. Predictors for traumatic brain injuries evaluated through accident reconstructions. Stapp car crash journal, 2007. 51: p.81–114.
43. Takhounts, E.G., Hasija, V., Ridella, S.A., Rowson, S., Duma, S.M. Kinematic Rotational Brain Injury Criterion (BRIC). In Prococeedings of 22nd International Technical Conference on the Enhanced Safety of Vehicles (ESV), 2011. Paper No. 11-0263.
44. https://helmets.org
45. http://www.onetri.com/Bike-Helmet-FAQ_ep_118-1.html
46. Vanden Bosche, K. Development and characterization of novelanisotropic foam for bicycle helmets, 2016, PhD Thesis, Katholieke Universiteit Leuven: Leuven.
47. Gale, A., Mills, N.J. Effect of polystyrene foam liner density on motorcycle helmet shock absorption. Plastics andRubber Processing and Applications, 1985. 5(2): p.101–108.
48. Di Landro, L., Sala, G., and Olivieri, D. Deformation mechanisms and energy absorption of polystyrene foams for protective helmets. Polymer Testing, 2002. 21(2): p.217–228
49. Hodgson, V.R., Skid Tests on a Select Group of Bicycle Helmets to Determine Their Head-Neck Protective Characteristics, 1991, Wayne State University: Detroit, Michigan.
50. De Bruyne, G. Heat loss of the human head under bicycle helmets for designing safer bicycle helmets, in Bio-Engineering (M3-BIOres) 2010, PhD Thesis, Katholieke Universiteit Leuven.
51. Mills, N.J., Gilchrist, A. Reassessing bicycle helmet impact protection In: Proceedings of the International Research Council on Biomechanics of Injury (IRCOBI) Conference, 2003. p.1-12.

52. Bruhwiler, P., Buyan, M., Huber, R., Bogerd, C., Sznitman, J., Graf, S, R¨osgen, T. Heat transfer variations of bicycle helmets. Journal of Sports Sciences, 2006. 24(9): p.999-1011.
53. De Bruyne, G., Aerts, J.M., Van der Perre, G., Goffin, J., Verpoest, I., Berckmans, D. Spatial differences in sensible and latent heat losses under a bicycle helmet. European Journal of Applied Physiology, 2008. 104(4): p.719-26.
54. http://www.giro.com/eu_en/a-plant-based-revolution-in-helmets/
55. Seidi, M., Hajiaghamemar, M., Ferguson, J., and Caccese, V. Injury Mitigation Performance of a Head Protection Wear with Polyurethane Honeycomb. SAE Technical Paper, paper nom. 2015-01-1443, 2015.
56. http://www.kraniums.com/kranium
57. http://www.koroyd.com/.
58. Kurt, M., Laksari, M., Kuo, C., Grant, G.A., Camarillo, D.B. Modeling and optimization of airbag helmets for preventing head injuries in bicycling. Annals of biomedical engineering, 2017. 45 (4): p.1148-11.6
59. Teng, T.-L., Liang, C.-C., Nguyen, V.-H. Assessment of a Bicycle Helmet Liner with Semispherical Cones. Proceedings of the Institution of Mechanical Engineers, Part L: Journal of Materials: Design and Applications, 2016. 230(1): p.1–9.
60. Mills, N., Polymer Foams Handbook: Engineering and Biomechanics Application and Design Guide 2007, Burlington, MA: Elsevier.
61. Gibson, L. and Ashby, M. Cellular solids : structure & properties - 2nd ed.1997, Cambridge, UK: Cambridge University Press.
62. Thompson, W., On the division of space with minimum partitional area Philosophical Magazine (Lord Kelvin) 1887. 24: p. 503-514.
63. Weaire, D. and Phelan, R. The structure of monodisperse foam. Philosophical Magazine Letters, 1994. 70(5):p.45-350.

64. Maiti, S.K., Gibson, L.J., Ashby, M.F. Deformation and energy absorption diagrams for cellular solids. Acta Metallurgica, 1984. 32(11): p. 1963-1975.
65. Huber, A.T., Gibson L.J. Anistropy of polymer foams. J Mater Sci 1988;23:3031–3040
66. CPSC, Consumer Product Safety Commission 16 CFR Part 1203 Safety Standard for Bicycle Helmets; Final Rule, 1998, Federal Register: Washington, D.C.
67. CAN/CSA, D113.2-M Cycling Helmets, 1989, Canadian Standards Association: Ontario, Canada.
68. CEN, EN 1078 Helmets for pedal cyclists and for users of skateboards and roller skates, 1997, Comité Européen de Normisation (European Committee for Standardization): Brussels, Belgium.
69. CEN, EN 1080 Impact protection helmets for young children, 1997, Comité Européen de Normisation (European Committee for Standardization): Brussels, Belgium.
70. AS/NZS, AS/NZS 2063:2008 (Incorporating Amendment No.1): Bicycle Helmets, 2009, Standards Australia/Standards New Zealand: Sydney, NSW, Australia.
71. Snell, 1995 Standard for protective headgear for use in bicycling -1998 Revision, in 2000, Snell Memorial Foundation, Inc.: North Highlands, CA.
72. Hynd, D., Cuerden, R., Reid, S., Adams, S. The potential for cycle helmets to prevent injury - A review of the evidence, Transport Research Laboratory Report PPR446, 2009.
73. UN/ECE, United Nations Economic Commission for Europe Regulation 22-05, Uniform provisions concerning the approval of protective helmets and their visors for drivers and passengers of motorcycles and mopeds.: Geneva.
74. Ebrahimi, I., Golnaraghi, F., Wang, G.G. Factors Influencing the Oblique Impact Test of Motorcycle Helmets. Traffic Injury Prevention, 2015. 16(4): p. 404-408.
75. Bourdet, N., Deck, C., Serre, T., Perrin C., Llari, M., Willinger R. In-depth real-world bicycle accident reconstructions.

International Journal of Crashworthiness, 2014. 19(3): p. 222-232.

76. Halldin, P., Gilchrist, A. and Mills, N.J. A new oblique impact test for motorcycle helmets. International Journal of Crashworthiness, 2001. 6(1): p. 53-64.
77. Aare, M. and Halldin, P. A New Laboratory Rig for Evaluating Helmets Subject to Oblique Impacts. Traffic Injury Prevention, 2003. 4(3): p. 240-248.
78. Mills, N.J. and Gilchrist, A. Oblique impact testing of bicycle helmets. International Journal of Impact Engineering, 2008. 35(9): p. 1075-1086.
79. Pang, T.Y., et al. Head and neck responses in oblique motorcycle helmet impacts: a novel laboratory test method. International Journal of Crashworthiness, 2011. 16(3): p. 297-307.
80. Deck, C., Bourdet, N., Calleguo, A., Carreira, P.R., Willinger, R. Proposal of an Improved Bicycle Helmet Standards. In Proceedings of the International Crashworthiness Conference. 2012, Milano, Italy.
81. Ivarsson, J., Viano, D.C., Lövsund, P., Parnaik, Y. Head Kinematics in Mini-Sled Tests of Foam Padding: Relevance of Linear Responses From Free Motion Headform (FMH) Testing to Head Angular Responses. 2013
82. Hansen, K., et al., Angular Impact Mitigation system for bicycle helmets to reduce head acceleration and risk of traumatic brain injury. Accident Analysis & Prevention, 2013. 59: p. 109-117.
83. Halldin, P. and Kleiven, S. The development of next generation test standards for helmets, in 1st International Conference on Helmet Performance and Design, P. Childs, A. Bull, and M. Ghajari, Editors. 15 Feb. 2013: Imperial College of London.
84. Tobback, B. and B. Boulanger, Evaluatie en optimalisatie van rotationele impact tests voor fietshelmen, in Industrial Sciences2011, Masters Thesis, Lessius Campus De Nayer: Mechelen.
85. M. Beusenberg, Shewchenko, N., Newman, J. A., De Lange, R. and Cappon, H. Head, Neck and Body Coupling in

Reconstructions of Helmeted Head Impacts. In: Proceedings of the International Research Council on Biomechanics of Injury (IRCOBI) Conference, 2001.

86. Chinn, B., Canaple, B., Derler, S., Doyle, D., Otte, D., Schuller, E., Willinger, R. COST 327 Motorcycle Safety Helmets, European Commission Directorate General for Energy and Transport, Brussels, Belgium, 2001.
87. Ghajari, M., Peldschus, S., Galvanetto, U., Iannucci, L., 2013. Effects of the Presence of the Body in Helmet Oblique Impacts. Accident Analysis & Prevention 50, 263–271.
88. Gilchrist, A. and N.J. Mills, Protection of the side of the head. Accident Analysis & Prevention, 1996. 28(4): p. 525-535.
89. Meyer, F., R. Willinger, and C. Deck, Helmet test method Influence of Neck, 2014, CEN TC 158 WG 11: Milan March 2014.
90. Depreitere, B., et al. Lateral Head Impacts and Protection of the Temporal Area by Bicycle Safety Helmets. Journal of Trauma-Injury Infection and Critical Care, 2007. 62(6): p. 1440-1445.
91. Mills, N.J., and Gilchrist, A. Response of helmets in direct and oblique impacts. International Journal of Crashworthiness, 1996. 2(1): p. 7–24.
92. Holborn, A.H.S. Mechanics of head injury. Lancet 1943. 2: p.438-441.
93. Gennarelli, T.A., Thibault, L.E., Ommaya, A.K. Pathophysiologic responses to rotational and translational accelerations of the head. 16st Stapp Car Crash Conference Proceedings. SAE No. 720970, 296-308, 1972.
94. Margulies, S.S., Thibault, L.E. and Gennarelli, T.A. Physical model simulations of brain injury in the primate. Journal of Biomechanics, 1990. 23(8): p. 823-836.
95. King, A.I., Yang, K.H., Zhang, L., Hardy, W., Viano, D.C. Is head injury caused by linear or angular acceleration?. In: Proceedings of the International Research Council on Biomechanics of Injury (IRCOBI) Conference, Lisbon, Portugal, 2003,p. 1-12.

96. Vanden Bosche, K., Mosleh, Y., Depreitere, B., Vander Sloten, J., Verpoest, I., Ivens J. Anisotropic polyethersulfone foam for bicycle helmet liners to reduce rotational acceleration during oblique impact. Proceedings of the Institution of Mechanical Engineers H, Journal of Engineering in Medicine, 2017. 231(9): p.851-861.
97. MIPS. Test Results. Available from: http://mipshelmet.com/how-it-works/test results.
98. Lazer. Standard Helmet vs SuperSkin - The scientific evidence. Available from: http://www.lazerhelmets.com/innovations/superskin/.
99. 6D Helmet, http://www.6dhelmets.com
100. ConsumerReports. Bike Helmet Buying Guide. April 2016; Available from: http://www.consumerreports.org/cro/bike-helmets/buying-guide.htm.
101. Klug, C., Feist, F., Tomasch, E. Testing of bicycle helmets for preadolescents. In: Proceedings of the International Research Council on Biomechanics of Injury (IRCOBI) Conference, 2015. p.136-155.
102. Depreitere, B., et al., Protective helmet, EP 1 776 022 B1, 2008 (Patent).
103. Börger, H., Verwendung eines Schaumstoffzuschnitts als Dämpfungselement und flächiges Dämpfungselement. DE 44 08 928 A1, 1995 (Patent).

Chapter 4

Effect of polymer foam anisotropy on energy absorption during combined shear-compression loading

Adopted from: Yasmine Mosleh, Kelly Vanden Bosche, Bart Depreitere, Jos Vander Sloten, Ignaas Verpoest, Jan Ivens. Effect of polymer foam anisotropy on energy absorption during combined shear-compression loading. *Journal of Cellular Plastics*, 2018. 54(3): p.597-613.

4.1 Introduction

Polymeric foams are cellular materials made of a three dimensional network of closed or open cells [1]. The processing method of foam strongly affects their cell morphology and subsequently their mechanical properties. There has been dedicated research in recent years to study the relationship between process, morphology and mechanical properties of the foams [2-4]. In general, elongational flow of molten foaming polymer leads to an anisotropic cell structure with elongated cells.

The high energy absorption capability of foams and their low weight make them an excellent choice in applications such as shock absorbers, packaging, protective helmets, and crashworthy vehicle interiors.

Moreover, foams are extensively used as core materials in lightweight sandwich structures and as thermal and acoustic insulators.
In-service loading conditions are often multi-axial due to the complex geometries of structures and intricate loading conditions. Therefore, investigation of the foam behaviour under both quasi-static and dynamic multi-axial loading is of great importance. Moreover, characterization of cellular materials under multi-axial loading allows the use of realistic and complex failure criteria in structural design, taking into account multiple loading directions.
Previously, several researchers have characterised cellular materials and sandwich structures using different multi-axial testing devices. The Arcan test rig [5], originally designed to investigate the biaxial failure of fibre reinforced composites, has been used by Gdoutos and Daniel [6] to obtain the multi-directional mechanical properties of PVC foams especially in tensile–shear mode. The mechanical behaviour of Rohacell-51WF foam under simultaneous shear-compression loading was studied by Mines and Birch [7]. Authors found a linear relationship between the compressive failure/plateau stress and shear stress. Doyoyo and Wierzbicki [8] used a modified version of the Arcan fixture to conduct a series of biaxial tests on isotropic and anisotropic aluminium foams and proposed a universal phenomenological yield criterion in principal stress space.
Mohr and Doyoyo [9] investigated combined shear-compression properties of aluminium honeycombs by introducing a new test method called Universal Biaxial Testing Device (UBTD), at different loading angles. The drawback of their set-up is that at angles higher than 30° the mode of stress changes from combined compression-shear to combined tension-shear. Benderly and Putter [10] studied the combined shear/compression failure envelope of PMI (Rohacell) foams using a modified four-point flexural testing method. Kintscher et al. [11] developed a test fixture which could apply simultaneous transverse shear and compression loads, using two independent load cells, to study stiffness and failure criteria of folded core structures. A similar set-up was also used by Hong et al. [12] to study the quasi-static behaviour of aluminium honeycombs under combined shear-compression loading.
Taher et al. [13] developed a modified Arcan test fixture (MAF) which was able to assess the multi-axial loading behaviour of foams at room or elevated temperatures. The MAF could measure high compression

to shear biaxial loading conditions that are not possible to measure with conventional Arcan fixtures.

Hou et al. [14] studied behaviour of aluminium honeycombs under shear-compression loading at impact velocity of 15 m/s by using a split Hopkinson pressure bar (SHPB). They reported a decrease in both initial peak and crush strength of aluminium honeycombs by increasing the loading angle from 0 to 60°. They observed two co-existing deformation patterns under combined shear-compression loading which occurrence was influenced by deformation rate. In another study, Hou et al. [15] conducted finite element analysis to study the combined shear-compression behaviour of aluminium honeycombs. They found elliptical stress envelopes on the plane of normal stress vs. shear stress for both the quasi-static and dynamic loadings. Furthermore, they observed a good agreement between experiments and FEM results.

Recently, Tounsi et al. [16] conducted dynamic combined shear-compression experiments to study the effects of loading angle on deformation mode of aluminium alloy honeycombs. They identified three deforming pattern modes, the distribution of which is related to the combined effects of the in-plane orientation angle and the loading angle. Ashab et al. [17] also carried out combined shear and compression experiments on aluminium honeycombs in quasi-static and dynamic modes under different loading angles. They proposed an empirical formula to describe the relationship between plateau stress and loading angle. Quasi-static combined shear-compression experiments on Nomex honeycombs were performed by Zhou et al. [18] to study macroscopic yield criteria. They used the Arcan set-up for their study. Zhang et al. [19] studied the yield behaviour of PMMA under combined shear–compression loading at different loading rates. Their research demonstrated that failure behaviour of PMMA is sensitive to loading rates.

In this chapter, a quasi-static combined shear-compression test set-up initially developed during PhD thesis of Kelly Vanden Bosche [20] is utilised to characterise the behaviour of isotropic EPS foams (with three different densities) and anisotropic PES foam, under quasi-static uniaxial compression and combined shear-compression loadings. The effect of deformation angle on stress-strain behaviour and energy absorption of the foams has been investigated. Moreover, it will be explained how the cell anisotropy can affect the energy absorption of foams under different deformation angles. This is particularly

interesting for designing structural parts where energy absorption is critical and multi-axial loads are present. In this case, it will be crucial to correctly position the cells in the anisotropic foam with respect to the loading direction for maximising energy absorption capacity.

4.2 Materials

4.2.1 Expanded polystyrene foam

Expanded Polystyrene bead foams (EPS) were sourced from Kemisol and Lazer Sports companies. The foams have densities of 40±3, 80±3 and 120±4 kg/m^3 (relative density of 0.38, 0.48, and 0.57, respectively). The production of the foams was by steam moulding of pre-expanded polystyrene beads.

4.2.2 Polyethersulfone foam

Thermoplastic PES (polyethersulfone) foam used in this study was sourced from DIAB company under the commercial name of Divinycell F50. The nominal density of Divinycell F50 is 50 kg/m3 (relative density = 0.37) and it has been specifically developed for aircraft interior applications. At sourcing, there was no information about geometrical or mechanical anisotropy of Divinycell F50. These are characterized in this chapter.

4.3 Methods

4.3.1 Quasi-static uniaxial compression test

Quasi-static compression tests were performed according to ASTM standard D1621/94 using a universal tensile testing machine (Instron 4467). Foams were compressed at a constant displacement rate of 2.5 mm/min between two steel plates. The displacement and the load were recorded. Samples were cut into cuboids of 5 cm (length) × 5 cm (width) × 2.5 cm (thickness). All experiments were performed at room temperature.

4.3.2 Biaxial shear-compression set-up and test method

The test apparatus for this study was developed as an insert into an existing biaxial test set-up for textiles, developed and built at KU Leuven (Figure 4-1). The combined shear-compression set-up comprises of two independent displacement actuators which apply

shear and compressive displacements in two orthogonal axes simultaneously as indicated in Figure 4-1.
Each axis has an independent displacement actuator and an independent load cell. The displacement rate of each axis can be varied from 0 to 20 mm/min generating any resultant angle of deformation, from pure compression (angle 0°) to simple shear (angle 90°). Different deformation angles (ɵ) were obtained by setting the ratio of "shear displacement rate"/"compression displacement rate", S/C, equal to the tangent of the deformation angle. Different foam specimens were tested over various deformation angles of 0° (pure compression), 15°, 45°, and 60°. Corresponding compressive and shear displacement rates of the set-up, for each deformation angle, are listed in table 4-1. All the experiments were performed at room temperature.

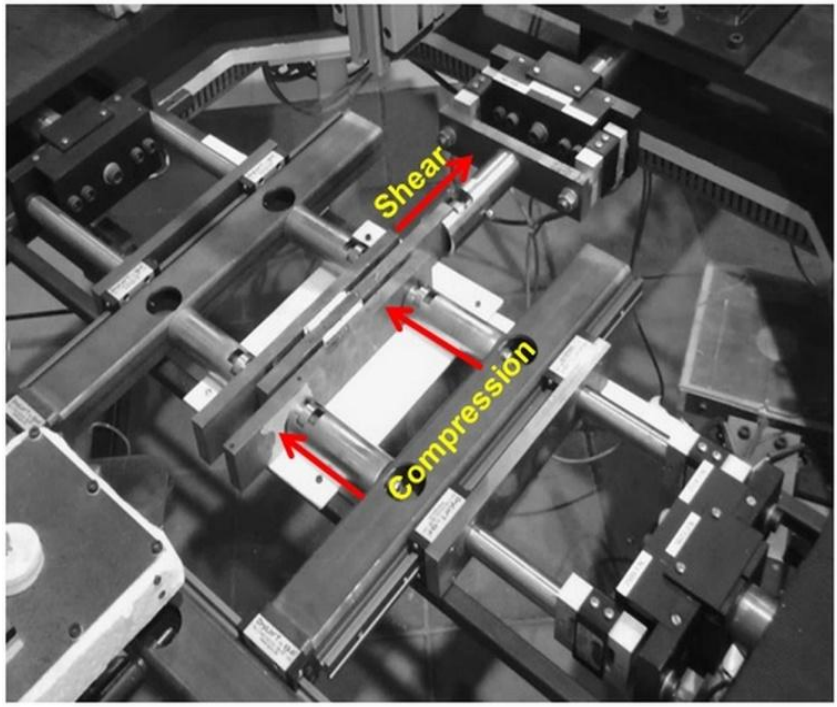

Figure 4-1: Biaxial shear-compression set-up; directions of compressive and shear forces are indicated with arrows.

Table 4-1: Corresponding shear and compressive displacement rates for different deformation angles.

Shear displacement rate: S (mm/min)	Compression displacement rate: C (mm/min)	Deformation angle (ɵ)
0	2.5	0°
1	3.73	15°
2.5	2.5	45°
2.6	1.5	60°

4.3.2.1 Sample preparation

In the biaxial set-up, as illustrated in Figure 4-2, two identical blocks of foam with dimensions of 5 cm (length) × 5 cm (width) × 2.5 cm (thickness) are glued to three parallel steel specimen holder plates in a symmetrical manner. The purpose of this symmetry is to avoid any bending moments during the test. For this, plates should be aligned parallel to each other.

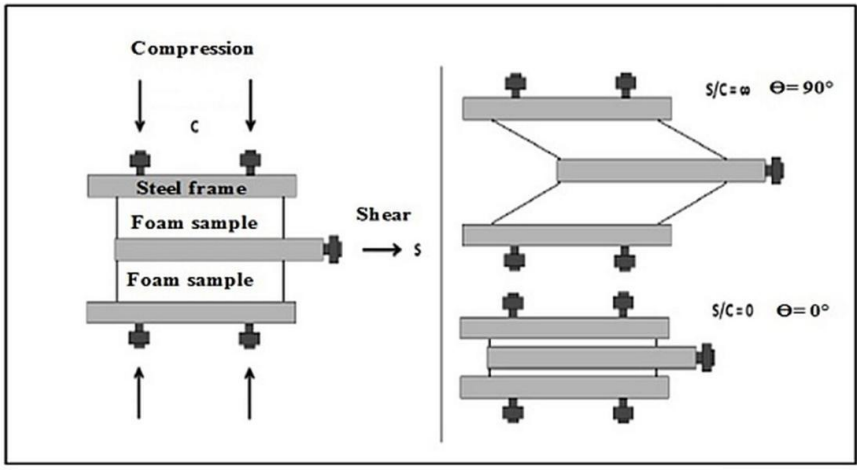

Figure 4-2: Illustration of specimen (top view) in biaxial fixture, ɵ=0° represents pure compression loading and ɵ=90° corresponds to simple shear loading.

In order to keep the three steel plates parallel, samples are cut into precise cuboids with orthogonal surfaces. Samples were glued to the test plates and fit into a special frame, as observed in Figure 4-3, to keep the plates perfectly aligned and leave the glue to harden and create the perfect bonding between the foam and steel plates. Two component fast epoxy glue (Araldite) with 5 min curing time were used for this purpose.

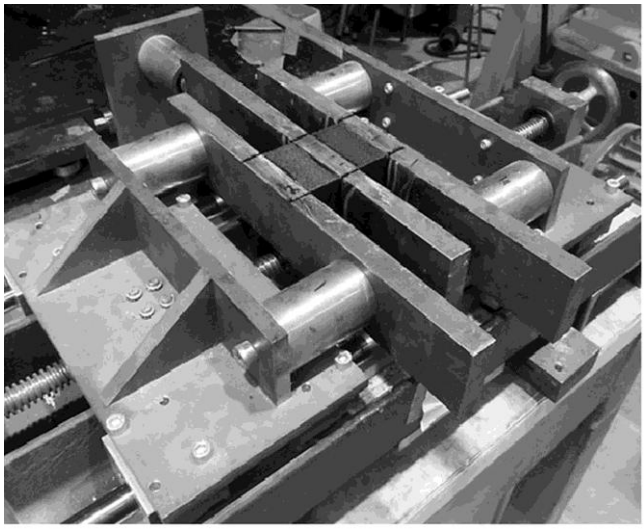

Figure 4-3: Sample preparation frame for biaxial shear-compression test.

4.3.2.2 Data acquisition

Crosshead displacements were used to calculate strains. Loads were measured separately by two independent load cells of 5 kN in both compression and shear direction. The output of the tests consists of two simultaneous shear force-shear displacement and compressive force-compressive displacement curves which are subsequently converted to stress-strain curves.

4.3.3 ESEM characterization

Micrographs of cut cross-sections of different foams were obtained using an environmental scanning electron microscope Philips XL30 ESEM FEG.

4.4 Results and discussion

In this study, the behaviour of isotropic EPS and anisotropic PES foams was investigated under uniaxial compression and biaxial shear-compression in quasi-static mode. Shear-compression experiments have been performed at four different deformation angles of 0° (pure compression), 15°, 45°, and 60°.

4.4.1 Compression test results on EPS and PES foams

Figure 4-4 (a and b) illustrates the compression behaviour of EPS and PES foams by loading in 3 orthogonal directions. All the specimens were tested at the same strain rates. As indicated in Figure 4-4, the compression behaviour of foams in quasi-static loading mode consists of three regions: (I) linear elastic up to the yield point, (II) plateau region, and (III) densification region. In Figure 4-4a, the effect of density of EPS foams on these three regions can be observed. Values of Elastic modulus, yield stress and onset of densification strain for EPS, when compressed in the 3 directions, are tabulated in table 4-2. The density variation, from 40 to 80 kg/m^3, does not only affect the elastic modulus and collapse stress but also the slope of the plateau region and strain at which densification starts. These effects are due to the change in foam microstructure with density such as the cell size and cell wall thickness. The compressive yield stress, σ_p, is defined as the intersection of the tangents of the plateau region and the elastic region. Compressive yield stresses of PES foam when compressed at A and C planes ($\sigma_{p,A}$ and $\sigma_{p,C}$, respectively) are indicated in Figure 4-4b. Moreover, as shown in Figure 4-4a, EPS foams with different densities show similar compression properties when compressed in all three orthogonal directions (x, y and z). Figure 4-4b shows the compressive curves of PES foam in the three directions. As observed, the compression stress-strain behaviour is significantly different in z direction (through the thickness direction) compared to the x and y directions. The latter shows the anisotropic behaviour of PES foam in rise direction (z) which is assumed to be due to cell elongation in z direction. This will be demonstrated further on with the help of SEM images of the cell structure.

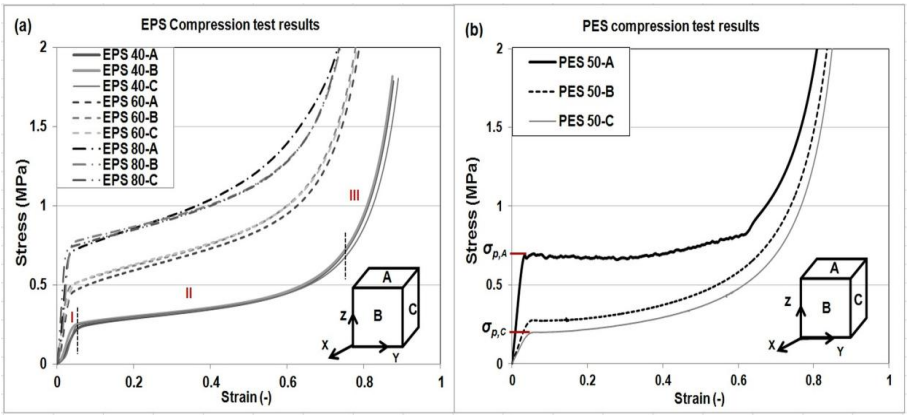

Figure 4-4: Compression graphs by loading of surfaces A, B, C: (a) EPS, (b) PES foam.

Table 4-2: Material properties and onset of densification strains of EPS foams and PES foam.

Sample code	E (MPa)	σ_y (MPa)	ε_d
PES-A	24.7±0.7	0.68± 0.01	0.70
PES-B	6.70±0.24	0.27± 0.01	0.72
PES-C	4.80±0.11	0.200± 0.004	0.72
EPS 40-A	6.5±0.5	0.23±0.02	0.80
EPS 40-B	7.1 ±1.2	0.24±0.01	0.80
EPS 40-C	8.0 ±1.4	0.24±0.01	0.80
EPS 60-A	14.9 ±1.0	0.44 ±0.02	0.75
EPS 60-B	16.4±0.5	0.49±0.02	0.75
EPS 60-C	17.0±2.0	0.51 ±0.02	0.75
EPS 80-A	26.0± 7.1	0.77±0.01	0.72
EPS 80-B	31.4 ±7.1	0.75±0.03	0.72
EPS 80-C	28.5±3.0	0.79±0.02	0.72

Figure 4-5 shows a micrograph of EPS foam. It is apparent that EPS has an isotropic cell structure approaching the equilibrium surface energy of the Kelvin cell structure.

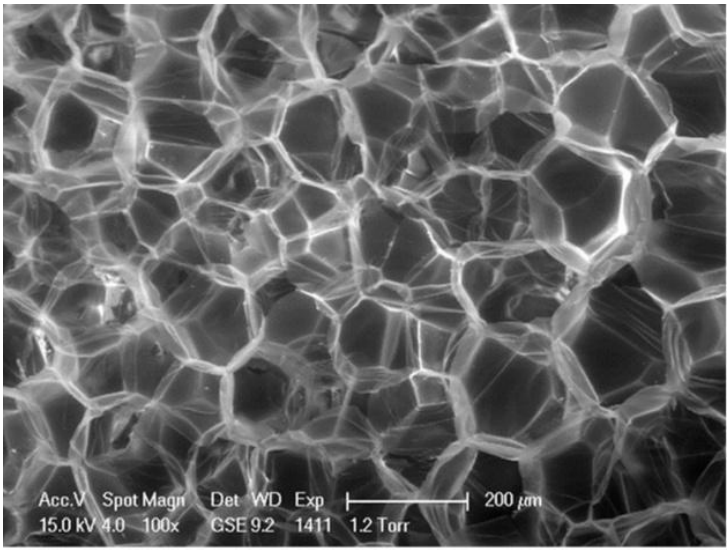

Figure 4-5: Micrograph of EPS foam, approaching the isotropy of typical Kelvin cells.

In contrast, Figure 4-6a shows the micrograph of PES in C plane. Elongated cells in z direction can be observed in Figure 4-6a. The cell geometrical anisotropy ratio, *R*, is measured by the ratio of the largest cell dimension to the smallest. A simple illustration of geometrical anisotropy ratio, R, is shown in Figure 4-6b.

The anisotropy ratio for the plastic yielding of closed cell rigid plastic foams is approximated by equation 4.1, [1]. $\sigma_{p,A}$ and $\sigma_{p,C}$ stand for the compressive yield stresses when the foam specimen is compressed on plane A and C, respectively. $\sigma_{p,A}$ and $\sigma_{p,C}$ for PES foam are indicated in Figure 4-4.

$$\sigma_{p,A}/\sigma_{p,C}=2R/\left(1+(1/R)\right) \quad (4.1)$$

For PES foam, $\sigma_{p,A}/\sigma_{p,C}$ is measured at around the value of 3.4 which leads to $R \approx 2.4$.

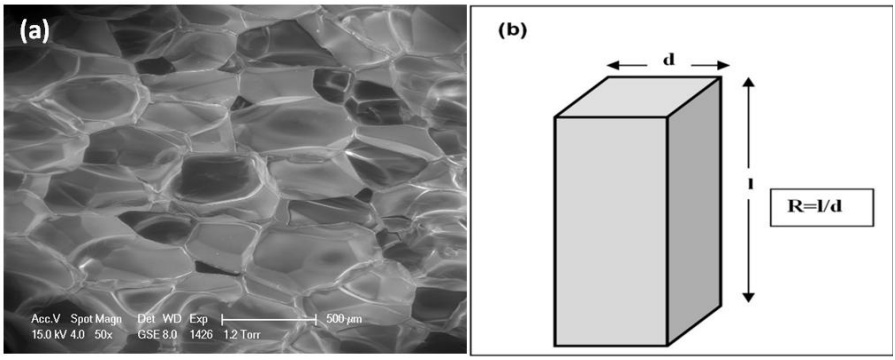

Figure 4-6: (a) Micrograph of PES at cross section of the C plane, (b) simple illustration of a single foam cell, d and l are dimensions of the cell and geometrical anisotropy ratio, R is given by l/d.

4.4.2 Combined shear-compression test results

4.4.2.1 Reproducibility of the test results

In order to illustrate the reproducibility of the tests, Figure 4-7 shows four repeat experiments which were conducted on EPS40 foams under a deformation angle of 45°. Results of the repeat tests show only a small deviation in stress levels, with standard deviation of ±0.01 MPa for the compression graph and ±0.008 MPa for the shear graph, indicating the good reproducibility of the experiments; all foam tests were conducted with 4 repeats.

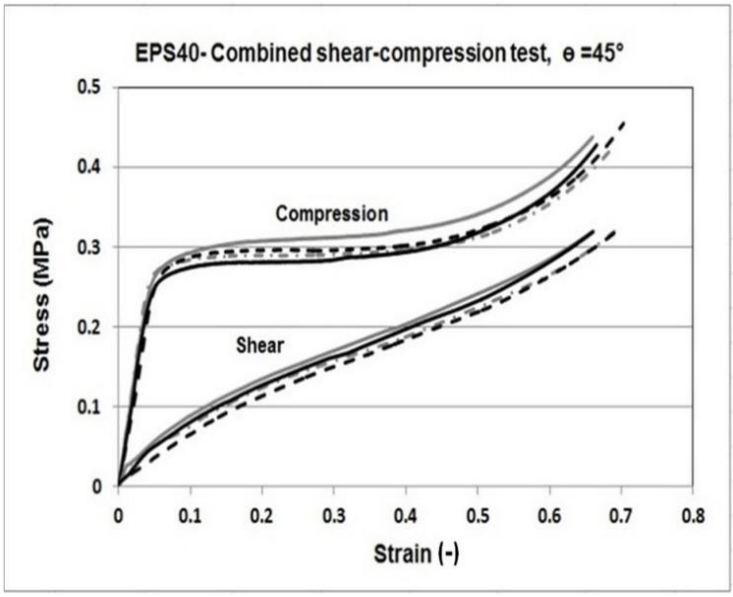

Figure 4-7: Shear-compression graphs of EPS40 at ɵ=45°, experiments were performed in 4 fold.

4.4.2.2 Effect of foam density and deformation angle on stress-strain response

The stress–strain response for different densities of EPS foam under a deformation angle of 45° is shown in Figure 4-8 (a and b) for both the compression and shear components separately. As observed in the compression curves, both the yield stress and plateau stress increase with density, whereas the strain at onset of densification decreases with an increase in foam density from 40 to 80kg/m^3. It is also observed in the shear graph that the shear stress values and the slope of the shear curve, at any given strain, increase with foam density.

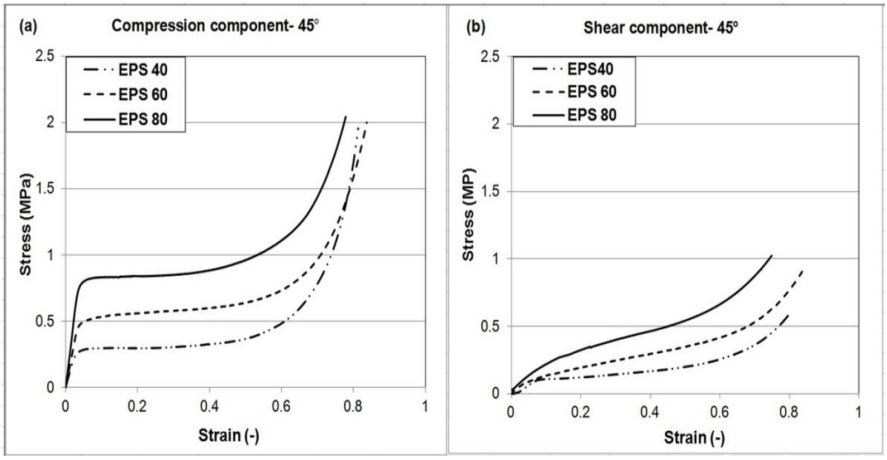

Figure 4-8: Biaxial test results of EPS foam, at deformation angle of 45°, with three different densities: (a) compressive stress-strain, (b) shear stress-strain.

Figure 4-9 (a and b) show the compressive and shear stress strain curves of EPS60 under three different angles of deformation. As observed in the compressive curves, the initial stiffness in the elastic region, yield stress, overall stress values and slope in the plateau region decrease with increasing the deformation angle.

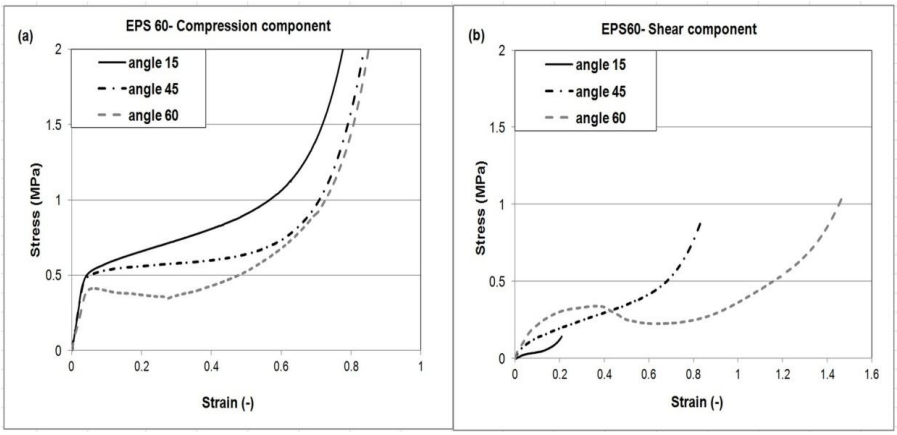

Figure 4-9: Biaxial test results of EPS60 at three different deformation angles of 15°, 45°, and 60°; (a) compressive stress-strain, (b) shear stress-strain.

This effect can be attributed to the shear load contributing to easier buckling in the compressive deformations when shear and compressive deformations are applied simultaneously. This leads to earlier onset of buckling in cell walls and struts, which can lead to lower elastic moduli and much earlier collapse/yield of the cells. This explains the significant decrease in plateau stress levels in Figure 4-9a by change of deformation angle. On the other hand, the initial slope of the shear curve and the plateau region increase at more shear dominant angles. This is due to exactly the opposite effect, specifically at lower shear angles the dominant deformation is in compression. Increased compression deformation assists the cell wall bending needed for shear deformation which can then occur at lower stresses.

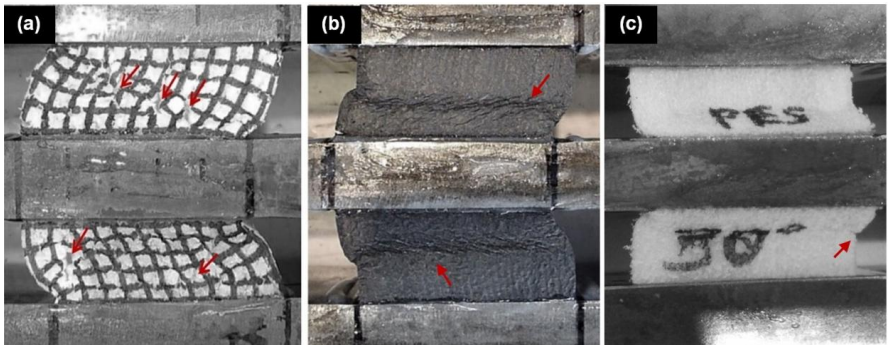

Figure 4-10: (a) Occurrence of micro cracks in EPS60 when deformed at angle 60°, as shown by the red arrows, (b) yielding of EPS80 when deformed at 60°, (c) yielding of anisotropic PES foam. Pictures were taken during testing when the dip in stress occurred.

A sudden drop in the shear and compressive stress curves, at a deformation angle of 60° (see Figure 4-9), can be related to the occurrence of micro-cracks in the sample as shown by red arrows in Figure 4-10a. In EPS80 yielding occurs in the central zone of the sample at an angle of 60°, as shown in Figure 4-10b. Figure 4-10c also shows the local yielding of PES foam. Similar results for the stress-strain curves are observed for anisotropic PES foam, when loaded at an angle of 60° (see Figure 4-11).

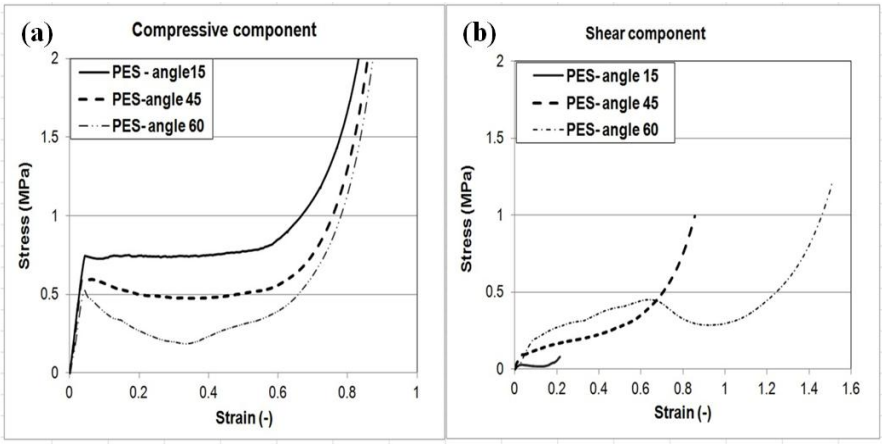

Figure 4-11: Biaxial test results of PES foam at three different deformation angles of 15°, 45°, and 60°; (a) compressive component, and (b) shear component.

4.4.2.3 Energy absorption

In applications such as packaging or occupant safety materials, the energy absorption capacity of the foam, up to a certain tolerable stress limit, is of most interest. To understand how varying the deformation angle affects the energy absorption capacity of the foams, the following analysis has been carried out. All the absorbed energies have been calculated up to the onset of densification. The strain at onset of densification is defined by the intersection of the tangents of the plateau region and the densification region in the compression graph [21]. For calculating the absorbed energy until the onset of densification, the curves are first analysed over the time domain in order to pinpoint the time at which the compressive curve reaches the onset of densification designated by point ***A*** (see Figure 4-12a). The corresponding point in the shear stress versus time curve is indicated by point ***B*** as shown in Figure 4-12a. The compressive and shear stress at the onset of densification is indicated by σ_A and τ_B, respectively. The compressive and shear stress-strain curves are then plotted as shown in Figure 4-12b. Subsequently, corresponding points C and D with respective stress values of σ_A and τ_B are marked in Figure 4-12b. The areas under the compressive and shear stress-strain curves up to points C and D are then integrated and named as compressive energy and shear energy, respectively.

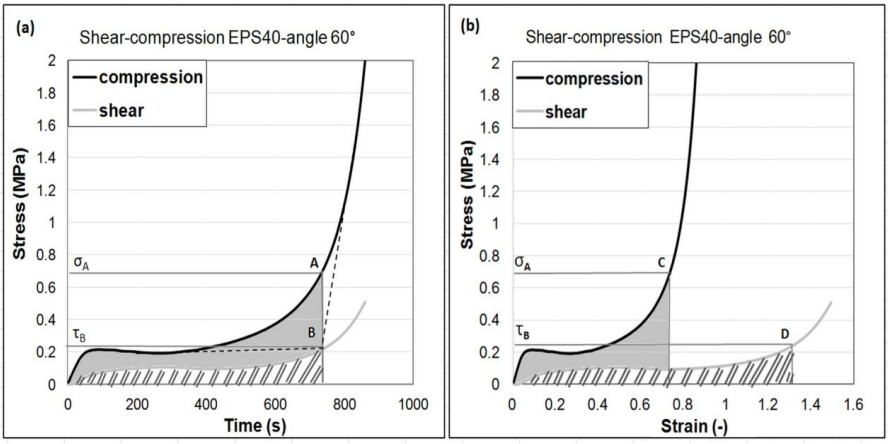

Figure 4-12: (a) Typical shear and compression stress-time curves for EPS 40; the onset of densification points are marked in both compressive and shear stress-time graphs as points A and B, (b) Energy under the stress-strain curves for both shear and compressive components until corresponding onset-of-densification points in strain domain, (C and D).

As shown in Figure 4-13 (a and b), in biaxial loading, the energy absorption capacity of EPS foams, in combined shear-compression loading, is a function of deformation angle as well as of foam density. A systematic increase in energy absorption with density for both compressive and shear energy absorption is observed for different angles. For each EPS density, the amount of energy absorption in compression decreases with increasing the angle of displacement towards shear dominant angles (from 15° to 60°). This is due to a decrease of the plateau stress with increase of deformation angle; the plateau region is the main region of energy absorption in foams. In contrast, shear energy absorption, for all the different densities, increases for shear dominant angles. This is due to the higher shear stress levels.

However, as observed in Figure 4-14, for the EPS foams, there is not a clear dependency of total energy absorption (which is a summation of shear and compressive energy) on angle of displacement for different densities. This can be attributed to the isotropic microstructure of EPS bead foams which leads to isotropic mechanical behaviour.

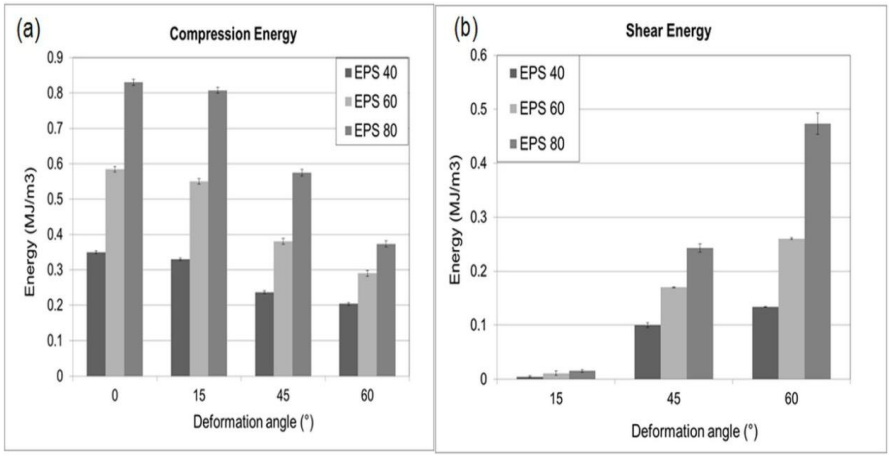

Figure 4-13: (a) Compressive energy absorption, (b) shear energy absorption of isotropic EPS foams, with densities of 40, 60 and 80 kg/m3, versus deformation angle.

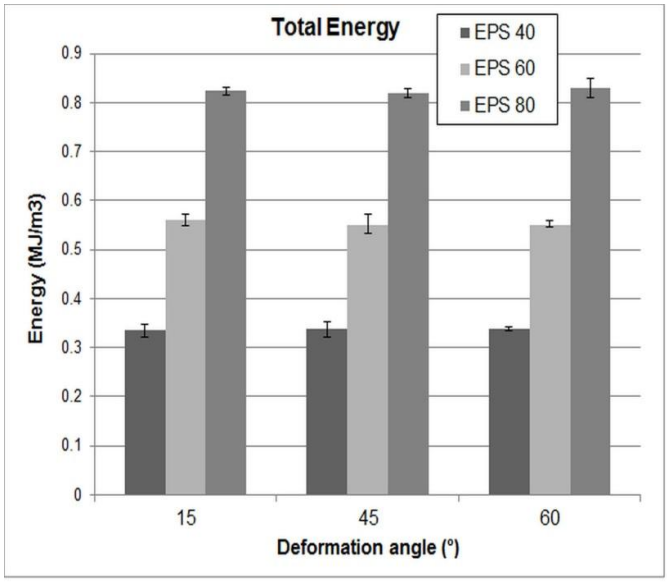

Figure 4-14: Total energy absorption of EPS foams with different densities versus deformation angle up to onset of densification.

In contrast to isotropic EPS, the total energy absorption in anisotropic PES foam demonstrates a direction dependency (Figure 4-15). It is interesting to note that the PES and EPS compared in this Figure are of similar relative densities (0.38 and 0.37 respectively).

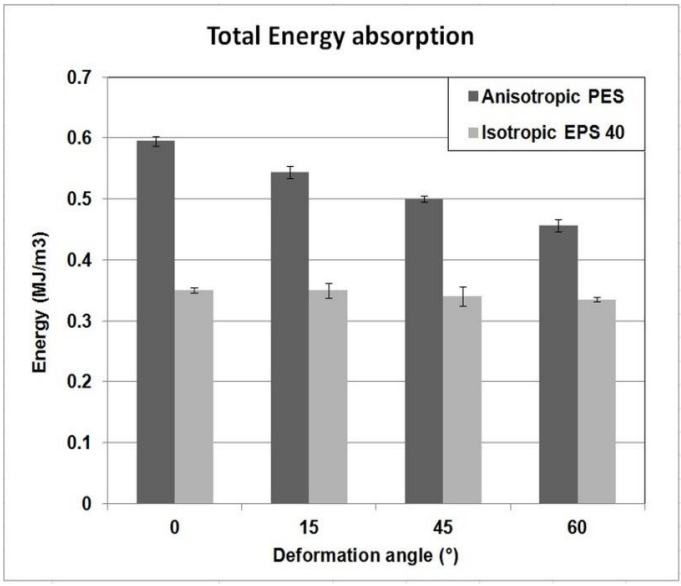

Figure 4-15: Total energy absorption of anisotropic PES50 compared to isotropic EPS 40 at different deformation angles.

The individual compressive and shear energies as function of deformation angle for PES foam are given in table 3. The data demonstrate that the energy absorption capacity in anisotropic foams is direction dependent, and larger than that of the EPS of similar relative density. The highest energy absorption occurs when the direction of the load is in line with the direction of cell elongation. The latter means that in energy absorbing applications, care should be taken how to locate the direction of anisotropy in a certain structural part to achieve the maximum energy absorbing capacity.

Table 4-3: Compressive and shear energy absorption of PES foam for different deformation angles [MJ/m³]; total energy values are plotted in Figure 4-15.

Deformation angle (ɵ)	**0°**	**15°**	**45°**	**60°**
Compression energy (MJ/m³)	0.59	0.55	0.35	0.20
Shear energy (MJ/m³)	0	0.004	0.15	0.26
Total energy (MJ/m³)	0.59	0.554	0.50	0.46

To explain the high energy absorption for anisotropic foam in the 0° direction, it is useful to check the data in table 4-3. As shown in equation 4.1, the plastic yield stress and consequently the plateau stress in compression for anisotropic foam is a function of almost twice the anisotropy ratio (R) of the cells. This leads to particularly high compressive stresses and thus compressive energy absorption at low deformation angle. It is apparent from the data in table 4-3 that the shear energy absorption at higher deformation angles, cannot fully compensate for the strong reduction in compressive energy absorption.

4.5 Conclusions

In this chapter, a combined shear-compression set-up was presented for quasi-static testing of foams. The advantage of this set-up is that any deformation angle can be mimicked by changing the ratio of shear displacement rate versus compression displacement rate. Moreover, this set-up enables independent measurement of shear and compressive components of the force. Combined shear-compression behaviour of EPS foams with three different densities and also anisotropic polyethersulfone foam (PES, anisotropy ratio ~2.4) were studied. The energy absorption capacity of the foams, up to the onset of densification point, was calculated for three different deformation angles. Effects of deformation angle and foam density on the biaxial stress-strain behaviour and energy absorption were investigated. Results show that by changing the deformation angle from pure

compression (ɵ=0°) to more shear-dominant deformation angles, the total energy absorption value of isotropic EPS foams remains constant. However, in case of the anisotropic PES foam, the total energy absorption up to the onset of densification decreases at more shear dominant deformation angles. In other words, the energy absorption capacity in anisotropic foams unlike isotropic ones is dependent on the loading direction. This means that when designing structural parts with energy absorbing functions, the exact positioning of the anisotropy direction of the foams can affect the energy absorbing performance of the part. This study concludes that to obtain the highest energy absorption performance, the direction of the elongated foam cells should be in line with the dominant loading direction. For helmets, the considerations are different; here one needs to have sufficient energy absorption in any direction, but one also needs to mitigate peak tangential forces. Therefore, for any oblique loading angle, the direction of anisotropy in the foam liner would be best along the radial direction (perpendicular to the surface of the head), so as to have sufficient shear deformation. The weakest direction in shear of the anisotropic foam is thus placed parallel to the skull surface, or more correctly formulated perpendicular to the radial direction of the head.

4.6 References

1. Gibson, L. and M. Ashby, *Cellular solids : structure & properties - 2nd ed.*1997, Cambridge, UK: Cambridge University Press.

2. Reignier, J., Gendron, R. Mechanical anisotropy of PS/CO2 microcellular foam sheet prepared by foaming extrusion. Journal of Cellular Plastics, 2016. 0(0): 1–15.

3. Tissandier, C., González-Núñez, R., Rodrigue, D. Asymmetric microcellular composites: Mechanical properties and modulus prediction Journal of Cellular Plastics, 2016. 52(4): p.365–398.

4. Kuboki, T., Mechanical properties and foaming behaviour of injection molded cellulose fiber reinforced polypropylene composite foams. Journal of Cellular Plastics, 2014. 50(2): p.129–143.

5. Arcan, M., Hashin, Z., Voloshin, A. A method to produce uniform plane-stress states with applications to fiber-reinforced materials. Experimental Mechanics, 1978. 18 (4): p.141-146.
6. Gdoutos, E.E., Daniel, I.M. Failure of cellular foams under multiaxial loading. Compos Part A, 2002. 33(2): p.163–76.
7. Li, Q.M., Mines, R.A.W., Birch, R.S. The crush behaviour of Rohacell-51WF structural foam. International Journal of Solids and Structures, 2000. 37(43): p.6321–41.
8. Doyoyo, M., Wierzbicki, T. Experimental studies on the yield behaviour of ductile and brittle aluminum foams. International Journal of Plasticity, 2003. 19(8): p.1195-1214.
9. Mohr, D., Doyoyo, M. Experimental investigation on the plasticity of hexagonal aluminum honeycomb under multiaxial loading. Journal of Applied Mechanics, 2004. 71(3): p.375-385.
10. Benderly, D., Putter, S. Characterization of the shear/compression failure envelope of Rohacell foam. Polymer Testing, 2004. 23(1): p.51-57.
11. Kintscher, M., Kärger, L., Wetzel, A., Hartung, D. Stiffness and failure behaviour of folded sandwich cores under combined transverse shear and compression. Composite Part A, 2007. 38(5): p.1288-1295.
12. Hong S.T., Pan, J., Tyan T, Prasad P. Dynamic crush behaviours of aluminum honeycomb specimens under compression dominant inclined loads. International Journal of Plasticity, 2008. 24(1): p.89-117.
13. Taher, S.T., Thomsen O.T., Dulieu-Barton, J.M., Zhang, S. Determination of mechanical properties of PVC foam using a modified Arcan fixture. Composite Part A, 2012. 43(10): p.1698 1708.
14. Hou, B., Ono, A., Abdennadher, S., Pattofatto, S., Li, Y., Zhao, H. Impact behaviour of honeycombs under combined shear-compression. Part I: experiments. International Journal of Solids and Structures, 2011. 48 (5): p.687–697.
15. Hou, B., Pattofatto, S., Li, Y., Zhao, H. Impact behaviour of honeycombs under combined shear-compression. Part II: analysis. International Journal of Solids and Structures, 2011. 48(5): p.698–705.
16. Tounsi, R., Markiewicz, E., Haugou, G., Chaari, F., Zouari, B. Dynamic behaviour of honeycombs under mixed shear-compression loading: experiments and analysis of combined

effects of loading angle and cells in-plane orientation. International Journal of Solids and Structures, 2016. 80: p.501–511

17. Ashab, A.S.M., Dong, R., Lu ,G.X., Wong, Y.C. Quasi-static and dynamic experiments of aluminum honeycombs under combined compression-shear loading. Material and Design, 2016. 97: p.183–194.
18. Zhou, Z., Wang, Z., Zhao, L., Shu, X. Experimental investigation on the yield behaviour of Nomex honeycombs under combined shear-compression. Latin American Journal of Solids and Structures, 2012. 9(4): p.515–530.
19. Zhang, J., Jin, T., Wang, Z., Zhao, L. Experimental investigation on yield behaviour of PMMA under combined shear–compression loading. Results in Physics, 2016. 6: p.265–269.
20. Vanden Bosche, K. Development and characterization of novelanisotropic foam for bicycle helmets, 2016, PhD Thesis, Katholieke Universiteit Leuven: Leuven.
21. Li, Q.M., Magkiriadis, I., Harrigan, J.J. Compressive Strain at the Onset of Densification of Cellular Solids. Journal of Cellular Plastics, 2006. 42: p.371–392.

Chapter 5

Introducing anisotropy in foams at macro level

Adopted from: Yasmine Mosleh, Bart Depreitere, Jos Vander Sloten, Jan Ivens. Decoupling shear and compression properties in composite polymer foams by introducing anisotropy at macro level. *Journal of reinforced plastics and composites*, 2018. 37 (10): p.657-667.

5.1 Introduction

In general, mechanical anisotropy in foams has a geometrical origin. It is the result of elongation of the foam cells in a particular direction, resulting in the directional dependence of the material properties. The cell shape anisotropy is measured by the ratio of the largest cell dimension to the smallest [1]. The cells of polymer foams tend to be elongated in the direction of foaming. The anisotropy in polymer foams can thus be induced via specifically designed processing methods [2-5]. However, it should be noted that achieving high level of anisotropy in the foam microstructure through a chemical foaming process is not straightforward, [5].

In this chapter, the composite foam concept is proposed to introduce mechanical anisotropy in a foam at the ''macro level'' by combining two different densities of a foam in layered and cylinder/matrix configurations. For this, in the first step, layers of EPS foams with two different densities (high and low density) are combined with each other, in two configurations namely ''parallel'' and ''series''. Parallel

means the layers are arranged parallel to the normal direction of the foam liner (direction of compression force) and series means the layers are arranged perpendicular to the normal direction. In this concept, the anisotropy in the foam is created without changing the thickness or overall density of the foam. Moreover, the level of anisotropy can be controlled and tailored in this approach. The compression, linear impact and biaxial combined shear-compression properties of layered composite foams are investigated and compared with single layer homogenous EPS foam with equivalent density and thickness. It will be shown that shear and compression resistance of the composite foam structure can be decoupled and that the shear resistance can become independent from the overall foam density. However, the compression resistance in the composite foam seems to be dependent on the overall density of the composite foam structure. Through a parametric study, it is observed that parameters such as the number of layers in the composite foam structure and the density difference between the high and low density foam layers, can affect the level of anisotropy and subsequently control the extent of decoupling of the shear and compression properties. Finally an optimised composite configuration namely cylinder/matrix is proposed for head protection applications e.g. in helmets, which will be elaborated in chapter 7.

5.2 Materials

5.2.1 Expanded polystyrene foam

Expanded Polystyrene bead foams (EPS) with actual densities of 40±3, 80±3, 100±4, and 120±4 kg/m^3 were sourced from Kemisol and Lazer Sports NV, both located in Antwerp (Belgium), in shape of blocks with a thickness of 25 mm. These foams are named EPS40, EPS80, EPS100, and EPS120, respectively.

5.2.2 Composite foam sample preparation

5.2. 2.1. Composite foam: layered configurations

Composite foams were prepared by combining discrete layers of EPS foam with two different densities (high and low density) in two configurations namely ''parallel'' and ''series'' as illustrated in Figure 5-1. Series here implies that the layers are arranged perpendicular to the direction of the compression force (indicated by a red arrow in Figure 5-1) and parallel means that the layers are arranged parallel to the direction of the compression force.

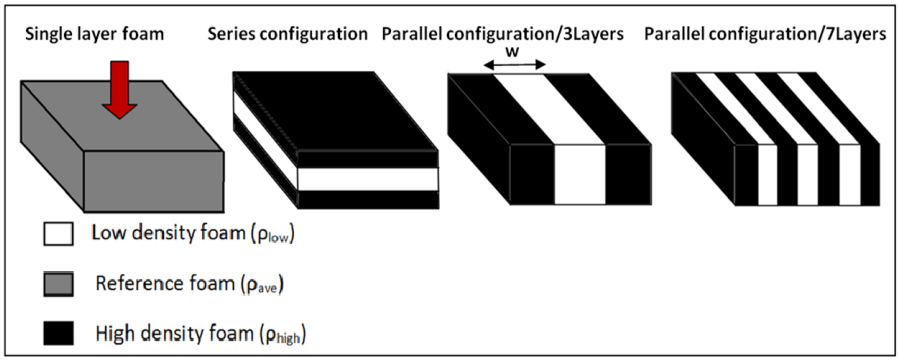

Figure 5-1: Illustration of single layer homogenous foam and layered composite foams with ''series'' and ''parallel'' configurations; composite foams with parallel configuration consist of 3 and 7 layers where foam layers are positioned in parallel with the direction of compression loading, indicated with a red arrow.

Composite foams with series configuration consist of three layers as shown in Figure 5-1 and they were prepared using EPS120 as high density and EPS40 as low density foam. Overall density of the composite foams with series configuration was aimed to be 80 kg/m^3. For this, the volume fraction for EPS120 and EPS40 in the composite foam sample is 50 %, respectively which means that for realizing the series configuration shown in Figure 5-1, the EPS40 layer is two times thicker than the EPS120 layers. The composite foam with series configuration in this chapter is compared to single layer homogeneous EPS foam with overall density of 80 kg/m^3.

For preparing composite foam with parallel configuration, EPS120 and EPS100 were chosen as high density foams and EPS40 as low density foam. Composite foams with parallel configuration were prepared with overall density of 80 or 100 kg/m^3 and they were compared to single layer homogeneous EPS foam with densities of 80 and 100 kg/m^3, respectively.

All the different composite foams with parallel configuration with their coding, aimed overall and actual densities, the constituent foams, and the number of layers of constituent foams are listed in table 5-1. To calculate the volume fraction of each foam component, a rule of mixture was used which is given in equation 5.1. In equation 5.1,

$\rho_{overall}$, ρ_{high}, and ρ_{low} stands for aimed overall density, density of high density foam, and density of low density foam, respectively. v_{high} is the volume fraction of high density foam. v_{low} stands for the volume fraction of low density foam and equals to (1-v_{high}).

$$\rho_{overall} = \rho_{high} \cdot v_{high} + \rho_{low} \cdot \left(1 - v_{high}\right) \quad (5.1)$$

The layers, in both series and parallel configurations, are adhered to each other using a Kip® 342 double-sided adhesive tape. The reason for using this tape was that it did not affect the impact properties with mechanisms such as artificial stiffening by a cured adhesive layer. This was verified by testing EPS80 foam pieces bonded together with the tape and no difference with non-bonded material was observed. In order to have cut layers with smooth surfaces, the layers were cut into desirable dimensions using a hot-wire foam cutter. Single layer homogenous EPS80 was considered as reference material and is used prevalently as liner in commercial bicycle helmets.

5.3 Test methods

5.3.1 Compression experiment

Compression tests in quasi-static mode were performed according to ASTM standard D1621/94 on a universal tensile testing machine (Instron). The compression experiments were displacement controlled and foam samples were compressed between two steel plates at the rate of 2.5 mm/min. Samples were cut into cuboids of 5 cm (length) × 5 cm (width) × 2.5 cm (thickness). All experiments were performed at room temperature and the tests were repeated at least three-fold.

Table 5-1. Different composite foams (all of them have parallel configuration) with their coding, overall density, number of layers and width of individual layers (w), and volume fraction of each foam constituent (v).

Composite foam code	$\rho_{overall}$ (kg/m^3)	ρ_{actual} (kg/m^3)	Layer number	Layer width, w (cm)	ν
EPS 100-40-100/3L(80)	80	80±4	3	5	1
EPS100			2	1.67	0.67
EPS40			1	1.67	0.33
EPS 120-40-120/3L(80)	80	81.2±0.2	3	5	1
EPS120			2	1.25	0.5
EPS40			1	2.5	0.5
EPS 120-40-120/3L(100)	100	98.0±1.0	3	5	1
EPS120			2	1.88	0.75
EPS40			1	1.25	0.25
EPS 120-40-120/7L(100)	100	97.0±3.0	7	5	1
EPS120			4	0.94	0.75
EPS40			3	0.42	0.25

5.3.2 Combined shear-compression experiments

The combined shear-compression experiments were used to benchmark different composite foam configurations against single layer EPS foam of equivalent density in oblique loading. Static bi-axial combined shear-compression tests were carried out at least three-fold on a biaxial test bench which is shown in Figure 5-2a. In biaxial testing, two independent displacement actuators apply shear and compressive displacements on foam samples simultaneously. The directions of compression and shear displacements are indicated by a black and red arrow in Figure 5-2a, respectively. In this set-up, foam specimens are placed between three parallel steel plates in a symmetrical manner. The foam samples are perfectly bonded to the steel plates using instant epoxy glue (Araldite). Experiments were performed at deformation angle of 45°, meaning similar shear and compression deformation rates of 2 mm/min were applied to the foam specimens. The angle of 45° was chosen to have a balanced contribution of both shear and

compression loading. The experiments were performed at room temperature. The combined shear-compression test set-up is described in more detail in chapter 4 of this thesis.

5.3.3 Drop weight impact experiment

Linear impact tests were performed by a drop weight impact tower, shown in Figure 5-2b.

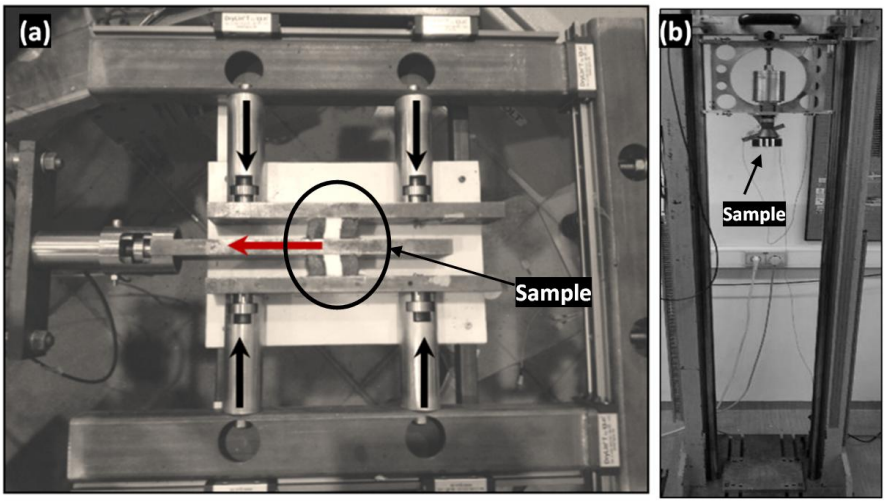

Figure 5-2. (a) Biaxial shear-compression set-up whilst testing EPS100-40-100/3L-parallel composite sample; compression and shear loading directions are shown by black and red arrows, respectively (view from top of the instrument); (b) Falling weight impact set-up, composite foam sample (with parallel configuration) is taped to impact projectile.

The impactor was equipped with a flat steel projectile with a circular cross section of 50 mm in diameter. The foam specimens were in the shape of cuboids with dimensions of 70mm (length) × 70mm (width) × 25mm (thickness). Impact tests were performed for two input energies of 66 J and 40 J. For input energy of 66J, the drop mass and drop height were set to 4.5 kg and 1.5 m, respectively. A drop mass and drop height of 2.37 kg and 1.2 m, respectively, resulted in input impact energy of 40 J. The foam samples were taped to the flat tub of the impactor (as shown in Figure 5-2b) and subsequently dropped on a flat anvil. For calculations of layer sizes in composite foam, care was taken that the area which was impacted by the projectile had the overall density of

the equivalent single layer EPS foam (80 or 100 kg/m^3) against which the impact performance of composite foams are benchmarked.

5.4 Results and discussion

5.4.1 Single layer EPS foams

5.4.1.1 Effect of density of EPS foam on static compression and linear impact behaviour

The compression behaviour of foams in quasi-static loading mode consists of three regions: (I) *linear elastic* up to the yield point; (II) *Plateau region* in which deformation continues at relatively constant stress level known as plateau stress. Most energy absorption occurs in the plateau region, hence the length of the plateau region and the plateau stress level are the defining factors in the stress absorption capability of a foam; (III) *Densification region* in which the stress rises steeply and the foam begins to respond as a compact solid. Figure 5-3a compares compressive stress-strain curves of EPS foams of three different densities (80, 100 and 120 kg/m^3). As observed in the compression curves, both yield stress and plateau stress increase with increasing the density while the densification strain decreases. Figure 5-3b presents force-time curves obtained from linear drop weight impact with input energy of 66J. By increasing the foam density, the peak force increases and the time duration of impact decreases as does the deformation of the foam, whilst all three foams absorb the same amount of energy (here all three foams can absorb the entire input energy of the impact). The time duration is related to the measured deformation. The shortening of the time duration means a decrease in maximum foam deformation during impact due to increase in the foam density. Energy absorption in EPS is controlled by microscopic and macroscopic phenomena. At microscopic level, EPS energy absorption can be optimized by tailoring the pre-expanded bead size as well as the size of elementary cells within the beads. At macroscopic level, the foam density is the crucial parameter affecting energy absorption capability and the acceleration values. By comparing the compression stress strain curves and linear impact force levels, it can be observed that the plateau stress value is linked to the peak stress level. Increase in plateau stress level for higher density foam leads to higher peak stress values in linear impact and a shorter impact duration.

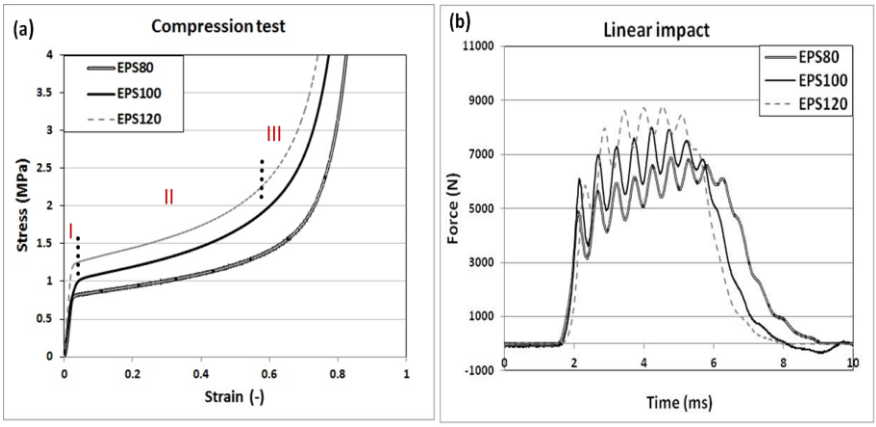

Figure 5-3: (a) Stress-strain curves obtained from quasi-static compression tests and (b) force time-curves of linear impact loading with input energy of 66J, for EPS foam with three different densities of 80, 100, and 120 kg/m^3.

5.4.2 Evaluation of layered composite foam: series configuration versus parallel configuration

5.4.2.1 Quasi-static compression behaviour

Figure 5-4a-b demonstrate EPS120-40-120 composites with parallel and series configurations both consisting of three layers and overall density of 80 kg/m^3. The stress-strain curves of composite foams and single layer EPS80, obtained from quasi-static compression experiments, are plotted in Figure 5-4c. It can be observed that the parallel configuration demonstrates similar macroscopic behaviour in comparison to single layer EPS80. It can be concluded that in a composite foam with a parallel configuration, the compressive response is dominated by the overall density. However, the series configuration demonstrates a step-wise behaviour in compression. For the series configuration, the compressive stress-strain curve comprises of two stress plateaus; the first stress plateau is related to the yielding of the EPS40 layer and the second plateau stress is the result of the yielding of the EPS120 layer. It should be noted that the length of each plateau region is directly related to the thickness of the corresponding layer. Figure 5-4d shows comparative curves of absorbed energy versus stress for each configuration. It can be observed that the series

configuration initially shows a gradual tendency to absorb energy whilst the parallel configuration, similar to homogenous EPS80, does not dissipate energy before a stress of 0.78 MPa. However, the overall energy absorption of the series configuration is less than for the parallel configuration (see Figure 5-4d). Therefore, it is expected that in linear impact where the loading is mainly in compression mode, the parallel configuration will be more efficient for absorbing the energy whilst experiencing lower peak forces which can be translated to peak acceleration.

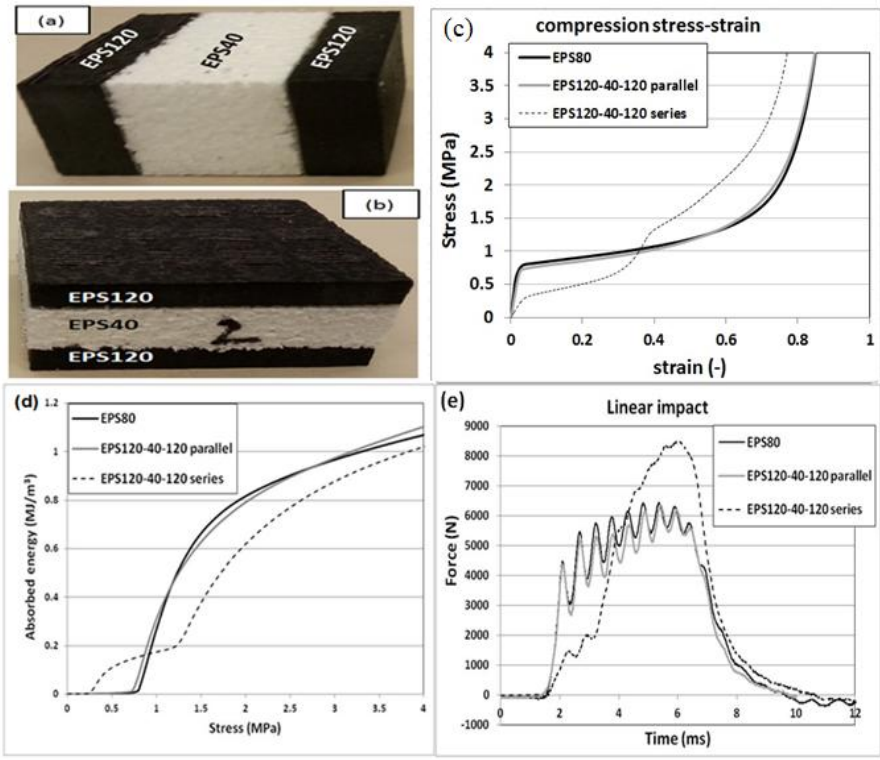

Figure 5-4: Layered composite foam comprised of EPS40 and EPS120 in (a) parallel configuration, and (b) series configuration.; (c) Stress-strain curves of composite foams in series and parallel configurations versus EPS80 obtained from quasi-static compression test; (d) Comparative curves of absorbed energy versus compressive stress for composite foams and single layer EPS80; (e) Force-time curves of layered foams versus EPS80, obtained from linear impact experiments with an impact velocity of 5.4 m/s.

5.4.2.2 Linear impact behaviour

One of the main functions of polymer foams in head protection is energy absorption during impact. Impact is a dynamic event and hence for a better evaluation of the foam performance in real applications, the foams are also studied in impact.

Force versus time curves obtained from impact experiments are plotted in Figure 5-4e. Similar to the quasi-static compression behaviour, the series configuration demonstrates a step-wise increase in force, attributed to the EPS40 and EPS120 layers respectively. As observed, for the same input energy of 66J, the series configuration experiences higher peak force and hence acceleration than homogenous EPS80. However, the layered foam with the parallel configuration follows the same trend as homogenous EPS80 in linear impact. Both the parallel configuration and the EPS 80 show a characteristic oscillatory behaviour during impact (Figure 5-4e). The reason for the occurrence of the oscillations in impact curves (in higher energy impact curves) is not yet fully understood but there are two hypotheses for this. One possible reason could be related to vibrations of the impact set-up. The second possible reason could be related to the material itself. In the framework of another project, impact experiments were performed on EPP foams using the same impact set-up with similar energy levels and similar oscillations were observed in those impact curves; however, it was observed that when the same EPP foam sample was impacted for the second time, the oscillations were no longer present in the second impact curves. EPP foams demonstrate a partially recoverable behaviour (excellent for multiple impact performance) unlike EPS foam which is a crushable foam (it means that the deformations surpassing the linear region will not disappear). This means that the oscillations might also come from the bending and yielding of inter-connected bead regions in the EPS foam. Apparently, the series configuration crushes in a different manner, which may be attributed to the stepwise deformation with the soft EPS40 material deforming and densifying first. It can be concluded that the parallel configuration outperforms the series configuration in linear impact and shows similar behaviour to EPS80. The behaviour of the parallel configuration in linear loading is dominated by overall density. Therefore, the parallel configuration is chosen as the suitable arrangement for oblique loading.

5.4.3 Further evaluation of composite foam with parallel configuration

5.4.3.1 Effect of density difference between high density and low density foam layers

In this section, subsequently the effect of density difference between low and high density foam layers of ''parallel composite foam'' in linear and biaxial loading is investigated.

5.4.3.1.1 Static compression and linear impact test

Figure 5-5a demonstrates the compression behaviour of layered composite foams namely, EPS120-40-120/3L (80) and EPS100-40-100/3L (80) both consisting of three layers and overall density of 80 kg/m^3. For each material a representative curve is shown. Standard deviations from at least 3 repeat measurements showed standard deviations on yield and plateau stress of less than 3%, so error bars were omitted from the graphs. Samples of EPS120-40-120/3L (80) and EPS100-40-100/3L (80) are shown in Figure 5-5b-c, respectively, before and after compression.

As observed in Figure 5-5a, the behaviour of the composite foams in the linear and plateau regions is very similar to EPS80. Only slightly earlier onset of densification can be observed in the composite foams in comparison to EPS80. This indicates that the uniaxial compressive behaviour of composite foam is dominated by the overall density of the composite foam.

Figure 5-5d-e demonstrate comparative impact curves of the composite foams for two different input energies of 40 and 66J, respectively. The impact curves of the composite foams and EPS80 are almost identical which could be expected from the almost identical static compression behaviour. This means in parallel layered composite foam, linear loading is dictated by overall density and not by structural anisotropy which is created by the composite concept. It can also be concluded that layered composite foam with similar density and thickness as single layer foam can have similar mechanical performance and impact resistance, when loaded parallel to the layers. Further analysis on parallel composite foam behaviour will be given in section 5.5 using analytical equations.

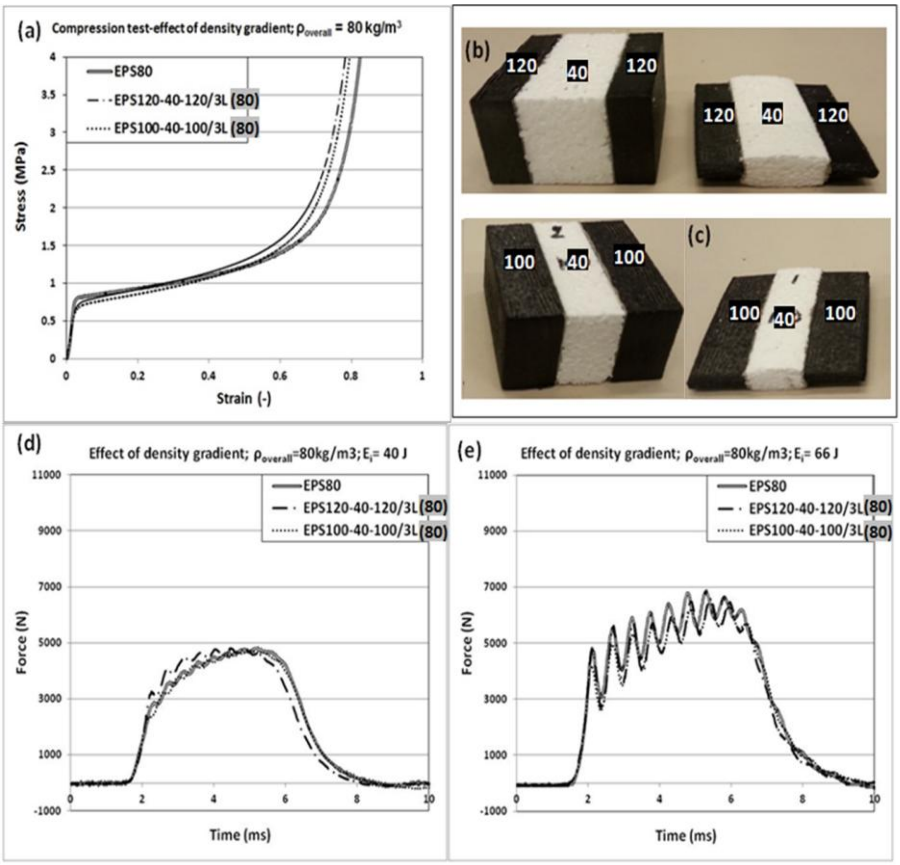

Figure 5-5: (a) Stress-strain curves obtained from quasi-static compression tests for EPS120-40-120 and EPS100-40-100 composite foams consisting of three layers with overall density of 80 kg/m3; (b) EPS120-40-120/3L(80) and (c) EPS100-40-100/3L(80) composite foam samples before and after compression; (d-e) Comparative impact force-time curves of EPS120-40-120/3L(80) and EPS100-40-100/3L(80) composite foams and EPS80, for input energy of 40 and 66 J, respectively.

5.4.3.1.2 Biaxial shear-compression test

Figure 5-6a-b, respectively, show the compressive and shear stress-strain curves of composite foams versus EPS80 in a comparative manner, as measured in a combined shear-compression test under a deformation angle of 45°. Figure 5-6c illustrates the orientations of the

shear (with red arrows) and compression (with green arrows) which are applied on the composite foams in the biaxial shear-compression experiment. The reason that the direction of shear is only in x direction and the shear resistance in y direction is not studied is that in x-direction one can exploit the series connection of the layers which will lead to a substantial lowering of the shear forces, whilst in y-direction, like in compression, a parallel loading is present which will hardly change the shear resistance compared to EPS80. For each material a representative curve is shown. Standard deviations from at least 3 repeat measurements showed standard deviations on yield and plateau stress of generally less than 3% for the compression results and less than 5% for the shear results, so error bars were omitted from the graphs.

As observed in Figure 5-6a, the compressive component curves in composite foams show similar compressive behaviour to EPS80, however earlier onset of densification can be observed. The differences in plateau stress between the materials are believed to be in the margin of error. It was observed that differences up to 5% were present between different batches of EPS 80 due to density variations between batches.

The earlier densification of the composite foams can be related to initial strain concentration in the weaker EPS40 layers in combined shear-compression, which are rapidly deformed up to densification, resulting in an increase in the stress level until the denser foam starts to crush. As shown in Figure 5-6b, the mechanical anisotropy of layered composite foam demonstrates its effect on the shear component curves in biaxial loading. It can be observed that by introducing anisotropy in layered composite foam, the shear and compression behaviour can be decoupled; the compression behaviour does not change whilst a significant reduction in shear stresses is obtained. It can be inferred that the compression behaviour is merely controlled by overall density, whilst the shear resistance can vary depending on the level of anisotropy. The further decrease in shear stress in EPS120-40-120 composite foam in comparison to EPS100-40-100 is related to the higher density difference in EPS120-40-120. The mechanism responsible is that for similar overall density, the high density layers in the EPS120-40-120 foam are thinner than in case of the 100-40-100 foam and the shear behaviour will be more dominated by the thicker weak EPS40 layer, because in shear the layers are loaded mechanically in series. It can be concluded that the decrease in shear

stress levels can be controlled by changing the density difference between the hard and soft layers, or in other words by controlling the relative thickness of the hard and soft layers.

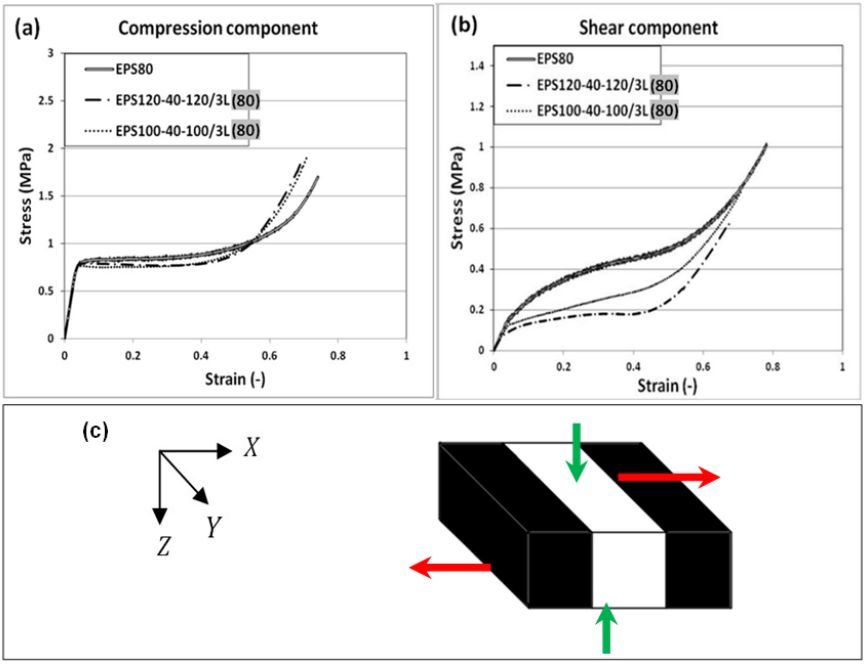

Figure 5-6: (a) compressive stress-strain and (b) shear-stress strain curves of EPS120-40-120 and EPS100-40-100 composite foams consisting of three layers with overall density of 80 kg/m3 versus EPS80 under combined shear-compression loading at deformation angle of 45°; (c) illustration of a composite foam sample under combined shear (red arrows) and compression (green arrows) loading in this experiment.

5.4.3.2 Effect of layer number (layer thickness) on the composite foams with parallel configuration

In this section the effect of the number of layers on quasi-static compression, linear impact and biaxial combined shear-compression behaviour of composite foam with parallel configuration is investigated and benchmarked against single layer EPS foam of equivalent overall density and thickness. For this, composite foams of EPS120-40-120 made of 3 and 7 layers have been prepared with overall density of 100 kg/m^3.

5.4.3.2.1 Static compression and linear impact test

Figure 5-7a demonstrates the comparative compressive curves of EPS120-40-120 (100) with 3 and 7 layers (with overall density of 100 kg/m^3) and EPS100. As observed in Figure 5-7a, composite foams demonstrate similar compressive behaviour to single layer EPS foam and the number of layers seems not to affect the overall compression behaviour. Similar to Figure 5-5a, the overall density governs the compressive response of composite foams.

The linear impact behaviour with input energy of 66J, shown in Figure 5-7b, can be correlated to the quasi-static compression test results. As expected from the quasi-static compression behaviour, the linear impact force-time curves in composite foams seem almost identical to the response of homogenous isotropic EPS foam. Compression samples of EPS 100-40-100 (100) materials with 3 and 7 layers can be seen in Figure 5-7c-d respectively.

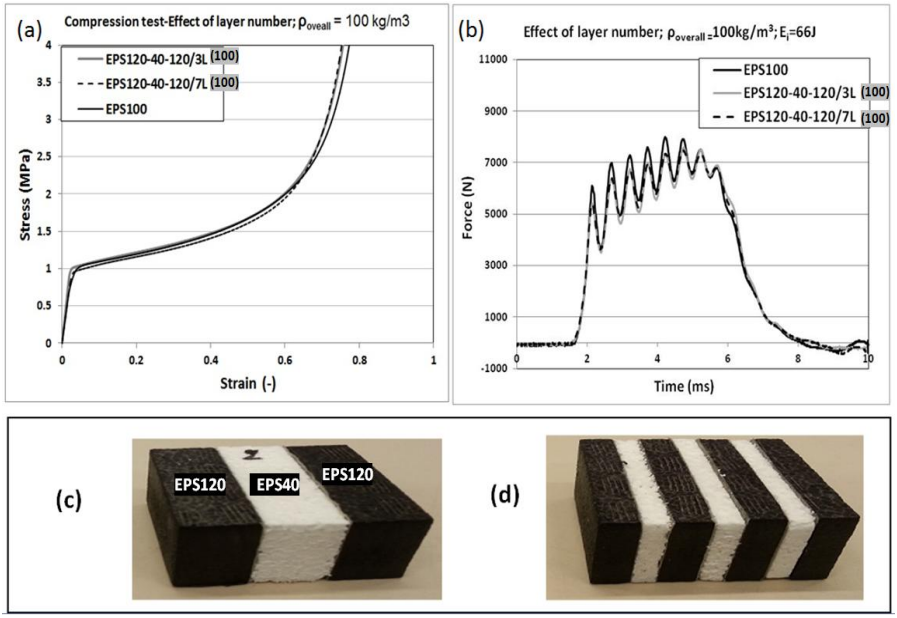

Figure 5-7: (a) Stress-strain curves of EPS120-40-120 (100) composite foams with 3 and 7 layers with overall density of 100 kg/m^3 versus EPS100 obtained from quasi-static compression tests; (b) Force-time curves of layered foams versus EPS100, obtained from linear impact experiments with input energy of 66J; (c-d) EPS120-40-120 (100) composite foam samples with 3 and 7 layers, respectively.

5.4.3.2.2 Biaxial shear-compression test

Compressive and shear stress-strain curves of EPS120-40-120 (100) composite foam samples (overall density of 100 kg/m^3) with 3 and 7 layers obtained from biaxial shear-compression tests are given in Figure 5-8a-b. The number of layers does not seem to significantly affect the compressive component of the biaxial loading and the overall density seems again the dominating factor here. However, the earlier onset of densification in composite foam can again be observed in comparison to single layer EPS100.

Significant decrease in shear stress levels for composite foam with 7 layers is observed in Figure 5-8b. The significant decrease in shear stress in EPS120-40-120 (100) composite with 7 layers is attributed to earlier onset of shear induced bending of the thinner layers. The evolution of deformation of composite foam EPS120-40-120 (100) with 3 and 7 layers during shear-compression experiments with time is shown in the snapshots in Figure 5-8c. The time points chosen are indicated in the corresponding compressive and shear stress-strain curves. The direction of shear and compression deformation applied by the biaxial set-up on foam samples is shown with red and yellow arrows, respectively. In Figure 5-8c it is shown that the deformation of the layers is complex. Phenomena like shear and compression induced bending and transverse shear in each layer can be observed. By comparing the shear curves in Figure 5-8b and the images in Figure 5-8c, it can be concluded that the bending of the thinner layers in the composite foam with 7 layers starts earlier and at lower stress than in case of the 3 layers, in fact significant bending already takes place before the first images taken at 1 minute. In composite foam with 7 layers at t=6 min, thinning of the EPS40 white layers demonstrates that the EPS40 layers are highly densified. This explains earlier densification in composite foams compared to single layer EPS100 which results in a sharper increase in stress levels in the compressive and shear curves (see Figure 5-6a-b).

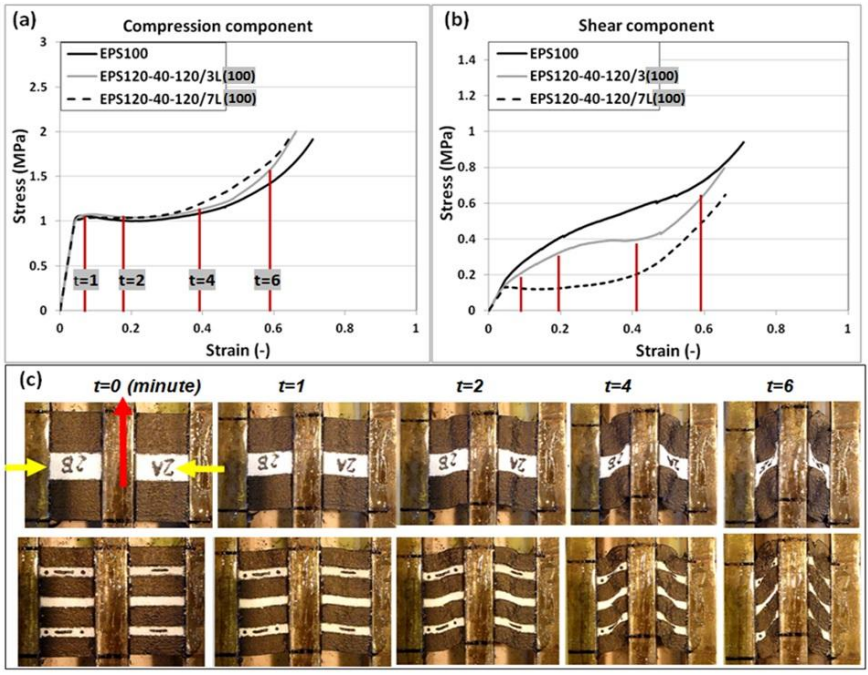

Figure 5-8: (a) Compressive stress-strain and, (b) shear-stress strain curves of EPS120-40-120 (100) composite foams with 3 and 7 layers with overall density of 100 kg/m^3 versus EPS100 under combined shear-compression loading at 45°; (c) The evolustion of deformation of EPS120-40-120(100) with 3 and 7 layers is shown by snapshots taken during shear compression tests; the direction of shear and compressive loading is shown by red and yellow arrows, respectively.

More analysis on the deformation mechanisms of the foam layers with some existing analytical formulas is given in section 5.5.
It can be concluded that the number of foam layers (and thus the layer thickness or the level of distribution between high and low density foam layers) in ''layered composite foam'' has a significant effect in further decoupling the shear and compressive properties of the foam for a given density. Therefore, it can be inferred that the composite foam has the potential that its properties can be tailored for the specific application by playing with parameters such as number of foam layers (and thus layer thickness) and the density difference

between foam constituents. It is believed that the behaviour observed in the static tests (compression and combined shear-compression) can be extrapolated to low velocity impact conditions. It is expected that in oblique impact, composite foams shows lower shear stress levels and thus reduce the rotational accelerations and velocities transferred to the head in applications such as helmets.

5.4.4 Introducing cylinder/matrix geometry in composite foam and its prospect in real applications

From the results section, it can be concluded that the composite foam concept is an effective way to create mechanical anisotropy in foams at a macro level and to decouple the compression and shear properties of the foam without changing its thickness or weight. However, a layered composite foam with parallel configuration, as shown in Figure 5-9, possesses a direction dependent mechanical behaviour (e.g. shear resistance when loaded in the x-z plane). Therefore, a column (e.g. cylinder)/matrix arrangement with hexagonal packing of the cylinders is proposed for the final application. In this case the x-y plane becomes isotropic. As explained before, for a plate-like configuration, loaded in the y-direction in figure 5-9, a parallel loading of the hard and soft foam is present, which will lead to the composite foam following the isostrain rule of mixtures and showing similar behaviour as foam of average density of the layers. In x-direction a series (isostress) connection is present and the composite foam behaviour will be closer to the behaviour of the soft foam, showing reduced shear resistance. In a column-matrix configuration the composite has a series connection in shear in all directions in the x-y plane and will thus show reduced shear resistance in any direction in the x-y plane. As shown, composite foams demonstrate reduced shear resistance whilst maintaining comparative compressive resistance to single layer foam under biaxial loading. The potential application of this behaviour of composite foam is in helmets for improved head protection in oblique impacts. It is believed that the lower shear resistance in a composite foam liner in a helmet could effectively mitigate rotational accelerations (caused by tangential forces) transferred to the head in oblique impacts. The great potential of composite foam with column (cylinder)/matrix configuration for helmet application will be investigated in chapter 7 and 8 of this thesis.

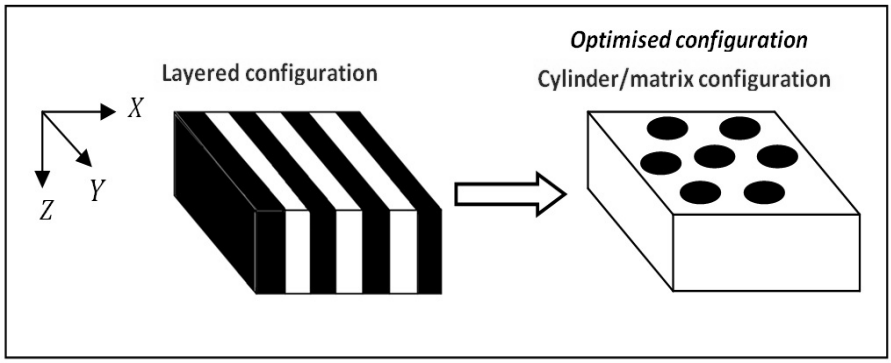

Figure 5-9: Illustration of composite foam with layered configuration versus cylinder/matrix configuration with hexagonal packing.

5.5 Simple analysis of composite foam behaviour

The regular and relatively simple geometries of layered composite foams in this chapter, as well as the column/matrix configurations, which will be described in chapter 7, do raise the question if their behaviour cannot be approximated using analytical formulas, before modelling their behaviour with finite element simulations, as is done in chapter 8.

The most important material property to consider for analysis, is the foam yield stress. The yield stress is typically considered equal to the plateau stress, which defines the energy absorbing capability of a foam structure.

5.5.1 Compressive yield stress

The first obvious question is if the composite foam behaviour can be described by simple rules of mixture based on the properties of the soft (low density) and hard (high density) foam and their respective volume fractions.

For the compressive yield stress of a composite, when loaded in the longitudinal direction of the reinforcement phase, it can be written, according to the isostrain assumption of classical composite micro-mechanics:

$$\sigma_c^y = \sigma_f^y \times V_f + \sigma_m^{'} \times (1 - V_f) \qquad (5.2)$$

where $\sigma_{f,y}$ is the compressive yield stress of the reinforcement phase, V_f is the volume fraction of the reinforcement phase and σ_m' is the stress in the matrix at the moment the reinforcement yields (assuming the matrix yield strain exceeds the reinforcing phase yield strain), which can be approximated by multiplying the reinforcement phase strain with the E-modulus of the matrix, assuming linear elastic behaviour of the matrix.
For most parallel plate configurations studied, a value for the compressive yield stress was measured. Equation 5.2 was used to provide theoretical predictions for the composite yield stress, as documented in table 5-2.

Table 5-2. Comparison of experimentally measured composite compressive yield stress and value determined according to the classical rule of mixture (ROM), for parallel plate configurations, where the high density foam is the reinforcement phase with V_f as the volume fraction of reinforcing phase, w as the width (or thickness) of reinforcing layer, and $\rho_{overall}$ is the overall density of composite foam.

sample	V_f	$\rho_{overall}$ (kg/m^3)	W (mm)	Experimentally determined yield stress (MPa)	Compressive yield stress according to ROM (MPa)
EPS 120-40-120/3L	0.50	80	12.5	0.75	0.73
EPS 100-40-100/3L	0.67	80	16.7	0.72	0.73
EPS 120-40-120/3L	0.75	100	18.8	1.00	1.01
EPS 120-40-120/7L	0.75	100	9.4	0.97	1.01

For all systems that could be evaluated, the compressive yield stress of the composite foam, follows the rule of mixture, based on the volume fraction of the reinforcing foam phase (high density foam) and the compressive yield stress of the reinforcing foam phase. This means that the reinforcing foam layers will yield or crush and not show any other failure behaviour like buckling or matrix shearing. This seems logical as the layer height is only 25 mm and the reinforcement foam layers used have appreciable width (thickness) (see table 5-2 and Figure 5-1), which means that they can be considered as short and sturdy.
To further elaborate on the compressive behaviour, various models used in literature were considered. Because most models available are

for columns, these can only give indications for the behaviour of the plate-like structures.
One of the first things to consider when plates or columns are loaded in compression in the lengthwise direction of these structures, is Euler buckling. The Euler buckling load for a straight column with pinned ends is given by Gere [6]:

$$P_{cr} = \frac{\pi^2 EI}{L^2} \tag{5.3}$$

$$I = \frac{\pi d^4}{64} \tag{5.4}$$

Where *E* is the modulus of the column material, *L* is the column height and *I* is the moment of inertia of the loaded cross-sectional area, with d the column diameter, in case of a cylindrical beam.
For the composite foam, the failure stress in buckling is found by multiplying the critical column buckling load with the number of columns per unit area (neglecting the elastic support provided by the matrix surrounding the cylinders):

$$\sigma_{cr} = NP_{cr} = V_f \frac{A}{A_{f,tot}} \frac{n}{A} \frac{\pi^3 E d^4}{64L^2} = V_f \frac{4A}{n\pi d^2} \frac{n}{A} \frac{\pi^3 E d^4}{64L^2} = V_f \frac{\pi^2 E d^2}{16L^2} \tag{5.5}$$

Where N is the number of columns per unit area (= number of columns n divided by total sample area A), and Af,tot is the total cross-sectional area of the columns.
For a plate, with simply supported boundary conditions, the following equation is found for the critical load [7]:

$$N_{cr,x} = \frac{\pi^2 D}{b^2} \left(\frac{b}{a} + \frac{a}{b} \right)^2 \tag{5.6}$$

$$D = E * \frac{bd^3}{12} \tag{5.7}$$

With *a* the plate dimension in the x-direction of loading, *b* the width of the plate and *D* the plate bending stiffness, with *E* the plate modulus and *d* the plate thickness. Again, for the composite foam, the critical

load is multiplied with the number of plates per unit area to obtain the failure strength.
However, this first Euler based column and plate buckling approximation does not yet consider the elastic sideways support provided by the matrix foam, which is expected to increase the critical load for buckling. For this case, the Winkler foundation analysis [8], for a beam in an elastic foundation can be applied. For the most unstable case of free ends, a simple expression is found:

$$P_{cr} = \sqrt{cEI} \tag{5.8}$$

Where *c* is the foundation modulus, or the matrix modulus in this case, *E* is the beam modulus and *I* is the moment of inertia of the beam. It can be seen that the buckling load now becomes independent of column length; this is because the analysis is for an infinitely long beam, which will likely buckle in a higher buckling mode (the first mode experiences the highest foundation resistance) and turns out to buckle near the beam ends only. With equation 5.8, it can be written for the failure stress of the composite:

$$\sigma_{cr} = NP_{cr} = \frac{V_f}{2}\sqrt{\frac{E_m E_f}{\pi}} \tag{5.9}$$

Where Vf is the volume fraction of columns, Em is the matrix modulus and Ef is the column (or fibre) modulus. Very interestingly, this result becomes even independent of column diameter.
For slender columns embedded in a weak foundation, the Winkler foundation analysis results in an overestimation, because the buckling of the columns is triggered by shearing of the foundation.
Rosen [9] approximated the compressive strength of unidirectional composites, assuming in-phase buckling of the fibres, controlled by the shear modulus of the matrix:

$$\sigma_c^* = \frac{G_m}{(1-V_f)} \tag{5.10}$$

Where G_m is the shear modulus of the matrix and V_f the fibre volume fraction.

The various models which were introduced above (which were mainly developed for columns), were applied to the composite foam from table 5-2 with the thinnest plates, being the system EPS 120-40-120-7L with 7 layers, of which the high density foam layers have thickness of 9.4 mm. For lack of models for plates, also the models developed for columns were employed, where the plate thickness (width shown in Figure 5-1) equalled the column diameter.
The results are shown in Figure 5-10.

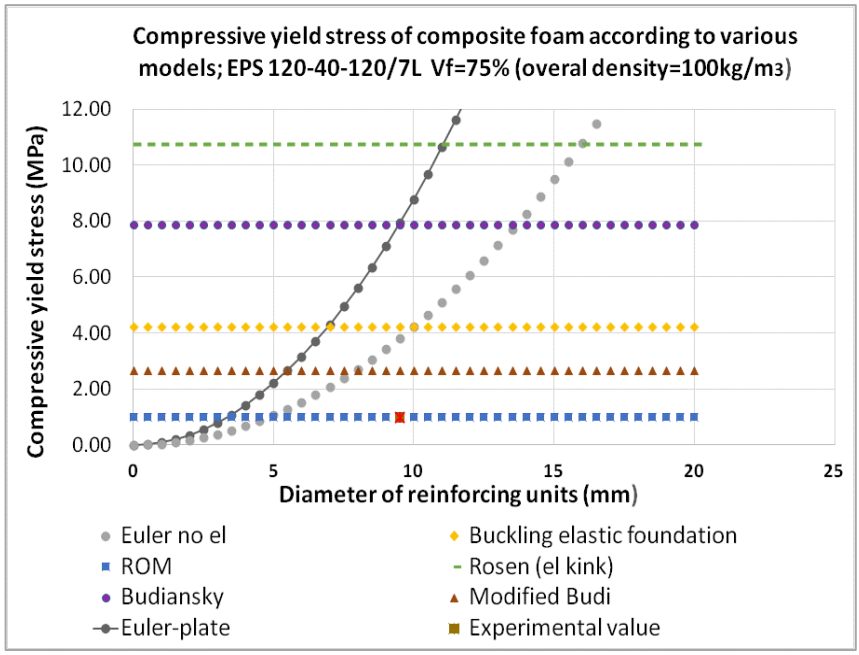

Figure 5-10. Various analytical models for composite compression yield stress applied to the composite foam with reinforcement layers of 9.4 mm thickness.

As was discussed before for table 5-2, the composite foam behaviour exactly follows the rule of mixture (ROM) for compressive yield stress. Only for small plate or cylinder dimensions (below a few mm width or diameter), buckling might become the dominant failure mechanism. However, such small dimensions are impractical for EPS-like foams.

5.5.2 Yield behaviour under combined shear-compression by introducing transverse load

The loading case of high interest in this work, is the combination of compression and transverse shear, with elastic support from the matrix. Unfortunately, such a case is not described in literature. However, if one is interested in more detail in the deformation mechanisms of individual foam layers or columns in composite foam structures, a finite element simulation approach is most suitable for this, to allow parametric studies on the system. Such endeavour is outside of the scope of the current thesis in which the main goal is the development of new materials and testing methods for head protection applications.

Beam-column theory [6] states that any eccentricity in the applied load, e.g. by applying shear deformation to the column loaded in compression, will lead to immediate bending, which will lower the critical compressive load with respect to the axial Euler buckling load.

Colums embedded in an elastic foundation will still exhibit bending, but at higher stress, depending on the foundation/matrix modulus.

For the compression strength of fibrous composites (so with fine fibres with very little buckling and bending resistance of themselves), Budiansky [9] considered the case of a misalignment in the load. Analogous to the Rosen equation, the compression strength is linked to the G-modulus of the composite:

$$\sigma_c^* = \frac{\tau_{comp}^*}{\gamma_{comp}^* + \varphi} \tag{5.11}$$

Where τ_{comp}^* is the in-plane shear strength of the composite, γ_{comp}^* is the accompanying shear strain in the composite and φ is the misalignment, which in this case can be expressed in terms of a shear strain. For in-plane shear, fibre and matrix are loaded in series (see Figure 5-9), and the composite shear strength and stiffness are largely controlled by the matrix shear strength and modulus. For the G modulus of the composite can be written:

$$G_{comp} = \frac{G_f G_m}{V_f G_m + (1 - V_f) G_f} \tag{5.12}$$

Where G_m and G_f are the shear moduli of matrix (here low density foam) and fibre (here high density foam), respectively. G_{comp} becomes approximately equal to $G_m/(1-V_f)$ when $G_m << G_f$. So when $\varphi = 0$ and this simplification is made, the Budiansky estimation becomes equal to the Rosen equation.
With the Budiansky equation, it becomes possible to make an analysis of a combined shear-compression loading. For a loading under 45°, it can be stated that the induced shear misalignment φ, becomes equal to the compression strain ε_c^*. Thus, it can be written:

$$\sigma_c^* = \frac{\tau_{comp}^*}{\gamma_{comp}^* + \sigma_c^*/E_{comp}} \tag{5.13}$$

Which equation can be solved for σ_c^*.
The Budiansky equation was employed in Figure 5-10. Where the label says Budiansky this is the solution for $\varphi = 0$; the modified Budiansky value is according to equation 5.13.
It is clear that the introduction of shear considerably lowers the predicted compressive strength of the composite foam when the assumed failure mode is fibre buckling of fine fibres. But still the failure by compressive yield of the composite, according to the rule of mixture, will happen first for the composite foams of this study. The compressive component of the failure stress in a combined shear-compression loading actually closely follows this predicted value by the ROM (see Figure 5-8a).
This was an important observation: in a combined shear-compression test under an angle of 45°, the compression component of the yield stress gave exactly the same values as the pure compression test under 0°. Apparently, the added transverse load does not affect the yield in compression of the material in any appreciable level. This also confirms that the yielding behaviour in compression is dominated by 'normal' yielding in compression (crushing) and not by bending or buckling phenomena. In transverse shear the behaviour is different.
Where the compression component of the composite foams seems to follow very well the rule of mixture for compressive yield stress of a composite, the shear component clearly is strongly dependent on the composite configuration, as was e.g. shown in Figure 5-8b. In a first approximation, the shear component would be determined by the

shear yield stress of the matrix, as the components are loaded in series during transverse shear.
As mentioned above, beam-column theory states clearly that any eccentricity during column loading will lead to instantaneous bending. It seems clear that the transverse shear behaviour of the composite foam will be dominated by a combination of matrix dominated shear and column or plate bending of the reinforcement phase. As this loading condition is not explicitly modelled in literature, a finite element simulation for this complex loading case seems most appropriate.

5.6 Conclusions

Cellular materials, particularly structural foams, play an important role in many passive safety applications, from automotive to packaging. Anisotropy in foams generally originates from cell elongation in a certain direction. In this chapter, a novel composite foam concept is proposed as an effective way to create mechanical anisotropy in foams at ''macro level''. Layered composite foams were produced by stacking discrete layers of EPS foams of two different densities in series and parallel configurations. The compression, linear impact and biaxial combined shear-compression properties of layered composite foams were investigated and compared with single layer homogenous EPS foam with equivalent density and thickness.
It was shown that shear and compression resistance of the composite foam structure can be decoupled and that the shear resistance can become independent from the overall foam density. It was shown that layered composite foam with parallel configuration outperforms the series counterpart in terms of effective energy absorption in linear loading. Moreover, for the same impact energy, the parallel configuration maintains lower peak forces/linear accelerations than the series configuration during linear impact. In addition, it was found that the behaviour of the parallel configuration in linear loading is dominated by the overall density of the composite foam. Therefore, parallel configuration was chosen for further investigation in biaxial (oblique) loading.
Biaxial shear-compression experiments on composite foams with parallel configuration have shown that the composite concept enables to decouple shear and compression properties of foams for a given overall density. Moreover, in composite foam (with parallel configuration) the level of decoupling between compressive and shear

properties can be tailored by parameters such as the number of layers and the density difference between hard and softer foam layers. Results showed that the compressive and linear impact behaviour of composite foam with parallel configuration is similar to single layer EPS foam with similar overall density. However, in oblique (biaxial) loading, composite foam demonstrates lower shear resistance than single layer isotropic foam whilst keeping similar levels of compressive stress. The level of reduction in shear resistance can be controlled by increasing the layer number and density difference between high and low density foam layers, where thinner high density layers lead to reduced shear resistance, due to enhanced shear induced bending.
Finally, composite foam with column (e.g. cylinder)/matrix configuration with a hexagonal packing is suggested as an optimized geometry for real applications. One of the potential applications of anisotropic composite foam is believed to be in protective helmets (e.g. bicycle helmets) with the aim of reducing rotational motion of the head. This will be further explored in chapter 7.

5.7 References

1. Gibson, L.J, and Ashby, M.F. Cellular solids: structure and properties. 2nd ed. Cambridge: Cambridge University Press, 1997.
2. Kleiner, F.G., Radojewski, L., Muhlbauer, L., Muller, K.H. Laminates of polyethylene foam with anisotropic pore structure, CA1071086 A, 1987.
3. Oliveira-Salmazo, L., Lopez-Gil, A., Silva-Bellucci, F., Job, A.E., Rodriguez-Perez, M.A. Natural rubber foams with anisotropic cellular structures: mechanical properties and modelling Industrial Crops and Products, 2016. 80: p.26–35
4. Bernardo, V., Laguna-Gutierrez, L., Lopez-Gil, A., Rodriguez-Perez, M.A. Highly anisotropic cross-linked HDPE foams with a controlled anisotropy ratio: Production and characterization of the cellular structure and mechanical properties. Materials & Design, 2017.114: p.83–91.

5. Vanden Bosche, K. Development and Characterization of Novel Anisotropic Foam for Bicycle Helmets (Ph.D. thesis). KU Leuven, 2016.
6. Gere, J.M. Mechanics of materials. 6th ed. *Bill Stenquist*, *2004*.
7. Gere, J.M. & Timoshenko, S.P., Mechanics of materials. 2nd ed. Boston PWS Pub Co. *1997*.
8. Bazant, Z.P. & Cedolin, L. Stability of Structures: Elastic, Inelastic, Fracture and Damage Theories. Oxford University Press. 1991
9. Budiansky & Fleck, Compressive failure of fibre composites. Journal of Mechanics and Physics of Solids, 1993. 41(1): p.183-211.

Chapter 6

Further development of oblique impact set-up

Oblique impact testing of the head describes an experiment in which both normal and tangential force components are applied to the head surface. A survey of different oblique impact set-ups found in literature was presented in Chapter 3 of this thesis. The design of oblique impact set-ups in different laboratories can be divided in two main categories. The first category includes the designs in which a helmeted headform is dropped from a height onto a horizontally moving impact surface (e.g. moving sled in the KTH set-up [1] or moving band in the KU Leuven set-up [2-3]). In this category the ratio between the horizontal and vertical velocity defines the impact angle. The second category includes designs that utilise an angled anvil to mimic a specific oblique impact angle. In these designs, the helmeted headform is dropped at a specified impact speed determined by the impact height onto the inclined anvil.

The first category of designs has the advantage that the drop height is not needed to be as high as in case of the second category (containing angled anvils) in order to achieve reasonably high reaction forces. Moreover, in the first category of oblique impact testers, the angle of impact can be easily adjusted by different combinations of drop height and horizontal impact surface speed. However, in practice, the moving (shooting) sled design is difficult to set up and tune. To regulate the timing between drop release and sled firing can be tricky and for each test a high speed video camera must be set-up during the test. Moreover, the oblique impact tester with moving sled/moving band

might be interesting for research purpose but adopting them for a standard test lab is rather complex and expensive. Therefore, the second category of oblique impact set-up including an angled anvil is believed to be the more suitable design for adaptation in future helmet testing standards.
This chapter comprises of two main parts. In the first part, the oblique impact set-up previously built in KU Leuven during the master thesis of Tobback and Boulanger [2] and the PhD thesis of Vanden Bosche [3], is critically examined and modified. For this the performance of this set-up is compared to the KTH moving sled set-up and the huge discrepancy between the oblique impact testing results is analysed. To understand the sources of this discrepancy, a series of controlled experiments is performed. Finally a more simplified set-up is proposed.
In the second part, a survey of commercial anisotropic cellular materials which are considered to be suitable in reducing rotational acceleration and velocity of the head is presented. Linear and oblique impact experiments are performed on them and the results are benchmarked against conventional EPS foam.

6.1 Introducing KU Leuven set-up and its different parts compared to KTH moving sled set-up

The initial version of KU Leuven oblique impact set-up was inspired by the KTH moving sled oblique impact tester explained in chapter 3. KU Leuven set-up shown in Figure 6-1 consists of several main parts:

- **Drop tower frame**: This set-up utilises a drop tower impactor initially designed for the testing of composite plates [4]. Therefore, there is a drop height limit of 2 meters in the existing frame.

- **Rotary band:** A rotating belt impact surface is incorporated in the drop tower assembly (see Figure 6-1) to apply horizontal speed to the impact target. A rotating band was chosen to overcome the complexities of tuning a moving sled impact target in the KTH set-up and still having a wide range of

allowable horizontal speeds, independent of the vertical velocity. The band can reach horizontal speeds of 10 ms^{-1} and is its surface is made of textured rubber surface (with rubbery protrusions) to maximize friction with the helmet.

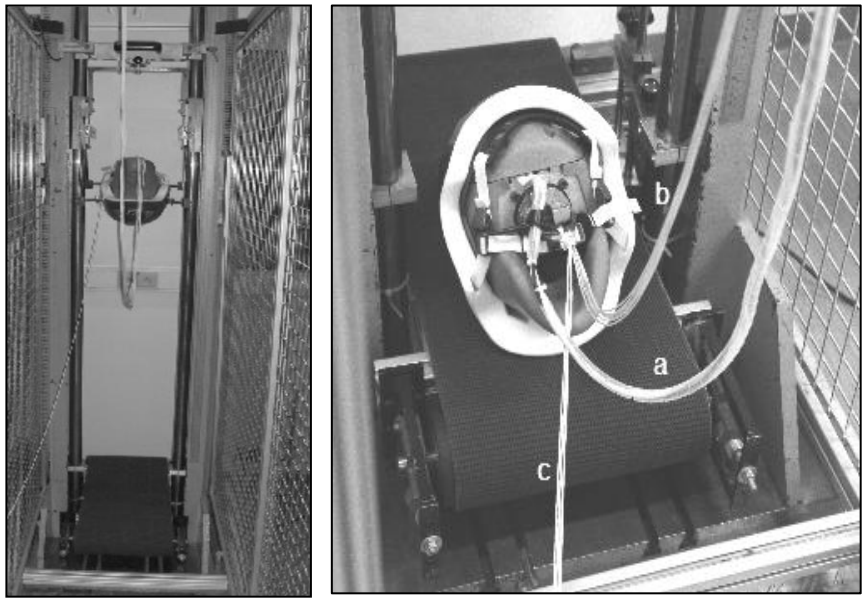

Figure 6-1: (left) overview image of the KU Leuven oblique impact set-up with head held in the support system, connected to the drop tower rail and ready to fall on the rotary band; (right) headform on the rotary band and connection cables are visible; *a* is instrumentation cord, b is a security cord, c is a second security cord for control by operator to catch the headform to prevent multiple impacts and damage to the instrumentation, [3].

- **Headform:** A hybrid III 50th percentile male anthropomorphic dummy head sourced from Humanetics is used in this set-up. This headform is chosen because its moments of inertia are more biofidelic than the EN-960 dummy head. The head is not connected to a neck and is allowed to rotate freely. The mass of the headform alone is 4.54 kg. The sensors in the head were

connected to the data logger interface via cables. In order to minimise the effect of the mass and tension of the cabling and cords, which can potentially affect the rotation of head/helmet system or be damaged during impact, a light-weight nylon cord was used to avoid straining of the cables. The head was also tied with a second slack cord so that the head could be caught after impact without damaging the instrumentation cables or inducing a second impact.

- **Instrumentations:** Rotational velocities about three directions of x, y and z (ω_x ω_y ω_z), are measured by an *IES* 3103 triaxial angular rate sensor (ARS) with an angular rate measurement range up to 4800 °/s (or 83.7 rad s^{-1}). The ARS is mounted in the centre of gravity (CG) of the headform as shown in Figure 6-2a. For measurement of linear accelerations in directions of x, y and z, three uniaxial MEMS 64C-2000-300 accelerometers with a measurement range of 0–2000g were mounted onto the ARS oriented along the coordinate axes of the head frame of reference as shown in Figure 6-2b.

- **Control, data acquisition and processing unit box:** A control, data acquisition and processing unit box for the sensors, including amplification, buffering, and filtering of the signals was developed in-house for this set-up. The signals were conditioned using an isolation amplifier from Analog Devices (AD210JN) and 100x amplification. They were subsequently filtered off-line in MATLAB using a Butterworth 6^{th} order filter with 90 Hz cut-off frequency [2-3], allowing the differentiation of the velocity signal to obtain the rotational accelerations. For the measurement presented in table 6-1 a 50 kHz sampling rate was use.

- **Guided support system:** A four-point support system is incorporated into the drop tower rails as shown in Figure 6-2c-d to position the headform and to avoid headform/helmeted

headform rotation just before impact. At the moment of impact of the helmet/headform, the support system continues to fall, loses contact and thus allows free rotation and motion of the helmeted headform.

Each of the four points is connected to a horizontal bar which itself is connected to a vertical bar as depicted in Figure 6-2a. They can be adjusted independently and can be moved vertically and can be also rotated. The length of the horizontal bar can be adjusted. These adjustments allow the support system to grip any helmet type and size.

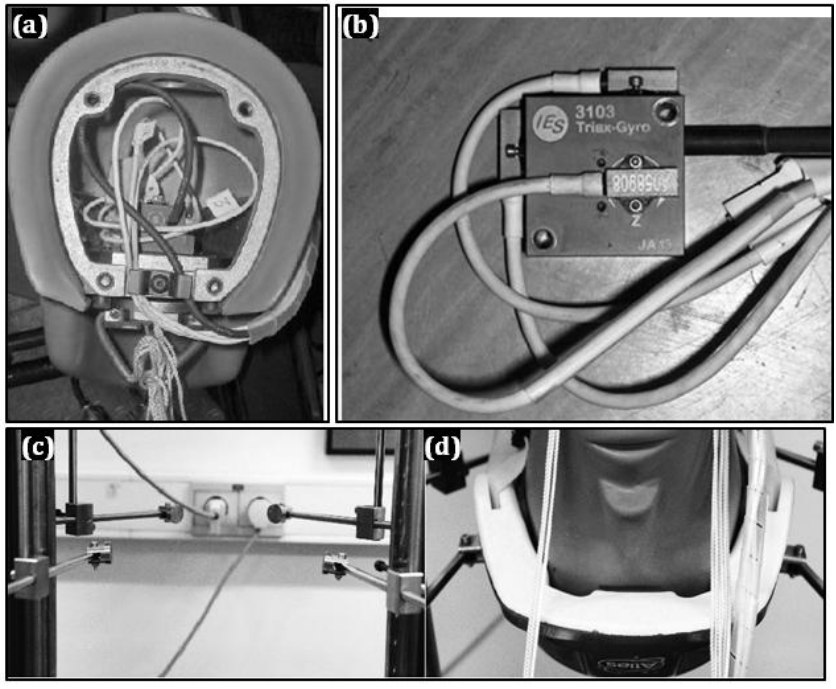

Figure 6-2: (a) Headform with sensors mounted at the CG of it; (b) triaxial ARS with three linear uniaxial accelerometers attached to it; (c) four-point guide support system; (d) support system holding a helmeted headform, [3].

Similar to the KU Leuven set-up, an identical hybrid III 50th percentile male headform is utilised in the KTH moving sled set-up. Regarding instrumentation, the KTH moving sled set-up is equipped with an array of 9 linear accelerometers (instead of an array of 3 linear accelerometers + ARS in the KU Leuven set-up) which measure linear and rotational accelerations in three directions of x, y, and z. A moving sled covered with sandpaper is used as impact surface; the sled is shot under the drop tower using pneumatic pressure. Moreover, in the KTH moving sled set-up, a pneumatic clamp is used to hold the head until just before impact. More information on the KTH moving sled set-up can be found in Halldin et al. [1].

Table 6-1: Data related to peak resultant linear, peak resultant rotational and peak resultant rotational velocity and the percentage of difference between the results obtained from experiments performed on identical helmets using KTH and KU Leuven set-ups. Similar impact conditions e.g. input velocities, and headform orientation are implemented in both experiment series.

	KTH moving sled set up	KUL set-up	difference
Peak resultant linear acceleration ($a_{r,max}$ in g)	129±6	69±8	-46%
Peak resultant rotational acceleration ($\alpha_{r,max}$ in krad/s^2)	10±1	17.7±0.9	43%
Peak resultant rotational velocity ($\omega_{r,max}$ in rad/s)	40±2	89±3	55%

6.2 Validation of the KU Leuven set-up

6.2.1 Comparison of the results obtained from KU Leuven and KTH moving sled set-ups

In order to critically assess the results obtained from KU Leuven oblique impact test apparatus, a series of oblique impact tests with the same impact conditions using both KU Leuven and KTH moving sled set-ups were performed during the thesis of Vanden Bosche [3]. Subsequently impact results in terms of resultant linear (a_r), rotational acceleration (α_r), and rotational velocity (ω_r) versus time curves were compared. For these experiments, commercial helmets SportAtlas

Hardtop Mini were used. The drop height was set to 0.7m, and the horizontal rotary band/moving sled speed was set to 6.8 ms^{-1}; the helmets were dropped on the crown. The results of the experiments in terms of peak linear acceleration, peak rotational acceleration and peak change in rotational velocity are summarized in table 6-1. As observed, the difference in measurements of these two different set-ups is remarkably large.

6.3 Investigation of sources of discrepancy in the results obtained from KTH and KU Leuven set-ups

The huge differences in the results obtained from these two set-ups can arise from three main sources

1. rotary band versus moving sled
    - The impact surface friction coefficient
    - The change in horizontal velocity profile of the band during impact
2. Sensoring system
3. Data processing box

6.3.1 Rotary band versus moving sled

To identify the effect of the rotary band versus the moving sled, additional oblique impact tests were performed. In these controlled tests, the rotary band was incorporated in the KTH set-up. Experiments are performed on identical helmets, orientation of the head and impact horizontal velocity of 6.8 ms^{-1} and the drop height of 0.7 m. Table 6-2 compares the results of these two experiments.

Table 6-2 shows that the discrepancies between the set-ups is significantly smaller, compared to the results shown in table 6-1, yet still significant, proving that the rotating band system is one of the origins of discrepancy. This can be caused by differences in elastic damping, a difference in coefficient of friction of the two surfaces, and differences in system inertia. Whereas the first element predominantly affects the linear accelerations (showing only a minor difference), the latter two elements influence the rotational acceleration and velocity.

Table 6-2: Data related to peak resultant linear, peak rotational and peak resultant rotational velocity the percentage of difference between the results obtained from experiments performed on identical helmets using KTH sensors and KTH moving sled or KU Leuven rotary band as impact surface in each set of experiments. Similar impact conditions are used in both experiment series.

	KTH sensors-moving sled	**KTH sensors-rotary band**	**difference**
Peak resultant linear acceleration ($a_{r,max}$ in g)	129±6	117±2	-9%
Peak resultant rotational acceleration ($\alpha_{r,max}$ in krad/s^2)	10±1	6.4±0.2	-36%
Peak resultant rotational velocity ($\omega_{r,max}$ in rad/s)	40±2	32±1	-20%

6.3.1.1 Surface measurements via friction test

It is known from basic mechanics that the moment of inertia of the helmeted head and the tangential frictional forces applied to it determines its rotational acceleration and velocity during impact. To obtain insight on the differences in surface properties of the elastomeric rotary band in the KU Leuven set-up and the sandpaper covered moving sled in the KTH set-up, friction experiments were performed [3]. For sake of completeness, the results are repeated here. For this an Instron tensile testing apparatus was utilised to which a low-friction pulley was attached. A polypropylene plate (simulating the helmet shell material) was drawn horizontally across the static rotary band surface or sandpaper surface of the moving sled. The PP plate could be loaded with different masses and could be also pulled with different pulley speeds. As observed in Figure 6-3, the friction coefficient of the sandpaper is lower than of the elastomeric band. Hence, there is a more efficient energy transfer from the rotary band to the helmeted head than for the sandpaper covered sled, which should result in higher rotational accelerations, opposite to the results shown table 6-2.

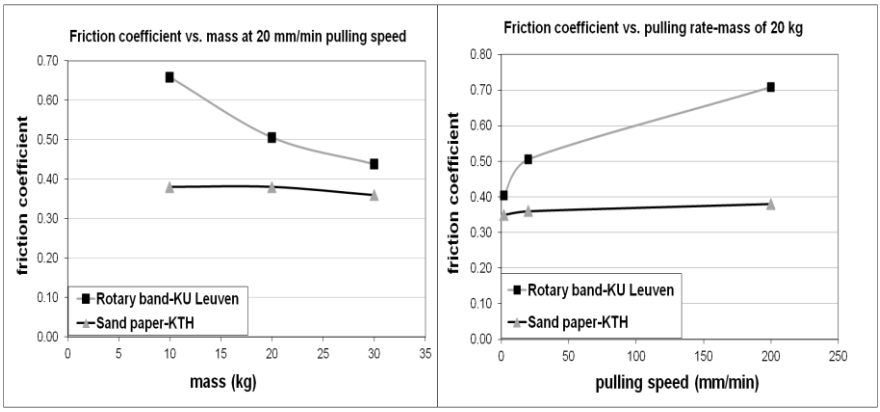

Figure 6-3: Friction coefficient of impact surface of KTH and KU Leuven set-ups obtained from sliding friction tests as a function of mass and at pulling speed of 20 mm/min (right), and as a function of pulley speed at constant weight.

However, the dynamic friction coefficient of sandpaper in KTH moving sled set-up is independent of the weight and the velocity. In contrast, the dynamic friction coefficient of the elastomeric band is found to be dependent on both mass and velocity. This could be due to the fact that the band is made of elastomeric materials and its surface has a comb-like structure which may explain the variable friction through the level of mechanical interlocking with the helmet surface. This dependence jeopardizes the repeatability of the experiments using the rotating band and adds unwanted variations. The friction coefficient values related to rotary band in Figure 6-3 are borrowed from the thesis of Vanden Bosche [3].

6.3.1.2 Other effects related to the rotary band

The rotary band is compressible and some part of the initial impact energy can be dissipated by the elastic compression of the rotary band, thus reducing the linear acceleration of the helmeted head and explaining the discrepancy (9%) in linear acceleration observed in table 6-2.

Moreover, the high speed camera in combination with tracking markers showed that the velocity of the band decreases to about 4.2 ms^{-1} when impacted by the helmeted headform and then is driven back again to 6.8 ms^{-1} during the course of the impact. The change in the horizontal velocity profile of the rotary belt is due to slip of the band on the rollers and insufficient power of the motor to maintain a constant

velocity during impact. This affects the energy transfer between the band and the helmeted headform. The KTH sled has a permanent decrease of velocity, to 5.5 ms^{-1}, as the head and helmet absorb some of its energy.

6.3.1.3 Conclusions drawn from studying the rotary belt versus moving sled

By comparing the data of table 6-2 where the helmet type, impact conditions, and sensors were identical, it can be observed that the peak resultant linear acceleration is somewhat reduced for the rotary belt due to compressibility of the rubber band and its dampening effect. Moreover, peak rotational acceleration and velocity of the helmeted head are lower when using the rotary belt as impact surface. This also indicates that less energy was transferred to the helmeted head from the belt. The lower peak rotational acceleration and velocity values of the helmeted headform, when impacting the rotary band (see table 6-2), is due to the more significant drop in rubber band velocity (4.2 ms^{-1}) than for the moving sled (5.5 ms^{-1}) at the moment of impact. In addition, the different friction coefficient of the textured rubber band versus sandpaper covered sled and the dependence of band friction coefficient on the speed and weight can add other sources of discrepancy. The higher friction coefficient of the rubber band leads to higher rotational acceleration whilst the higher deceleration of the rubber band when impacted by the head results in lower rotational acceleration of the head. Therefore, there is a competing effect between these two phenomena. The resulting lower rotational acceleration and velocity of the head in case of the rubber band shows that deceleration of the rubber band is the dominating phenomenon.

In a nutshell, the rotating band system shows a number of advantages such as compactness, the ease of speed control, and the energy transfer efficiency due to the high friction of the band surface. However, the compressibility of the band, the weight dependent friction coefficient of the band surface, and the change in horizontal velocity profile during impact add some complexities and cause discrepancy between the results obtained by KU Leuven and KTH moving sled set-ups. Some of these disadvantages can be overcome by redesigning the rotary belt and using a less compressible material with a stable friction coefficient instead of textured rubber band, and also by using a stronger motor to reduce the significant drop of the band velocity during the impact; but even by overcoming all these issues with the rotary belt, the set-up still

remains complex and for future standardization, the consensus is that a simpler approach is needed by using anvils instead [5].

6.3.1.4 Replacement of rotary band with anvil to simplify KU Leuven set-up

In order to tackle the abovementioned issues with the rotary band and to have a simpler, cheaper, and more compact testing rig which can be adopted in future helmet testing standards [5], the rotary band was replaced by a steel anvil covered with sandpaper. Anvils with different angles of 0°, 15°, 45°, and 60° were designed to be incorporated into the current drop impact tower. Figure 6-4 illustrates the anvil designs. As shown in Figure 6-4, the anvil was designed with 3 different parts:

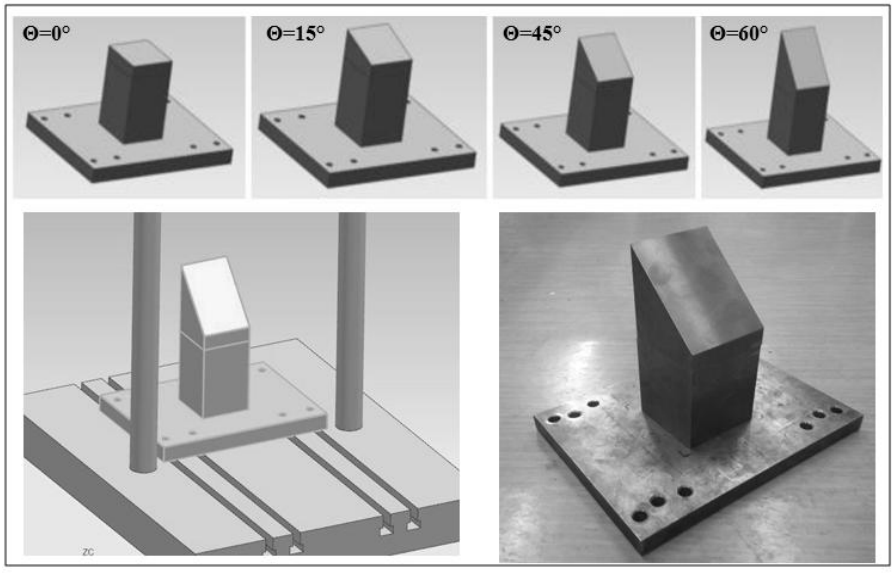

Figure 6-4: (Above) from left to right illustrations of the designed anvil with different angles of 0°, 15°, 45°, and 60°; (below left) illustration of the anvil being assembled onto the drop tower plate; (below right) an example of the 45° anvil from steel and custom made in MTM workshop.

- The lower plate made of steel
- A rectangular prism that leaves enough space for the support system, holding the helmeted headform, to slide down without interfering with the head movement,
- The triangular prisms with different surface angles relative to the horizontal line (0°, 15°, 30°, 45°, and 60°). The triangular prisms with different surface angles can be bolted to the rectangular prism.

These parts are assembled and slid into the drop tower plate and connected to it by two long vertical screws.

6.3.2 Sensor system

The sensors could be another source of discrepancy between the results acquired by KTH moving sled and KU Leuven set-ups. The sensors in the KTH setup, an array of 9 accelerometers, are regularly calibrated with well-established calibration methods, and the sensors are applied in the range of calibration. Moreover, the calculation of rotational accelerations from linear accelerometers is straightforward, the angular velocities are obtained by integrating the rotational accelerations which is a numerically stable process that reduces noise; therefore, the results obtained by KTH are considered reliable and used here as a benchmark. In the framework of this project and the project of Kelly Vanden Bosche, experiments were carried out using the rotary band in combination with a 9 accelerometer array (at KTH) and a 3 linear accelerometers + triaxial gyroscope (at KU Leuven). This allows comparing the performance of sensors of the set-ups while all other parameters (identical helmets, impact conditions, head orientation and impact surface) were kept constant. Experiments were carried out using the same initial conditions as in section 6.2. Table 6-3 summarizes the results of these experiments. As observed, there is a significant difference in the measured values between the two sensor systems. It can be concluded that there might be issues or errors with either the ARS calibration, or data acquisition/processing in the KU Leuven set-up. In the next sections each of these possibilities will be further investigated.

Table 6-3: Comparison of experimental results obtained from KTH moving sled set-up (with KTH accelerometer sensors) using KU Leuven rotary band, and experiments carried out on KU Leuven set-up (with angular rate sensor/accelerometer sensors) using the rotary band. All results are for the same helmet model, same initial input velocities, and same headform orientation [2].

	KTH sensors-band	KUL sensors-band
Peak resultant linear acceleration (a_r in g)	117±2	69±8
Peak resultant rotational acceleration (α_r in krad/s²)	6.4±0.2	17.7±0.9
Peak resultant rotational velocity (ω_r in rad/s)	32±1	89±3

6.3.2.1 Calibration of the sensors

As explained earlier, the sensors in KU Leuven set-up consist of a triaxial gyroscope and 3 linear accelerometers. The triaxial gyroscope was calibrated by the manufacturer within a limited range and checked in the MTM lab up to 93±1 °/s and a frequency of 3 Hz which is significantly slower than the average frequency of the impact pulse (on average around 100 Hz for a helmet test) [3]. To exclude errors due to calibration, the gyroscopes need to be calibrated in its full range of operation (up to 4500 °/s). This is not straightforward, therefore a set-up for calibration was proposed, which will be elaborated in the next sections.

6.3.2.1.1 Calibration of linear accelerometers

The three linear accelerometers 64C MEMS were calibrated internally using a triaxial piezoelectric PCB calibrator model number: 394C06. The test confirmed the calibration by the manufacturer and that the accelerometers work properly.

6.3.2.1.2 Calibration of triaxial gyroscope

For calibration of the gyroscope an in-house test set-up was designed during the master's thesis of Amato and De Ghellinck [6]. The calibration set-up is illustrated in Figure 6-5.

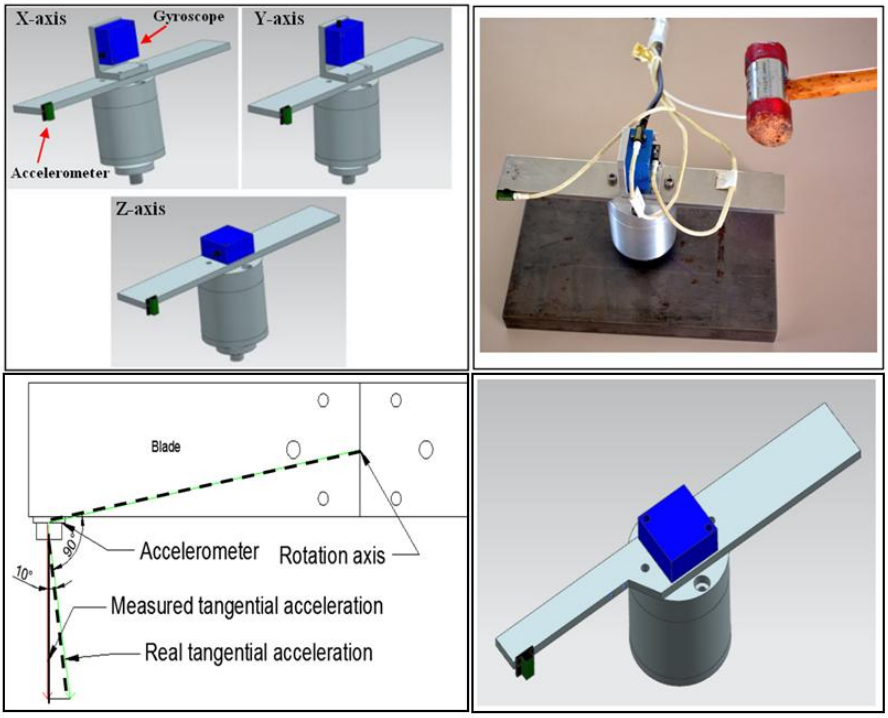

Figure 6-5: (Upper left) Illustration of the calibration set-up showing gyroscope mounted to the blade in three directions x, y and, z going clockwise; (upper right) image of custom made calibration set-up and the rubber hammer used to hit the extremity of the blade; (lower Left) Measured and real acceleration before modification of the blade; (lower right) illustration of modified blade.

In this set-up a rigid blade, made of aluminium, is bolted to a multi part aluminium cylinder in which two bearings enable its (almost friction-free) rotation around a vertical axis. The blade is positioned horizontally to exclude the influence of gravity**.** The plinth (not represented in the Figure 6-5), in which the thread below the cylindrical part of the set-up is inserted, is made of steel to be heavy enough to reduce the vibrations and movement during the rotation of the blade. A calibrated accelerometer is placed at the end of the blade to measure the tangential acceleration. The gyroscope (in blue) is placed in the middle of the rotating blade to measure its rotational (angular) velocity around the rotating axis. In order to measure the angular velocity around all three axes of the gyroscope, an L-shaped

piece is attached on the blade as in Figure 6-5 which allows the gyroscope to rotate around each of its axes. In this experiment, basic angular motion theory is used to compare the signals of the accelerometer and the gyroscope. The linear accelerometer will provide the tangential linear acceleration (a_t) which by integrating it, tangential linear velocity (V_t) is obtained (equation 6.1). Dividing the tangential linear velocity by the distance between the accelerometer and the centre of the axis of rotation, $\boldsymbol{r}$, gives angular velocity (ω) as shown in equation 6.2.

$$V_t = \int_0^t a_t . dt \quad [\mathrm{m/s}] \tag{6.1}$$

$$\omega = {}^{V_t}/_{r} [^\circ/\mathrm{s}] \tag{6.2}$$

To start the rotation of the blade, the extremity of the blade is hit with a rubber hammer, as shown in Figure 6-5 (upper right), and the signals from both sensors are logged. In the initial design of the calibration set-up shown in Figure 6-5 (upper left), the accelerometer only measured part of the real tangential acceleration and there was an angle of 10° difference between the measured and the real tangential acceleration as shown in Figure 6-5 (lower left). Although during calibrating the gyroscope in lower frequency range no significant issue was identified, this angle induced noticeable errors at higher angular velocities. To tackle this, there was some correction to the current calibration set-up by cutting the blade in half along the centre line as shown in Figure 6-5 (lower right).
By plotting the rotational velocity signal obtained from the gyroscope and the integrated signal of the accelerometer, a delay between the two signals can be observed in Figure 6-6. As observed, the signal provided by the accelerometer (in voltage) reaches its maximum with a delay of 2 milliseconds in comparison to the signal of the gyroscope. This discrepancy was observed in all test repetitions and for all three directions of the gyroscope.

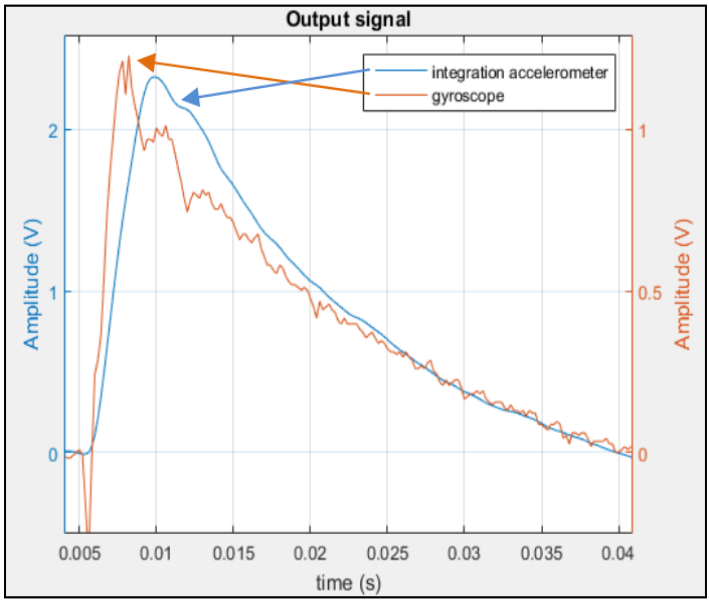

Figure 6-6: Comparison of integrated signal of linear accelerometer and signal obtained from gyroscope after hitting the blade with rubber hammer.

The following three possible sources for the mismatch of the signals were considered:
1. Error in sensors (accelerometer, gyroscope or both)
2. Incorrect digitizing or computing.
3. Poor or incorrect amplification/isolation in the signal processing box.

Extensive study was carried out to examine each of these three hypotheses, from which it was concluded that the error was caused by the signal processing box and more in detail, the bandwidth of the accelerometer amplifier was not adequate for the frequency range of the experiments (100-250 Hz). Bandwidth of an amplifier (or any other electronic component) is a frequency range at which the signal is modified correctly independent of the frequency within this range. After modification of the signal processing box, the tests were repeated showing a very good match between the signals (Figure 6-7).

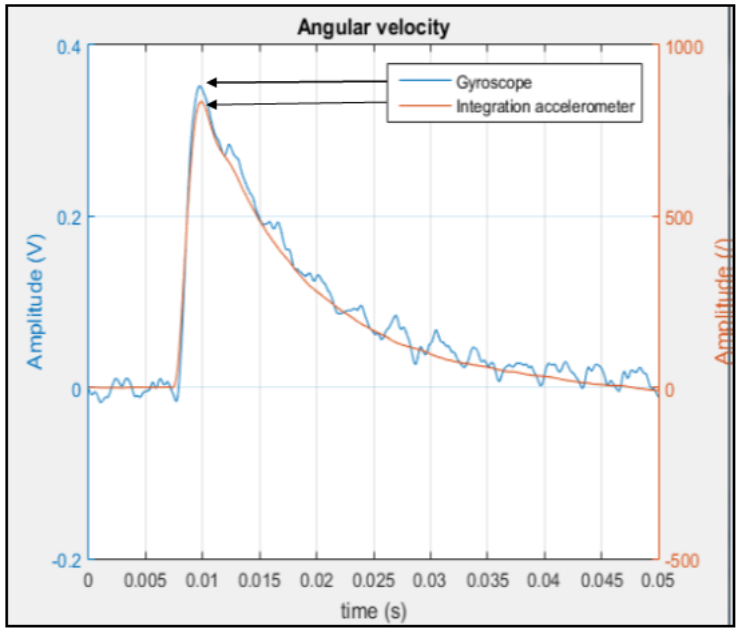

Figure 6-7: Comparison of integrated signal of linear accelerometer and signal obtained from gyroscope after correcting the signal processing box.

The set-up was then used to calibrate the gyroscope and to see if the gyroscope response was consistent with the linear calibration curve provided by the manufacturer, yet in a wider frequency range. During calibration experiments it was noticed that the calibration curves have different slope than the theoretical calibration curve provided by the manufacturer. After opening the amplification box it was discovered that the supply voltage of the gyroscope was set incorrectly to higher voltages (than the voltage suggested by the ARS datasheet which is 10v). This is believed to be the reason that much higher rotational acceleration and rotational velocity values were previously measured by KU Leuven sensors during helmet testing (see table 6-3). Setting higher supply voltage for the gyroscope in the signal processing box leads to overamplification of the gyroscope response. Extensive detail of the procedures can be found in [6]. After setting the supply voltage back at 10v, the calibration experiments were repeated. Figure 6-8 depicts the calibration curves up to angular velocity of 600 ° /s. It can

be seen that the calibration curves obtained from the experiments follow the theoretical linear calibration curve provided by the manufacturer quite well.

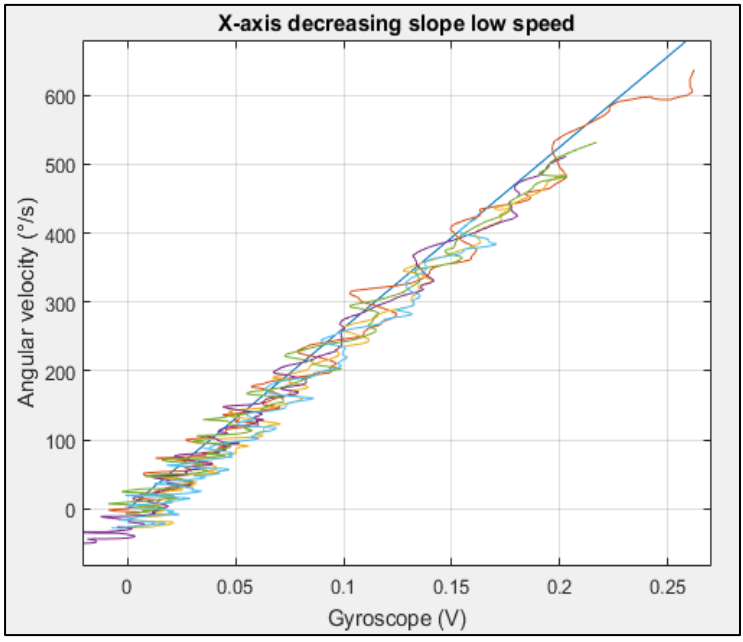

Figure 6-8: Calibration curves of gyroscope up to angular velocity of 600 ° /s.

Figure 6-9 presents the calibration curves up to the angular velocity of 3500 °/s. As observed, the experimental curves correlate well with the linear calibration curve provided by the manufacturer. Some deviations from the linear calibration curve are caused by the vibrations of the set-up but overall all the experimental curves follow the linear calibration curve.
It can therefore be concluded that the calibration of the sensors is not the cause of the discrepancies observed in table 6-3.

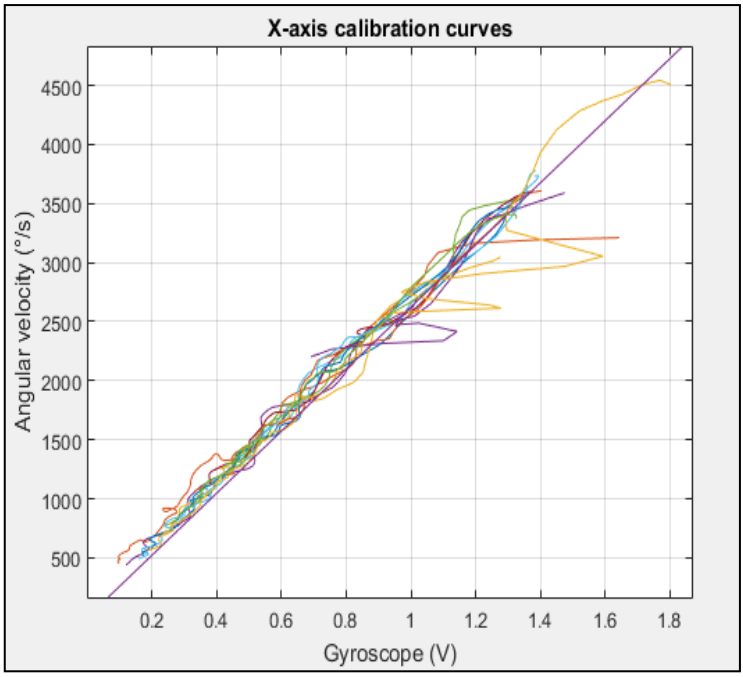

Figure 6-9: Calibration curves up to the angular velocity of 3500 ° /s.

6.3.2.2 Conclusions drawn from studying the sensors

Linear accelerometers were calibrated again. A set-up for calibration of the triaxial gyroscope (ARS) was designed, manufactured and utilised. During the gyroscope calibration experiments, it was found that the sources of discrepancy are related to the signal processing box and not to the sensors. More particularly, it was found that the bandwidth of the accelerometer amplifier (in the data processing box) was below the impact testing range. This could explain the difference in linear accelerations in table 6-3. Moreover, during gyroscope calibration experiments, it was discovered that the previous researchers set the supply voltage of the gyroscope incorrectly to higher voltages which well explained the much higher rotational acceleration and rotational velocity measured previously by KU Leuven sensors during helmet testing. Moreover, from the calibration experiments it can be concluded that the gyroscope works properly. The gyroscope was calibrated for a wide angular rate range (up to 3500 °/s).

6.4 Performing experiments on finalised KU Leuven set-up

6.4.1 Simplified KU Leuven oblique impact set-up

A picture of the modified KU Leuven oblique impact test set-up with its different parts is shown in figure 6-10. As shown in Figure 6-11b-c, the headform is held by the support system at a height of 1.5 m resulting in an impact velocity of 5.4 m/s. The anvil with an angle of 45° was used for the oblique impact test. Foam samples of EPS with density of 80±3 kg/m^3 in the shape of cuboids and dimensions of 80 mm (length) × 80 mm (width) × 25 mm (thickness) were glued firmly on the 45° anvil. The head was subsequently dropped on the sample. To be sure that the direction of the dummy head in the impact plane is kept constant, a smart phone with digital spirit level application was utilised by placing the smart phone on top of the jaw of the dummy head and taking care that it always indicated an inclination of 0° in every direction in-plane before each test (see Figure 6-11d).

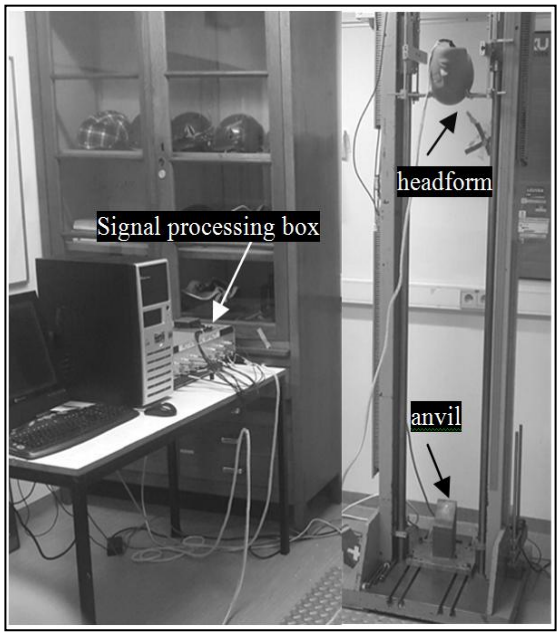

Figure 6-10: Complete image of modified KU Leuven set-up.

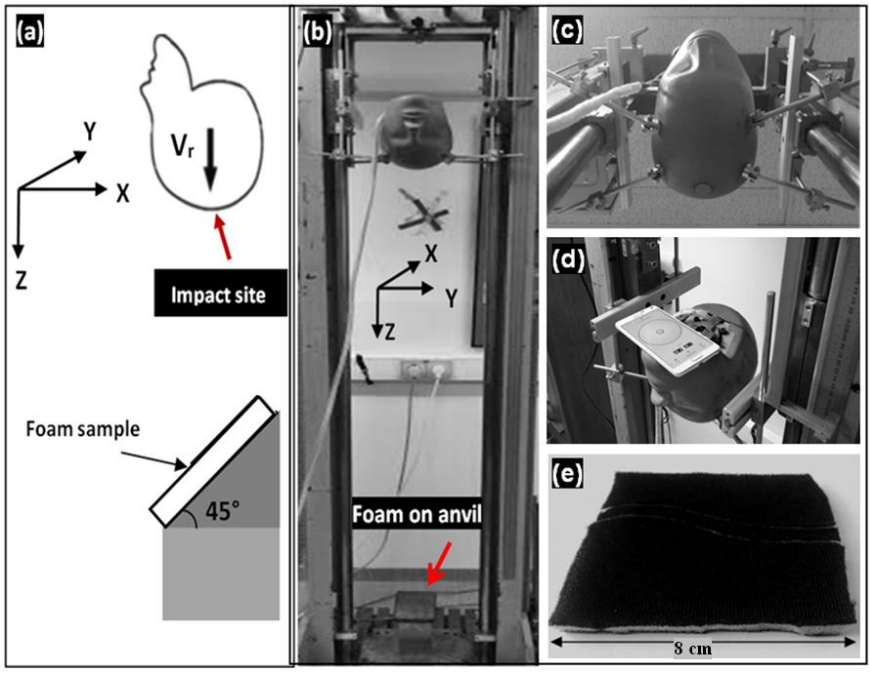

Figure 6-11: (a) Illustration of the oblique impact set up equipped with a hybrid III dummy head which falls on the foam sample at an impact angle of 45 °, the drop direction is shown by a black arrow; sample placed on the 45 ° anvil is shown by the red arrow; (b) front view of the set-up; (c) the headform held by the support system ;(d) fixing orientation of dummy head with digital spirit level; (e) comfort padding.

Since the friction coefficient between the head and the foam plays a role in rotational movement of the head, a thin layer (about 2 mm thickness) of comfort padding obtained from the SportAtlas company in Sweden was placed on all the samples to ensure a constant friction coefficient between the headform and all the foam samples. The comfort pad, shown in Figure 6-11d, was placed and fixed on the foam surface using double sided tape. In this configuration the headform is impacted at its crown and the rotation of the head is mainly around ear-to-ear axis (y axis). To obtain the results, a sampling rate 7000Hz was used. Signals were subsequently filtered off-line in MATLAB using a second order Butterworth filter with a cut-off frequency of 175Hz.

6.4.2 Reproducibility of the oblique impact tests

Figure 6-12 left, right, and below demonstrate the resultant linear acceleration, rotational acceleration and rotational velocity obtained from oblique impact experiments on EPS80 foam samples. As shown, the testing results are quite reproducible.

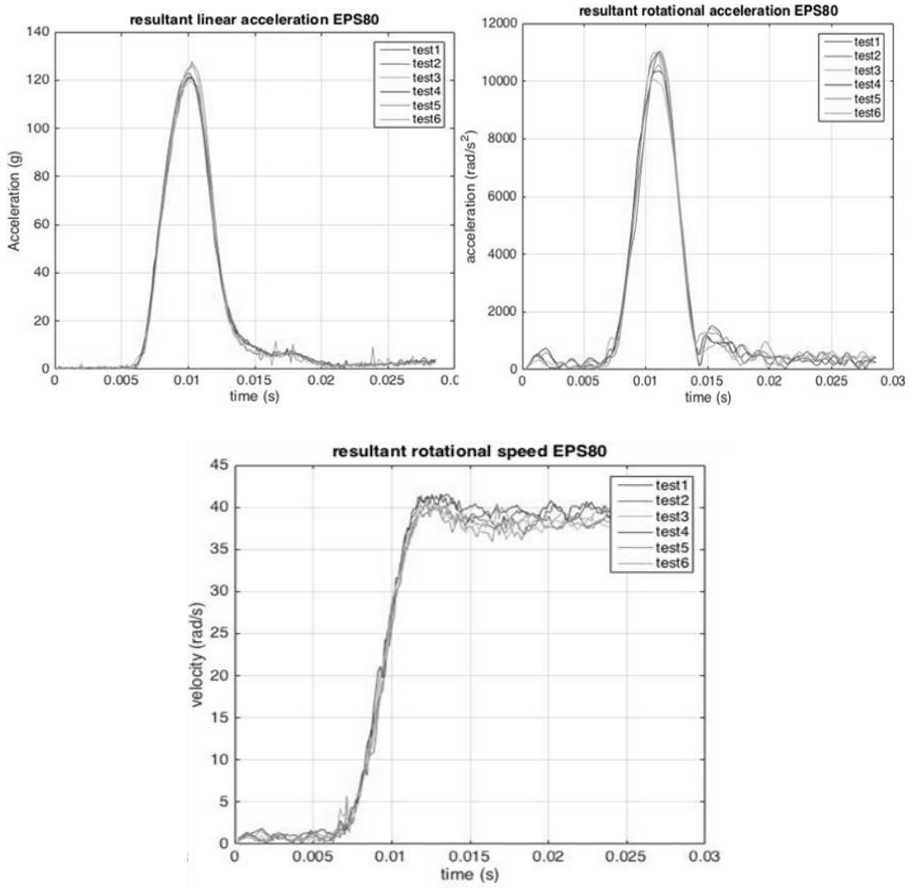

Figure 6-12: (Left) resultant linear acceleration, (right) rotational acceleration, and (below) rotational velocity obtained from oblique impact of EPS80 foam samples placed on an anvil with angle of 45° and the head is dropped from impact height of 1.5 m.

6.5 Oblique impact experiments on several commercial materials

In order to have an initial assessment of available commercial anisotropic materials which can be potentially suitable for head protection in terms of reduction of rotational acceleration in oblique impacts, several materials were selected to be tested using the simplified KU Leuven oblique impact set-up. After extensive search and performing quasi-static mechanical tests (compression and combined shear-compression), the following materials were selected: IMPAXX (extruded polystyrene) foam, PES foam and a special poly amide honeycomb from Econcore.

6.5.1 Selected commercial anisotropic materials

6.5.1.1 EPS80

Expanded polystyrene foam with density of 80±3 kg/m^3 is sourced from Lazer Sport NV in the form of blocks with thickness of 25 mm. EPS80 is used as reference isotropic foam and the performance of other foams are compared with it.

6.5.1.2 IMPAXX Foam

IMPAXX-700 is a closed cell extruded polystyrene foam sourced from Dow chemical with nominal density of 45±5 kg/m^3. IMPAXX foams are proposed for automotive applications (e.g. bumpers or doors) and their function is to absorb the impact energy during crash [7]. The IMPAXX foam has anisotropic mechanical behaviour. This is shown in Figure 6-13 in which quasi-static compression stress-strain curves on IMPAXX foam samples in three orthogonal directions are shown. The anisotropy is induced during the extrusion process of IMPAXX foam by restricting the expansion in one direction. The anisotropy ratio of IMPAXX-700 foam studied here is around 2.7. The production of these materials is limited to flat sheets but it is suggested by the manufacturer that these foams can be thermoformed [8].

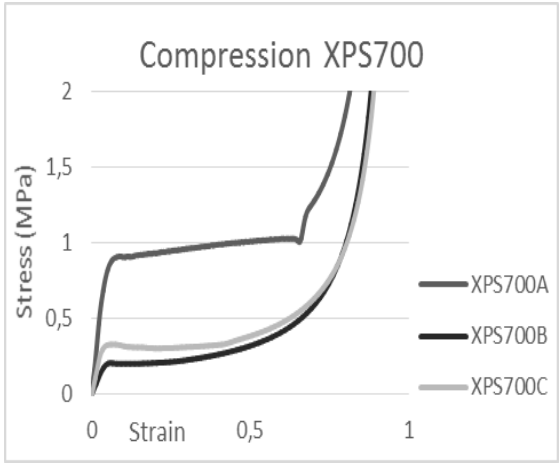

Figure 6-13: Representative compressive stress-strain curves of Impaxx-700 in three orthogonal directions of A, B, and C and it can be seen that A is the cell elongation direction.

6.5.1.3 PES foam from DIAB

Thermoplastic PES (polyethersulfone) foam used in this study was sourced from DIAB company under the commercial name of Divinycell F50. It is developed for aircraft interior applications. The nominal density of Divinycell F50 is 50 kg/m^3 and it has been specifically developed for aircraft interior applications. The study of compression and combined shear-compression behaviour and microstructure of this foam was presented earlier in chapter 4 of this thesis. The anisotropy ratio of this foam was found to be around 2.4.

6.5.1.4 PES foam from ULTRATECT®

Highly anisotropic polyethersulphone (PES) foam, sourced from ULTRATECT® and produced by Thermoplast Composite GmbH [9-10], with density of 57 kg/m^3 and anisotropy ratio around 10. This PES foam was indicated by Verschueren [11] (by oblique impact testing on flat foams) and Vanden Bosche [2] (by oblique impact testing on helmet prototypes) as an alternative to foam which has the potential for a significant reduction of rotational acceleration [12]. However this foam can only be produced in flat slabs and can only be moderately shaped via a cold-forming technique. More details on this foam can be found in thesis of Vanden Bosche, [3]. In this thesis, this foam is used for benchmarking purpose.

6.5.1.5 Polyamide honeycombs

Honeycombs in general have intrinsic anisotropic mechanical properties due to their structure and hence they were considered in our survey of finding potentially suitable commercial anisotropic cellular materials. The thermoplastic honeycomb studied here is shown in Figure 6-14a. It is made of impact absorbing polyamide developed by Toray. The honeycomb structure itself is manufactured by Econcore. This honeycomb has a density of 140±5 kg/m^3, wall thickness of 400 µm, cell size of 6 mm and slab thickness of 10 mm. The honeycomb has been tested in oblique impact in two main directions namely "parallel" and "perpendicular" as shown in Figure 6-14a. The shear properties of honeycombs in these two directions are different and depending on which direction is oriented along the prime direction of the head rotation, it can affect the rotational acceleration of the head. Impact samples are prepared by fixing 2 layers on top of each other with double sided tape. Figure 6-14b compares the quasi-static compression behaviour of honeycomb with the reference EPS80 foam. As observed in the compression curve of the honeycomb, there is a high collapse stress followed by a significant drop during the crushing phase in the plateau region. The low plateau stress means that a thicker layer of honeycomb is needed to absorb similar level of impact energy in comparison to EPS foam. Therefore, in the impact experiments presented in the next sections, two layers of honeycomb are attached to each other by double sided tape.

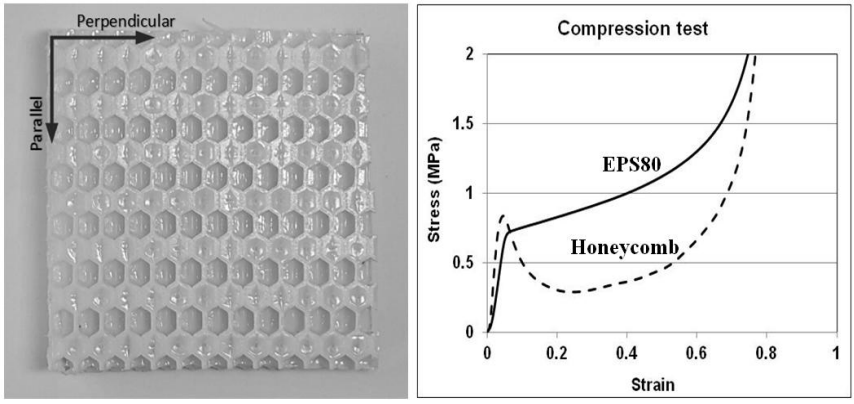

Figure 6-14: (Left) an image of the thermoplastic polyamide honeycomb from above; (right) quasi-static compression stress-strain curve of honeycomb when compressed along the cell direction versus EPS80.

6.5.2 Linear impact results

Linear impact tests were performed using the drop-weight impact tower set-up equipped with a flat steel projectile with a circular cross-section (radius of 50mm), attached to a frame. The total drop weight was set at 4.5 kg resembling the average weight of a hybrid III dummy head as it is used in oblique impact experiments. The drop height was fixed at 1.5 m resulting in impact velocity of 5.4 m/s. Impact samples were cut into cuboids of 70mm ×70 mm × 25mm (thickness of 20 mm in case of honeycombs and PES Ultratect) and placed on the steel plate; the projectile subsequently falls on the foam/honeycomb samples.
Figure 6-15 presents the linear impact behaviour of these commercial materials compared to EPS80. The IMPAXX and PES DIAB foams show significantly lower impact forces (or accelerations) than EPS80, yet at the expense of longer impact duration. Honeycomb shows similar levels of impact force compared to EPS80. These preliminary tests show that IMPAXX and PES foam could outperform the conventional EPS80 in linear impact. The next step is to examine their performance in oblique impact. It should be noted that the impact tests are all performed at room temperature, while in an application such as a helmet, the standards require the impact tests to be performed also at low (-20°C) and high (+50°C) temperatures.

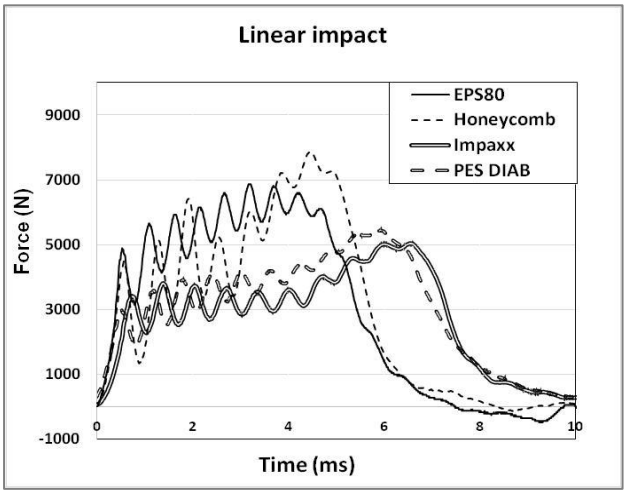

Figure 6-15: Force-time curves obtained from linear impact test of different commercial foams versus EPS80 when impacted at velocity of 5.4 m/s and input energy of 66J.

6.5.3 Oblique impact results

The resultant linear and rotational accelerations and rotational velocity curves (a_r, α_r and ω_r, respectively) are presented in Figure 6-16a-c.

The peak values of linear and rotational accelerations for different foams and the reduction percentage compared to EPS80 are summarized in table 6-4.

It can be observed that PES Ultratect foam with a density around 57 kg/m^3 demonstrates a reduction in both linear and rotational accelerations and rotational velocity in comparison to EPS80 which confirms the earlier observation by Verschueren [10] and VandenBosche [3]; moreover it has – with a thickness of 20 mm – an areal weight of 1140 g/m^2, which is 40% less than EPS80. Although this foam can be used in flat form in interiors such as crashworthy vehicles, forming this foam into the intricate shape of a helmet is difficult. This is because as explained earlier, the highly anisotropic structure is a result of its special processing method which can only produce flat panels [10]. Moreover, according to Vanden Bosche [3] thermoforming of this foam will damage its cell structure and it is important to keep the anisotropy direction in the radial direction in respect to the head to see the reduction of rotational acceleration. Hence from a processing aspect, this particular foam is not suitable for helmets at industrial scale though it outperforms current EPS foam.

PES DIAB foam with micro-size cells and an anisotropy ratio around 2.4 (much lower than PES Ultratect) also demonstrates a reduction in both linear and rotational accelerations of the head, about 23% and 29%, respectively. Also the rotational velocity is reduced compared to EPS80, with a weight reduction of 35%. The peak rotational acceleration in PES DIAB is slightly higher than for PES Ultratect which is believed to be related to the higher degree of anisotropy and lower shear resistance in PES Ultratect, and despite the lower density of the DIAB foam and the lower thickness of the PES Ultratect foam. Therefore it is believed that reduction in rotational acceleration will be augmented for similar thickness and density of both PES types because of the higher anisotropy level in PES Ultratect. According to the manufacturer, PES DIAB can be formed into complex shapes in hot or cold temperatures. Therefore, it can be an interesting alternative anisotropic material for further investigation for helmet application.

IMPAXX foam also outperforms EPS foam by reducing linear and rotational accelerations and rotational velocity by 12%, 21%, and 12%,

respectively. This is accompanied by a weight reduction of more than 40%. The IMPAXX foam had a big variation in its density and the samples with density around 50 kg/m^3 could absorb the linear impact without densifying. Therefore, IMPAXX700 foam can also be an interesting material either in flat shape (e.g. car interiors) or helmet application.

The thermoplastic honeycomb studied here also demonstrates a significant reduction in linear and rotational accelerations and rotational velocity when the main axis of rotation is in parallel or perpendicular direction of the honeycomb as shown in Figure 6-14a. From Figure 6-16, it can be observed that in honeycombs the level of reduction in rotational acceleration and velocity is direction dependent in the plane of impact. It can be observed that the reduction in rotational acceleration depends on how the honeycomb is placed on the anvil. The rotational accelerations in honeycombs can be reduced up to 51% when the main direction of rotation is along the perpendicular direction. This reduction is more significant than when the parallel direction of the honeycomb is oriented along the direction of the rotation (31%). The maximum rotational velocity along perpendicular direction is around 32 rad/s in comparison to parallel direction which is around 35 rad/s and both significantly lower than in case of EPS80 (40 rad/s). This is due to the lower shear resistance of the honeycomb in perpendicular direction. This lower shear resistance of the honeycomb in what is in reality the machine direction of the Thermhex honeycombs, can be explained by the weld lines created during honeycomb production. As can be seen in Figure 6-14, the weld lines are oriented in what was called the parallel direction, leading to thicker honeycomb walls in this direction. However, the much higher density of the employed honeycombs must be taken into account, and the abovementioned reductions are achieved with areal weight of 2800 g/m^2, which is 40% higher than the reference EPS80 foam.

The HIC_{15} and RIC values for the different foams are calculated and tabulated in table 6-5. Similar conclusions can be drawn that all the anisotropic foams demonstrate lower HIC and RIC values than EPS80. Moreover, these foams are lighter which is advantageous for helmet application. RIC and HIC values of the thermoplastic honeycombs are also lower than for reference EPS80 foam. However, the thermoplastic honeycombs have a considerably higher density than EPS foam. As mentioned earlier these experiments have only been performed at

room temperature and repeating these experiments in low and high temperatures is also required for helmet applications.

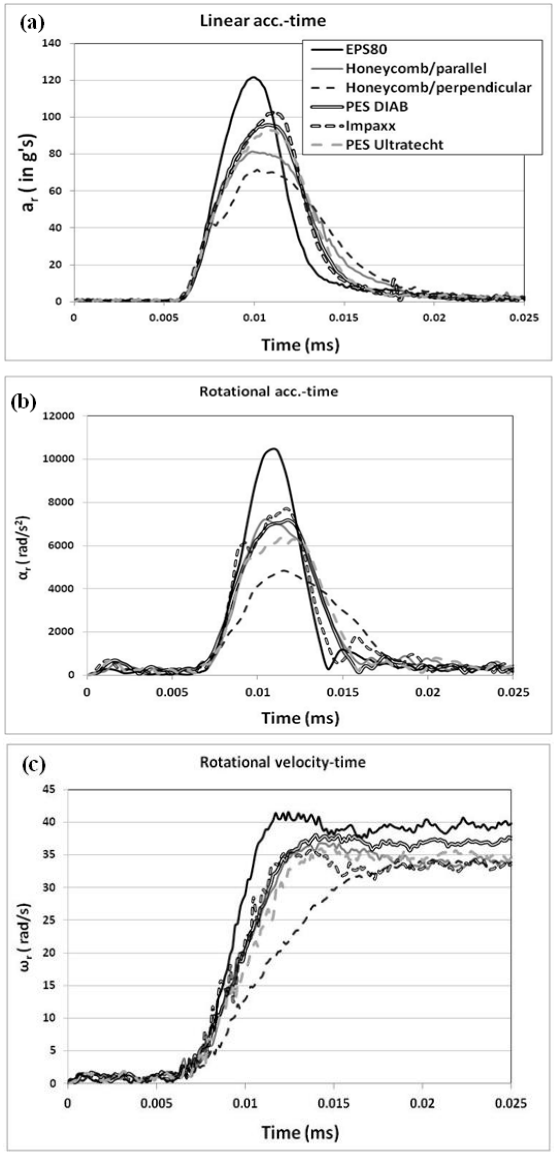

Figure 6-16: Oblique impact results for different commercial materials versus EPS80, (a) linear acceleration, (b) rotational acceleration, and (c) rotational velocity.

Table 6-4: Summary of peak resultant linear ($a_{r,max}$) and peak resultant rotational accelerations ($\alpha_{r,max}$) of different anisotropic commercial materials obtained from oblique impact tests and their reduction in comparison to EPS80 foam.

sample	Areal weight (g/m^2)/ thickness (mm)	$a_{r,max}$ (in g)	Reduction (%)	$\alpha_{r,max}$ (in rad/s^2)	Reduction (%)
EPS80	2000 / 25	123±2	-	10400±400	-
PES Ultratect	1140 / 20	95±1	-22%	7093±366	-31%
PES DIAB	1250 / 25	94±1	-23%	7330±400	-29%
IMPAXX	1125 / 25	108±5	-12%	8145±377	-21%
Honeycomb-parallel	2800 / 20	80±1	-35%	7180±343	-31%
Honeycomb-perpendicular	2800 / 20	72±3	-41%	5018±536	-51%

Table 6-5: Summary of HIC15 and RIC values of different anisotropic commercial materials and their reduction in comparison to EPS80 foam.

sample	Areal weight (g/m^2)/ thickness (mm)	HIC_{15}	Reduction (%)	RIC	Reduction (%)
EPS80	2000 / 25	402±18	-	16870±1000	-
PES Ultratect	1140 / 20	282±8	-29%	8190±560	-51%
PES DIAB	1250 / 25	295±6	-26%	9150±355	-4 5%
IMPAXX	1125 / 25	342±24	-15%	11109±1053	-34%
Honeycomb-parallel	2800 / 20	227±6	-43%	8335±340	-50%
Honeycomb-perpendicular	2800 / 20	169±12	-57%	4045±770	-76%

6.6 Conclusions

The first part of this chapter focused on critical comparison of KU Leuven and KTH moving sled oblique impact set-ups and further development and simplification of the initial KU Leuven oblique impact set-up [2-3]. As the first step to validate the test set-up, during the PhD thesis of Vanden Bosche, oblique impact experiments were performed on helmets by both KU Leuven set-up and KTH set-up and the results were compared in table 6-1. Significant differences in test results (in terms of linear acceleration, rotational acceleration, and rotational velocity) obtained by these two test set-ups were observed. In this thesis, the first goal was to find the sources of these significant differences, to ratify them and to propose a modified test set-up which is simpler to be adopted for future helmet standardization tests.
To identify the sources of discrepancy between the two set-ups, controlled tests were performed and it was concluded that the discrepancy may arise from three main sources:

- The impact surface: rotary band in case of KU Leuven set-up versus moving sled in case of KTH set-up
- Sensors in the centre of gravity of the headform: for KU Leuven set-up comprise of an array of a triaxial gyroscope (ARS) + 3 linear accelerometers and for the KTH set-up, an array of 9 linear accelerometers.
- Signal processing box which contains amplifiers/isolators

By comparing the sled and the rotating belt set-up, it can be concluded that:

- The rotating belt set-up is compact, easy to control and cheaper than the sled set-up.
- Friction experiments indicated that the rubber surface of the belt is more efficient in transferring the horizontal velocity to the impacted headform, however, the rubber surface dissipates some of the impact energy; additionally, its dynamic coefficient of friction is dependent on the velocity and the vertical load. The changing friction coefficient of the rotary band surface increases test variability in a way that is difficult to control. Moreover, this can be one of the sources of discrepancy between results obtained by KU Leuven versus KTH moving sled set-ups.

- Additionally, the rotating belt slips during impact. As this slip is uncontrolled, it negatively affects the repeatability of the tests.

To overcome the shortcomings of both set-ups and to have a cheaper, simpler and compact set-up, an angled anvil impact set-up is preferred, even though using anvil (instead of rotary band/moving sled) couples horizontal and vertical velocities.

Experiments summarized in table 6-3 also showed that there might be an issue with the sensors or signal processing box. By comparing the 9 linear accelerometer array in the KTH set-up with the 3 linear accelerometers + triaxial ARS array in the KU Leuven set-up, it can be concluded that:

- It is necessary to calibrate the ARS in the right velocity range. For this, an in-house calibration set-up was proposed, manufactured and utilized to validate the calibration of the gyroscope in its full working range.
- The same set-up was used to check the data acquisition and processing unit and in this way an error in the amplification was found which did explain the rest of the difference between the experimental results obtained by the two set-ups.
- The numerically unstable differentiation of the ARS signal to obtain rotational accelerations requires the use of an adequate butterworth type of frequency filter to remove signal noise and obtain a decent acceleration curve. Care must be taken that the filter does not alter the result.
- In general, the 9 accelerometer array is more expensive but robust. The 3 linear accelerometers+ARS array is a more economic choice but is less stable than the 9 accelerometer array.

In the second part of this chapter, several commercial anisotropic foams namely, PES Ultratect, PES DIAB, IMPAXX and a thermoplastic polyamide honeycomb were investigated and benchmarked against conventional EPS foam. The goal was to identify the most interesting materials which can reduce linear and rotational acceleration and rotational velocity. Linear and oblique impact tests on flat samples of these materials were performed at impact velocity of 5.4 m/s. The results show that all these anisotropic materials could outperform

EPS80, however, some of these materials like PES Ultratect could only be used in flat shape and are hence not suitable for helmet production. Thermoplastic honeycomb samples were tested in both in-plane directions and in both cases they showed the highest reduction in rotational acceleration/velocity, and also linear acceleration. Moreover, the honeycomb can be thermoformed thus can be used specifically for helmets. However, they have a relatively high density of 140 kg/m^3. Nevertheless, it can still be an option to be used in some parts of the helmet or in bicycle helmets where there are many ventilation holes and as a compensation, the manufacturer can or must use higher density liners.

6.7 Suggestions for further improvement of the KU Leuven set-up

There are some suggestions for further modification of the KU Leuven set-up as following:

- The weight of the whole setup could be increased in order to reduce overall vibrations of the set-up as advocated by helmet testing standards (weight of the set-up around 500 kg). This could be done by placing a concrete heavy block underneath the plinth of the current setup and bolting it in place.
- There is a drop height limitation for the current impact which is 2m. This puts a constraint on the input impact velocities that the helmets can be tested at. Therefore, using a spring in the set-up which can increase the helmeted headform velocity could be considered.
- In the current set-up, the support system is not sufficient to perform the impact tests at any position of the head. Therefore, another suggestion for further improvement of the set-up could be designing a new support system which allows testing of the headform in temporal, frontal and occipital sites.
- Using wireless sensors can be another proposition which simplifies the experiments by omitting the probability of interference of the cables during experiments.

6.8 References

1. Aare, M. and Halldin, P. A New Laboratory Rig for Evaluating Helmets Subject to Oblique Impacts. Traffic Injury Prevention, 2003. 4(3): p. 240-248.
2. Tobback, B. and Boulanger, B. Evaluatie en optimalisatie van rotationele impact tests voor fietshelmen, in Industrial Sciences 2011, Masters Thesis, Lessius Campus De Nayer: Mechelen.
3. Vanden Bosche, K. Development and characterization of novelanisotropic foam for bicycle helmets, 2016, PhD Thesis, Katholieke Universiteit Leuven: Leuven.
4. MTM. Impact testing (low speed impact). Available from: https://www.mtm.kuleuven.be/equipment/impact-lvi/impact-lvi
5. CEN/TC158-WG11. CEN/TC 158 - WG11 Rotational test methods. 2014.
6. Amato, J., and De Ghellinck, J. Analysis and improvement of a rotational impact setup used to test bicycle helmets, 2015, Mater thesis, Katholieke Universiteit Leuven: Campus GroupT.
7. Slik, G., Kleiner, B., Vogel, G. Enhanced occupant safety through use of highly efficient energy absorbing foam. in FISITA 2008. Munich, Germany.
8. Tech Data Sheet IMPAXX™ 700 Energy Absorbing Foam. Available from: https://www.rollbarpadding.com/FS/CO/84/0/IMPAXX700.pdf
9. Technical description of anisotropic PES foam, (ULTRATECT). Available from: http://www.thermoplast-composite.de/gb_schaum.html.
10. Zapf, A., *Processing hints for ULTRATECT-foam*, 2008.
11. Verschueren, P. Biomechanical analysis of head injuries related to bicycle accidents and a new bicycle helmet concept, 2009, PhD Thesis, Katholieke Universiteit Leuven: Leuven.

12. Vanden Bosche, K., Mosleh Y., Depreitere, B., Vander Sloten, J., Verpoest I., Ivens J. Anisotropic polyethersulfone foam for bicycle helmet liners to reduce rotational acceleration during oblique impact. Proceedings of the Institution of Mechanical Engineers H, Journal of Engineering in Medicine. 2017, 231 (9): p.851-861.

Chapter 7

Novel composite foam concept for protective helmets to mitigate rotational acceleration of the head in oblique impacts: An experimental approach

Adopted from:
Yasmine Mosleh, Jos Vander Sloten, Bart Depreitere, Jan Ivens. Novel composite foam concept for head protection in oblique impacts. *Advanced Engineering Materials, 2017. 19 (10).* atr.num. 1700059.
&
Yasmine Mosleh, Leonard Pastrav, Aart W. Van Vuure, Bart Depreitere, Jos Vander Sloten, Jan Ivens. Optimization of composite foam concept for protective helmets to mitigate rotational acceleration of the head in oblique impacts: A parametric study. *Advanced Engineering Materials,* 2018. 20(2). atr.num.1700443.

7.1 Introduction

Oblique impact is the most common situation that cyclists experience during traffic accidents [1-4]. In an oblique impact, the human head undergoes radial and tangential forces. Radial and tangential forces give rise to both linear and rotational (angular) accelerations of the

head. Rotational kinematics of the head is known to be linked to the majority of traumatic brain injuries (TBI) e.g. subdural haematoma and diffuse axonal injuries, [4-8]. The role of rotational acceleration in TBI during direct or indirect impact was first cited in the pioneering work of Holborn. [4] In later research conducted by Gennarelli et al. [5-8], it was proposed that rotational acceleration contributes more than linear acceleration to occurrence of traumatic brain injuries such as concussive injuries, diffuse axonal injuries (DAI), and acute subdural haematomas (ASH). The higher susceptibility of the brain to the shear strain induced by rotational acceleration is due to the fact that the brain tissue is nearly incompressible and its bulk modulus is around six orders of magnitude larger than its shear modulus [9-10], hence for a given impact, the brain is more prone to shear deformation. Kleiven concluded that strain in the brain is more sensitive to rotational rather than linear movement, [10]. As explained earlier in chapter 3, it is believed that by limiting the tangential force transferred to the head, the rotational movement of the head can be mitigated. To reduce the transferred tangential force from the helmet to the cyclist‘s head during impact, it is proposed to use anisotropic foams instead of conventional isotropic foams as helmet liners. The hypothesis is that by introducing anisotropy in a foam liner with the direction of anisotropy perpendicular to the head surface, the shear resistance transmitted to the head can be reduced [11-12].To prove this hypothesis, further research was carried out to study the performance of anisotropic polyethersulfone (PES) foams particularly for bicycle helmets. For this helmet prototypes were made of PES foams and oblique impact experiments were carried out on helmet prototypes as well as standard helmets made of isotropic EPS foams. Oblique impact test results of helmet prototypes showed reduction in peak linear and rotational accelerations of the head up to 39% and 42%, respectively [13-14]. However, in that study PES foam had a different density and solid material properties than EPS foam in reference helmets, which hindered the researchers to conclude that the superior performance of PES over EPS helmet liners was solely due to mechanical anisotropy. Additionally, practical realization of PES foam as an alternative material for helmet liners, in terms of processing and manufacturing on an industrial scale, is significantly challenging. This is because the particular PES foam with high degree of anisotropy can only be processed in the form of slabs and processing the flat PES into the intricate shape of a helmet without damaging the cell structure

appears very time consuming and labour intensive and obviously is not suitable for industry.
In chapter 5, a composite foam, comprising of two different densities of expanded polystyrene (EPS) in column (e.g. cylinder)/matrix configuration, is proposed as a smart structural solution to create mechanical anisotropy in foams at a ''macro level'' without changing the thickness or overall weight of the foam. In this chapter, composite foams with cylinder/matrix configurations have been produced and their behaviour in biaxial combined shear-compression loading and oblique impact is investigated and compared with single layer EPS foam of equivalent density and thickness. The composite foam concept gave the opportunity for a proof of principal study which shows that the mechanical anisotropy as a single variable leads to mitigation of rotational acceleration and velocity of the head during oblique impacts in head protection applications e.g. bicycle helmets. In addition, through a parametric study, it is shown that the level of rotational acceleration and velocity mitigation in composite foams can be tailored and optimized. This can be achieved by changing parameters such as the number of cylinders in the structure, and the compliance of the matrix foam. Moreover, an optimized structure for the best performance in rotational acceleration and velocity mitigation is proposed, supported by applying global head injury criteria.

7.2 Materials

7.2.1 Expanded polystyrene foam and soft polyurethane foam

Expanded Polystyrene bead foams (EPS) with densities of 40±3, 60±2, 80±3, and 120±4 kg/m^3 were sourced from Kemisol and Lazer Sports NV (located in Antwerp, Belgium), in the form of blocks with thickness of 25 mm. These foams are named EPS40, EPS60, EPS80 and EPS120, respectively. Soft open cell polyurethane foam was sourced from Huntsman Polyurethanes in shape of slabs with a density of 130±3 kg/m^3. Compression stress-strain curves of the different foams are shown in Figure 7-1a. To obtain the compressive stress-strain curves of foams, quasi-static compression tests were performed according to ASTM standard D1621/94 using a universal tensile testing machine (Instron) at room temperature. Table 7-1 summarizes the elastic modulus, yield stress and onset of densification strain obtained from compression graphs. All the experiments were performed at least 3-fold.

7.2.2 Composite foam sample preparation

Composite foam with cylinder/matrix configuration where cylinders are arrayed in a square packing (square packing is chosen over hexagonal packing to reduce the complexities of preparation of the composite foam samples in the lab) is shown in Figure 7-1b. In this concept, the cylinder consists of a type of foam with higher compressive and shear properties (modulus and yield/plateau stress) than the matrix foam. Cylinders are surrounded by the matrix foam in this configuration. The cylinder-matrix configuration has largely transversely isotropic mechanical properties in the x-y plane which represents the impact plane in this case. The direction of mechanical anisotropy in this composite foam configuration is in z direction (see Figure 7-1b). This means in case such a structure is used as a helmet liner, the direction of anisotropy would be perpendicular to the surface of the head.

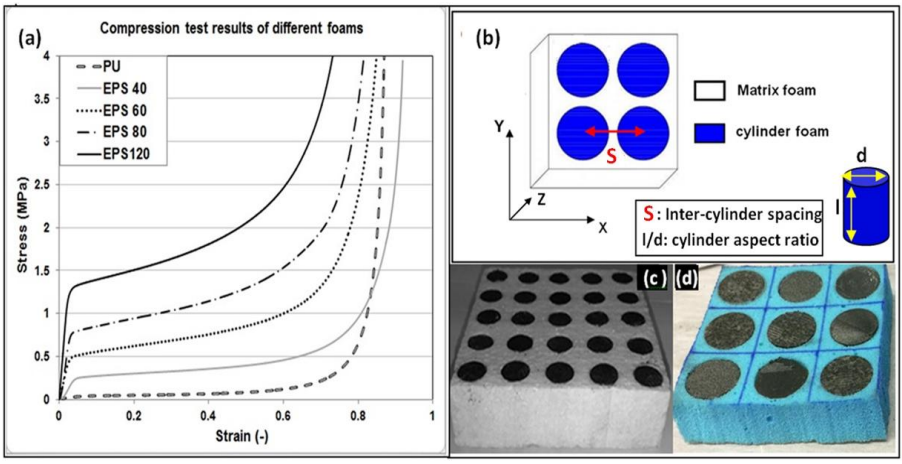

Figure 7-1: (a) Quasi-static compression stress-strain curves of different foams (representative curve of at least 3 tested specimens of each foam); (b) Illustration of composite foam with cylinder/matrix configuration where the cylinders are arrayed in square packing; Composite foam specimens of (c) EPS60m/EPS120f/5×5; (d) PU/EPS120f/3×3.

Matrix foam was chosen from a lower density foam, more precisely foam with lower shear and compressive resistance e.g. EPS40, EPS60 and soft polyurethane. EPS120 was chosen for the cylinders. The list of different composite foam configurations, their coding and cylinder diameters, cylinder aspect ratio and inter-cylinder distance in each configuration, are presented in table 7-2. Cylinder aspect ratio (l/d) and inter-cylinder spacing (S) are illustrated in Figure 7-1b.

Table 7-1: A summary of values for elastic modulus, yield stress and onset of densification strain of different foams which are obtained from quasi-static compression stress-strain curves presented in Figure7-1a.

Foam type	Elastic Modulus (MPa)	Yield stress (MPa)	Densification strain
EPS40	7.1 ± 1.2	0.24±0.01	0.80
EPS60	16.4±0.5	0.49±0.02	0.75
EPS80	28.5±3.1	0.79±0.02	0.72
EPS120	57.2±3.0	1.29±0.02	0.60
PU	0.145±0.010	0.024±0.001	0. 80

Sample coding in table 7-2 is as follows: **''matrix foam (m) /cylinder foam (f) / number of columns of cylinders × number of rows of cylinders''**. For instance, ''EPS60m/EPS120f/5×5'' stands for a composite foam sample with EPS60 as the matrix foam and EPS120 as cylinder foam with 25 cylinders arrayed in a square packing. PU/EPS120f/3×3 represents a composite foam sample with soft polyurethane as matrix foam and EPS120 as cylinder foam with total number of 9 foam cylinders arrayed in a square packing (see Figure 7-1c-d). The overall density of composite foams was kept at 80 kg/m^3 except for PU/EPS120 composites. Single layer EPS80 was chosen as reference material to which the performance of all composite foams was compared. The thickness of reference EPS80 and composite foams was 25 mm.

Table 7-2: A summary of the evaluated composite foam samples for oblique impact, with their coding, cylinder diameter (d), inter-cylinder distance (S), cylinder aspect ratio (l/d) and cylinder volume fraction (ν).

Sample code	Cylinder	Matrix	Number of cylinders	d (mm)	S (mm)	l/d	ν
EPS80 Reference	**EPS80**	**EPS80**	-	-	-	-	-
EPS40m/EPS120 /3×3	**EPS120**	**EPS40**	9	21.2	25.3	1.18	0.5
EPS40m/EPS120 /5×5	**EPS120**	**EPS40**	25	12.7	15.5	1.97	0.5
EPS60m/EPS120 /3×3	**EPS120**	**EPS60**	9	17.3	24.3	1.44	0.33
EPS60m/EPS120 /5×5	**EPS120**	**EPS60**	25	10.4	15.1	2.40	0.33
PU/EPS120f/ 3×3	**EPS120**	**PU**	9	21.2	25.3	1.18	0.5
PU/EPS120f/ 5×5	**EPS120**	**PU**	25	12.7	15.5	1.97	0.5

In order to prepare the cylinder/matrix configuration, firstly, matrix foams were cut into cuboids. Secondly, cylindrical holes were cut using a thin cylindrical hollow drill which was mounted on a drilling machine. Subsequently, cylinder-shape EPS120 foams were cut out of a flat foam slab using the drill, and the cylinders were placed to fill up the holes made in the matrix foam. A thin layer of flexible glue named Pattex 100% Repair Gel® was used to bond the cylinders and matrix. This glue contains no solvent and retains flexibility after setting without stiffening effect on foam behaviour as was verified by impact testing. In order to obtain composite foam samples with an average density of approximately 80 kg/m^3, the cylinder diameters were chosen in such a way that the volume fraction of cylinders and matrix in the composite foam lead to an overall density of the foam of 80 kg/m^3. To achieve this in case of EPS40m/EPS120f and EPS60m/EPS120f, the cylinder volume fraction was fixed at 0.5 and 0.33, respectively.

7.3 Experimental methods

7.3.1 Shear-compression test

In order to measure decoupled shear and compressive stress-strain curves of the foam specimens, a biaxial combined shear-compression set-up was utilized. The combined shear-compression set-up comprises of two independent displacement actuators which apply simultaneous shear and compressive displacements in two orthogonal axes resulting in combined shear and compressive loading of the foam specimens. This set-up was extensively described in chapter 4 of this thesis. The biaxial shear-compression tests are performed at deformation angle of 45° meaning that both shear and compressive displacement rates were set at 2 mm/min. Foam samples for this test were cut in cuboids with dimensions of 50 mm (length) × 50 mm (width) × 25 mm (thickness).

It should be remarked that because the size of the shear-compression samples is different than the size of the impact samples (80 × 80 mm), the dimensions of the cylinders used in the shear-compression samples will be different than for the equivalent impact samples (the cylinders are thinner; for the 3 × 3 configuration the cylinders in the shear-compression samples have diameter 13.3 mm; for the 2 × 2 configuration the cylinders have diameter 19.9 mm). It should then also be immediately remarked that this is not an issue, because our goal is comparison in behaviour between the two test set-ups as function of number of cylinders and matrix compliance, not direct transfer of measured properties. This set-up allows investigation of the qualitative relationship between shear stress level and rotational acceleration.

7.3.2 Oblique impact test

In order to experimentally measure linear and rotational acceleration during an oblique impact, a test set-up was developed at KU Leuven which is illustrated in Figure 7-3a-b. In this set-up, a hybrid III dummy head is mounted on a drop tower via a grip system which is shown in Figure 7-2a. The dummy head is equipped with three linear accelerometers in x, y, and z directions and a triaxial gyroscope in its centre of gravity. The linear accelerometers measure linear accelerations in x, y, and z directions whilst the gyroscope measures the rotational velocities around x, y, and z axes. Rotational accelerations can be obtained by differentiation of rotational velocity

versus time curves. The head was fixed at a height of 1.5 m resulting in an impact velocity of 5.4 m/s. This impact velocity is used in the current bicycle helmet safety standard (EN1078) to evaluate helmets in linear impacts. The height was measured from the first point of contact between the head and the foam. Impact experiments were performed at an oblique angle of 45°. Foam samples were all in the shape of cuboids with dimensions of 8 cm (length) × 8cm (width) × 2.5 cm (thickness). The samples were fixed firmly on the 45° anvil using a double sided adhesive tape (Kip® 342) as shown in Figure 7-2b.

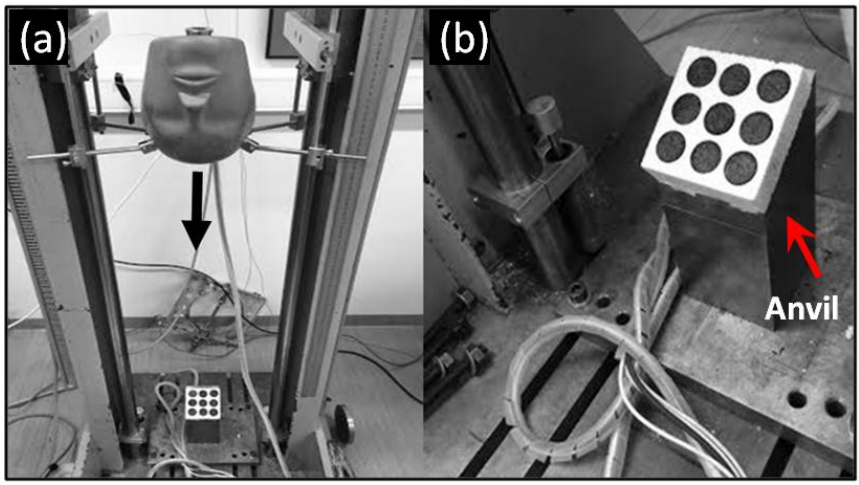

Figure 7-2: (a) Illustration of oblique impact set up equipped with hybrid III dummy head which falls on the foam 11sample at an impact angle of 45°, the drop direction is shown by a black arrow; (b) EPS40m/EPS120f/3×3 composite foam firmly fixed with double sided tape to the 45° anvil.

The head was subsequently dropped on the foam sample. Moreover, a layer of comfort pad, with thickness around 2 mm and obtained from a commercial helmet (Hardtop from SportAtlas, Sweden), was glued by double sided tape on the surface of all the samples in order to have a constant friction between the dummy head and the foam samples. The addition of comfort pad in between the dummy head and the foam liner gives a more realistic friction condition like in real helmets. Different friction coefficients between the head and different foam configurations can affect the rotational behaviour; therefore it is

important to keep the friction between the head and the foam surface for all the configurations similar. All the experiments were performed at least three times and for each material configuration a representative curve was chosen for interpretation of the results.

7.3.3 Global head injury criteria

The oblique impact test results are analyzed according to global head injury criteria such as HIC [15], RIC [16], HIP[17], BRIC [18], and GAMBIT [19] in order to evaluate and compare the performance of composite foam versus single layer EPS80. These global injury criteria are explained in detail in chapter 3.

7.4 Results and discussion

7.4.1 Combined shear-compression behaviour of composite foams

In order to mimic oblique loading but in a quasi-static test, combined shear-compression experiments were performed on different composite foam configurations for a deformation angle of 45°. Compressive and shear stress-strain curves can be obtained simultaneously from each test. Figure 7-3a-b demonstrates the compressive and shear stress-strain curves, respectively, of different composite foams. As observed, composite foams in general demonstrate significantly lower shear stress levels than single layer EPS80 whilst keeping a comparative compressive stress level in biaxial loading. This can be attributed to anisotropic mechanical properties of composite foam inherent to the structure which leads to decoupling of shear properties from compressive properties hence showing decrease in shear resistance. From Figure 7-3b, it can be inferred that two main parameters strongly affect shear stress levels in biaxial behaviour of composite foams, namely the number of cylinders in the structure or in other words, the diameter of the cylinder cross-section, and the compliance of the matrix foam.

In case of EPS40m/EPS120f composite foams, increasing the number of cylinders from 4 to 9, leads to further mitigation in shear stress levels. This phenomenon can be hypothesized to be attributed to earlier onset of shear induced local bending of the cylinders with smaller cross-section in combined shear and compression loading. This will be further elaborated in section 7.5.

Another possible reason is that increasing the number of cylinders means more interface area between cylinder and matrix foams and hence easier deformation under shear, in case sliding could not entirely be avoided at the interface. Moreover, by changing the matrix from EPS40 to soft PU foam, a further decrease in shear stress is observed. This is due to significantly weaker mechanical properties and higher compliance of soft PU foam (see Figure 7-1a) which leads to easier shear deformation in the matrix and allows easier bending of the cylinders.

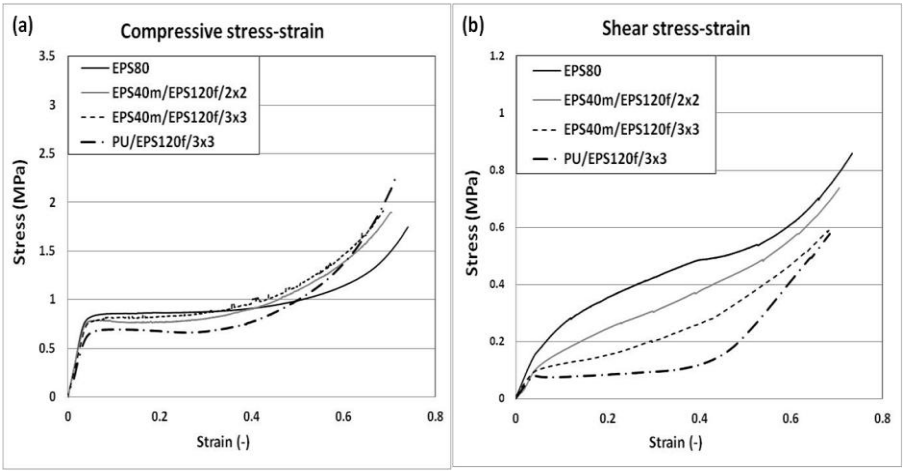

Figure 7-3: (a) compressive stress-strain and (b) shear-stress strain curves of different composite foams versus EPS80 under combined shear-compression loading at deformation angle of 45°.

Compressive stress-strain components of EPS40m/EPS120f demonstrate similar behaviour to EPS80, and overall density seems to govern the compressive behaviour. However, a decrease in compression stress levels can also be observed in case of the PU/EPS120f/3×3 composite in comparison to EPS40/EPS120/3×3 and EPS80, see Figure 7-3a. This is because soft PU matrix with very weak compressive resistance does not contribute much to the overall compressive properties of the structure, unlike EPS40, and the compressive load in the PU/EPS120f/3×3 composite is taken mainly by the cylinder foam. The cylinders can also locally bend more easily with the lower sideways support of the PU foam.

7.4.2 Oblique impact test results

7.4.2.1 Effect of cross-sectional diameter of cylinders on linear and rotational accelerations

Figures 7-4a-c demonstrate the resultant linear and rotational acceleration and rotational velocity versus time of EPS60m/EPS120f with 9 and 25 cylinders compared to single layer EPS80, obtained from oblique impact at an angle of 45°. Figure 7-4d-f shows the oblique impact results of EPS40m/EPS120f with 9 and 25 cylinders. At first glance, it can be concluded that the composite foam concept can reduce rotational acceleration in comparison to a single layer which confirms the initial hypothesis that by creating anisotropy, rotational acceleration transmitted to the head can be reduced without change in the weight and thickness of the liner. Moreover, the effect of reducing the diameter of the cylinders (by increasing the cylinder number from 9 to 25) on reduction of resultant rotational acceleration in EPS60m/EPS120f is highlighted in Figure 7-4b. A small decrease in linear acceleration and rotational velocity can also be observed in Figure 7-4a and 4c. The decrease in rotational accelerations by increasing the number of cylinders is more pronounced in EPS40m/EPS120f composite foams as shown in Figure 7-4e. For the case of linear acceleration and rotational velocity, also a noticeable reduction in maximum values occurs for EPS40m/EPS120 with 25 cylinders (see Figure 7-4d&f).

Average resultant linear and rotational acceleration peak values and maximum resultant rotational velocity are tabulated in table 7-3. The reduction in peak rotational acceleration by increasing the number of cylinders from 9 to 25 (decreasing the diameter of the cylinders from 21.2 to 12.7 mm), can be attributed to lower shear resistance of the composite foam configuration with thinner cylinders, as observed earlier in the biaxial tests (see Figure 7-3b), leading to lower shear force transmitted to the dummy head. The lower shear force transmitted to the head is believed to be the reason for reduction of rotational movement of the head.

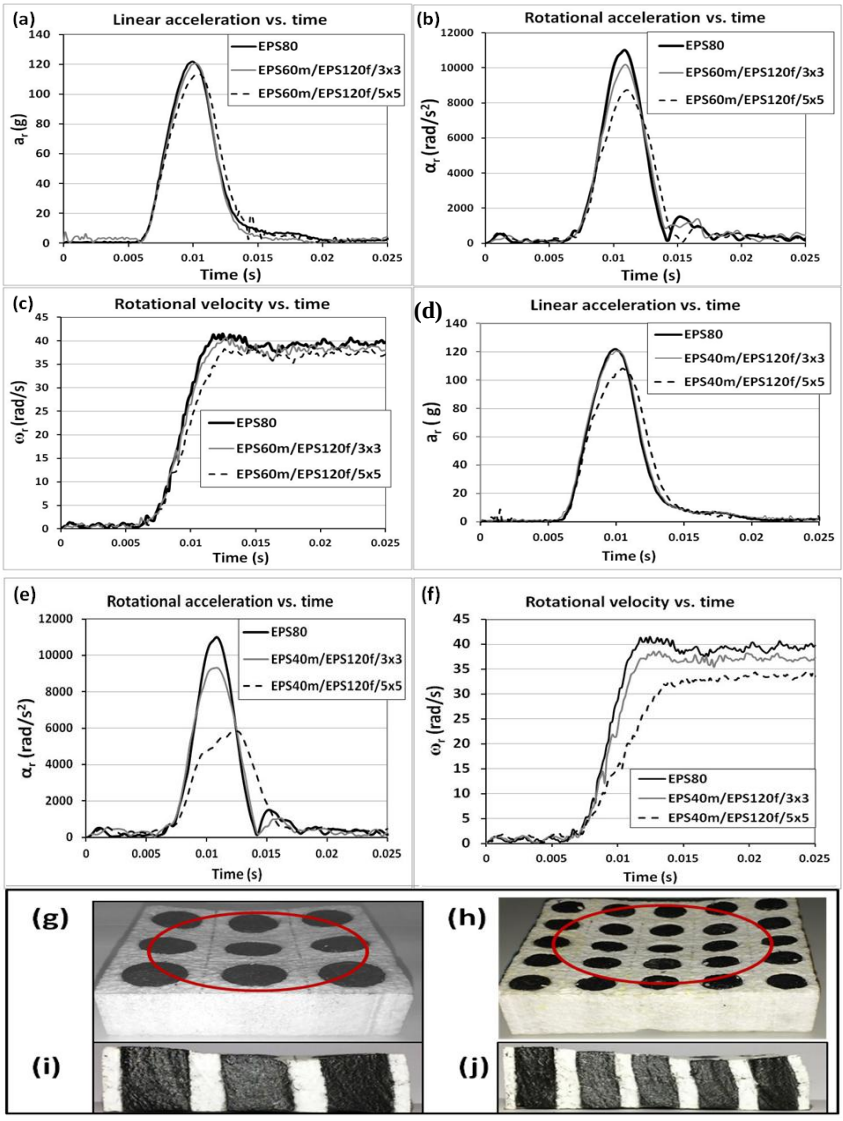

Figure 7-4: Effect of number of foam cylinders in oblique impact behaviour of composite foams of EPS60m/EPS120f and EPS40m/EPS120f with 9 and 25 cylinders versus EPS80; (a,d) Resultant linear acceleration; (b,e) Resultant rotational acceleration; (c,f) Resultant rotational velocity; Pictures of EPS60m/EPS120f with 9 and 25 cylinders (g-h) ; Images of the over-the-thickness cross section of composite foam after oblique impact where bending of the cylinders can be clearly observed (i-j).

Equation 7.1 demonstrates the relationship between a tangential force (in our case the tangential force is the shear force transmitted to the head surface) and the rotational acceleration. In this equation, F_t (N) stands for tangential force to the surface of the head, I ($kg.m^2$) is the moment of inertia of the head and R (m) is the distance between the tangential force and the centre of gravity of the head; α represents the rotational acceleration (rad/s^2). It can be seen that the magnitude of tangential (shear force) transferred to the head has a direct relationship to the rotational movement of the head and a decrease in shear stress can result in reduction in rotational movement (acceleration/velocity) [3].

$$F_t = I\alpha/R \qquad (7.1)$$

As visualized in Figure 7-4g-h, in EPS60m/EPS120f composite foam, by increasing the number of cylinders, a given impact area contains more cylinders with smaller cross-sections which can bend in shear and hence, cause a lower shear resistance of the composite foam structure. Figure 7-4i-j demonstrates the cross sections of the impacted composite samples of EPS60m/EPS120f with 9 and 25 cylinders respectively, which are cut from the middle of the impact specimen. As is shown, more bended cylinders can be seen in case of EPS60m/EPS120f/5×5 (Figure 7-4j).

This means that by optimization of the structure via the diameter of the cylinders, a targeted reduction of linear acceleration versus reduction in rotational acceleration and velocity can be realised in the composite foam concept.

7.4.2.2 Effect of matrix compliance on linear and rotational accelerations

The effect of matrix foam compliance on resultant linear and rotational acceleration and rotational velocity of composite foams with 9 cylinders compared to single layer EPS80 is demonstrated in Figure 7-5a-c. As observed by decreasing the matrix foam mechanical resistance (or increasing compliance, see Figure 7-1a) from EPS60 to soft PU, there is a clear reduction in rotational accelerations. A similar trend can also be observed in Figure 7-5d-f, in which the number of cylinders, for all the composite foams, is kept constant (25 cylinders) to be able to independently investigate the effect of matrix foam. As observed in these composite foams with 25 cylinders, by increasing matrix compliance from EPS60 to soft PU, there is a significant reduction in linear and rotational accelerations and rotational velocity. The reduction in linear acceleration is attributed to the very low contribution of the weak PU matrix in the compressive resistance of the overall composite foam (see Figure 7-3a).

The values of peak accelerations and maximum rotational velocities are tabulated in table 7-3. The effect of matrix stiffness can be attributed to the fact that the weaker matrix foam allows for easier shear deformation of the whole composite foam structure as well as easier bending of the cylinders in the structure. When comparing EPS40m/EPS120f and EPS60m/EPS120f, two competing effects will play a role. The weaker matrix in case of EPS40 will lead to lower resistance to stress, but the bending stiffness of the cylinders will be higher in this case, because the cylinders are thicker (the bending stiffness has a power four relationship with cylinder radius) to obtain the constant overall density of 80 kg/m^3 (see table 7-2 for cylinder diameter). Apparently, in this case the effect of the weaker matrix is larger, since the stress levels for the EPS40 system are lower which leads to lower peak accelerations.
When comparing EPS40m/EPS120f/5×5 with PU/EPS120f/5×5, the thickness of the cylinders remains the same, but the matrix becomes again somewhat softer; this leads to a (limited) further decrease of the

impact stress levels. It was noted that for the PU matrix, there is some time delay in the response peaks; this may be attributed to the very low stiffness of this foam (see Figure 7-1a) where there is hardly talk of a yield or plateau stress.

7.4.3 Correlation between oblique impact and biaxial shear-compression test results

By correlating the results of oblique impact tests with combined shear-compression experiments, both under an angle of 45°, it can be concluded that optimization of parameters such as the number and the thickness of the cylinders as well as the compliance of the matrix foam lead to remarkable mitigation in shear stress levels (see Figure 7-3) and rotational movement of the head (see Figure 7-4 and Figure 7-5).

As a preliminary attempt to correlate the results of oblique impact with combined shear-compression results, both under an angle of 45°, the maximum deformation of each impacted sample was measured and translated into strain. The maximum strains measured from impacted samples of EPS80, EPS40m/EPS120f/3×3, and PU/EPS120f/3×3 were equal to 0.16, 0.17, and 0.18 respectively. From these strains the corresponding shear stress can be estimated from Figure 7-3b and this is equal to 0.31, 0.14 and 0.08 MPa, respectively.

It is believed that there is an intertwined relationship between the shear stress level in the foam structure and the level of rotational acceleration and velocity experienced by the head when the foam structure is incorporated in head protective applications (e.g. helmets). It can then be concluded that the biaxial shear-compression test can be employed as an effective preliminary test to qualitatively compare the performance of different foam liners in mitigation of rotational acceleration of the head in oblique impact. Moreover, it can be inferred that by introducing anisotropy in the foam liner and by controlling decoupling of compressive and shear properties of the foam liner in a way that compressive properties are comparable with standard foam liners whilst shear properties are reduced, a better performance in reducing rotational movement can be observed.

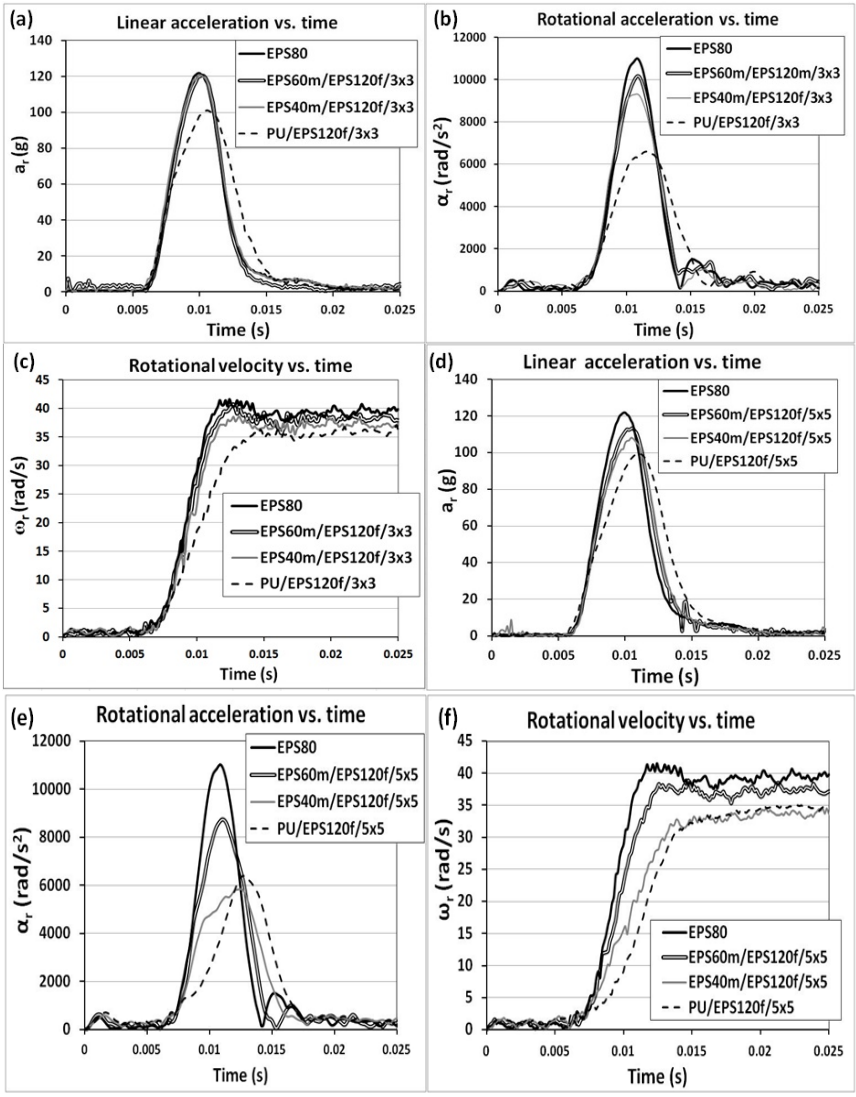

Figure 7-5: Effect of matrix foam compliance in oblique impact behaviour of composite foams versus EPS80, with a matrix of EPS40, EPS60 or PU and 3×3 or 5×5 configuration; (a,d) Resultant linear acceleration versus time; (b,e) Resultant rotational acceleration versus time; (c,f) Resultant rotational velocity versus time.

Table 7-3: Tabulated values of peak resultant linear and rotational acceleration and rotational velocity.

Sample code	$a_{r,max}$ (g)	$\alpha_{r,max}$ (rad/s²)	$\omega_{r,max}$ (rad/s)
EPS80 Reference	123±2	10400±400	40.0±1.0
EPS40m/EPS120f/3×3	122±2	9480±200	38.5±1.0
Reduction percentage	0%	-9%	-1%
EPS40m/EPS120f/5×5	106±2	5780±300	32.5±0.5
Reduction percentage	-14%	-44%	-19%
EPS60m/EPS120f/3×3	122±2	9990±60	39.0±1.0
Reduction percentage	0%	-4%	-1%
EPS60m/EPS120f/5×5	114.5± 1.5	8500±200	37.5±0.5
Reduction percentage	-7%	-18%	-6%
PU/EPS120f/3×3	100±0	6530±100	35.0±0.0
Reduction percentage	-19%	-37%	-12.5%
PU/EPS120f/5×5	98±5	6300±300	32.5±0.5
Reduction percentage	-20%	-40%	-19%

7.4.4 Evaluation of composite foam performance in oblique impact based on global head injury criteria

There are several head injuries induced by head impact. Some of these injuries such as skull fracture are mainly attributed to high linear acceleration. Some other lesions such as acute subdural haematomas and diffuse axonal injuries are mainly attributed to rotational acceleration (and velocities).There are other head injuries such as concussions that are known to be connected to a combination of linear and rotational accelerations. Here by using simplified models known as

global head injury criteria, a preliminary attempt is made to quantify the level of protection of composite foam in comparison to single layer EPS foam. The oblique head impact results are analysed based on most relevant global head injury criteria namely, HIC_{15}, RIC, HIP_{max}, GAMBIT and BRIC. These global injury criteria are all described in detail in chapter 3 of this thesis. Each of these values signifies the probability of head injury occurrence and not its severity and decreasing these values gives some indication of lower injury risk. Therefore, calculating the impact results based on each criterion can be a suitable measure to qualitatively compare the performance of different foams with each other. Calculated values for each criterion for composite foams and reference EPS80 are tabulated in table 7-4.

Table 7-4: Tabulated values of calculated HIC_{15}, RIC, HIP_{max}, GAMBIT, and BRIC values for different composite foams and reference EPS80.

Criterion / *Sample code*	HIC_{15}	*RIC*	HIP_{max} *(kW)*	*GAMBIT*	*BRIC*
EPS80 Reference	**402 ±18**	**16870±100**	**26.8±0.8**	**0.64±0.02**	**1.12±0.01**
EPS40m/EPS120f/3×3	**413±8**	**13720±400**	**26.2±0.4**	**0.61±0.00**	**1.08±0.03**
EPS40m/EPS120f/5×5	**328±2**	**5910±400**	**19.2±0.2**	**0.47±0.01**	**0.84±0.01**
EPS60m/EPS120f/3×3	**413 ±17**	**14980±500**	**27.3±0.8**	**0.63±0.08**	**1.09±0.02**
EPS60m/EPS120f/5×5	**378±12**	**11750±700**	**24.4±0.6**	**0.57±0.01**	**1.02±0.02**
PU/EPS120f/3×3	**320±10**	**6980±100**	**20.1±0.6**	**0.48±0.01**	**0.92±0.01**
PU/EPS120f/5×5	**290±20**	**5520±150**	**18.3±1.0**	**0.45±0.02**	**0.86±0.01**

7.5 Simple analysis for column-matrix configurations

In chapter 5 (section 5.5), the compressive yield stress of composite foams with layered (plate-like arranged in parallel with the loading direction) configuration was evaluated with simple analytical expressions from literature. This showed that for the parallel loaded configuration the composite foam behaviour closely follows the rule of mixture for compressive yield stress.

It was also discussed that the values for yield stress do not change when the composite foam was loaded under an angle of 45°; the compressive component in this case showed exactly the same yield stress as in a simple compression test in 0° direction; however plateau stresses demonstrate reduction when loaded at 45° compared to 0°.

For the column-matrix configurations in this chapter, only static shear-compression tests under an angle of 45° were conducted. The results are summarised in table 7-5.

Table 7-5. Comparison of experimentally measured composite compressive yield stress and value determined according to the classical rule of mixture (ROM), for composite foam with column-matrix configuration, loaded by combined shear-compression under 45°; experimental value shows compression component of stress; ROM is for 0° loading. $\rho_{overall}$ is overall density of composite foam, V_f is the volume fraction of reinforcing phase and d is the diameter of foam columns.

sample	V_f	$\rho_{overall}$ (kg/m³)	d (mm)	Experimental compressive yield stress (MPa)	Compressive yield stress according to ROM (MPa)
EPS40m/EPS120f/ 2×2	0.5	80	19.9	0.76	0.73
EPS40m/EPS120f/ 3×3	0.5	80	13.3	0.76	0.73
PU/EPS120f/ 3×3	0.5	-	13.3	0.70	0.65

As can be seen, like in chapter 5.5, the compression component of the composite yield stress closely follows the rule of mixture for compressive yield stress. This again indicates that under compression, for the systems studied, the failure mode is rather normal foam yield under compression, rather than behaviour dominated by bending or buckling.
The same further analysis, as used in chapter 5 (section 5.5) can also be used for the column-matrix configurations.
Figure 7-6 repeats the analysis, used in chapter 5 (section 5.5), for the system with a weak polyurethane matrix foam (PUm/EPS120f/3×3). It is shown that even here, the experimental compressive component of yield stress is best predicted by the ROM for pure compression. All equations for fine fibres (Rosen, Budiansky) now predict lower yield stress values, because of the very low support of the surrounding matrix foam and the very low buckling resistance of fine fibres. But the high density foam columns with a diameter of 13.3 mm cannot be considered as fine fibres without buckling resistance. On the other hand, the beam-on-an-elastic-foundation prediction is already higher than the experimental value, partly because this model does not include shear. But still the overall picture is that the compressive component of yield stress follows the ROM for compressive yielding. Only for columns with a very small diameter (order a few mm), for values which are not realistic for EPS foam columns, a shift in failure mode (to buckling dominated behaviour) may be expected.
For the EPS 40m/EPS120f samples, the analysis is completely analogous to the analysis in Figure 5-10 in section 5.5. As mentioned, the experimental compression component of the yield stress was equal to the pure compression yield stress for the layered composite foam samples in chapter 5 and Figure 5-10 in section 5.5 showed that in compression the normal compressive yielding would be dominant.
Again, in transverse shear the picture is different. In transverse shear, next to matrix dominated shear, also bending of the reinforcement layers will occur. This can explain behaviour as shown in Figure 7-3b, where thinner columns and a softer supporting matrix lead to increased bending and a lowering of the shear stress levels.

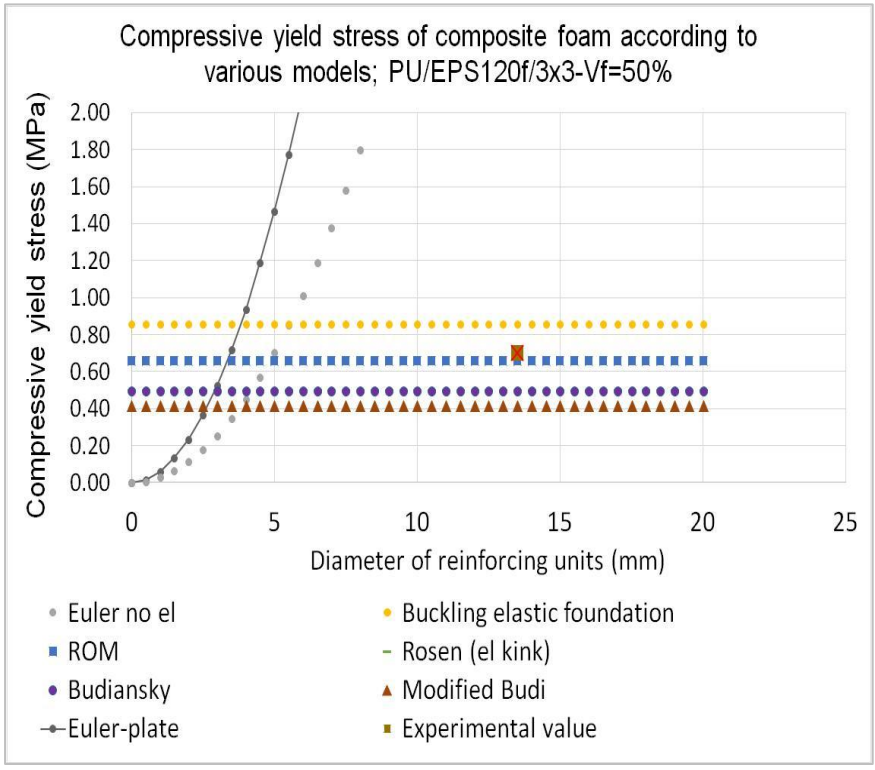

Figure 7-6: Various analytical models for composite compression yield stress applied to the composite foam with reinforcement columns of 13.3 mm diameter in a weak PU matrix.

7.6 Conclusions

The composite foam concept with a cylinder/matrix configuration was proposed in chapter 5 as a smart design that can be incorporated in head protection applications (e.g. protective helmets or energy absorbent panels for interiors of vehicles) to mitigate rotational acceleration and velocity beyond the capacity of single layer homogenous foam. In this study, composite foams with cylinder/matrix configurations were produced in the shape of flat samples. Oblique impact experiments were performed on composite foams at impact velocity of 5.4m/s and oblique angle of 45°.

Through an experimental parametric study on the composite foam structure, it is shown that the level of mitigation of linear and rotational accelerations and rotational velocity experienced by the head can be tailored and optimized in the composite foam concept. It is observed that the parameters such as number and thickness of cylinders, and the matrix compliance, play an important role in the relative extent to which linear and rotational accelerations transferred to the head (and rotational velocity) can be mitigated.

Oblique impact tests using an anvil inclined at 45° showed that peak rotational acceleration and velocity of the EPS40m/120f/5x5 and PU/EPS120f/5×5 composite foam were significantly reduced up to 44% and 19% respectively when compared to the values for standard EPS80. Oblique impact results of all the composite foams and reference EPS80 were analysed based on the most common global head injury criteria such as HIC, RIC, HIP, GAMBIT and BRIC. EPS40m/120f/5×5 and PU/EPS120f/5×5 demonstrated the highest reduction of each criterion (ranging from -19% to -67%) which can be interpreted as a reduced probability of head injury occurrence by using these composite foams.

Furthermore, it was shown there is a clear correlation between biaxial combined shear-compression and oblique impact results. The foams with lower shear stress levels transmitted lower rotational accelerations to the dummy head during oblique impact.

7.7 References

1. Otte, D., Chinn, B., Doyle, D., Mäkitupa, S., Sturrock , K., Schuller, E. Contribution to Final Report of COST 327 Project. University of Hannover,1999.
2. Richter, M., Otte, D., Lehmann, U., Chinn, B., Schuller, E., Doyle, D. Head injury mechanisms in helmet protected motorcyclists: Prospective multicenter study. Journal of Trauma, 2001. 51:949–958.
3. Verschueren, P. Biomechanical Analysis of Head Injuries Related to Bicycle Accidents and a New Bicycle Helmet Concept (Ph.D. thesis). KU Leuven, 2009.
4. Holborn, A.H.S. Mechanics of head injury. Lancet, 1943. 2: p.438- 441.
5. Gennarelli, T.A., Ommaya, A.K., Thibault, L.E. Comparison of translational and rotational head motions in experimental

cerebral concussion. In: Proceedings of 15th stapp car crash conference, SAE P-39, p.797–803. Coronado, CA, 1971.
6. Gennarelli, T., Thibault, L., Ommaya A.K. Pathophysiologic responses to rotational and translational accelerations of the head. Stapp car crash journal, 1972. 16: p.296–308.
7. Gennarelli, T.A., et al., Diffuse axonal injury and traumatic coma in the primate. Annals of Neurology, 1982. 12(6): p. 564-74.
8. Gennarelli, T.A., Thibault L.E. Biomechanics of acute subdural hematoma. Journal of Trauma, 1982. 22 (8): p.680–686.
9. McElhaney J.H., Roberts V.L., Hilyard J.F. Properties of human tissues and components: nervous tissues. In: Handbook of Human Tolerance. Automobile Research Institute Inc. p.143-151.Tokyo, Japan, 1976.
10. Kleiven, S. Evaluation of head injury criteria using an FE model validated against experiments on localized brain motion, intra-cerebral acceleration, and intra-cranial pressure. International Journal of Crashworthiness, 2006. 11:p.65–79.
11. B. Depreitere, J. Goffin, C. Van Lierde, B. Haex, J. Vander Sloten, R. Van Audekercke, G. Van Der Perre, I. Verpoest, P. Verschueren, H. Delye Protective Helmet, E.P. Office, Editor, K.U.Leuven Research & Development, 2008.
12. Verschueren, P. Biomechanical analysis of head injuries related to bicycle accidents and a new bicycle helmet concept, 2009, PhD Thesis, Katholieke Universiteit Leuven: Leuven.
13. Vanden Bosche, K. Development and Characterization of Novel Anisotropic Foam for Bicycle Helmets, 2016, PhD Thesis, Katholieke Universiteit Leuven: Leuven.
14. Vanden Bosche, K., Mosleh, Y., Depreitere, B., Vander Sloten, J., Verpoest, I., Ivens, J. Anisotropic polyethersulfone foam for bicycle helmet liners to reduce rotational acceleration during oblique impact. Proceedings of the Institution of Mechanical Engineers, Part H: Journal of Engineering in Medicine, 2017. 231(9):p.851-861.
15. Versace, J. A review of the severity index, in 15th Stapp Car Crash Conference1971. p. 771-796.
16. Kimpara, H., Iwamoto, M. Mild traumatic brain injury predictors based on angular accelerations during impacts. Annals of Biomedical Engineering, 2012. 40(1):p.114–126.
17. Newman, J.A.S., Shewchenko, N. Welbourne, E. A proposed new biomechanical head injury assessment function—the maximum

power index. In: 44th Stapp Car Crash Conf. SAE paper no. 2000-01-SC16.2000.
18. Takhounts, E.G., Hasija, V., Ridella, S.A., Rowson, S., Duma, S.M. Kinematic Rotational Brain Injury Criterion (BRIC). In: Proceedings of 22nd International Technical Conference on the Enhanced Safety of Vehicles (ESV). Paper no. 11-0263. Washington, D.C., 2011.
19. Newman, J. A generalized acceleration model for brain injury threshold (GAMBIT). In: Proceedings of the International Research Council on Biomechanics of Injury (IRCOBI) Conference, 1986.p.121–131.

Chapter 8

Novel composite foam concept for protective helmets to mitigate rotational acceleration of the head in oblique impact: Numerical approach

Adopted from: Yasmine Mosleh , Martin Cajka, Bart Depreitere, Jos Vander Sloten, Jan Ivens. Designing safer composite helmets to reduce rotational accelerations during oblique impacts, Proceedings of the Institution of Mechanical Engineers Part H Journal of Engineering in Medicine, 2018. 232(5):p.479-491.

8.1 Introduction

Composite foam concept comprising of two different densities of EPS foams in a ''column (cylinder)/matrix'' configuration is proposed in chapter 5 to introduce anisotropy in foam liners at a "macro level". In chapter 7, composite foam samples with a column (cylinder)/matrix configuration were actually produced and oblique impact tests (using hybrid III dummy head) on flat foam samples, at an oblique angle of 45°, indicated that the concept of composite foam could be a promising structural solution to reduce rotation of the head. Moreover, it was proved that the mechanical anisotropy as a single variable in a foam liner leads to mitigation of rotational acceleration and velocity of the head during oblique impacts. In addition, through a parametric study, it has been shown that the extent of rotational acceleration and

velocity mitigation in composite foams can be tailored by changing parameters such as the diameter of columns (cylinders) in a given structure and the compliance of the matrix foam.
In this study, the performance of the composite foam concept with column/matrix configuration in flat and helmet shape is further investigated by performing finite element simulations of linear and oblique impacts. The results obtained by FE simulations of oblique impact are also compared with experimental tests results. The aim is to investigate the structural parameters that can further improve and optimize the performance of composite foams in mitigation of rotational acceleration and velocity during oblique impact. These parameters include the diameter of the columns in a given structure, cross-sectional shape of the columns and the matrix compliance (by inversing matrix and column foams). The anisotropic composite foam concept can be utilised in head protection applications, aiming here specifically at bicycle helmets. This concept can be used in other protective helmets such as motorcycle helmets, equestrian helmets, and ski helmets, or e.g. in automotive headliners.

8.2 Experimental part

8.2.1 Materials

8.2.1.1 EPS foams

For the experimental part of this study expanded polystyrene (EPS) foams with actual densities of 40±3, 80±3, and 120±4 kg/m^3 were sourced from Kemisol and Lazer Sports NV (Belgium), in shape of blocks with a thickness of 25 mm. These foams are referred to as EPS40, EPS80 and EPS120, respectively.

8.2.1.2 Composite foams with different configurations

The composite foams have a column (cylinder)/matrix configuration as shown in Figure 8-1 where columns (here cylinders) are arrayed in a square packing. As mentioned in chapter 5 and chapter 7, in order to have transversely isotropic behaviour in the plane of the impact, in real applications, a hexagonal packing of the columns is preferred; however, to make composite sample production less complex, a square packing was chosen for the experimental parametric study in chapter 7. To be able to compare simulation results with experiments, the same square packing is used in the simulations. The composite foams are

aimed to have overall density of 80 kg/m^3 and their performance is compared with single layer EPS80 of equivalent thickness. To obtain the overall density of 80 kg/m^3, the volume fraction of EPS120 and EPS40 in the composite foam sample is targeted to be 50%. Figure 8-1 demonstrates different configurations of composite foam and their coding throughout the chapter. For instance, EPS40m/EPS120f/4×4 stands for a composite foam sample in which EPS40 is used as matrix foam and EPS120 as cylinder foam (foam column) with a total number of 16 columns arrayed in a square packing. Different configurations of composite foams in this chapter with their geometrical information are tabulated in table 8-1.

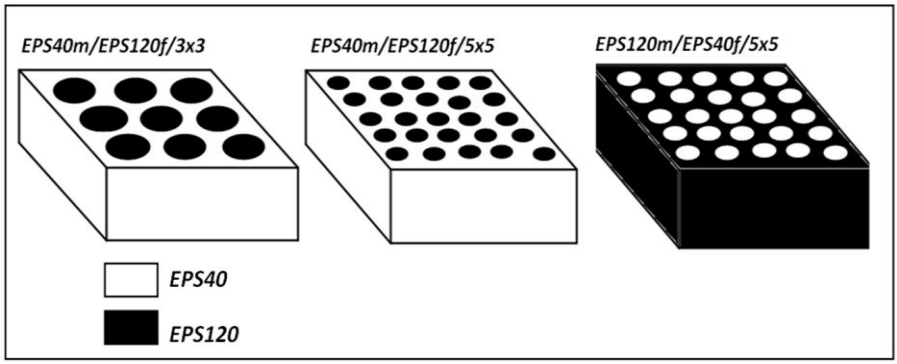

Figure 8-1: Illustrations of different column ("fibre")/matrix composite foams with their coding, where foam columns are embedded in matrix foam in a square packing.

8.2.2 Testing methods

8.2.2.1 Quasi-static compression experiments

Quasi-static tests of EPS foams with three different densities of 40, 80 and 120 kg/m^3 were performed according to ASTM standard D1621/94 using a universal tensile testing machine (Instron). Foams were compressed at a constant displacement rate of 2.5 mm/min. Foam samples were in the shape of cuboids with dimensions of 50 mm (length) × 50 mm (width) × 25 mm (thickness).

Table 8-1: Simulated flat foam samples with their coding and constituents comprising matrix foam, foam column and column cross sectional shape and size.

Composite foam coding	Matrix foam	Column foam	Cross-sectional geometry	Diameter of columns (mm)
EPS40m/EPS120f/3×3	EPS40	EPS120	circle	21.2
EPS40m/EPS120f/4×4	EPS40	EPS120	circle	15.8
EPS40m/EPS120f/5×5	EPS40	EPS120	circle	12.6
EPS120m/EPS40f/5×5	EPS120	EPS40	circle	12.6
EPS40m/EPS120f/5x5 square	EPS40	EPS120	square	11.3
EPS40m/EPS120f/5×5 hexagonal	EPS40	EPS120	hexagonal	14.0
Helmet EPS40m/EPS120f circular big	EPS40	EPS120	circle	11.6
Helmet EPS40m/EPS120f circular small	EPS40	EPS120	circle	5.8

8.2.2.2 High strain rate compression experiments

For investigating the high strain rate compression behaviour of EPS foams, a drop tower impactor was used. In these experiments, EPS foam samples (with three densities of 40, 80, and 120) were impacted at a velocity of 5.4 m/s (initial strain rate of $215s^{-1}$) by a flat steel projectile with a circular cross section of 5 cm diameter. To achieve the impact velocity of 5.4 m/s, the impact height was 150 cm; the weight of the impactor was 4.5 kg resembling the average weight of human head. EPS foam samples were cut into cuboids with dimensions of 5 cm (length) × 5cm (width) × 2.5cm (thickness).

8.2.2.3 Oblique impact experiments

The oblique impact experiments were performed using a drop weight impact tower. In this experiment, a hybrid III dummy head (*50^{th}* percentile *male)* is utilized as headform. The dummy head was fixed at a height of 150 cm resulting in an impact velocity of 5.4 m/s. The velocity of 5.4 m/s is used in the current bicycle helmet safety standard (EN1078) to evaluate helmets in linear impact. A steel anvil with angle of 45° was used for the oblique impact test. The hybrid III

dummy head is equipped with an array of three linear accelerometers and a triaxial gyroscope in its centre of gravity allowing the measurement of the three linear accelerations and three rotational velocities in x, y, and z directions, respectively. Foam samples in the shape of cuboids and dimensions of 80 mm (length) × 80 mm (width) × 25 mm (thickness) were fixed firmly on the 45° anvil using double sided adhesive tape (Kip® 342). The head was subsequently dropped on the sample. Since the friction coefficient between the head and the foam plays a role in rotational movement, a thin layer (about 2 mm thickness) of comfort pad obtained from SportAtlas company in Sweden was placed on all the samples to ensure a representative friction coefficient between the head and all the foam samples. The comfort pad was placed and fixed on the foam surface using double sided tape.

The oblique impact tests were performed on EPS80, and composite foams of EPS40m/EPS120f/3×3 and EPS40m/ EPS120f/5×5, to have a qualitative comparison with simulation results of the same composite foam configurations and also to compare the performance of composite foam versus single layer EPS foam (of the same thickness and density) in real experiments. All materials were tested at least three times to ensure the repeatability of the results and a representative curve for each material has been chosen for interpretation of the results. All experiments were performed at room temperature.

8.3 Simulation part

8.3.1 Description of FE model and simulation parameters

Numerical simulations were performed to investigate the linear and oblique impact performance of composite foams in comparison to single layer EPS foam using Abaqus/Explicit. The FE impact simulations consist of three main parts, the EPS foam, the headform and the anvil. The impact simulations were carried out for two different impact velocities of 5.4 m/s and 6.5 m/s.

For the simulation of oblique impact behaviour, two different configurations were considered which are shown in Figure 8-2a&c. In the first case (Figure 8-2a), the flat foam sample with dimensions of 8 cm (length) × 8 cm (width) × 2.5 cm (thickness) is placed on a 45° anvil and the headform (approximated as a sphere) is dropped vertically on

the foam specimen with the specified impact velocities. In the second configuration, the foam is shaped on the spherical headform and covers half of the headform, resembling a hemispherical helmet and dropped on 45° anvil which is illustrated in Figure 8-2c. For simulating linear impact, the helmeted headform is dropped on the 0° (flat) anvil as shown in Figure 8-2b.

Headform: For the purpose of simplification, the headform is approximated as a sphere. The radius of the spherical head model was set at 8.5 cm. The weight of the headform was set to 4.5 kg similar to the weight of an hybrid III dummy head. In these simulations, the headform is modelled as a rigid body and the linear and rotational accelerations transferred to the headform were read from the centre of mass.

EPS foam: The EPS foam liner was modelled in Abaqus using the crushable foam model for isotropic material with volumetric hardening [1] in conjunction with a linear elastic model. Material properties of EPS crushable foams such as Young's modulus, yield stress and plateau stress for the constitutive model used in the current study were determined by performing quasi-static compression experiments (see Figure 8-3a). Poisson's ratio can be considered being independent of the strain rate and equivalent to zero for EPS in this range of density [2-3]. The strain hardening of the polymeric foam is defined by the constitutive stress-strain relationship which is a function of strain rate. The yield stress at an initial strain rate of 215 s^{-1} (when the foam is impacted by the projectile with a velocity of 5.4 m/s) for each foam density, was obtained from dynamic compression experiments and fed into the material model in Abaqus which will be further discusses in section 8.4.1. For meshing of the foam, C3D8R elements were used with distortion control which does not allow elements to invert during large deformations. The columns (fibres) and matrix foam were bonded perfectly to each other in the model.

The Anvil: The anvil was also modelled as a rigid part. The friction coefficient between the headform and the foam in the configuration where the foam was placed on the anvil (Figure 8-2a) and also between the hemispherical helmet and the anvil (Figure 8-2b) was set to $f=0.3$ in first approximation. The foam was connected to the anvil, in Figure 8-2a, or to the headform, in Figure 8-2b, using coupling where all the degrees of freedom of the foam surface in contact with the anvil or with the headform were restrained.

For the case of simplicity, for both simulations a friction coefficient of 0.3 was chosen, as the purpose of the simulations was comparison of different foam configurations. For polymer to steel, as in the second case, a sliding friction coefficient of 0.3 is realistic [4].

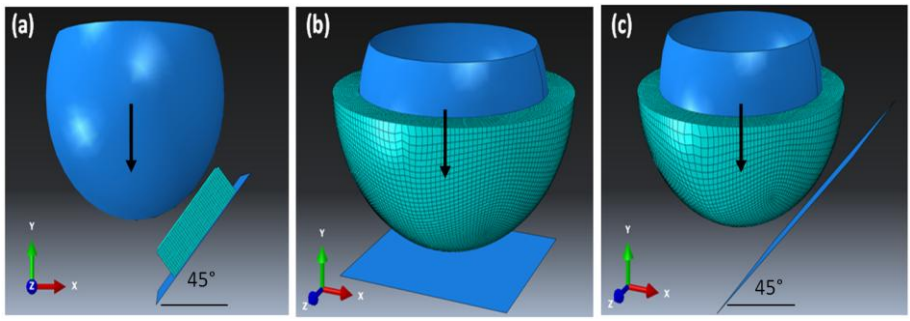

Figure 8-2: Illustrations of (a) Oblique impact of the head on a foam where the foam sample is placed on the anvil at an angle of 45°; (b) Linear impact of helmeted head on anvil at angle of 0° ; (c) Oblique impact of helmeted head at an angle of 45°, black arrow demonstrates the direction of the impact velocity.

8.4 Results and discussions

8.4.1 Static and dynamic compression

The quasi-static compression tests were performed on EPS foams of different densities (40, 80, and 120 kg/m^3) and stress-strain curves are illustrated in Figure 8-3a. Based on the experimental compression test results, the parameters for the crushable foam model in Abaqus can be determined and provided as input to the model. The static compressive stress–strain curves for EPS foams obtained from FE modelling are shown and compared to the experimental curves in Figure 8-3a, demonstrating that the crushable foam model can be used. The dynamic compressive stress-strain curves of these EPS foams obtained from FE modelling when impacted at velocity of 5.4 m/s (initial strain rate of 215 s^{-1}) are also plotted and compared with curves obtained from experiments in Figure 8-3b. As observed, a good quantitative match between experimental and modelling results can be observed for both quasi static and dynamic compressive stress-strain curves of EPS foams, when the crushable foam model is applied.

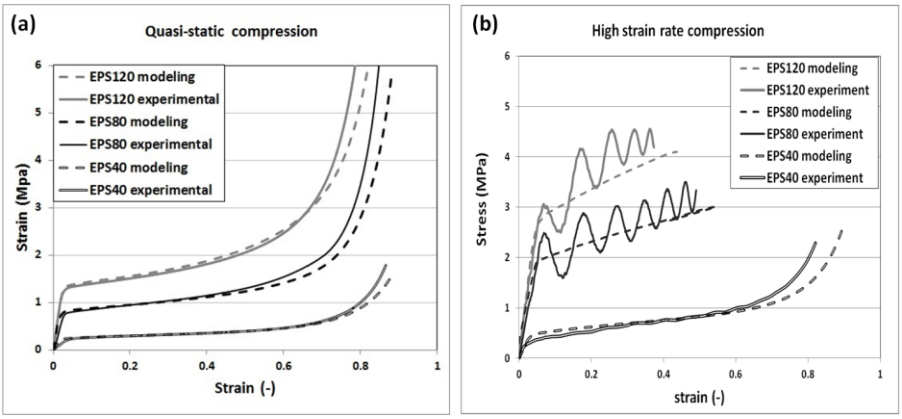

Figure 8-3: Comparison between compressive stress strain curves for EPS foam with three different densities (80, 100 and 120 kg/m^3) obtained from experiments and FE modelling (a) static compression; (b) dynamic compression.

8.4.2 Simulation of oblique impact of head on flat foam

8.4.2.1 Effect of column number on oblique impact performance of inclined flat composite foam

Figure 8-4a-f demonstrate resultant linear and rotational accelerations and rotational velocity versus time, transferred to the headform. These results are acquired when the headform impacted EPS40m/EPS120f flat composite samples with 9, 16, and 25 columns (here cylinders) at 45° oblique angle at two different impact velocities of 5.4 m/s and 6.5 m/s. As observed in Figure 8-4a&d, only a slight decrease can be observed in linear acceleration transferred to the headform by increasing the number of columns in the composite foam from 9 to 25. However, a significant reduction in rotational acceleration and rotational velocity can be observed. The mitigation of rotational acceleration in composite foams is believed to be linked to introducing anisotropy in the foam structure and as a result reducing shear stress transferred to the head. The reduction of shear stress in composite foam in comparison to single layer EPS foam corroborates the results presented in chapter 7, performing combined shear and compression experiments mimicking oblique loading.

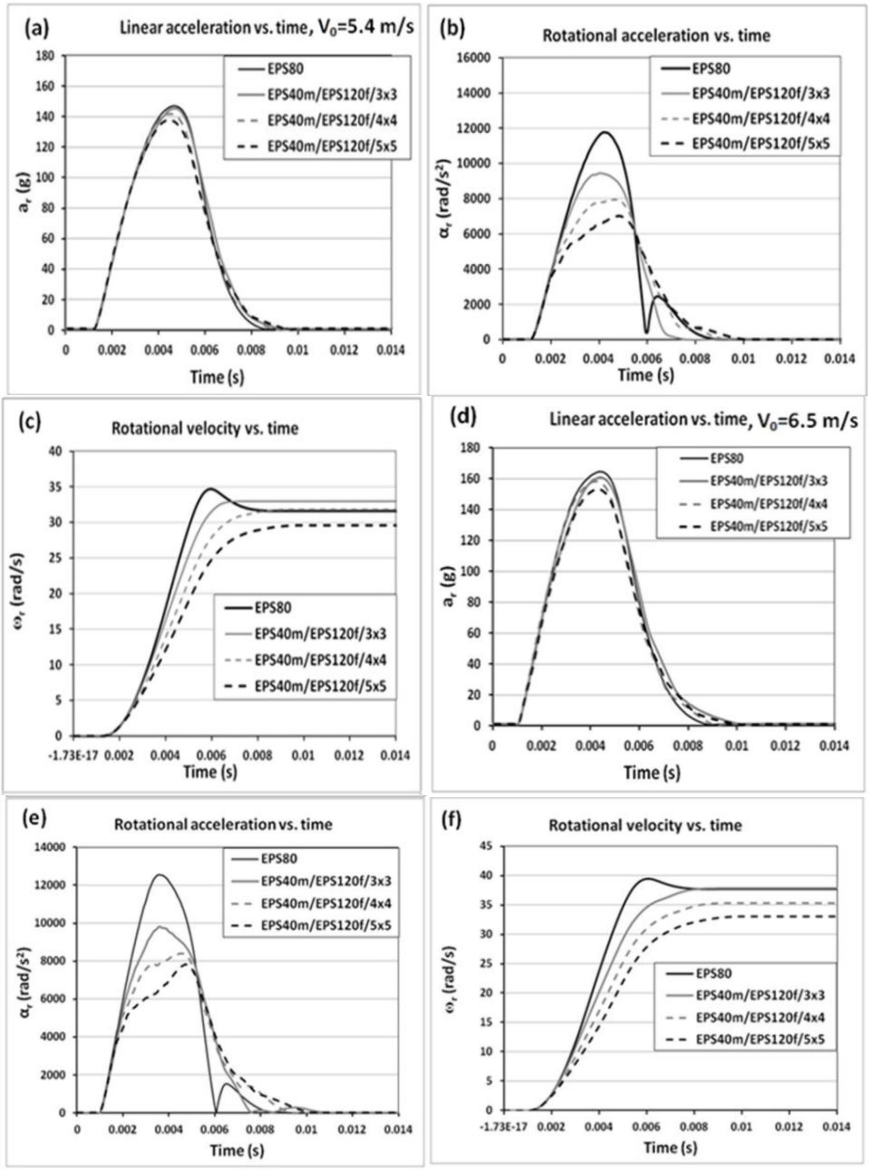

Figure 8-4: Simulation results: Effect of column number in oblique impact behaviour of composite foams versus EPS80 when the headform impacted flat foam laid on the anvil at an angle of 45°; with impact velocity of 5.4 m/s and 6.5 m/s, respectively; (a&d) Resultant linear acceleration versus time; (b&e) Resultant rotational acceleration versus time; (c&f) Resultant rotational velocity versus time.

In addition, as shown in Figure 8-4, by increasing the number of foam columns (cylinders) in composite foam from 9 to 25, further mitigation of rotational acceleration and velocity can be observed. This is due to the fact that by increasing the number of EPS120 columns, they become thinner leading to easier shear induced bending of the columns and hence lower shear force transmitted to the dummy head. This was discussed in chapter 7 (section 7.5). The shear force transmitted to the head is believed to be linked to head injury risks. However, more important will be the transferred rotational energy, hence the importance of pulse duration of the experienced rotational acceleration, as will be analysed further on in section 8.4.2.4 with various head injury criteria, in which pulse duration is included.

The deformation mode of the EPS120 columns embedded in EPS40 matrix is shown in Figure 8- 5a-b and is dominated by shear induced bending. To validate the modelling findings and to assess the efficiency of the model in predicting the composite foam behaviour in a qualitative manner, oblique impact experiments have been performed as explained earlier in section 8.2.2.3. Oblique impact results are presented for EPS40m/EPS120f with 9 and 25 columns in comparison to single layer EPS80 in Figure 8-6.

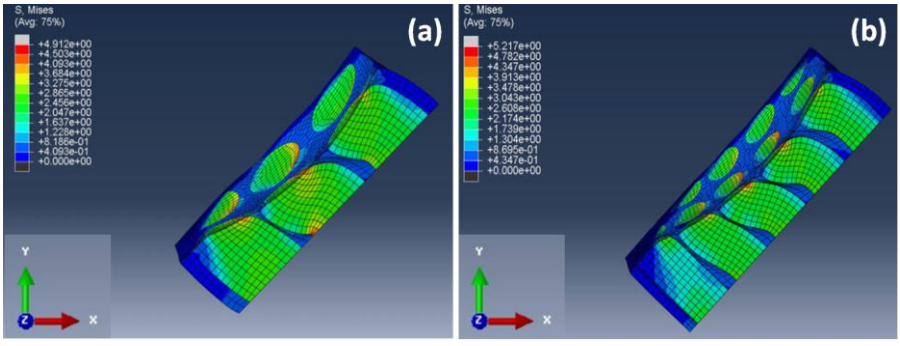

Figure 8-5: Deformation of composite foam samples when impacted by the headform at oblique angle of 45° (a) EPS40m/EPS120f/3×3, (b) EPS40m/EPS120f/5×5; bending and shearing mode of deformation of columns during impact can be observed in these samples.

The results of Figure 8-6 were obtained when a hybrid III dummy head impacted the foam samples with impact velocity of 5.4 m/s at an angle of 45°. Similar trends as for the simulation results (Figure 8-4a-c) can be observed in the experimental results shown in Figure 8-6a-c. The absolute values of the different simulated properties are even within 20% of the experimental values. As predicted by simulations, by decreasing the diameter of the columns in the composite foam structure, the rotational acceleration and velocity of the dummy head can be significantly reduced. Both the experimental and modelling results indicate a prolongation of impact duration around 2 ms for EPS40m/EPS120f/5×5 composite in comparison to EPS80 reference foam. The effect of these changes in rotational acceleration and velocity values, combined with the effect on impact duration, will be analysed further on with various head injury criteria in section 8.4.2.4.

As mentioned, there are differences up to about 20% in the absolute values of linear and rotational accelerations and rotational velocity between the simulation and real experiments. One possible reason for this discrepancy in absolute values can be due to the different geometries of the headform; in experiments a hybrid III dummy head is used whilst in the simulations the headform is approximated as a sphere and this will affect the moment of inertia and dynamics of the rotation. The difference in shape may also affect the size of the contact area, which will also affect the induced stresses. Another reason is the possibly different friction coefficient between the dummy head and the comfort pad placed on the foam, than the value of 0.3 that was assumed in the models. Due to lack of data (at the time that the modelling was performed) on the value of the friction coefficient between the hybrid III dummy head and the foam samples, this was not further verified. To study the influence of the various relevant friction coefficients is one of the recommendations for future work. However, the main goal of the simulation was to enable the comparison of different geometrical configurations in composite foam in comparison to single layer EPS foam and also to optimize the foam structure for the best performance in rotational movement mitigation of the head. The experimental results confirm the predictions of the current simulations. The models show similar trends for the various foam configurations as in the experiments.

Figure 8-6d-e demonstrate the different cross sections of the impacted composite samples of EPS40m/EPS120f with 9 and 25 columns respectively, which are cut from the middle of the impacted specimen. Similar to the simulations shown in Figure 8-5a-b, the deformation mode of the foam columns in Figure 8-6d-e is dominated by shear induced bending.

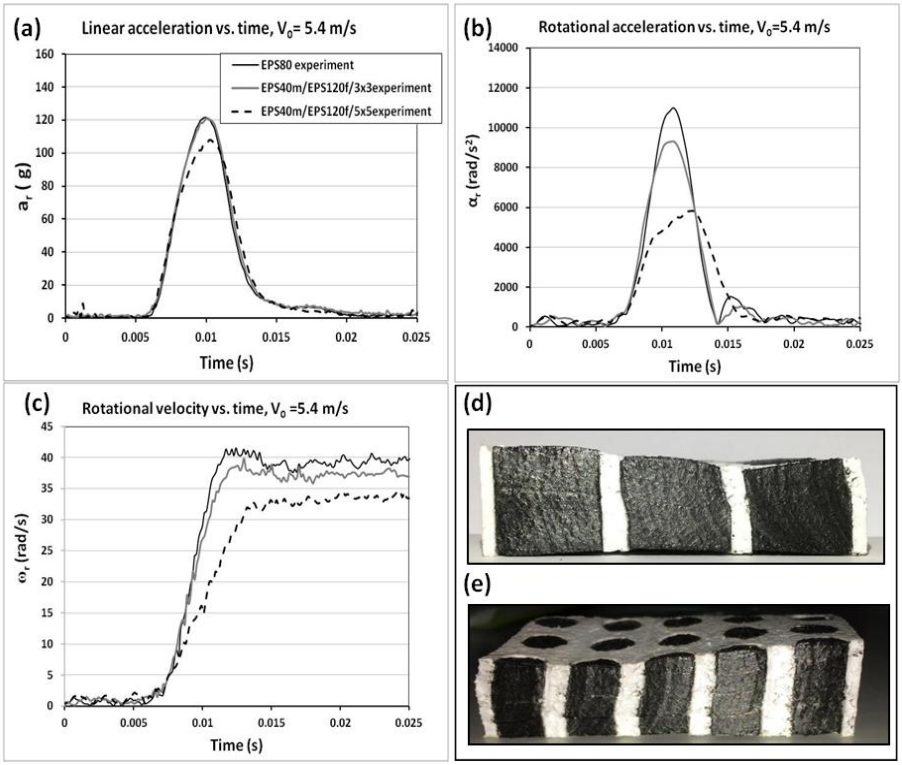

Figure 8-6: Experimental results showing the effect of number of foam columns on oblique impact behaviour of composite foams of EPS40m/EPS120f/3×3 and EPS40m/EPS120f/5×5 versus EPS80 at angle of 45° and impact velocity of 5.4 m/s, (a) Resultant linear acceleration; (b) resultant rotational acceleration; (c) resultant rotational velocity; Images of the cross section of composite foam after oblique impact which have been cut from the middle of the impacted foam sample where bending of the columns can be clearly observed (e-f).

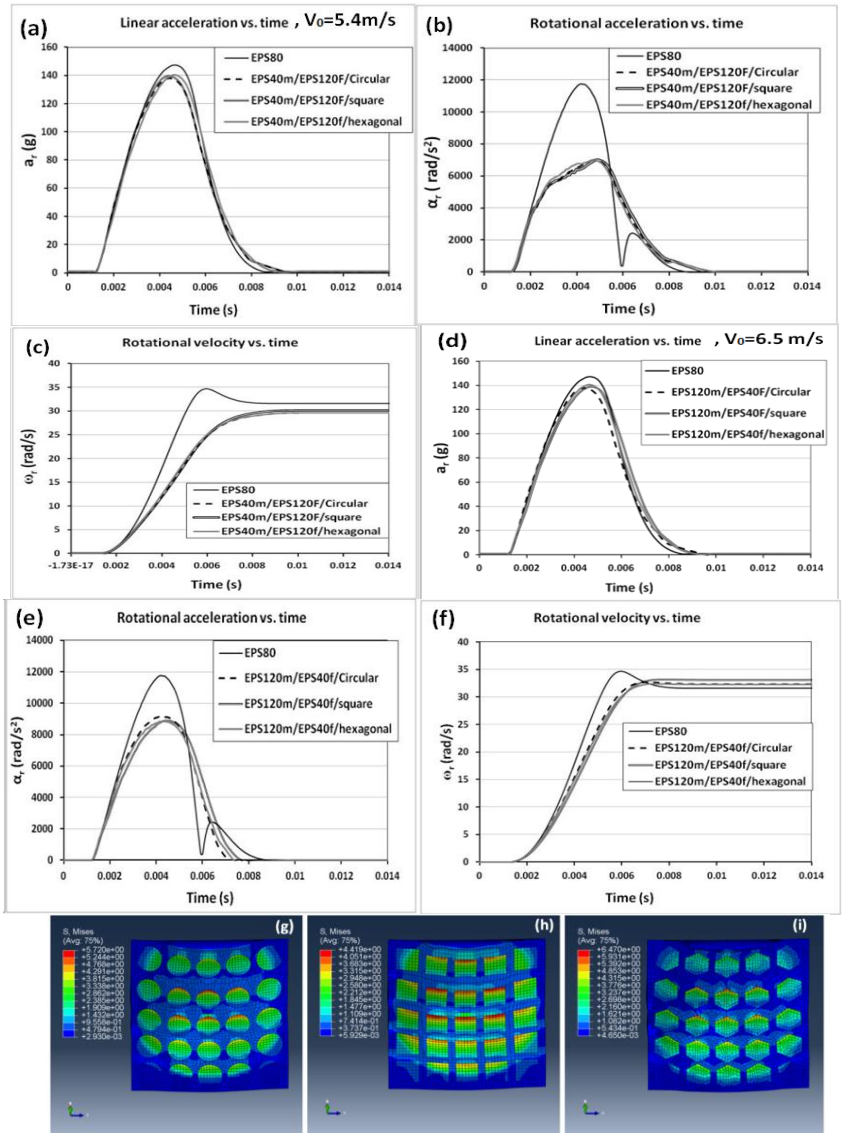

Figure 8-7: Oblique impact simulations of composite foams of EPS40m/EPS120f/5×5 versus EPS80 when headform impacted the flat foam laid on the 45° anvil with impact velocity of 5.4 m/s and 6.5 m/s, respectively; (a&d) Resultant linear acceleration versus time; (b&e) Resultant rotational acceleration versus time; (c&f) Resultant rotational velocity versus time; (g-i) Illustrations of impacted EPS40m/EPS120f/5×5 composite foams when column foam has a circular , square and hexagonal cross section, respectively.

8.4.2.2 Effect of the shape of the cross section of columns on oblique impact performance of composite foams

To investigate the effect of the geometrical shape of foam column cross section, oblique impact of the head on flat composite foams of EPS40m/EPS120f comprising of 25 columns and three different geometrical shapes of the cross-section of the column foam (circular, square, and hexagonal) was simulated, at constant column volume fraction. Figure 8-7a-f demonstrate the resultant linear and rotational accelerations and rotational velocity transferred to the headform at two different impact velocities of 5.4 m/s and 6.5 m/s.

As observed in Figure 8-7, the shape of the cross section hardly affects the linear and rotational acceleration and rotational velocity in composite foam.

The parameter showing a significant effect on the performance of the composite foam is the size of the cross section of the column, rather than its shape. This observation can be explained by the fact that in composite foam, bending of the foam columns plays an important role in composite foam deformation.

The bending moment of inertia of a column (here cylinder), is a function of its radius to the power 4 ($I=\pi\frac{r^4}{4}$). So when bending is the important mode of deformation during rotational (shear) loading, the thickness of the columns will have a strong effect, with much lower resistance for thinner columns. In this analysis, the exact shape of the column has a much smaller effect on the bending resistance, which manifests itself in only small changes of the rotational acceleration and velocity.

8.4.2.3 Effect of matrix foam stiffness on oblique impact performance of composite foam

In order to investigate the effect of matrix foam compliance on the efficiency of composite foam in head protection, Figure 8-8 shows the 45° oblique impact simulation curves of EPS40m/EPS120f/5×5 and EPS120m/EPS40f/5×5 versus EPS80 for two impact velocities of 5.4 and 6.5 m/s. The number of columns ('fibres'), for both the composite foams, is kept constant (25 columns) to be able to independently investigate the effect of matrix foam compliance.

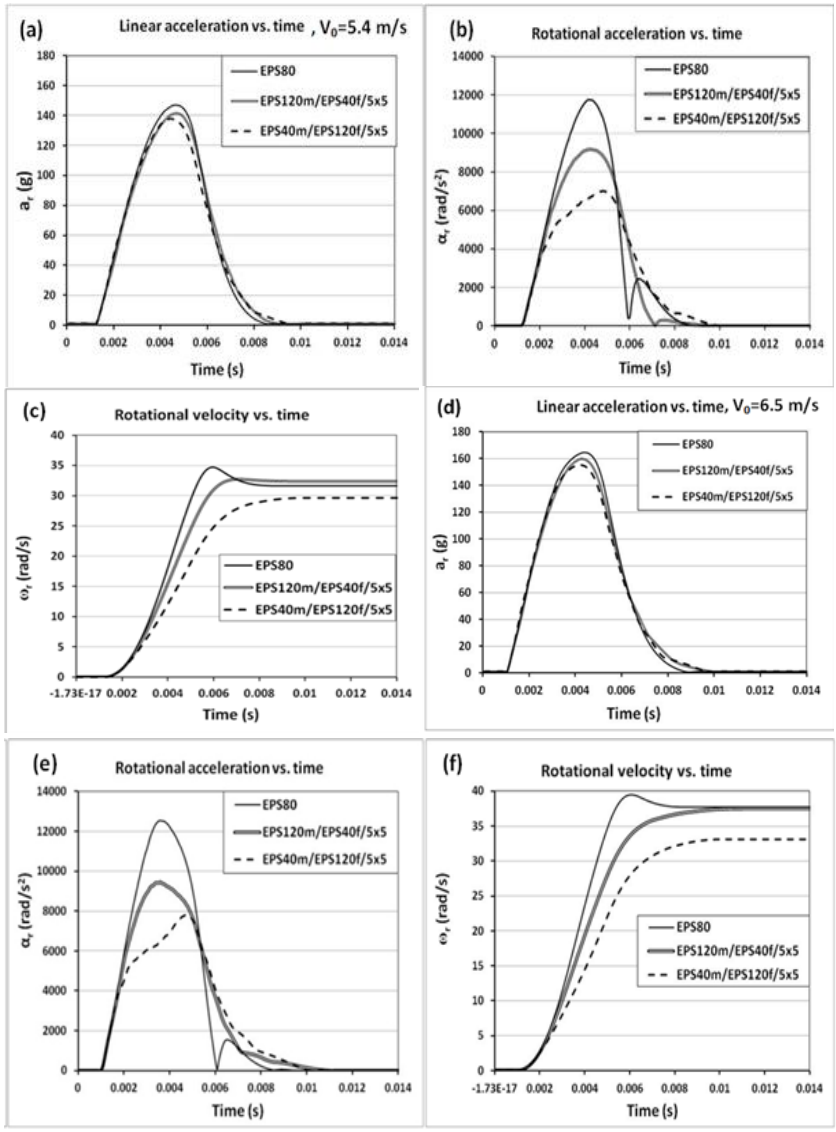

Figure 8-8: Effect of matrix stiffness in oblique impact behaviour of composite foams of EPS40m/EPS120f/5×5 and EPS120m/EPS40f/5×5 versus EPS80 obtained from FE simulations when headform impacted the flat foam laid on the 45° anvil with impact velocity of 5.4 m/s and 6.5 m/s, respectively; (a&d) Resultant linear acceleration versus time; (b&e) Resultant rotational acceleration versus time; (c&f) Resultant rotational velocity versus time.

Table 8-2: Tabulated values of peak resultant linear and rotational accelerations and resultant rotational velocity obtained from oblique impact simulations for different composite foams and EPS80 at impact velocities of 5.4 and 6.5 m/s; the reduction percentages of calculated values compared to EPS80 are also included below each value.

Sample code	V_0 (m/s)	$a_{r,max}$ (g)	$\alpha_{r,\ max}$ (rad/s²)	$\omega_{r\ max}$ (rad/s)
EPS80	**5.4**	147	11660	34.7
	6.5	164	12555	39.5
EPS40m/EPS120f/3×3	**5.4**	141 -4%	9431 -19%	32.9 -5%
	6.5	160 -2%	9790 -22%	37.5 -5%
EPS40m/EPS120f/5×5	**5.4**	134 -9%	7650 -34%	29.6 -15%
	6.5	155 -6%	8000 -36%	33.0 -16.5%
EPS120m/EPS40f/5×5	**5.4**	140 -5%	9430 -19%	32.7 -6%
	6.5	160 -2%	9900 -21%	37.4 -5%

8.4.2.4 Analysis based on global head injury criteria

For a more relevant analysis of the results, it is discouraged to draw conclusions solely based on peak acceleration values and to neglect the impact time duration. Therefore, the test results are analyzed according to the global head injury criteria such as Head Injury Criterion (HIC) [5], Rotational Injury Criterion (RIC) [6], Generalised Acceleration Model for Brain Injury Threshold (GAMBIT) [7], and rotational BRain Injury Criterion (BRIC) [8]. Each of these criteria is described in detail in chapter 3 of this thesis. The calculated values of

abovementioned criteria can be used to comparatively evaluate and benchmark the composite foams versus EPS80 and are listed in table 8-3.

Table 8-3: Calculated values of of HIC_{15}, RIC, BRIC, and GAMBIT criteria for different composite foams and EPS80 at impact velocities of 5.4 and 6.5 m/s; the reduction percentages of calculated values compared to EPS80 are also included below each value.

Sample code	V_0 (m/s)	HIC_{15}	RIC	BRIC	GAMBIT
EPS80	**5.4**	595	16064	1.04	0.75
	6.5	830	20363	1.16	0.82
EPS40m/EPS120f/3×3	**5.4**	594 0%	11213 -30%	0.94 -10%	0.67 -10%
	6.5	825 -1%	13102 -35%	1.05 -9%	0.75 -8.5%
EPS40m/EPS120f/5×5	**5.4**	513 -14%	5978 -62%	0.83 -20%	0.61 -8.5%
	6.5	714 -14%	7288 -64%	0.91 -21%	0.69 -16%
EPS120m/EPS40f/5×5	**5.4**	549 -8%	10706 -33%	0.94 -10%	0.67 -11%
	6.5	742 -11%	11997 -41%	1.05 -9%	0.75 -8.5%

As observed in table 8-3, HIC values show a modest decrease around 14% for EPS40m/EPS120f/5×5 and around 8% for EPS120m/EPS80f/5×5. RIC values of EPS40m/EPS120f composites however, exhibit significant decreases and by increasing the number of columns from 9 to 25, a decrease from -35% to -64% can be observed.

Moreover, it can be observed that by using EPS40 as matrix, RIC values can be much further decreased compared to EPS120m/EPS40f/5×5 in which higher density EPS120 is the matrix. This enhanced performance for the case of strong and stiff columns in a weaker matrix, was even stronger in experimental results. In a similar trend, BRIC and GAMBIT values are reduced by using composite foam and the increase in column number and by using softer EPS40 as matrix can further extend the reduction in values.

8.4.3 Simulation of helmeted head

One of the most interesting application areas for the composite foam concept could be in protective helmets. Therefore, in the following section, the simulation effort is further extended to linear and rotational impact of a helmeted head.

8.4.3.1 Linear impact

Figure 8-9a-b demonstrates the linear impact versus time curves obtained from linear impact simulations of a helmeted head with impact speed of 5.4 and 6.5 m/s, respectively.

In Figure 8-9, composite foam with EPS40 as matrix foam and EPS120 as column foam were applied. The column foams have a circular cross section and composite helmets with two different column diameters of 11.6 and 5.8 mm were simulated and are named as helmet-EPS40m/EPS120f-circular-big and small, respectively.

As observed, the peak resultant linear acceleration in the composite foam helmet is slightly reduced. The helmet with smaller foam column diameter transfers lower peak linear acceleration to the headform. However the reductions in linear accelerations are not remarkable. It can be concluded when the dominant mode of deformation is in compression as can be seen in Figure 8-9c-d, the behaviour of composite foam is dominated by the overall density. Composite foam shows similar behaviour in compression and linear impact to single layer EPS foam of the same density.

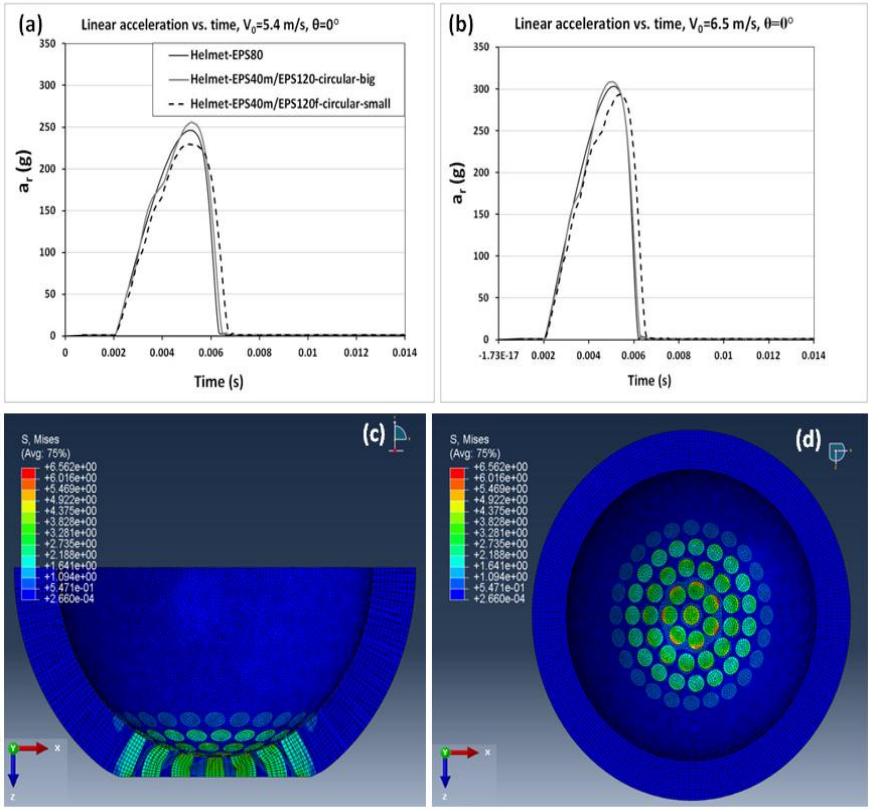

Figure 8-9: Simulation results: Effect of the cross sectional diameter of the foam column on performance of a helmet in linear impact in comparison to an EPS80 reference helmet at impact velocity of 5.4 m/s (a) and 6.5 m/s (b); Illustration of impacted helmet made of EPS40m/EPS120f, (c) side view showing the buckling of foam columns, (d) view from the top.

8.4.3.2 Oblique impact

Figure 8-10a-c demonstrate the resultant linear and rotational accelerations and rotational velocity transferred to the headform during the oblique impact simulations with impact velocity of 5.4 m/s. As observed, the composite foam helmet slightly mitigates linear acceleration in comparison to the homogenous EPS80 helmet. Similar to oblique impact simulations of flat foam, it can be observed that by using composite foam as a helmet can significantly mitigate the rotational acceleration and velocity transferred to the head. By decreasing the diameter of the foam columns from 11.6 to 5.8 mm in the helmet structure, the rotational acceleration peak can further decrease. The decrease in rotational acceleration shown in Figure 8-10b is not limited to mitigation in peak values but also lower acceleration values can be observed during the whole impact duration. The appearance of an initial shoulder in the rotational acceleration curve of the composite foam helmet (see Figure 8-10b) can be related to the presence of two different foam densities of EPS40 and EPS120 in the helmet structure and also by the sudden bending of the columns. The results of oblique impact with a velocity of 5.4 m/s show that helmets containing foam columns with a diameter of 5.8 mm, demonstrate superior performance over helmets with thicker columns. Similar conclusions can be drawn from oblique impact simulation curves with impact velocity of 6.5 m/s presented in Figure 8-10d-f.

It should be noted that in both Figure 8-10b&e, the second rotational acceleration peak has a negative sign but here as in all rotational acceleration curves the absolute values are reported. Figure 8-10g also shows the side view of the helmeted head (with column diameter of 5.8 mm) impacting the 45° anvil. The bending and shearing of the columns at the moment of impact can be seen in this figure. Figure 8-10h gives a view of the top of the impacted helmet and the associated stress map.

The peak resultant linear and rotational acceleration and resultant rotational velocity for composite helmets and the homogenous EPS80 helmet are tabulated in table 8-4. Moreover, the impact results have been analyzed based on global injury criteria, particularly HIC, RIC, BRIC, and GAMBIT.

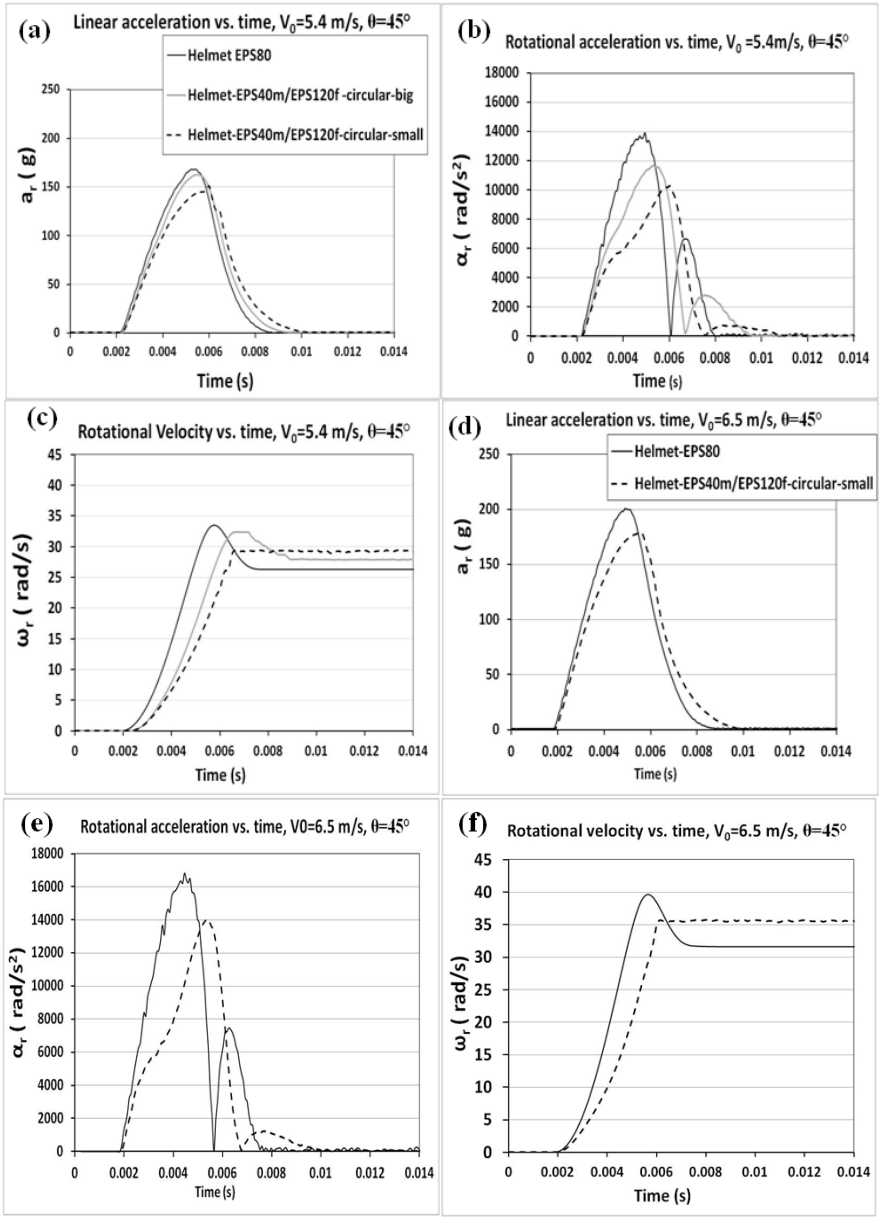

Figure 8-10 a-f. See next page g&h!

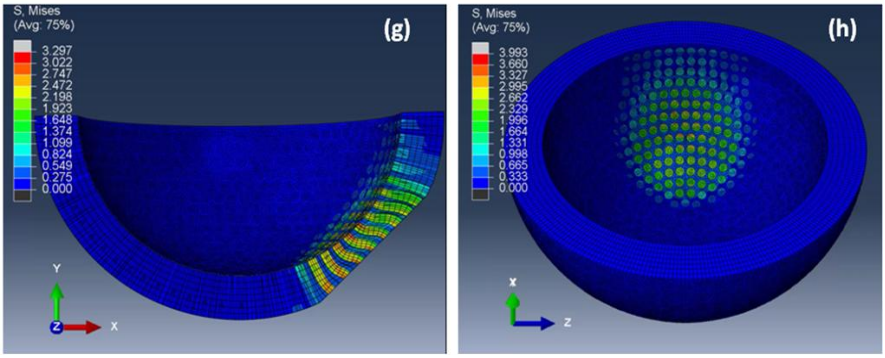

Figure 8-10: Simulation results: Oblique impact of helmeted head at angle of 45° and impact velocity of 5.4 m/s, with two different diameters of foam column, called big (diameter of 11.6mm) and small (diameter of 5.8 mm) in comparison to EPS80 helmet, (a) linear acceleration versus time, (b) rotational acceleration versus time and (c) rotational velocity versus time; Oblique impact results of helmet with small diameter versus EPS80 helmet with impact velocity of 6.5 m/s, (d) linear acceleration versus time, (e) rotational acceleration versus time and, (f) rotational velocity versus time; Illustration of impacted helmet made of EPS40m/EPS120f with column diameter of 5.8 mm, (g) the side view showing the bending and shearing of foam columns, (h) view from the top.

These values can be used to comparatively evaluate the composite foams and EPS80 helmets. As shown in table 8-5, the composite foam helmets can reduce the probability of head injury according to the different injury criteria. Moreover, similar to conclusions deduced from comparing peak resultant linear and rotational accelerations, reducing the diameter of the column foam significantly reduces the calculated values for each of these criteria.

Composite foam helmet with smaller foam column ("fibre") diameter of 5.8 mm shows a reduction in HIC values of around 20%. Moreover, composite foam helmets could half the RIC value, showing the merit of the composite concept at specifically reducing rotational acceleration.

In a similar trend, BRIC and GAMBIT values are also reduced by using the composite foam helmet. These results demonstrate the efficacy of the composite foam concept to be used as structural solution for producing safer helmets which can further mitigate rotational

accelerations and velocity. This concept can also be used in combination with other smart designs which specifically aim at mitigation of the head rotational movement such as MIPS [16], for a possible synergy. Further research on such a possibility is highly recommended.

Table 8-4: Tabulated values of peak resultant linear and rotational accelerations and resultant rotational velocity obtained from simulations of oblique impacts with impact velocities of 5.4 and 6.5 m/s, for different composite helmets in comparison to EPS80 helmet; The reduction percentage of calculated values compared to EPS80 are also included below each value.

Helmet code	V_0, (m/s)	$a_{r,max}$ (g)	$\alpha_{r,max}$ (rad/s²)	$\omega_{r,max}$ (rad/s)
EPS80	5.4	168	13900	34
	6.5	200	16800	39.6
EPS40m/EPS120f-big	5.4	162 -4%	11700 -16%	32 -6%
EPS40m/EPS120f-small	5.4	144 -14%	10177 -27%	29 -15%
	6.5	178 -12%	14000 -17%	35.5 -10%

Table 8-4: Calculated values of HIC_{15}, RIC, BRIC, and GAMBIT criteria for different composite helmets in comparison to EPS80 helmet; The reduction percentage of calculated values compared to EPS80 are also included below each value.

Helmet code	V_0 (m/s)	HIC_{15}	RIC	BRIC	GAMBIT
EPS80	5.4	673	19500	1.08	0.87
	6.5	1051	30300	1.27	1.04
EPS40m/EPS120f-big	5.4	648 -4%	14256 -27%	0.98 -9%	0.79 -9%
EPS40m/EPS120f-small	5.4	529 -21%	9826 -50%	0.88 -18.5%	0.70 -19.5%
	6.5	840 -20%	16306 -46%	1.11 -12.5%	0.90 -13.5%

8.5 Conclusions

In this chapter, composite foams comprised of two different densities of EPS foam (40 and 120 kg/m^3) with a column/matrix configuration are proposed as a substitute for single layer EPS foam of equivalent weight and thickness for head protection, aiming at reduction of rotational movement of the head during oblique impacts. A finite element model of linear and oblique impact of composite foam with different configurations has been employed on foams in flat and helmet shapes. A parametric study on the composite foam configuration was performed to optimize its performance. Results show that parameters such as matrix compliance and the column diameter can dramatically affect the extent of the rotational acceleration and velocity mitigation. By using more compliant matrix foam, and by decreasing the diameter of the columns or in another words by increasing the number of the columns within the composite structure (for the same overall density), the rotational movement of the head can be further mitigated.

The application of such geometry can be wherever head protection is of great concern e.g. in the interior of crashworthy vehicles (headliners

in car interiors). The concept can be employed in complex geometries such as bicycle helmets, e.g. by using a two part mould, where first the first density and secondly the second density foam would be applied. Moreover, in column/matrix configuration, the foam columns are best to be arrayed in a hexagonal packing to have a transversely isotropic foam structure and direction independent in-plane impact properties in a real application, however in a helmet, it also depends on the complete topology (e.g. ventilation openings).

8.6 References

1. Zhang, J., Kikuchi, N., Li, V., Yee, A., Nusholtz, G. Constitutive modelling of polymeric foam material subjected to dynamic crash loading. International Journal of Impact Engineering. 1998, 21(5): p. 369–386.
2. Rizov, V.I. Low velocity localised impact study of cellular foams. Materials & Design, 2007. 28(10):p.2632-2640.
3. Cui, L., Kiernan, S., Gilchrist, M.D. Designing the energy absorption capacity of functionally graded foam materials. Material Science and Engineering A. 2009, 507:p.215–25.
4. Ashby, M.F. Materials selection in mechanical design, 4th ed. Butterworth-Heinemann, 2010.
5. Versace, J., A review of the severity index. In: 15th Stapp Car Crash Conference,1971. p. 771-796.
6. Kimpara, H., Iwamoto, M. Mild traumatic brain injury predictors based on angular accelerations during impacts. Annals of Biomedical Engineering, 2012;40(1):p.114–126.
7. Newman, J. A generalized acceleration model for brain injury threshold (GAMBIT), In: Proceedings of the International Research Council on Biomechanics of Injury (IRCOBI) Conference. 1986:p.121–131.
8. Takhounts E.G., Hasija, V., Ridella, S.A., Rowson, S., Duma, S.M. Kinematic Rotational Brain Injury Criterion (BRIC). In: Prococeedings of 22nd International Technical Conference on the Enhanced Safety of Vehicles (ESV), Washington, D.C., June13-16, 2011, Paper No. 11-0263.

Chapter 9

Study on the effect of shell material and multilayer foam liner on performance of bicycle helmets

Adopted from: Yasmine Mosleh, Martin Cajka, Bart Depreitere, Jos Vander Sloten, Jan Ivens. Study on the effect of shell material and multilayer foam liner on performance of bicycle helmets in linear and oblique impacts. (submitted)

9.1 Introduction

One of the functions of the outer shell in a helmet is to distribute the impact load over a larger area, avoiding concentrated loads and penetration of sharp objects. Another function of the outer shell is enabling the sliding of the head when impacting the road surface. The sliding of the head on the road surface can help minimizing the head rotation and neck injury. Additionally, a part of the impact energy is dissipated by shell deformation. In commercial bicycle helmets, a very thin shell composed of thermoplastic material such as polycarbonate (PC), acrylonitrile-butadiene-styrene copolymer (ABS) or polymer composite is used. Bicycle helmets covered with a hard shell were

found to be safer than helmets without this shell during skid-type impact onto a concrete surface [1-2].

Helmet liners which are typically comprised of polymer foams, are designed to absorb impact energy whilst keeping forces/accelerations transmitted to the head below a critical threshold [3-4]. Over the last decade, a design concept which focuses on varying foam density through the thickness by combining layers with different densities (in a series configuration) or functionally graded foams has been proposed to improve the energy absorption capability of helmet liners [5-7]. Preliminary impact simulations by some researchers suggest that using layered foam or functionally graded foams instead of single layer foam in helmets could improve impact absorption and reduction in peak acceleration compared to conventional single layer helmet liners for low and medium impact velocities (4.4m/s-5.4m/s). They attribute this slight improvement to increasing the dissipated plastic energy density and the contact area between the head and the helmet liner. Yet these studies are not fully conclusive and further research is needed [6].

In chapter 5, 7, and 8 of this thesis, it was shown that composite foams with parallel layers or columns demonstrate clear reductions in rotational acceleration and velocity as well as a reduction in shear stresses. Nevertheless, in this chapter, it is attempted to further verify and shed light on the performance of layered foam with a series configuration advocated by some studies in the literature (although inconclusively).

This chapter has two main objectives. The first part of this chapter deals with investigating the effect of the thickness and material type of the helmet shell on the helmet performance in linear impact by blunt and sharp projectiles. For this study polycarbonate (PC), self-reinforced polypropylene (CURV®) and silk/HDPE composite were chosen as different shell materials.

The second objective of this chapter is to investigate the performance of layered EPS foams, with varying density through the thickness, versus single layer EPS foam of equivalent weight and thickness. For this, experiments and FE simulations of linear and oblique impact on multi-layered foams and homogeneous EPS foam in the shape of a flat sample or helmet are performed.

9.2 Experimental

9.2.1 Materials

9.2.1.1 Helmet shell material and production method

The effect of helmet shell thickness and material type have been studied by performing drop weight impact on cuboids of EPS foam (density of 60 kg/m^3) covered with shell material. For investigating the effect of materials type, three different shell materials namely Polycarbonate (PC) sheet, self-reinforced polypropylene composite (CURV®) and Silk/HDPE composite, all with a thickness around 1.5 mm were investigated. For studying the effect of shell thickness, polycarbonate (PC) shells with two different thicknesses of 0.5 and 1.5 mm were prepared and subsequently tested in linear impact.

Polycarbonate (PC) sheets with thickness of 0.5 mm and 0.75mm were sourced from the helmet manufacturing company Lazer Sport in Belgium. The PC shell with thickness of 1.5 mm was produced by compression moulding using a Fontijne hot press. For this, two PC sheets of 0.75 mm thickness were pressed at a temperature of 200 °C while applying a pressure of 15 bars for 5 minutes. The samples were subsequently cooled to 90°C at the same pressure and a cooling rate of 5 °C/min. After 15 min holding time at 90°C the samples were cooled to room temperature and removed from the hot press.

Self-reinforced polypropylene (CURV®) composite shells with an average thickness of 1.4 mm, were obtained from Propex Fabrics (Germany).

Silk/HDPE composite shells with a thickness of 1.5 mm were prepared using a cocoon silk twill woven fabric as fibres and a modified high density polyethylene as matrix. The silk twill weave with areal weight of 80 g/m^2 was sourced from the company Hermes (France). The high density polyethylene modified with maleic anhydride (HDPE-MA), Bynel 40E529, in the form of pellets, was supplied by DuPont and the pellets were subsequently processed into a film with a thickness of 0.065 mm by Amcor. The thermoplastic silk/HDPE composite shells were also produced by compression moulding using a hot press (Fontijne). Processing temperature was set at 150 °C. The applied pressure was set to 15 bar for 8 min. Then samples were cooled to 90°C at the same pressure. After 15 min holding time at 90°C the samples were cooled to room temperature and removed from the hot press. Fibre volume fraction of silk fibre in the composite plate was 50%. The sample code of the different shells and their actual thickness are listed in table 9-1.

Table 9-1: Different shell materials and their thicknesses.

Shell sample code	Material type	Thickness (mm)
PC 0.5	Polycarbonate	0.48 ±0.05
PC 1.5	Polycarbonate	1.49±0.02
Curv	Self-reinforced polypropylene composite	1.39±0.01
Silk/HDPE	Composite of silk twill weave/high density polyethylene	1.50±0.03

9.2.1.2 Multi-layer EPS foam liner

Multi-layer liners were prepared by combining discrete layers of EPS foam with three different densities of 40±3, 80±3, and 120±4 kg/m^3 (EPS40, EPS80 and EPS120), respectively. EPS foams were sourced from Kemisol and Lazer Sport in shape of blocks with a thickness of 25 mm. Three different configurations used in this study namely B120/80/40T, B40/80/120T, and B120/40/120T are illustrated in Figure 9-1, where the B (bottom) side is close to the head. As illustrated in Figure 9-1, e.g. B120/80/40T refers to the configuration where higher density foam (EPS120), is close to the head and EPS40 is adjacent to the helmet shell. The overall density and thickness of all three configurations were aimed at 80 kg/m^3 and 24 mm, respectively. To achieve the overall density of 80 kg/m^3 for *EPS40/80/120* layered composite foams, all three layers of EPS40, EPS80, and EPS120, were cut into the thickness of 8 mm (one third of overall thickness of foam specimen). For cutting the foam layers, a hot wire was used to ensure a smooth surface. In the *EPSB120/40/120T* configuration, for achieving the overall density of 80 kg/m^3, EPS120 and EPS40 layers were cut into thickness of 6 and 12 mm, respectively, to obtain overall density of 80 kg/m^3. The layers were bonded together using double-sided tape (Kip® 342). Single layer EPS80 was considered as the reference material to which the performance of multi-layer foams is compared. EPS is used prevalently as liner in commercial bicycle helmets.

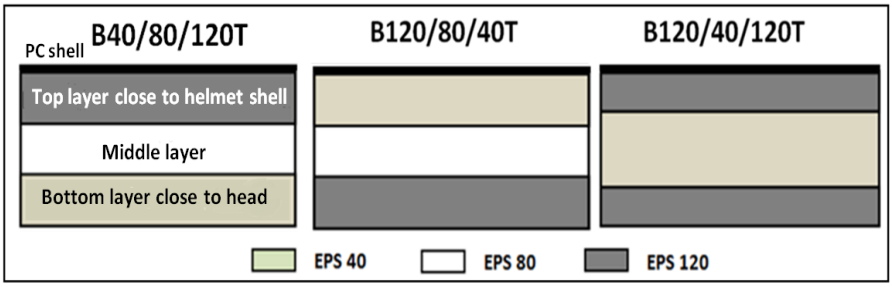

Figure 9-1: Illustration of different configurations of composite foams from left to right, B40/80/120T; B120/80/40T, and B120/40/120T, respectively, where B is the bottom location near the head and T is the top position adjacent to the helmet shell.

9.2.2 Testing methods

9.2.2.1 Linear impact testing of different shells

Impact tests were performed using a drop tower impactor. Two different projectiles were used for impacting the different shells which are shown in Figure 9-2a-b. Figure 9-2a demonstrates a steel flat tub with a diameter of 50 mm and a steel finger projectile with a hemispherical tip and diameter of 16 mm for applying localized loads is shown in Figure 9-2b.

The drop height and weight were set at 1.5 m and 4.5 kg respectively, resulting in impact velocity of 5.4 m/s. This corresponds to the velocity suggested by the current European bicycle helmet standard, EN 1078. For preparing samples for impact tests on different shells, the shells were cut and glued to EPS60 foam cuboids with the dimension of 100 mm×100 mm×25 mm using double-sided adhesive tape Kip® 342 as illustrated in Figure 9-2c. Instead of gluing the samples to the impact tub, they were clamped between two heavy steel rings with an opening of 70 mm, as shown in Figure 9-2d. The bolts on the ring were tightened carefully by applying the same amount of torque (20 N.m) on every bolt using a torque meter to avoid variation in clamping force.

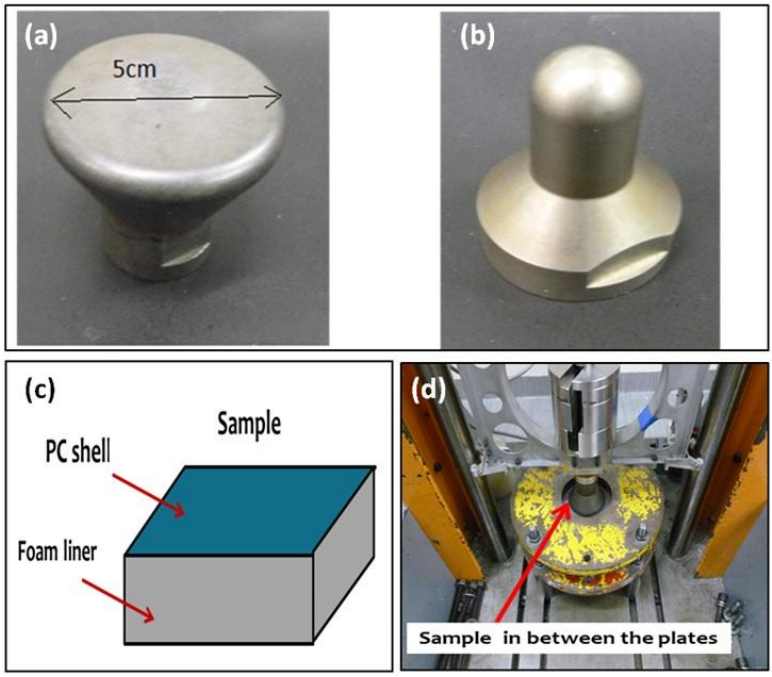

Figure 9-2: Projectiles used in drop weight impact experiments on different shells (a) steel flat tube with circular cross section of 50 mm diameter; (b) steel finger projectile with 16 mm diameter. (c) Illustration of a foam specimen covered with PC shell used for impact testing. (d) Example of a foam sample covered with shell fixed in between two steel rings with an opening of 70 mm in drop impact tower and impacted by flat steel tub.

9.2.2.2 Compression tests of foam liners

Quasi-static tests were performed according to ASTM standard D1621/94 using a universal tensile testing machine (Instron 4467). Foams were compressed at a constant displacement rate of 2.5 mm/min between two parallel steel plates. The displacement and the load were recorded. Samples were cut into cuboids of 50 mm (length) × 50 mm (width) × 24 mm (thickness). All the tests were performed at room temperature and repeated at least 3 fold.

9.2.2.3 Linear impact tests of foam liners

Linear impact tests on foam samples were performed using a drop-weight impact tower set-up equipped with a flat steel projectile, which is shown in Figure 9-3a-b. The circular cross section of the steel projectile has a radius of 50mm and it is attached to a frame.

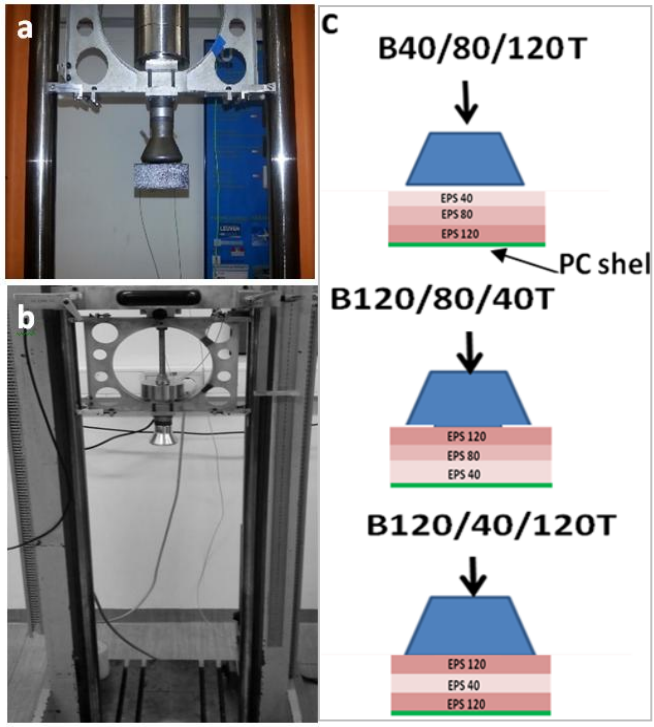

Figure 9-3: (a-b) Drop weight impact tower; (c) Illustrations of three configurations of composite foams connected to flat steel tub.

The total drop weight was set at 4.5 kg resembling the average weight of a hybrid III dummy head that is used in oblique impact experiments. The drop height was fixed at 1.5 m resulting in an impact velocity of 5.4 m/s. The impact force on the projectile was monitored by a Kistler load cell, type 9041A; the displacement was monitored with a laser sensor. Foam specimens were prepared in the form of cuboids with dimensions of 70mm (length) × 70mm (width) × 24mm (thickness) and taped to the projectile using double sided adhesive tape (Kip® 342). As illustrated in Figure 9-3c, a PC shell with thickness of 0.5 mm

was also taped to the outer surface of each foam liner specimen using the same double sided tape.

9.2.2.3 Oblique impact testing of foam liners

An illustration of the oblique impact set-up used in this study is shown in Figure 9-4a. In this set-up, a hybrid III dummy head is utilized as the headform and is incorporated into the existing drop weight impact tower, supported as shown in Figure 9-4b. The grips are mounted on the rails of the drop tower impact set-up. An array of three linear accelerometers and a gyroscope in the centre of gravity of the dummy head allow the measurement of the three linear accelerations and three rotational velocities in x, y, and z directions, respectively. The head was fixed at a height of 1.5 m resulting in an impact velocity of 5.4 m/s. An anvil with an angle of 45° was used for the oblique impact test. Foam samples in the shape of cuboids and dimensions of 80 mm (length) × 80 mm (width) × 24 mm (thickness) were glued firmly on the 45° anvil as shown in Figure 9-4b. The head was subsequently dropped on the sample.

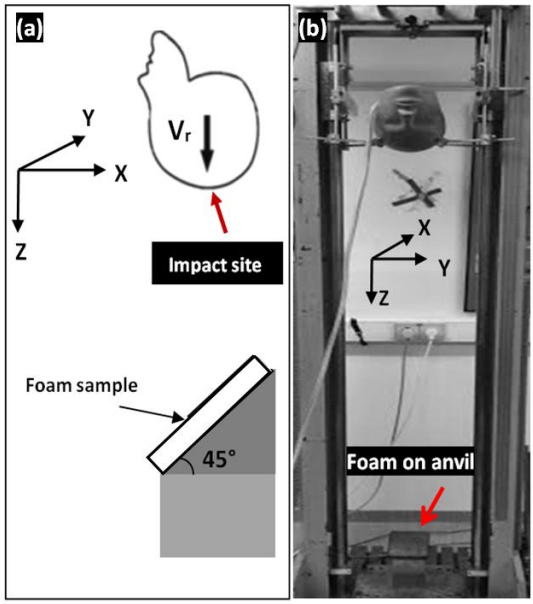

Figure 9-4: Illustration of oblique impact set up equipped with hybrid III dummy head which falls on the foam sample at an impact angle of 45 °, the drop direction is shown by a black arrow; sample laid on 45 ° anvil is shown by red arrow, (a) illustrative side view and (b) front view.

All materials were tested at least three-fold to ensure the repeatability of the results and a representative curve was chosen for comparative curves. All experiments were performed at room temperature. The oblique impact test results are subsequently analyzed according to global head injury criteria such as HIC (linear head injury criterion) and RIC (rotational head injury criterion), for a more relevant analysis of the results.

9.3 Simulation part

9.3.1 Modelling description

The FE impact simulation of physical oblique impact consists of three main parts: the EPS foam, the headform and the anvil. The impact simulations were carried out for two different impact velocities of 5.4 m/s and 6.5 m/s. For the simulation of oblique impact behaviour, two different configurations were considered which are shown in Figure 9-5. In the first case (Figure 9-5a), the flat foam sample with dimensions of 8 cm (length) × 8 cm (width) × 2.5 cm (thickness) is placed on a 45° anvil and the headform is dropped vertically on the foam specimen with the specified impact velocities. In the second configuration, the foam is placed on the spherical headform and covers half of the spherical headform, resembling a hemispherical helmet which is illustrated in Figure 9-5b-c.

The headform is subsequently dropped on the 0° and 45° anvil simulating linear or oblique impact, respectively. For the purpose of simplification, the headform is approximated as a sphere. The radius of the spherical head model was set at 8.5 cm. The weight of the headform was set to 4.5 kg similar to the weight of a hybrid III dummy head. In these simulations, the headform is modelled as a rigid body and the linear and rotational accelerations transferred to the headform are measured from the centre of mass.

The EPS foam liner was modelled in Abaqus/Explicit using the crushable foam model for isotropic material with volumetric hardening in conjunction with a linear elastic model. Material properties of EPS crushable foams such as Young's modulus, yield stress and plateau stress for the constitutive model used in the current study were determined by performing quasi-static compression experiments. Comprehensive description on modelling the EPS foam is given in chapter 8.

For meshing of the foam, C3D8R elements (linear brick elements) were used with distortion control which does not allow elements to invert

during large deformations. The anvil was also modelled as an analytically rigid part. The foam was connected to the anvil, in Figure 9-5a, or to the headform, in Figure 9-5b, using coupling where all the degrees of freedom of the foam surface which was in contact with the anvil (in Figure 9-5a) or with the headform (in Figure 9-5b-c) were restrained.

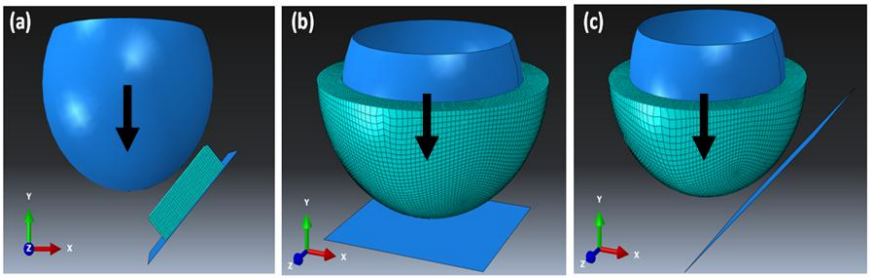

Figure 9-5: Illustrations of (a) Oblique impact of the head on a foam where the foam sample is placed on an anvil at an angle of 45°; (b) Linear impact of helmeted head on anvil at angle of 0° ; (c) Oblique impact of helmeted head at an angle of 45°, the black arrow demonstrates the direction of the impact velocity.

The friction coefficient between the headform and the foam in the configuration where the foam was placed on the anvil (Figure 9-5a) and also between the hemispherical helmet and the anvil (Figure 9-5b-c) was set to *f=0.3*. For the case of simplicity, for both simulations a friction coefficient of 0.3 was chosen. As explained earlier in chapter 8, the value of 0.3 is an assumption. However, the knowlege of exact friction coefficient in real experiments do not hinder the main goal of this modelling study which is to compare different configurations of layered EPS foam, relative to each other and to single layer EPS.

9.4 Results and discussions

9.4.1. Experimental results

9.4.1.1 Effect of shell material on impact performance of helmet

Linear impact tests were performed on different shells with 2 projectiles, a steel finger projectile (Figure 9-6a) and a steel flat projectile (Figure 9-6b) to see the effect of local shell deformation on the impact results.

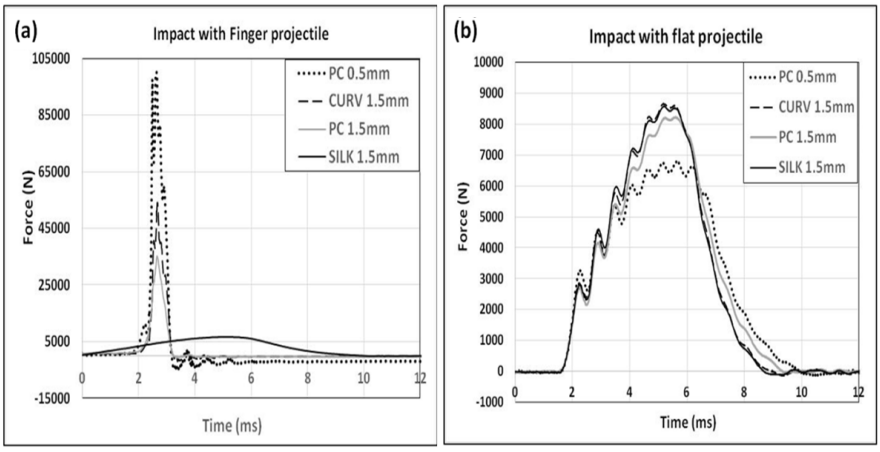

Figure 9-6: Linear impact force-time graphs with (a) finger steel tub and, (b) flat steel tub. High peak forces lead to high peak accelerations which should be avoided.

As shown in Figure 9-7a-d, during the impact tests using the steel finger projectile all the foam samples covered with PC shells (both thickness of 0.5 and 1.5 mm) and Curv® shells were perforated, except for the samples with silk/HDPE composite shell. This is due to higher penetration impact resistance of silk/HDPE composite. The combination of tough silk fibres (with strain to failure of 20%) and a thermoplastic matrix such as HDPE-MA with high strain to failure (820%) leads to higher deformability and a better spread of the damage in the composite shell, avoiding localization and perforation at this impact velocity. Previous research carried out by several researchers on penetration resistance of glass and carbon fibre reinforced composites indicated that the fibre volume fraction was the dominant factor controlling penetration impact and that the matrix type had no noticeable effects [8, 9]. However, other researchers demonstrated the crucial effect of the matrix in impact resistance of composites reinforced with tough fibres (e.g. tough stainless steel and silk fibres), [10-12]. The reason could be that during impact, tough fibres surrounded by a matrix with a high strain to failure, can still fail first and, thus, their toughness can be exploited to its full potential. Impact results on different shells indicate the importance of a suitable tough composite shell in protecting the head against perforation by sharp objects which is more probable in e.g. the case of mountain biking.

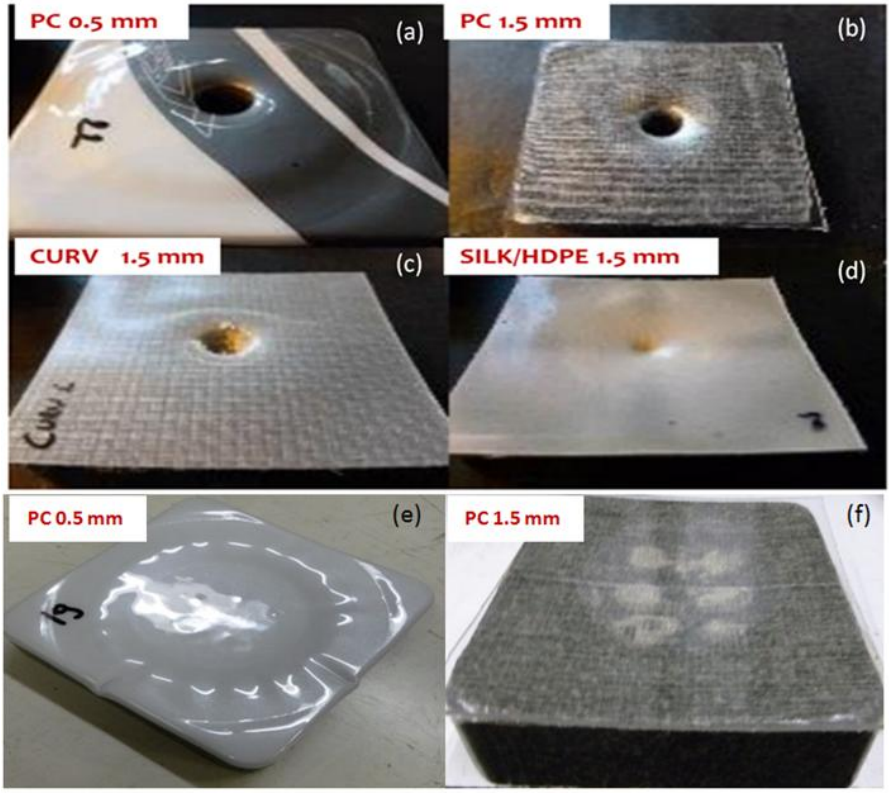

Figure 9-7: Perforated samples of EPS foam covered with (a) PC shell with thickness of 0.5 mm, (b) PC shell with thickness of 1.5 mm, (c)) Self-reinforced PP (CURV) shell with thickness of 1.5 mm, (d),) Silk/HDPE composite shell with thickness of 1.5 mm, impacted by steel finger projectile with impact velocity of 5.4m/s ; samples of EPS foam covered with (e) PC shell with thickness of 0.5 mm, (f) PC shell with thickness of 1.5 mm, impacted by flat steel projectile at velocity of 5.4 m/s.

During the impact tests using the steel flat projectile, none of the shells were punctured. All samples except for PC0.5 showed a similar peak force and impact time duration. As observed in Figure 9-6b and within the limited test range, the thickness of PC shells plays a dominant role in peak force/acceleration which can be related to lower bending stiffness of PC0.5 allowing for larger deformation between the projectile and the sample (see Figure 9-7e-f).

9.4.1.2 Compression and linear impact experiments on layered foams

The compressive stress-strain curves of multi-layer composite foams EPS40/80/120, and EPS120-40-120 versus single layer EPS80, obtained from quasi-static compression experiments, are plotted in Figure 9-8a. It can be observed that layered EPS foams demonstrate a step-wise behaviour in compression. For EPS40/80/120, the compressive stress-strain curve comprises of three stress plateaus; each of which relates to a different density layer. The first stress plateau is related to the yielding of the EPS40 layer, the second plateau stress is the result of the yielding of the EPS80 layer and finally the EPS120 layer undergoes compression loading. EPS120-40-120 composite foam sample demonstrates two plateaus in the compressive stress-strain curve attributed to EPS40 and EPS120 layers, respectively. In general in multi-layer foam, when the layers are loaded in series, the number of steps appearing in the stress-strain curve is equal to the number of different densities in the configuration. In addition, the length of each plateau region is directly related to the thickness of the corresponding layer. In the helmet application, it is important that the foam liner can absorb the energy whilst keeping the stress below the injurious level. The magnitude of compressive stress is correlated with the acceleration experienced by the dummy head. To compare the energy absorption efficiency of layered EPS liner with single layer EPS80, Figure 9-8b shows absorbed energy density versus stress for each configuration. It can be observed that the multi-layer foams initially demonstrate a gradual tendency to absorb energy whilst the single layer EPS80, does not dissipate energy before a stress of 0.78 MPa. However, after the stress level of 0.78 MPa, EPS80 foam outperforms the layered foams in energy absorption at intermediate stress levels. It is believed that the analysis of energy absorption efficacy of the foams in quasi-static compression can be a good indication of the behaviour of the foams in dynamic linear impact inside a helmet.

To evaluate this hypothesis, linear impact has been performed on all three configurations of layered foam and compared with EPS80. As shown in Figure 9-8c, the layered EPS foam liners demonstrate higher force (accelerations) levels than EPS80. This is in line with findings of energy density versus stress graphs (Figure 9-8b). The initial energy recommended for testing bicycle helmets is higher than the observed threshold of 0.18 MJ/m^3.

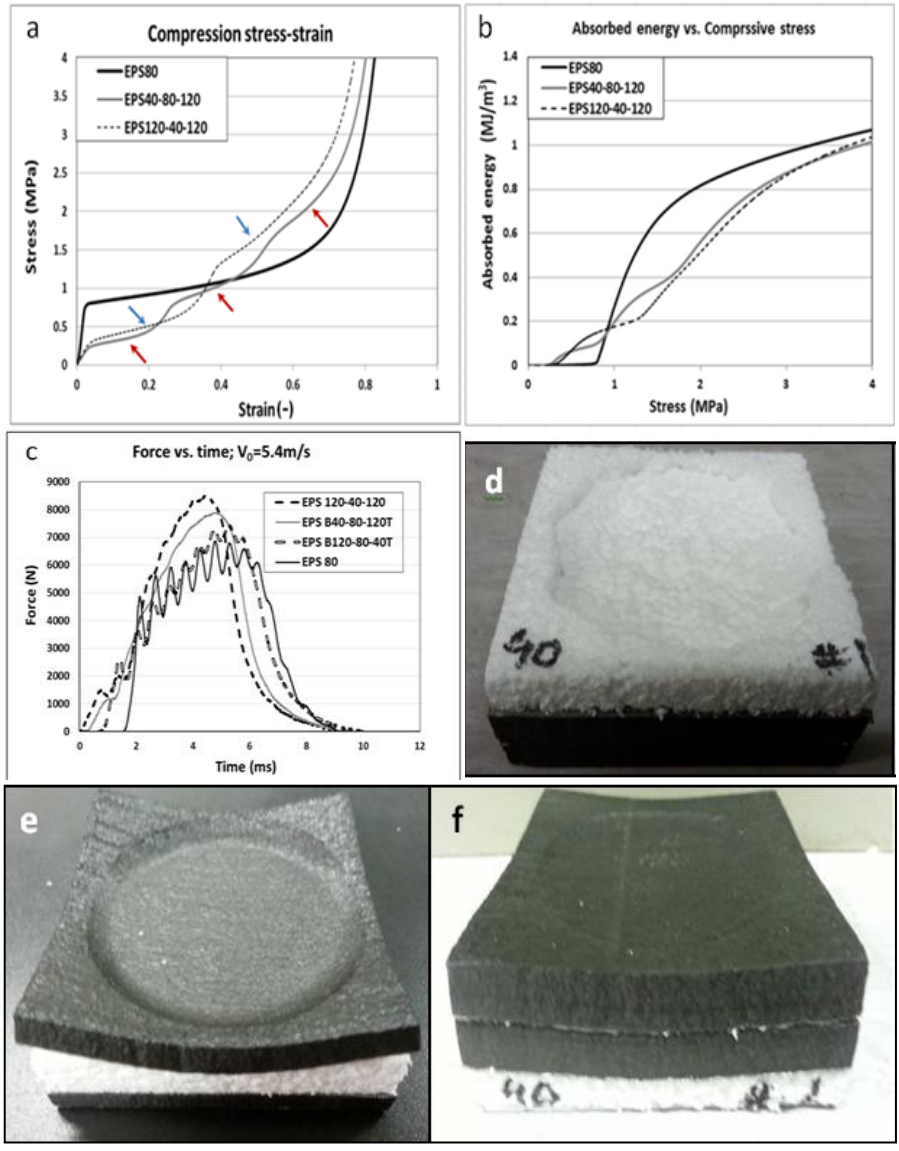

Figure 9-8: (a) Stress-strain curves of layered composite foams versus EPS80 obtained from quasi-static compression test; (b) Comparative curves of absorbed energy versus compressive stress for layered composite foams and EPS80; (c) Force-time curves of layered foams versus EPS80, obtained from drop weight impact experiments with an impact velocity of 5.4 m/s; (d-f) Impacted samples of B40/80/120T, B120/40/120T and B120/80/40T respectively.

This can be further explained with a basic energy density calculation. For the impact velocity of v=5.4 m/s (as suggested by EN1078), a mass of the head of m=4.5 kg, the total impact energy is 65.6 J. Assuming the elastic energy and energy absorption by the shell during the impact are negligible, this energy has to be absorbed in the impacted liner volume. According to Ashby and Gibson [13], the load distribution area during a helmeted head crash is in the order of A= 0.01 m^2. In the FE simulations in chapter 8, an estimation of the experienced contact area gives values of approximately 0.005 m^2. The Ashby value of 0.01 m^2 will be more conservative. With a liner thickness of 25 mm, an approximate absorbed energy density in the foam liner for a bicyclist crash can be calculated, resulting in a higher energy absorption per unit volume demand than 0.18 MJ/m^3:

Absorbed energy per unit volume [MJ/m^3] = $\frac{\frac{1}{2}mv^2}{A.t} = \frac{\frac{1}{2}\times 4.5\times (5.4)^2}{0.025\times 0.01} = 0.262$ MJ/m^3

Therefore, it is believed that the layered foam liners can demonstrate superior impact protection in helmets, yet only at low impact energies. Another interesting observation is that the configuration of the layered EPS foam, particularly the sequence of the different density layers, affects the impact performance. As observed, by placing the higher density foam layer close to the head in case of EPSB120/80/40T, the foam liner can absorb the energy in lower force/accelerations levels in comparison to EPSB40/80/120T. This can be attributed to the fact that placing lower density foam close to the head leads to a more concentrated load due to its weaker compressive properties. In contrast, by placing the higher density layer close to the head in the gradient, the load further spreads and a less localized load can be seen (see Figure 9-8d versus f). The highest peak force is related to EPSB120/40/120T. A possible explanation can be related to the higher thickness of EPS40 layer in this case, in comparison to the gradient configurations of EPSB120/80/40T and EPSB40/80/120T to achieve the similar overall density of 80 kg/m. At the moment of impact, lower density EPS40 is the first layer that deforms and enters the densification region. This leads to a higher portion of overall thickness that is densified by the time the EPS120 layers take over the load. The thicker densified region causes EPSB120/40/120T to act as a foam of higher density in the higher stress range and overall the material

experiences higher force/acceleration levels, as is observed in Figure 9-8a-c.
In conclusion, there seems to be a correlation between the energy absorption ability of multi-layered EPS foams during compression and linear impact tests. Also it can be concluded that layered EPS foam liners can outperform single layer EPS foam, with similar overall density, yet only in low energy impacts and when higher density foam is positioned adjacent to the head. The conclusion of this section will be further scrutinized by numerical modelling for both linear and oblique impacts and for two different impact velocities (relevant for testing bicycle helmets) in the next sections.

9.4.1.3 Experimental oblique impact

In this section, the performance of multi-layered EPS foam liner versus EPS80, when impacted at an oblique angle of 45° is discussed. Flat foam specimens were placed on the 45° anvil, and the hybrid III dummy head was subsequently dropped on the foam samples with an impact velocity of 5.4 m/s. Figure 9-9a-c demonstrate the resultant linear and rotational accelerations and rotational velocity versus time of multi-layer foams in comparison to EPS80. As observed, peak linear accelerations of layered EPS liners are similar to EPS80 except for EPSB120/80/40T, which can be related to a less localized impact loading, as discussed before in section 9.4.1.2. Slight prolongation of the impact duration can also be observed in the layered foams which can be related to the stepwise deformation in layered foam, starting in the softer layers, which can prolong the contact time between the head and foam specimen. The longest impact duration can be observed for EPSB120.40.120T configuration which can be attributed to the thicker soft EPS40 layer.
Layered EPS foam liners demonstrated lower peak rotational acceleration in comparison to EPS80. The lower rotational acceleration and lower rotational velocity slope can be related to the lower shear stresses (lower shear resistance in the softer layers) transmitted to the head in the earlier stages of contact. Easier shear deformation of the EPS40 layers in the layered foam structures can lead to reduction of shear stress transfer to the head and hence lower rotational acceleration values. However, it is believed that for higher impact energies, the soft layer densifies quicker leading to higher shear resistance of the structure. This further investigated by numerical modeling in the following sections.

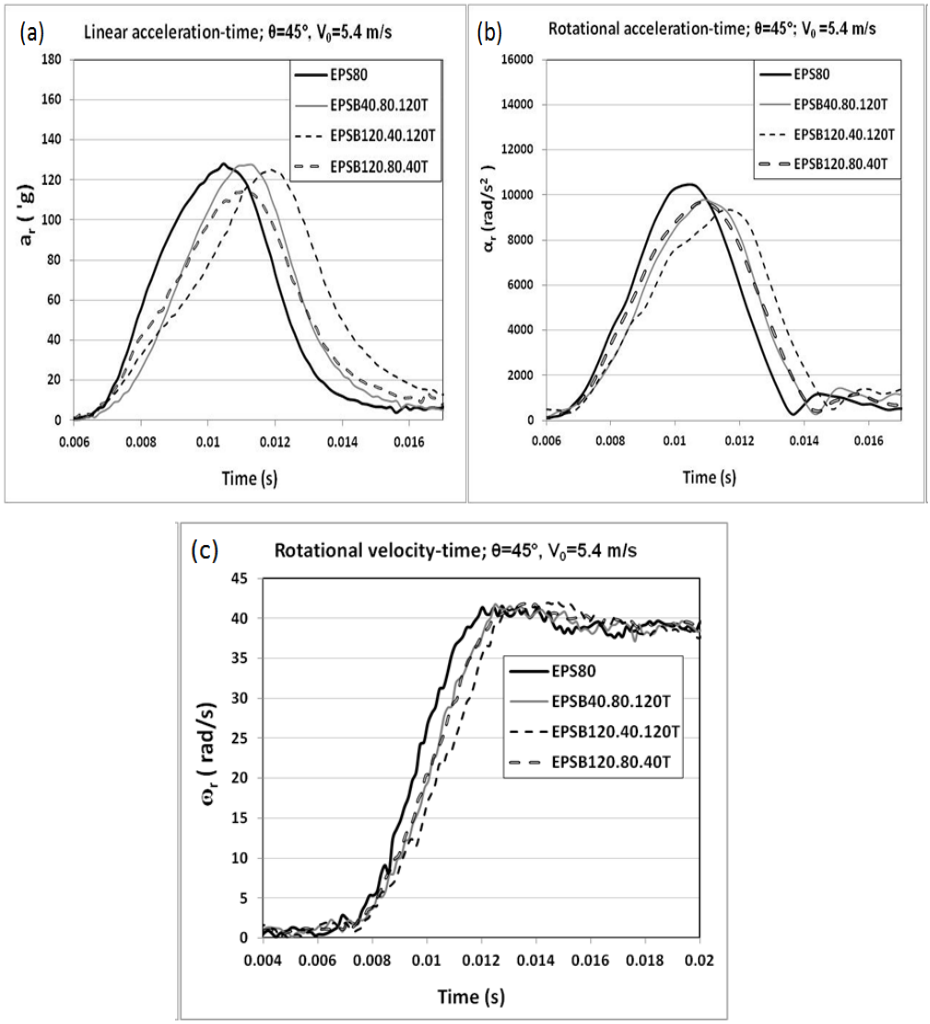

Figure 9-9: Oblique impact behaviour of three different configurations of layered composite foam versus EPS80 obtained from oblique impact experiments in which flat foam specimens are placed on an anvil at 45° and are impacted by the dummy head at an impact velocity of 4.5 m/s, (a) resultant linear acceleration-time, (b) rotational acceleration-time, and (c) rotational velocity-time.

9.4.2 Impact simulation results

The purpose of this section is to first assess the eligibility of the current numerical simulations for evaluation of the performance of different foam configurations in linear and oblique head simulations, which can save time and labor of actual experimentation. Secondly, a qualitative comparison will be done of different layered EPS configurations versus single layer EPS as a helmet foam material.

9.4.2.1 Oblique impact simulations of flat foam samples

Figure 9-10a-c, respectively, show the calculated linear and rotational acceleration and rotational velocity versus time of multi-layer composite foams in comparison to EPS80. In these simulations, the foams were fixed on the 45° anvil (see Figure 9-5a). Subsequently, the spherical headform dropped on the foam specimens with impact velocity of 5.4 m/s.

By comparing Figure 9-9a-c and Figure 9-10a-c, it can be concluded that there is a good agreement between experimental and simulation results in terms of predicting the trends and relative behaviour of the different configurations of multi-layer composite foams with respect to each other and to EPS80. The shape of the linear and rotational acceleration versus time and rotational velocity versus time curves are very similar to the results obtained from the experiments. All the layered composite foams show lower rotational acceleration values and also a lower slope of the rotational velocity, for the used impact velocity of 5.4 m/s. Moreover, EPSB120/80/40T seems to be the best configuration since it also transfers lower linear acceleration levels in comparison to EPS80, as was also observed during the experiments.

In both simulation and experimental results a prolongation of impact duration around 2 ms can be seen for multi-layer foams in comparison to EPS80. As mentioned earlier this could be due to the stepwise deformation in the layered foam. In layered foams deformation starts in the softer layers which can be observed in Figure 9-11, in which evolution of deformation in different layered foams is shown in progression of time.

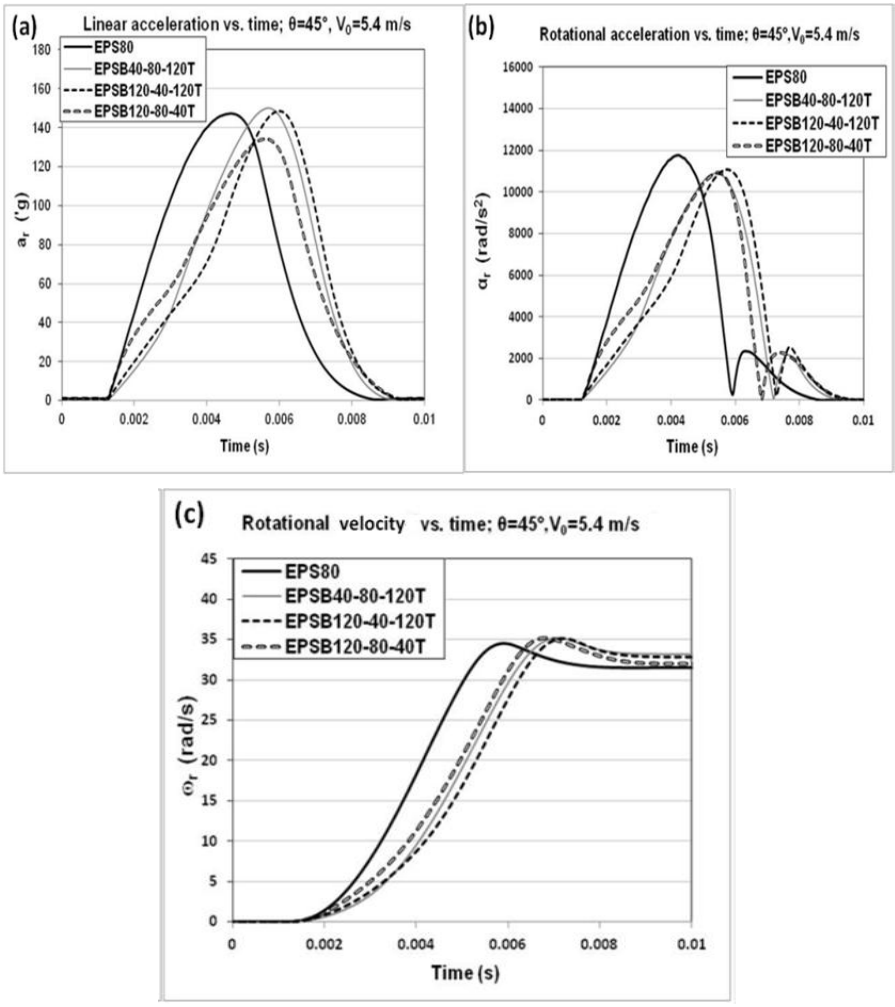

Figure 9-10: Simulated oblique impact behaviour of three different configurations of layered composite foam versus EPS80 obtained from oblique impact experiments in which flat foam specimens are placed on an anvil at 45° and are impacted by the dummy head at impact velocity of 4.5 m/s, (a) resultant linear acceleration-time, (b) rotational acceleration-time, and (c) rotational velocity-time.

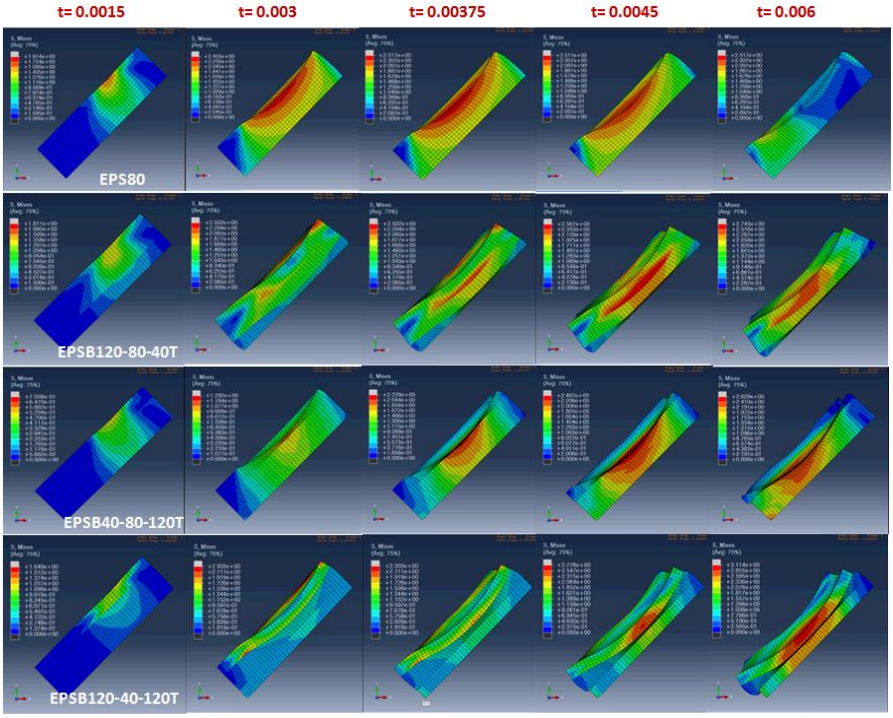

Figure 9-11: The evolution of deformation of EPS80 foam and layered EPS foams with time during oblique impact (impact velocity of 5.4 m/s) is shown by snapshots from simulations.

However, absolute values of linear and rotational acceleration in simulation curves show higher values compared to experimental curves. As explained in chapter 8, one of the reasons for this discrepancy in absolute peak values between simulations and experimental curves can be that the simulated headform is approximated as a sphere whilst in actual experiments in this study a hybrid III dummy head was used. Possible difference in friction coefficient between the dummy head and the foam (covered by comfort pad) during experiments than the value of 0.3 that was assumed in the model can be another source of discrepancy.

9.4.2.2 Linear impact simulations of helmeted heads

Figure 9-12a-b demonstrates the linear acceleration versus time curves obtained from linear impact simulations of helmeted heads with impact speed of 5.4 and 6.5 m/s, respectively.

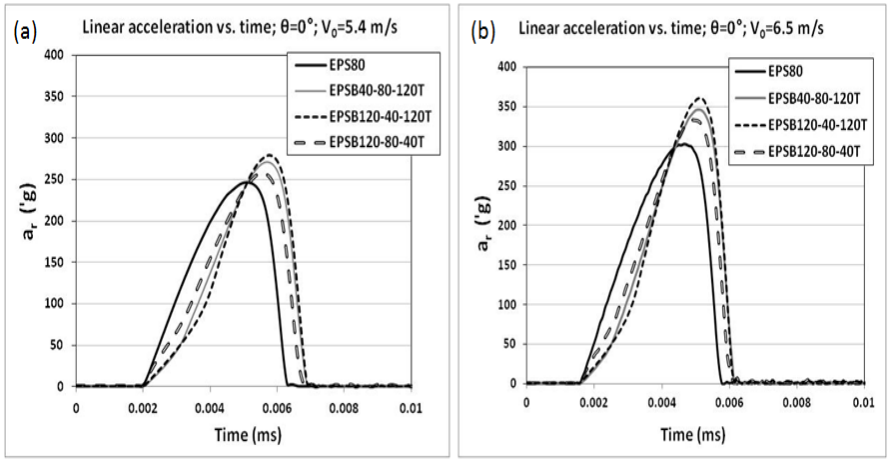

Figure 9-12: Simulated performance of helmets made of layered composite foam in linear impact in comparison to EPS80 reference helmet at impact velocity of (a) 5.4 m/s, and (b) 6.5 m/s (a_r is resultant linear acceleration).

It can be seen that the numerical results are in line with the conclusion which was drawn from compression and linear impact experimental results (Figure 9-8). Multi-layer EPS liners demonstrate higher peak linear acceleration in comparison to EPS80. For both impact velocities of 5.4 and 6.5 m/s, it can be observed that the highest peak acceleration is related to the EPSB120/40/120T configuration, which is believed to be related to the thicker layer of EPS40 which densifies prior to the higher density layers and leads to a bigger ratio of the densified layer in comparison to other configurations. Similar to observations in drop weight impact experiments on flat samples, it can be seen that the configuration where the higher density layer is closer to the head transfers lower accelerations to the head, however it cannot outperform EPS80.

9.4.2.3 Oblique impact simulations of helmeted head

Figure 9-13a-c demonstrates the linear and rotational accelerations and rotational velocity transmitted to the headform whilst impacting the 45° anvil, with impact velocity of 5.4 m/s.

As observed, for the impact velocity of 5.4 m/s, the EPSB120/80/40T helmet transfers slightly lower peak linear and rotational accelerations to the head compared to EPS80 helmet whilst EPSB120/40/120T and EPSB40/80/120T helmets show similar peak linear and rotational accelerations to EPS80 helmet.

These results are somewhat different from the experiments and simulations of flat foam samples, where all layered foam samples showed reduced rotational acceleration. In addition, in the helmeted head simulations, all the layered EPS foam configurations demonstrate lower slope before reaching peak accelerations for both linear and rotational accelerations and prolongation of the impact duration around 2 ms, compared to EPS80. This can be related to the weaker EPS40 layers in layered foams. However, at higher impact velocity of 6.5 m/s as shown in Figure 9-13d-f, EPS80 demonstrates lower linear and rotational acceleration peaks than the layered foam configurations, except for EPSB120/80/40T. As shown earlier in Figure 12a-b, in linear impact, EPS80 outperforms all three layered EPS foam configurations.

The values for peak resultant linear and rotational acceleration, and rotational velocity obtained from linear and oblique impact simulations of helmeted head for both impact velocities of 5.4 and 6.5 m/s are tabulated in table 9-2 and table 9-3.

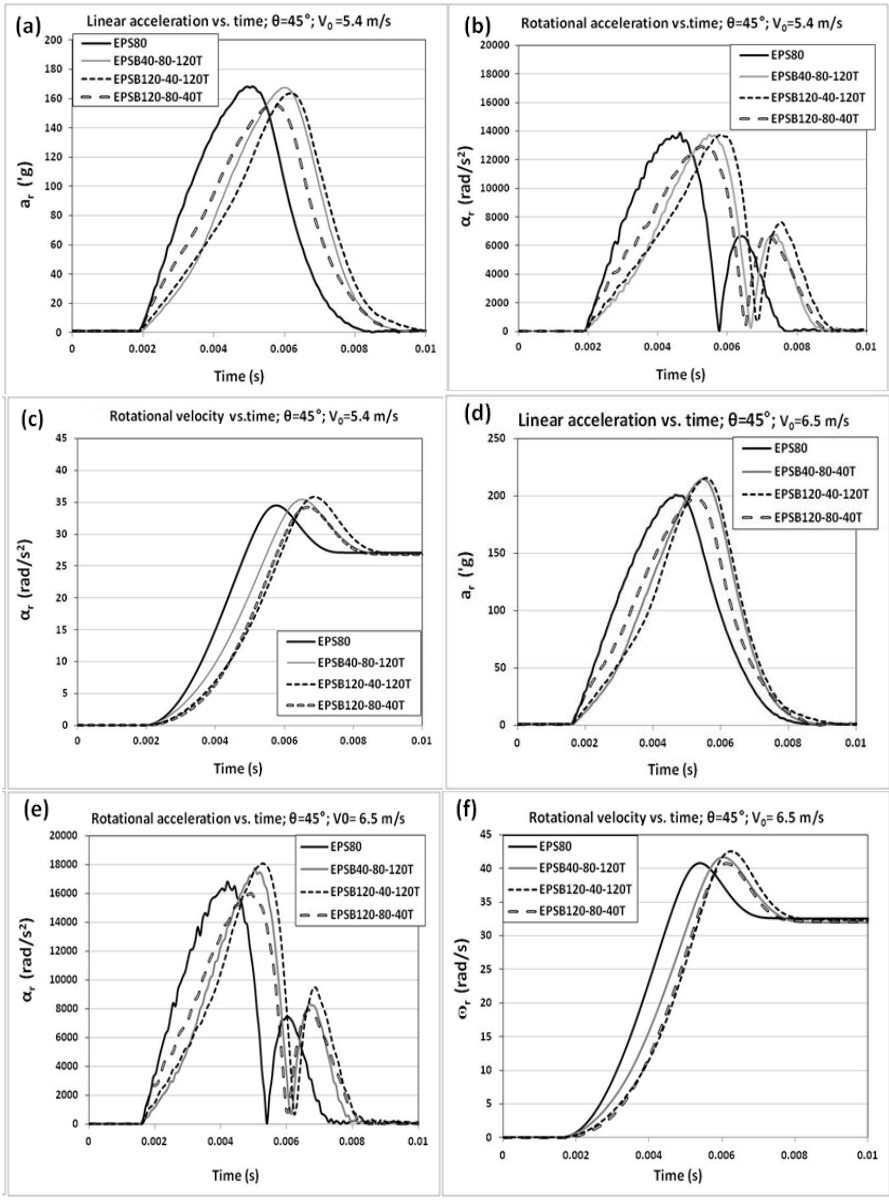

Figure 9-13: Simulated performance of helmets made of three different configurations of layered composite foams versus EPS80 obtained from FE simulations of oblique impact at angle of 45° and two impact velocities of 5.4 and 6.5 m/s; (a&d) resultant linear acceleration-time, (b&e) rotational acceleration-time , and (c&f) rotational velocity-time.

Table 9-2: Tabulated values of peak resultant linear acceleration, from linear impact simulations of helmeted head at two impact velocities of 5.4 and 6.5 m/s.

	V_0=5.4 m/s, θ=0°	V_0=6.5 m/s, θ=0°
Sample code	$a_{r,max}$ (g)	$a_{r,max}$ (g)
EPS80	246	300
EPSB40/80/120T	270	346
EPSB120/40/120T	278	360
EPSB120/80/40T	258	333

Table 9-3: Tabulated values of peak resultant linear and rotational accelerations, and peak resultant rotational velocity, from oblique impact simulations of helmeted heads at two impact velocities of 5.4 and 6.5 m/s.

	V_0=5.4 m/s, θ=45°			V_0=6.5 m/s, θ=45°		
Sample code	$a_{r,max}$ (g)	$\alpha_{r,rmax}$ (rad/s²)	$\omega_{r,max}$ (rad/s)	$a_{r,max}$ (g)	$\alpha_{r,max}$ (rad/s²)	$\omega_{r,max}$ (rad/s)
EPS80	141	13600	34.4	200	16836	40.8
EPSB40/80/120T	142	13775	35.4	182	17562	41.5
EPSB120/40/120T	140	13731	35.8	186	18053	42.5
EPSB120/80/40T	133	12863	34.1	200	15951	40.7

9.4.2.4 Analysis of the data based on global injury criteria

In order to avoid drawing conclusions on performance of multi-layer foam solely based on peak acceleration and to take into account pulse duration, the test results are analyzed according to global head injury criteria such as HIC (linear head injury criterion), and RIC (rotational head injury criterion). The calculated HIC_{15} and RIC values for linear and oblique impacts are tabulated in table 9-4. As shown in table 9-4, in linear impact the helmets with the layered configurations demonstrate higher HIC_{15} values than standard EPS80 helmets for both impact velocities of 5.4 and 6.5 m/s. However, in oblique impact, for impact velocity of 5.4 m/s, HIC and RIC values for layered foam and specifically the EPS120B-80-40T material show slightly lower values than EPS80 and also for impact velocity of 6.5 m/s, only the EPS120B-80-40T helmet can slightly outperform the EPS80 helmet.

As can be observed in table 9-4, at impact velocity of 5.4 m/s, the calculated RIC values for multi-layer composite are slightly lower than for EPS80 helmet. The decrease in RIC values in case of the EPSB120/80/40T Prototype is up to 10 %. For impact velocity of 6.5 m/s, only the EPSB120/80/40T helmet exhibits a lower RIC value than EPS helmet (8.5%).

From simulation results it can be concluded that multi-layer foams cannot outperform single layer EPS foam of the equivalent weight and thickness in linear impact. In oblique impact, results of simulation for impact velocity of 5.4 m/s show that layered composite helmets can outperform EPS80 helmet, however for a higher impact velocity of 6.5 m/s only the EPSB120/80/40T helmet can slightly outperform the EPS80 helmet by reducing peak linear and rotational accelerations. However, no clear change in peak rotational velocity by using multi-layer composite helmets was observed.

Concluding, both the simulation results and the earlier experimental results indicate that no significant benefits for impact energy absorption may be expected from layered foam liner configurations, notwithstanding some positive reports in literature [5, 6]. However, instead of using layered foam configurations which are loaded in series during impact, as an alternative parallel loaded composite foam configurations were evaluated, which turned out to give very clear reductions in rotational acceleration [14-16]. This is discussed in detail in chapters 5, 7, and 8.

Table 9-4: Calculated values of HIC, RIC, and HIP criterion for different layered composite foam configurations versus EPS80.

	V_0=5.4 (m/s) θ=0°	V_0=6.5 (m/s) θ=0°	V_0=5.4 (m/s) θ=45°		V_0=6.5 (m/s) θ=45°	
Sample code	**HIC_{15}**	**HIC_{15}**	**HIC_{15}**	**RIC**	**HIC_{15}**	**RIC**
EPS80	100%	100%	100%	100%	100%	100%
EPSB40/80/120T	122%	138%	94%	92%	99%	101%
EPSB120/40/120T	127%	145%	86%	89%	103%	103%
EPSB120/80/40T	106%	130%	84%	89%	91%	93%

9.5 Conclusions

This chapter comprises of two main parts. In the first part, the effect of helmet shell material and thickness on the impact resistance of a helmet against blunt and sharp projectiles was studied by performing drop weight impact tests. For this, composite shells of self-reinforced PP and silk/HDPE were benchmarked against conventional PC shells. The results indicate that only a tough composite of silk/HDPE can protect the helmets against perforation by sharp projectiles. Moreover, it was observed that using a thinner PC shell could lead to lower peak accelerations upon loading with a flat projectile, attributed to lower bending stiffness which allows for higher deformability, yet at the cost of reduced penetration resistance by a sharp projectile.

In the second part of this chapter, multi-layer EPS foams with three different configurations were prepared and their performance in compression and linear impact was compared with single layer EPS of similar thickness and weight. Results from compression experiments showed that the multi-layer foams initially absorb the energy more efficiently, however, after a certain stress level (in case of our material around 0.78 MPa), single layer EPS80 outperformed composite foams by absorbing more energy at intermediate stress levels. In the next step, the performance of multi-layer foams as a helmet liner in linear

and oblique impact was investigated via finite element simulations. Results demonstrated that the multi-layer composite foam with equal thickness and overall density did not outperform the single layer EPS80 foam in linear impact for both impact velocities of 5.4 and 6.5 m/s which are relevant velocities for bicycle helmet testing. In oblique impact, only the EPSB120/80/40T configuration in which the high density EPS120 layer is the closest to the head can slightly outperform EPS80 based on the peak acceleration values and HIC and RIC calculations. Based on the results of this chapter, notwithstanding earlier positive reports in literature, it seems multi-layer configurations are merely an equal alternative for single layer foam with the same density and thickness when protection as a helmet liner is targeted.

9.6 References

1. Di Landro, L., Sala, G., and Olivieri, D. Deformation mechanisms and energy absorption of polystyrene foams for protective helmets. Polymer Testing, 2002. 21(2):p. 217–228.
2. Hodgson, V.R., *Skid Tests on a Select Group of Bicycle Helmets to Determine Their Head-Neck Protective Characteristics*, 1991, Wayne State University: Detroit, Michigan.
3. Miltz, J., Ramon, O. Energy absorption characteristics of polymeric foams used as cushioning materials, Polymer Engineering and Science, 1990. 30: p.129–133,
4. Mills, N.J., Fitzgerald, C., Gilchrist, A., Verdejo, R. Polymer foams for personal protection: cushions, shoes and helmets. Composites Science and Technology, 2003. 63: p.2389-2400.
5. Cui, L., Kiernan, S., Gilchrist, M.D. Designing the energy absorption capacity of functionally graded foam materials. Materials Science and Engineering: A, 2009. 507(1-2):p. 215-225
6. Forero Rueda, M.A., Cui, L., Gilchrist, M.D. Optimisation of energy absorbing liner for equestrian helmets. Part I: Layered foam liner Materials & Design, 2009. 30:p.3405-3413.
7. Cui, L., Forero Rueda, M.A., Gilchrist, M.D. Optimisation of energy absorbing liner for equestrian helmets. Part II:

Functionally graded foam liner. Materials & Design, 2009. 30:p.3414–9

8. Caprino, G., Lopresto, V. Factors affecting the penetration energy of glass fibre reinforced plastics subjected to a concentrated transverse load. In: Proceedings of 9th European Conference on Composite Materials (ECCM-9), Brighton, UK, 2000.
9. Caprino G, Lopresto V. On the penetration energy for fibre-reinforced plastics under low-velocity impact conditions. Composite Science and Technology, 2001; 61: p.65–73.
10. Van Vuure, A.W., Vanderbeke. J., Osorio, L., Trujillo, E., Fuentes, C., Verpoest, I. Natural Fibre Composites: Tough silk and strong bamboo. In: Proceedings of 17th International Conference on Composite Materials (ICCM-17), Edinburgh, UK, 2009.
11. WO2007110758, Silk fibre composites
12. Mosleh, Y., Clemens, D., Gorbatikh, L., Verpoest, I., Van Vuure, A.W. Penetration impact resistance of novel tough steel fibre-reinforced polymer composites. *Journal of Reinforced Plastics and Composites, 2015. 34* (8): p.624-645.
13. Gibson, L. and Ashby, M. Cellular solids : structure & properties - 2nd ed.1997, Cambridge, UK: Cambridge University Press.
14. Mosleh, Y., Vander Sloten J., Depreitere B., Ivens J. Novel composite foam concept for head protection in oblique impacts. *Advanced Engineering Materials*, 2017. DOI: 10.1002/adem.201700059.
15. Mosleh, Y., Pastrav, L., Van Vuure, A., Depreitere, B., Vander Sloten, J., Ivens J. Optimization of composite foam concept for protective helmets to mitigate rotational acceleration of the head in oblique impacts: A parametric study. *Advanced Engineering Materials, 2017*. DOI: 10.1002/adem.201700443.
16. Mosleh, Y., Cajka, M., Depreitere, B., Vander Sloten, J., Ivens. J. Designing safer composite helmets to reduce rotational accelerations during oblique impacts. *Proceedings of the Institution of Mechanical Engineers H, Journal of Engineering in Medicine,* 2018. 232(5):p.479-491.

Chapter 10

Conclusions and future work

The most important achievement of this thesis is the proposition of a new anisotropic foam concept namely ''composite foam''. The composite foam, comprising of two different densities of a foam in a column/matrix configuration, is shown to be capable of reducing rotational acceleration and velocity of the head during oblique impacts in head protection applications such as different types of protective helmets (e.g. bicycle helmets, motorcycle helmets, ski helmets, and equestrian helmets).
This thesis is comprised of two main themes. In this conclusion chapter, in a retrospective manner, all the questions that were raised in chapter 2 (statement of purpose) are systematically addressed and answered.

1. Proposition of a new anisotropic foam concept for protective helmets:

- **Given the complications of chemical processing of anisotropic foam and more importantly its processing into intricate geometries for some applications, e.g. helmets, what can be a**

smart structural solution to create the anisotropy in foam without going through the difficulties of a chemical foaming route?

A ***novel composite foam concept*** was proposed to introduce mechanical ***anisotropy in a foam at the "macro level"*** by combining two different densities of a foam, initially in **layered configurations,** and eventually as **a column/matrix configuration**. For this, at first, discrete layers of EPS foams with two different densities (high and low density) were stacked upon each other, in two configurations namely ***"parallel"*** and ***"series"*** and compared to isotropic EPS foam of equivalent density and thickness. The compression experiments on layered composite foams showed that the ***parallel configuration outperforms the series counterpart in terms of effective energy absorption versus generated stress levels.*** In linear impact, for a given impact energy, the parallel configuration maintained peak forces/linear accelerations similar to isotropic foam of the same overall density but demonstrated lower peak forces/linear accelerations than the series configuration.
In biaxial shear-compression experiments, the composite foams with parallel ***configuration demonstrated reduced shear resistance whilst maintaining comparative compressive resistance to single layer isotropic foam***; this proved that the mechanical anisotropy was created in the foam and ***the shear and compressive response were decoupled***. However, composite foams with parallel plate configuration exhibited unwanted direction dependent mechanical behaviour in the plane of the impact when used in a real application (e.g. helmets). Therefore, composite foam with ***a column (e.g. cylinder)/matrix configuration*** was proposed as optimised geometry for real applications.

- **Can the shear and compressive properties of a foam in oblique loading be decoupled from each other without changing the overall density of the foam?**

Thanks to the composite foam concept, the shear and compression properties in a foam were decoupled irrespective of its density. The level of decoupling can be tailored.
Biaxial shear-compression experiments on ***layered composite foams with parallel configuration*** (composed of discrete layers of high

density and low density EPS foam) showed that the ***shear and compression properties of these foams were decoupled*** and they demonstrated lower shear properties than single layer isotropic EPS foam (of similar overall density and thickness) whilst preserving the levels of compressive stress (chapter 5). Additionally, ***the level of decoupling between compressive and shear properties can be tailored*** by parameters such as ***the number of layers*** or more precisely ***the thickness of the layers*** and the ***density difference between high density and low density foam layers***.
In the next step, the ***column/matrix configuration*** was used as an optimized geometry. In chapter 7, the biaxial shear-compression experimental results on column/matrix composite foams further confirmed the decoupling of shear and compressive properties in composite foam. Furthermore, in both layered composite foams and column/matrix composite foams ***the level of decoupling of shear and compression stresses*** or in other words ***the level of anisotropy*** can be ***tailored and optimised***. For instance, the liner composition can be varied near the helmet edge to compensate for the smaller liner volume that needs to absorb the impact energy, or on locations where the skull is thinner (temporal region).

- **Does anisotropy in a foam liner as a single variable (without changing other parameters such as foam density, solid foam material or foam thickness) lead to reduction of rotational acceleration and velocity in comparison to isotropic foam?**

Composite foams with column (cylinder)/matrix configurations comprised of two different densities of EPS foam have been produced and tested in oblique impact. The actual oblique impact experiments on flat composite samples were performed at impact velocity of 5.4 m/s and an oblique anvil angle of 45°. The results showed that ***the composite foam could significantly reduce the rotational acceleration and velocity compared to the isotropic foam counterpart (of equivalent density and thickness).***
The composite foam concept finally enabled a ***proof of principle study*** which confirmed that the ***anisotropy as a single variable*** leads to ***mitigation of rotational acceleration and velocity*** of the head during oblique impacts. The performance of the composite foam concept in flat and helmet shape was further investigated by performing ***finite element simulations of oblique impacts***. The results obtained by FE

simulations further demonstrated the superior performance of ***the anisotropic composite foam compared to isotropic single layer foam in reducing rotational acceleration and velocity of the head during oblique impact.***

- **When a suitable material concept is found, more particularly the proposed composite foam, what parameters within the concept can be varied to optimise the performance of the foam liner?**

In chapters 7 and 8 a dedicated parametric study was used to show that the ***level of rotational acceleration and velocity mitigation in the composite foams can be tailored and optimized***. The results demonstrated that by ***decreasing the diameter of the cylinders*** (made of higher density foam) in the composite foam structure and also by ***using a more compliant matrix foam (****or increasing* ***the compliance gradient between column and matrix foams)***, the level of rotational acceleration and velocity mitigation can be further improved.
In addition, FE simulations showed that ***the shape of the cross-section of the columns*** in composite foams hardly affects the linear and rotational acceleration values. Additionally, for obtaining the best performance of composite foams, ***the matrix foam*** should be made of the **lower density foam** and the ***foam columns*** should consist of ***higher density foam***. The impact results obtained from both experiments and simulations were analysed based on several ***global head injury criteria*** *(such as HIC and RIC)* and the composite foam demonstrated superior performance compared to single layer EPS foam.

- **Can quasi-static combined shear compression tests on flat foams be linked to their performance in oblique impacts in flat or helmet shape?**

In chapter 7, it was shown that there is ***a clear correlation between biaxial combined shear-compression and oblique impact results***.
Through a parametric study on column (cylinder)/matrix composite foam, it was shown that a systematic ***reduction in the shear stress component of the foam liner subjected to a static biaxial shear-***

compression load resulted in improved ***mitigation of rotational acceleration and velocity*** of that foam liner ***in oblique impact***.

This correlation is very important because the full helmet impact tests are cumbersome as a method to develop and compare materials for helmets, as they always require prototype helmets. But the parametric study on different composite foam configurations via quasi-static shear-compression and oblique impact experiments shed light on the existence of a qualitative correlation between shear stress levels of the foam in the combined shear-compression test with rotational acceleration and velocity in oblique impact.

- **Can the proposed anisotropic material concept be applied to complex geometries such as bicycle helmets?**

Although the development of the actual helmet manufacturing process is beyond the scope of this thesis, the author is convinced that a composite foam with a column/matrix configuration can be processed into intricate shapes and be utilized in helmet liners. One method of processing could be via a two stage process. High density foams with cylinder-shape can be produced by moulding or extrusion and cut to the right size. In the next step, the high density foam columns are placed in the strategic places (depending on the topology of the helmet) inside the helmet mould as inserts by a robot and are fixated in place via some pins. Subsequently, the low density foam will be injected and expanded. This requires sufficient thermal stability of the high density foam at the processing temperature of the low density matrix. Alternatively, the low density matrix is produced first with metallic inserts, which are subsequently replaced by the high density foam columns.

- **What is the effect of the helmet shell material on the impact performance when impacted by sharp and blunt projectiles?**

In chapter 9, the ***effect of helmet shell material and thickness*** on the impact resistance of a helmet against blunt and sharp projectiles was studied by performing drop weight impact tests. For this, composite shells of self-reinforced PP and silk/HDPE were benchmarked against conventional PC shells. The results demonstrated that tough composite of silk/HDPE can protect the helmet liner against perforation by sharp

projectiles when impacted at velocity of 5.4 m/s. Moreover, it was observed that using a thinner PC shell could lead to lower peak accelerations upon loading with a flat projectile, attributed to lower bending stiffness which allows for higher deformability, yet at the cost of reduced penetration resistance.

2. Further development and utilization of relevant testing machines:

2.1 Biaxial combined shear-compression tester:

- **Does the biaxial shear-compression test set-up generate reproducible and consistent results?**

Biaxial shear-compression experiments on EPS foams with three different densities under different loading angles have been performed. The test results shown in chapter 4 were consistent and reproducible with minimum scatter.

- **What is the effect of foam anisotropy and loading angle on the energy absorption capability of foams in biaxial shear-compression loading?**

The combined shear-compression behaviour of EPS foams with three different densities and anisotropic polyethersulfone foam (PES with anisotropy ratio ~2.4) was studied under different loading angles (deformation angles). The biaxial shear-compression experiments showed that by changing the loading angle from pure compression (θ=0°) to more shear dominant, the total energy absorption capacity of the isotropic EPS foams (up to the onset of densification) is independent of the loading angle. In contrast, in case of the anisotropic PES foam, the total energy absorption of the anisotropic PES foam decreases at more shear dominant deformation angles. In other words, the energy absorption capacity in anisotropic foams is dependent on the loading direction. This means that for the highest overall energy absorption the direction of anisotropy of the foam in the part must be aligned along the most probable loading direction.

2.2 Oblique impact set-up:

- **What are the sources of difference in the initial design of the KU Leuven oblique impact set-up with the KTH moving sled set-up? Impact surface? Sensoring system? Data acquisition box?**

To further develop the KU Leuven oblique impact set-up, a critical comparison between KU Leuven and KTH-MIPS (Stockholm) moving sled ***oblique impact test set-ups*** has been made (chapter 6). The helmet testing results obtained by these two set-ups showed a big discrepancy. To identify the sources of this discrepancy, controlled tests were performed and it was concluded that the discrepancy can be caused by three main sources. 1) impact surface, 2) sensoring system, and 3) data acquisition box.
The rubber impact surface of the rotary band in the KUL set-up was more efficient in transferring the horizontal velocity to the impacted headform due to its much higher coefficient of friction. However, it was found that the dynamic friction coefficient of the rotary band surface (unlike the sand paper in the KTH moving sled set-up) is dependent on the velocity and the vertical load. The changing friction coefficient of the rotary band surface increases test variability in a way that is difficult to control. Moreover, the rubber surface dissipated some of the impact energy. Also slippage of the rotary band during the helmet experiments adds to the results variability and actually resulted in a lower horizontal velocity transfer than for the KTH moving sled set-up.
Secondly, the sensor set-up was investigated. It is necessary to calibrate the Angular Rate Sensor (gyroscope) in its full angular velocity range; for this an in-house calibration set-up was designed and utilized. Calibration experiments showed that the gyroscope works properly.
Thirdly, the signal processing box was investigated. During ARS calibration experiments, an error in the amplification was found responsible for some of the differences in experimental results obtained from the two set-ups. As both the moving sled and the rotating belt add complications to the set-ups, a simplified set-up using an **inclined anvil surface** was made and utilized for the oblique impact testing of various foam liner materials in this thesis.

- **How can the ARS be calibrated in the relevant angular velocity range?**

For the ***calibration of the triaxial gyroscope (ARS)*** in its full working range, ***a new in-house test set-up*** was designed, manufactured and utilised (chapter 6). This set-up consists of a rigid blade which is bolted to a multi-part cylinder in which two bearings enable its (almost friction-free) rotation around a vertical axis. In this set-up, a calibrated accelerometer is placed at the end of the blade to measure the tangential acceleration. The gyroscope subsequently is placed in the middle of the rotating blade to measure its rotational (angular) velocity around the rotating axis. An L-shaped piece in this set-up enables measurement of the angular velocity of the triaxial gyroscope (ARS) around all three axes. Calibration experiments showed that the ARS sensor works properly in its full working range.

Suggestions for future work

The composite foam is shown to be a promising concept to be employed in the next generation of helmet liners for reducing head rotational acceleration and velocity during oblique impacts. Therefore, to apply the composite foam concept for the intricate shape of e.g. bicycle helmets, an industrially viable manufacturing method is one of the important aspects for future research and development. Two-step processing methods were proposed in the previous paragraph but require further elaboration.

High density foam cylinders can be produced by moulding or extrusion, cut to size and placed as inserts in the helmet mould, secured by pins. The low density matrix foam would then be injected and expanded around the high density cylinders. Effects of temperature and expansion pressures on the cylinder inserts require further investigation.

Alternatively, the matrix foam can be processed first using metallic inserts or machined (from a soft foam such as flexible PU) to create the necessary holes. Subsequently, the foam for the columns (from a second foam type or density) would be inserted in the holes. The method of inserting the foam cylinders without damage needs to be

developed and the influence on the interaction between the two foams needs to be studied.

This thesis proved that (macroscopic) anisotropy, as the only varying parameter in a foam, can result in reduction of rotational acceleration and velocity to the head via reducing shear stresses in the foam liner. The next compelling question is to what extent the anisotropy level in the foam liner could be optimised to maximise mitigation of rotational acceleration whilst reducing the shear resistance. This can be achieved with a dedicated parametric study on the column/matrix composite structure via finite element modelling, by changing parameters such as foam column diameter, varying cross-sectional shape of the foam columns along its length (which affects its bending moment of inertia), and the density gradient between column and matrix foams (or the compliance gradient), for a given helmet geometry. Furthermore, other light-weight materials or even strut-like 3D-printed open structures could be envisaged to create macroscopic anisotropy.

The FE head-helmet model used in this thesis was simplified, compared to a real helmet. The modelling can be further elaborated and improved by using a more realistic head model and using real helmets, with their aerodynamic shape, including the outer shell and the internal soft padding, retention system and straps. Especially the introduction of ventilation holes will require modifications to the column/matrix configurations to optimise the helmet impact performance.

As friction and sliding play an important role in oblique impact, applying a more accurate friction coefficient between head and helmet and the helmet and the anvil will further improve the impact simulations. These aspects will be studied in the PhD research of Dimitrius Zouzias and Antonia Trotta.

Current material models in impact modelling of the foams utilise compression and tension stress-strain curves obtained from actual experiments. In a combined compression-shear loading, the compression stress component leads to foam crushing and increased foam density; it is highly unlikely that this modified material will fail at the same tensile stress level as observed in simple tensile tests. Therefore, new material models will need to be developed and implemented in FE software packages like ABAQUS or LS DYNA.

It is expected that combining a composite foam liner with other innovative designs such as a MIPS slip layer inside a helmet will further reduce accelerations and velocities and improve helmet impact

performance. Possible synergistic effects could be subject of further research.

Another suggestion for further future investigation is related to the medical aspect of head protection. In this thesis, the results obtained by oblique impact on different composite foams versus isotropic reference materials have been evaluated based on global head injury criteria. It is well known that, although indicative, these global criteria do not correlate well with all head injuries. Hence, the use of injury-specific criteria using state of the art head models will allow further optimisation of the performance of these materials in head injury prevention.

In this thesis, during the parametric study on various composite foam configurations, it was shown that there is a correlation between quasi-static shear-compression experiments of the foams with the oblique impact tests. Oblique impact is a dynamic event; hence for a possibly better correlation between combined shear-compression and oblique impact experiments, a test set-up which can measure combined shear-compression behaviour of the foams at high strain rates will further improve this correlation. This aspect is currently under investigation in the PhD of Chen Ling.

Moreover, the KU Leuven oblique impact set-up can be further improved and here are some suggestions:

- The weight of the whole setup could be increased in order to reduce overall vibrations of the set-up by placing a heavy mass underneath the plinth of the current setup and bolting it in place.
- Currently, there is a drop height limitation of 2m in the KU Leuven set-up which limits the impact testing velocity and energy. Therefore, using a spring in the set-up which can increase the helmeted headform velocity is proposed.
- The support system is not sufficient to perform the impact tests at any position of the head. Therefore, the design of a new support system which enables testing of the headform in temporal, frontal and occipital sites, is needed.
- For further simplification of the oblique impact experiments, using wireless sensors is proposed to avoid the interference of the cables during experiments.

Scientific record

Articles in internationally reviewed academic journals:

1. Yasmine Mosleh, Bart Depreitere, Jos Vander Sloten, Jan Ivens. Decoupling shear and compression properties in composite polymer foams by introducing anisotropy at macro level. Journal of Reinforced Plastics and Composites, 2018. 37 (10): p.657-667.
2. Yasmine Mosleh, Martin Cajka, Bart Depreitere, Jos Vander Sloten, Jan Ivens. Designing safer composite helmets to reduce rotational accelerations during oblique impacts. *Proceedings of the Institution of Mechanical Engineers H, Journal of Engineering in Medicine,* 2018. 232(5):p.479-491.
3. Yasmine Mosleh , Leonard Pastrav, Aart Willem Van Vuure, Bart Depreitere, Jos Vander Sloten , Jan Ivens. Optimization of composite foam concept for protective helmets to mitigate rotational acceleration of the head in oblique impacts: A parametric study. *Advanced Engineering Materials*, 2018. 20 (2). atr.num.1700443.
4. Yasmine Mosleh, Kelly Vanden Bossche, Bart Depreitere, Jos Vander Sloten, Ignaas Verpoest, Jan Ivens. Effect of polymer foam anisotropy on energy absorption during combined shear-compression load. Accepted by the Journal of Cellular Plastics, 2018. 54(3): p.597-613.
5. Yasmine Mosleh, Jos Vander Sloten, Bart Depreitere, Jan Ivens. Novel composite foam concept for head protection in oblique impacts. Journal of Advanced Engineering Materials, 2017. 19(10). atr.num.1700059.
6. Kelly Vanden Bosche*, Yasmine Mosleh*, Bart Depreitere, Jos Vander Sloten , Ignaas Verpoest, Jan Ivens. Anisotropic polyethersulfone foam for bicycle helmet liners to reduce rotational acceleration during oblique impact. *Proceedings of*

the Institution of Mechanical Engineers H, Journal of Engineering in Medicine, 2017. 231(9):p.851-861. *joint first authors.

7. Yasmine Mosleh, Dorien Clemens, Larissa Gorbatikh, Ignaas Verpoest, Aart Willem Van Vuure. Penetration impact resistance of tough novel steel fibre-reinforced polymer composites, Journal of reinforced plastics and composites, *2015* .34(8):p.624-635.
8. Yasmine Mosleh, Martin Cajka, Bart Depreitere, Jos Vander Sloten, Jan Ivens.'' Study on the effect of shell material and multilayer foam liner on performance of bicycle helmets in linear and oblique impacts'' (submitted).
9. Yasmine Mosleh*, Nadereh Golshan Ebrahimi, Alireza Mahdavian, Mohsen Ashjari. TPU/PCL/nanomagnetite ternary shape memory composites: Studies on their Thermal, Dynamic-Mechanical, Rheological, and Electrical Properties. Iranian Polymer Journal-Springer publishing, 2014. 23(2):p.137-145.*
10. M. Ashjari, A. Mahdavian, N. G. Ebrahimi, Y. Mosleh. Efficient Dispersion of Magnetite Nanoparticles in Polyurethane Matrix Through Solution Mixing and Investigation of the Nanocomposite Properties, *Journal of Inorganic and Organometallic Polymers and Materials, 2010. 20(2):p.213-219.*

Conference papers/presentations:

1. Yasmine Mosleh , Martin Cajka, Bart Depreitere, Jos Vander Sloten, Jan Ivens. Composite foam for designing safer helmets in real life impacts, CellMAT conference, 6-9 December 2016, Dresden, Germany.(presentation without paper)
2. Yasmine Mosleh, Bart Depreitere, Jos Vander Sloten, Jan Ivens**.** Design and optimization of layered composite foam liners and shell material for protective helmets, ECCM17 Conference, European conference on composite materials, 26-30 June 2016. (full paper in proceedings)
3. Yasmine Mosleh, et al., "Static and Dynamic Response of Novel Anisotropic Foam
   Concept For Protective Helmets", 20th European Conference on Composite Materials
   ICCM20-19-24 July 2015, Copenhagen, Denmark. (full paper in proceedings)
4. Yasmine Mosleh, Kelly Vanden Bosche, Jos Vander Sloten, Ignaas Verpoest, Jan Ivens, " Characterisation of EPS Foams under Combined Shear-Compression Loading", *SAMPE Europe Technical Conference-SETEC 14, 10-11 September 2014, Tampere, Finland.* (full paper in proceedings)
5. Yasmine Mosleh, Kelly Vanden Bosche, Jos Vander Sloten, Ignaas Verpoest, Jan Ivens, " Combined Shear-Compression Test to Characterize Foams under Oblique Loading for Bicycle Helmets",*16th European Conference on Composite Materials-ECCM16, 22-26 June 2014, Seville, Spain.* (full paper in proceedings)
6. Yasmine Mosleh, Kelly Vanden Bosche, Miguel Rodriguez Perez, Jos Vander Sloten, Jan Ivens, Ignaas Verpoest, " Development of Anisotropic Foams and Characterisation methods for Bicycle helmets", *Composite Week @ Leuven, 16-20 September 2013, Leuven, Belgium.* (full paper in proceedings)
7. Yasmine Mosleh, Aart Willem Van Vuure, Sophie Vande Walle, Larissa Gorbatikh, Ignaas Verpoest, "On the Potential of Fine

Steel Fibres to Create Stiff but Tough Polymer Composites", 1*5th European Conference on Composite Materials-ECCM15, 24-28 June 2012, Venice, Italy.* (full paper in proceedings)

8. Y. Mosleh, N. G. Ebrahimi, A. Mahdavian. M. Ashjari, "Crystallization and Glass Transition Behavior of PU/PCL/nanomagnetite Ternary Composite", *9th International Seminar on Polymer Science and Technology, Tehran, Iran, October 17-21, 2009.*
9. M. Ashjari, A. Mahdavian, N. G. Ebrahimi, Y. Mosleh,"Effect of Mixing Process on the Preparation of Nano-Fe3O4 Doped Thermoplastic Polyurethane", *International Conference on Nanoscience and Technology (ICONSAT2010), Mumbai, India, February 17-22, 2010.*

Patent:

Anisotropic composite structure, liner and helmet comprising such a structure and use of and method of producing such a structure. Inventors: Yasmine Mosleh, Jan Ivens PCT/EP2017/066233. WO2018002283A1. (2017)

Contribution to bicycle helmet Demo Day:

Task: Preparation of the helmet prototype/presentation

Yasmine Mosleh, Kelly VandenBosche,Ignaas Verpoest, Jan Ivens, Bart Depreitere, Jos Vander Sloten, Ontwikkelen van anisotrope materiaal concepten voor fietshelmen ter reductie van rotationele acceleratie Bicycle Helmet Demo Day. Leuven, 5 July. *Article in "De Standaard" 6 July 2016.*

Master student supervision:

Bart Van De Poel. ''DEVELOPMENT OF A STANDARD TEST METHOD FOR SHEAR-COMPRESSION TESTING OF FOAMS'' 2013-2014.

Jeroen Peetroons. '' DEVELOPMENT AND CHARACTERISATION OF ANISOTROPIC MATERIALS FOR BICYCLE HELMETS'' 2014-2015

Jamie Amato & Joachim De Ghellinck. ''ANALYSIS AND IMPROVEMENT OF A ROTATIONAL IMPACT TEST SET-UP USED TO TEST BICYCLE HELMETS'' 2014-2015.

Sven Hendrickx. ''CHARACTERIZATION OF ANISOTROPIC FOAM COMPOSITES FOR REDUCING THE SHEAR RESISTANCE IN BICYCLE HELMETS'' 2015-2016

Olivier Van Bladel. '' CHARACTERISATION OF POLYMER FOAMS UNDER INFLUENCE OF SIMULTANEOUS SHEAR AND COMPRESSION'' 2015-2016.

Maarten Vanhulst. ''OPTIMIZATION OF ANGULAR ACCELERATION-REDUCING PROPERTIES OF ANISOTROPIC COMPOSITE FOAMS'' 2015-2016.

Frederick De Hollander & Serdar Sengun '' ROTATIONAL IMPACT EXPERIMENTS OF NEW GENERATION OF BICYCLE HELMET LINERS AIMING AT ROTATIONAL ACCELERATION MITIGATION'' 2015-2016.